DEVELOPMENT OF METHODS TO SCREEN AND EVALUATE SMALL MOLECULE BINDERS OF THE PROTEASOME

by

Marianne Elizabeth Maresh

A Dissertation

Submitted to the Faculty of Purdue University

In Partial Fulfillment of the Requirements for the degree of

Doctor of Philosophy

Department of Medicinal Chemistry and Molecular Pharmacology

West Lafayette, Indiana

May 2021

THE PURDUE UNIVERSITY GRADUATE SCHOOL
STATEMENT OF COMMITTEE APPROVAL

Dr. Darci J. Trader, Chair

Department of Medicinal Chemistry and Molecular Pharmacology

Dr. Vincent Jo Davisson

Department of Medicinal Chemistry and Molecular Pharmacology

Dr. Michael Wendt

Department of Medicinal Chemistry and Molecular Pharmacology

Dr. Qing Deng

Department of Biological Sciences

Approved by:

Dr. Andy Hudmon

This work would not have been possible without my family. Thank you to my mom, dad, and brother for their unconditional love and support. I am also extremely grateful to my fiancé, Keith. I am thankful for you every day and could not have done this without you. Thank you for always pushing me to be my best, loving me no matter what, and being there for me.

ACKNOWLEDGMENTS

I would like to thank my advisor, Professor Darci J. Trader, for her support, advice, and inspiration during the completion of this work. I am incredibly thankful to have an advisor that is so passionate not only about her science, but the success of her students. I would also like to extend gratitude to my lab mates, Christine Muli, Andres Salazar-Chaparro, Tom Tian, Saayak Halder, and Mackenzie Clement. I have cherished our friendship and deeply appreciate all the scientific input you have provided. Thank you to Dr. Breanna Zerfas for not only her contribution to my growth as a scientist, but also being a great friend and source of support. Several figures were created with BioRender.com.

TABLE OF CONTENTS

LIST OF FIGURES

ABSTRACT

The proteasome is responsible for the majority of protein degradation in the cell. Dysregulation of proteasome activity is implicated in a variety of diseases such as cancer, neurodegeneration, and aging. As a result, it has emerged as therapeutic target and significant research to elucidate the impacts of modulating its activity with small molecules is ongoing. While a variety of small molecule binders have been identified and shown to be effective in treating diseases such as cancer, there is a lack of standardized assays to identify new binders and evaluate their impacts in biologically relevant settings. In this work, we present a suite of assays that can be used to screen proteasome subunits for new binders and determine the impacts of small molecules in yeast with reduced proteasome capacity. We also explore stimulation of the immunoproteasome (iCP), a proteasome isoform that is expressed during inflammatory conditions.

We first developed a method to screen one-bead-one-compound (OBOC) libraries in which hits could be prioritized. Our method involves labeling a target protein with a near-infrared range fluorophore and incubating it with OBOC library beads in a well plate. The plate can then be imaged for fluorescence and the signal can be quantified. This provides a basis to rank hits. We used this screening method to identify TMM-6, a peptoid that covalently binds the oncoprotein gankyrin. Since this method does not require the function of a protein to be known, it is ideal for screening noncatalytic proteasome subunits.

We then optimized an assay to monitor the chronological lifespan (CLS) of yeast in response to dosage with small molecules that stimulate the proteasome. Through alterations of growth media, we successfully reduced the time required to perform this assay from over a month to just one week. Similarly, the assay was scaled down to a 96-well plate format to make it more amendable to high-throughput applications. We used this assay to evaluate the impacts of the proteasome stimulator ursolic acid (UA) on the CLS of yeast with reduced proteasome capacity. We found that dosage with UA resulted in slight lifespan extension.

The iCP generates peptides that are compatible with major-histocompatibility complexes type I (MHC-I) and several viruses are known to deploy proteins that interact with the iCP to inhibit its activity. We hypothesize that iCP inhibition could be rescued with a small molecule stimulator and in turn increase the pool of MHC-I compatible peptides, allowing virally infected cells to be recognized by the immune system. Here, we report UA and structurally similar

compounds as potent iCP stimulators. Stimulation was demonstrated in both a biochemical assay and in cells induced to express the iCP.

This work resulted in several new assays that can be used to quickly identify quality binders to proteasome subunits and evaluate their impacts in aged yeast. We anticipate usage of these assays will result in the discovery of new proteasome binders that impact its activity. Particularly, we are interested in determining the impacts of targeting noncatalytic proteasome subunits, as their therapeutic potential remains largely underexplored. We also identify new iCP stimulators and plan to further explore the impacts of iCP stimulation on MHC-I expression.

CHAPTER 1. THE PROTEASOME AS A THERAPEUTIC TARGET AND METHODS TO IDENTIFY SMALL MOLECULE MODULATORS OF ITS ACTIVITY

1.1 Overview of Protein Degradation by the Proteasome

1.1.1 The Ubiquitin-Dependent Pathway

The ubiquitin proteasome system (UPS) is responsible for degradation of up to 80-90% of proteins in the cell that are worn out or misfolded.[1,2] At the center of the UPS is the proteasome, a large multi-catalytic enzymatic complex that is responsible for hydrolyzing proteins into small peptide fragments. These fragments are then recycled by the cell. The proteasome exists in several isoforms that carry out ubiquitin-dependent or ubiquitin-independent protein degradation (**Figure 1.1**).[2–4] The 26S proteasome is responsible for ubiquitin-dependent degradation of proteins. It is composed of two parts, a 19S regulatory particle (RP) and a 20S core particle (sCP).[3,5] The RP is responsible for recognizing ubiquitinated substrates, removing the ubiquitin tags, unfolding the protein through an ATP-dependent process, and shuttling the protein into the catalytic core.[2,6] The sCP is composed of a series of four heptameric rings that arrange in an α-β-β-α fashion. The α rings form a gate structure which exists in an open or closed confirmation to allow or block entry of a protein substrate into the proteasome.[4,7–9] The β rings house three catalytic subunits, β1, β2, and β5 which exhibit different cleavage specificities (caspase-like, trypsin-like, and chymotrypsin-like, respectively).[2,10] These subunits are responsible for the hydrolysis of the unfolded protein into short peptide sequences. Proteins that are folded are typically too bulky to

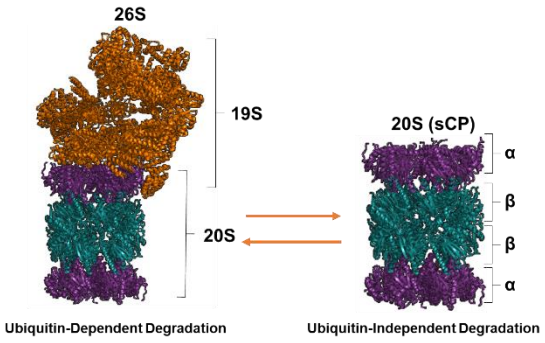

Figure 1.1. Isoforms of the Proteasome. The proteasome exists in equilibrium between two isoforms, the 26S and the 20S. The 26S carries out ubiquitin-dependent degradation while the 20S facilitates ubiquitin-independent degradation of protein substrates. The 26S is composed of the 19S regulatory particle (RP) and the 20S core particle (sCP). The RP recognizes ubiquitinated substrates and prepares them for cleavage by the sCP. The sCP can exist without an RP. The sCP consists of four heptameric rings. The α rings make up a gate structure that allows entry of unfolded proteins. The β-rings house three catalytic subunits that are responsible for hydrolyzing the unfolded protein into short peptide sequences that can be recycled by the cell. The 20S can hydrolyze small, intrinsically disordered proteins that are not tagged with ubiquitin.

be degraded by the sCP directly without unfolding by the RP. This offers a layer of protection to prevent excessive degradation of proteins that are still needed by the cell.[6]

The 26S carries out ubiquitin-dependent protein degradation in which the protein substrate must first be labeled with a chain of ubiquitin proteins. This is facilitated by the ubiquitin enzyme cascade consisting of E1, E2, and E3 enzymes. E1 enzymes activate ubiquitin and transfer it to an E2 enzyme.[11] The E2 enzyme will then transfer the ubiquitin to a target protein with support from an E3 ligase enzyme.[11] Multiple ubiquitin are successively attached to a target protein to build a polyubiquitin chain.[12] Ubiquitin chains are built through linkage of one ubiquitin to the next through attachment by one of several lysine residues. Generally, protein substrates tagged for proteasomal degradation have chains of four to five ubiquitin proteins that are attached through K48 linkage.[13] After linkage of ubiquitin to the target protein, it can then be recognized by the proteasome and degraded.

The RP of the 26S proteasome houses two subunits, Rpn-10 and Rpn-13 that recognize ubiquitin-tagged proteins.[14,15] The ubiquitin chain is then removed from the target protein either through the RP subunit Rpn-11 or other deubiquitinating enzymes recruited by the RP.[6] The exact mechanism of protein unfolding by the RP is not completely understood, but it is believed that interactions between disordered regions of the target protein with Rpt subunits of the RP facilitates protein unfolding.[16,17] The linearized protein is then shuttled into the catalytic core of the sCP where it is hydrolyzed into peptide fragments.

Ubiquitin-dependent protein degradation by the 26S is critical to removing well-folded proteins from the cell. Dysregulation or disruption of this process impacts proteostasis and can result in cell death. As previously mentioned, the 26S proteasome exists in equilibrium with the sCP in the cell. The sCP is also capable of degrading a subset of proteins that are not tagged with ubiquitin, resulting in ubiquitin-independent protein degradation.

1.1.2 The Ubiquitin-Independent Pathway

The structural diversity of proteins found within the cell are vast, ranging from large, well ordered and tightly folded, to small, disordered proteins. As discussed above, well-folded proteins are primarily degraded by the proteasome through a ubiquitin-dependent manner which is carried out by the 26S proteasome. However, there are several instances in which small, disordered proteins must be degraded. These proteins are small enough to directly enter the gate formed by

the α subunits and are readily degraded by the sCP.[18] The sCP is sometimes linked to an 11S cap structure.[18,19] Similar to the RP, this cap can facilitate opening of the gate formed by the α rings to allow entry of small proteins into the catalytic core for degradation.

Proteins that are degraded in this fashion are either intrinsically disordered, or contain large regions that are structurally disordered.[20] Interestingly, many of these proteins are prone to aggregation which leads to cell death and implicated in several neurodegenerative disorders such as Parkinson's Disease and Huntington's Disease.[21–23] Other groups of small disordered proteins include cell cycle regulating proteins and transcription factors.[24] As such, proper function of the ubiquitin independent proteasomal degradation pathway is critical to maintaining homeostasis and cell health, as decline of this pathway could disrupt the ability of the cell to properly divide.

1.1.3 Protein Clearance During Inflammatory Conditions

During inflammatory conditions such as viral infection or injury, cells undergo several changes. One of which is production of an isoform of the proteasome known as the immunoproteasome (iCP) (**Figure 1.2**). Upon stimulation by cytokines such as interferon gamma (IFN-γ), the cell begins synthesizing three new proteasome catalytic subunits, β1i, β2i, and β5i.[25] These subunits are incorporated into newly synthesized proteasomes to produce the iCP. These new subunits exhibit slightly different cleavage specificities than their standard counterparts, resulting in better production of peptides that can be loaded into major histocompatibility complexes type I (MHC-I).[26] This is due to increased production of peptides that have hydrophobic C-termini, a necessary feature for peptides to be loaded into MHC-I complexes, by the iCP as compared to the sCP.[27] Both cellular proteins and viral proteins are degraded by the iCP to form antigenic peptides. Loaded MHC-I complexes are then displayed on the outside of the cell surface and alert the immune system of an infection or abnormal condition.[25,28] Like the sCP, the iCP is also capable of degrading misfolded and damaged proteins to prevent excess accumulation.[27]

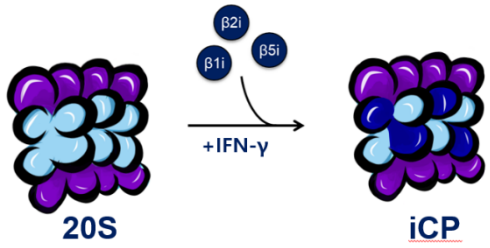

Figure 1.2 The Immunoproteasome. Upon stimulation by IFN-γ, cells begin producing new catalytic proteasomal subunits, β1i, β2i, and β5i, forming the immunoproteasome (iCP). These subunits are incorporated into new proteasomes as they are assembled. The iCP is more efficient at generating peptide fragments that are compatible with MHC-I complexes that are displayed on the outside of the cell and can alert the immune system of an infection. The iCP is endogenously expressed in some cell types, such as cells derived from bone marrow and some immune cells

Viral infection often leads to release of cytokines, including IFN-γ, near infected cells resulting in expression of the iCP.[26,29] Partially as a result of the increased pool of MHC-I-compatible peptides produced by the iCP, MHC-I expression on the cell surface increases. Since viruses must evade the immune system for successful infection, some directly target the iCP and inhibit it to prevent the generation of antigenic peptides.[30] Several viruses including human immunodeficiency virus (HIV),[31,32] Hepatitis C,[33] and Epstein-Barr virus[34] are all known to deploy proteins that interact with the iCP. These proteins work to inhibit the iCP, thereby reducing degradation of viral proteins and subsequent loading of viral antigens into MHC-I complexes for immune system detection. This is one of several ways viruses work to evade the immune system and establish successful infection.

Since the iCP plays a critical role in producing MHC-I-compatible peptides, it is also endogenously expressed in antigen-presenting cells such as dendritic cells.[27,30] Recent research has also shown iCP expression has implications in the differentiation of several tissue types[35–37] and division of T-cells.[38] This strongly suggests that there are other important functions of the iCP outside of generating MHC-I-compatible peptides, but the understanding of the iCP in these rolls is not yet fully elucidated.

1.2 The Proteasome as a Therapeutic Target

1.2.1 Proteasome Dysregulation and Cancer

Since tight regulation of protein synthesis and degradation is critical to cell viability, disruption of the proteasome can have devastating impacts on cell health. When protein synthesis is not matched by degradation, proteins accumulate leading to cell stress and the activation of several pathways that eventually result in death if left unchecked.[39,40] Dysregulation of the proteasome is implicated in several disease states, including cancer. Cancer cells generally have lost control over cell cycle regulatory processes, which results in uncontrolled cell proliferation and tumor progression.[36,37] Since the proteasome is responsible for degrading transcription factors and cell cycle regulating proteins, it has a direct role in the onset and progression of some cancers.[41] Mutations in the genome of cancer cells often leads to abhorrent protein production, resulting in faster synthesis of proteins than their healthy counterparts.[41,42] Therefore, increased protein

production must be matched by enhanced elimination. As a result, some cancer cells rely more heavily on proteasome activity for sufficient protein clearance to avoid death. [38]

In particular, the hematological cancer that results from malignant B-cells, multiple myeloma (MM), is known to rely more heavily on proteasome activity than normal cells.[43,44] B-cells are primarily responsible for producing immunoglobulins, proteins that are secreted by the cell to bind and neutralize components of a pathogen.[29] B-cells require complex regulation of proteasome activity during this differentiation process.[45] When B-cells turn malignant, as in the case with MM, they begin producing abnormally large amounts of immunoglobulins.[46] Since these cells produce large amounts of proteins in the form of immunoglobulins, they are extremely reliant on proteasome activity for survival.[47] As a result, the proteasome has emerged as an important therapeutic target for this type of cancer. Increased reliance on proteasome activity by MM cells provides a way to discriminate between cancer cells and healthy cells. Attention has been turned to methods to modulate proteasome activity to exploit this difference. Specifically, it has been hypothesized that inhibition of the proteasome's activity could lead to excess buildup of proteins in MM cells and trigger apoptosis.[44,47] Large amounts of research has led to the discovery of several small molecules that inhibit proteasome activity, which will be discussed in a later section. It has been demonstrated that disruption of proteasome activity through the use of a small molecule inhibitors triggers apoptosis of MM cells and other B-cell cancers.[45] Excitingly, a few small molecules proteasome inhibitors have been approved by the Food and Drug Administration (FDA) for the treatment of MM.[44,48] These small molecule inhibitors have greatly enhanced the quality of life and life expectancy of patients diagnosed with MM.

While the role of the standard proteasome in cancer progression is well characterized, recent evidence suggests the iCP is overexpressed in several cancers including MM,[49] prostate cancer,[50] and some forms of breast cancer.[51] The reasons why the iCP is overexpressed remains to be fully elucidated. iCP expression has been linked to resistance of cancer cells to sCP inhibitors, suggesting that it may be deployed by cancer cells to overcome sensitivity to chemotherapy agents that inhibit the proteasome.[49,52] The mechanism of inducing iCP expression differs depending on the type of cancer. In the case of solid tumors, the microenvironment is vastly different than that of healthy tissues.[51] This is partially due to the presence of tumor-infiltrating lymphocytes which release large amounts of IFN-γ.[53] Release of this cytokine triggers expression of the iCP in cancer cells within the tumor.[36,37,51] Interestingly, cancer patients with high expression of the iCP were

associated with better prognosis and improved survival rates, indicating that the iCP plays an important role in the progression of cancer and may serve as an interesting therapeutic target for these cancers.[51]

Cancers that do not form solid tumors such as MM and other hematological malignancies are known to overexpress the iCP, despite the lack of tumor-infiltrating lymphocytes no presence of IFN-γ.[54,55] This is likely partially due to the fact that cells from hematopoietic origins such as the blood cells that lead to hematological malignancies already express a basal level of the iCP.[54,55] Studies have also shown that overexpression of the iCP in some hematological cancers is not dependent on the transcription of genes that are triggered by IFN-γ stimulation.[51,56]

Since tight regulation of protein synthesis and degradation is crucial to cell survival, cancer cells must carefully regulate proteasome activity to ensure increased protein synthesis is matched by degradation. This leaves cancer cells more vulnerable to proteasome inhibition and subsequent death than normal cells. As a result, the proteasome has emerged as an important target in the development of new chemotherapy agents against several types of cancer. The iCP is also known to be overexpressed in many cancers, although the exact implications of this remain unclear. It is important to note that iCP expression in cancer cells must be tightly regulated, as the iCP will increase the pool of antigenic peptides, leaving cancer cells vulnerable to immune system detection. As a result, iCP expression varies greatly among cancers and although small molecule inhibitors have been developed with the intent to use against cancer, their use must be carefully tailored to specific types of cancer.[57] The discovery and use of proteasome inhibitors as chemotherapy agents will be discussed in a later section.

1.2.2 Proteasome Dysregulation and Aging

Aging is accompanied by several changes in cellular processes including protein degradation, which can result in accumulation of damaged proteins and eventually cell death.[58] In fact, decline in protein clearance pathways is one of the driving forces of aging.[59] Research indicates that both autophagy and the UPS decline with age and this is compounded by dysregulation of the transcriptome and proteome.[60,61] The results of protein accumulation on aged cells can be devastating. Decline of protein clearance pathways with age leads to secondary pathologies such as neurodegenerative diseases which are characterized by protein buildup and aggregation.[58] Reduction in proteasome activity is observed in several aged human tissues such as

the heart,[62] brain,[63] and fibroblasts.[64] Conversely, proteasome activity in the fibroblasts of centenarians has been shown to be significantly higher than other older humans, resembling that of younger humans.[65] Other long-lived species, such as naked mole rats, which are among the longest living rodents, have been shown to have higher proteasome activity than other mammals of similar size with significantly shorter lifespans.[66] Although naked mole rats and other similar sized rodents experience similar amounts of protein damage, the amount of ubiquitinated proteins in naked mole rat tissues was shown to be significantly lower than other aged rodents. Along similar lines, studies with transgenic mice with reduced proteasome activity revealed these rodents had faster onset and rapid progression of aging compared to control mice with normal proteasome activity.[66] This suggests that decreased proteasome activity plays an important role in the onset of aging. The clear link between the decline of the UPS and onset of aging has warranted investigation into the proteasome as a therapeutic target for aging.

Outside of rodents, other model organisms have emerged as important tools to study the relationship between proteasome activity and aging onset. Yeast, for example, share significant structural similarity to human proteasomes and are known to undergo similar mechanisms of aging.[67,68] Yeast are also relatively easy to genetically manipulate to reduce or increase expression of various proteasome subunits. Studies with yeast have revealed that knocking down transcription of proteasome subunits resulted in a significant shortening in lifespan compared to yeast with normal proteasome expression.[69] Conversely, overexpression of these genes led to lifespan extension. Enhancing autophagy has also been shown to increase the lifespan of yeast, further providing evidence that elimination of proteins is critical to the onset of aging.[70]

1.3 Small Molecule Proteasome Activity Modulators

1.3.1 Proteasome Inhibitors and Cancer

As previously described above, the proteasome has emerged as an interesting therapeutic target in several types of cancers. Since cancer cells produce more proteins than normal cells, they must maintain a careful balance between synthesis and degradation to ensure survival. As a result of this increased dependence on the proteasome, many research groups have turned their attention to developing small molecules that inhibit its activity. Increased reliance of cancer cells on proteasome activity should make them more sensitive its inhibition than noncancerous cells.[43,71]

The results of this research yielded several small molecule inhibitors of the proteasome. Some of these have been approved by the FDA for cancer treatment and therefore represent an important class of chemotherapy agents.

The first small molecule inhibitor of the proteasome discovered that was adopted in the clinic is bortezomib, which was approved by the FDA for treatment of MM in 2003 (**Figure 1.3**). Bortezomib is a dipeptide that houses a boronic acid moiety that binds the β5 subunit of the sCP.[44]

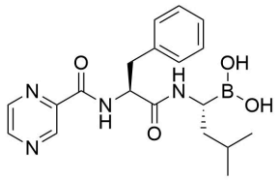

Figure 1.3 Structure of Bortezomib. Bortezomib is a dipeptide inhibitor of the proteasome. It contains a boronic acid moiety that interacts with the catalytic threonine of the β5 subunits of the sCP. Bortezomib is a reversible binder of the sCP and has been successfully used to treat MM patients who are resistant to other chemotherapies.

The boronic acid interacts with the catalytic threonine residue in the active site of the β5 subunit and prevents it from cleaving incoming protein substrates, thereby inhibiting proteasome activity.[44,72] Bortezomib binds reversibly to the β5 subunit and proteasome activity is completely restored within 48-72 hours after administration. Bortezomib is an attractive drug because it proved to be potent against some types of MM that had become resistant to other forms of treatment.[72,73] Although it is well established bortezomib triggers apoptosis in cancer cells, the mechanism behind induction of apoptosis remain unknown. It is theorized that blocking proteasome activity prohibits degradation of cell cycle regulating proteins such as p53 and prevents activation of the NF-κB pathway.[74,75] While bortezomib is remarkably effective at triggering apoptosis in cancer cells, it is important to note that it also inhibits proteasomes of normal cells. Although these cells are more tolerant of proteasome inhibition, this off target effect often leads to significant side effects such as neuropathy, nausea, vomiting, and diarrhea, which may warrant discontinued use in patients who exhibit severe side effects.[44,76] Similarly, boronic acid moieties are also known to interact with serine proteases and other cellular enzymes.[77,78] Although the concentration of bortezomib required to inhibit the proteasome is lower than that required to inhibit serine proteases.

In addition to the potential of severe side effects, cancer patients eventually acquire resistance to bortezomib, rendering the drug less effective at suppressing cancer cell proliferation.[44] The exact mechanism of resistance to bortezomib remains unclear.[79] It was originally hypothesized that mutations in the PSMB5 gene, which encodes the β5 subunit, were responsible for resistance, but research has shown that this is not the case.[79–81] Although mutations in the PSMB5 gene are sometimes observed in MM patients, they do not appear to correlate to

bortezomib resistance. As a result, more research is necessary to elucidate mechanisms of patient resistance to bortezomib.

Because resistance is not uncommon, some research groups turned their attention to making second generation proteasome inhibitors, leading to the discovery of carfilzomib (**Figure 1.4**).[48] Like bortezomib, carfilzomib also binds the β5 subunit of the sCP.[82] However, the warhead that interacts with the β5 subunit and prevents it from cleaving proteins is an epoxyketone, not a boronic acid as in bortezomib. Epoxyketones are used in several small molecule inhibitors of the proteasome.[83] The epoxyketone of carfilzomib interacts with the catalytic threonine residue of the β5 subunit.[84,85] Unlike bortezomib, carfilzomib is an irreversible binder of the proteasome.[86] Generally, it appears to be better tolerated by patients than bortezomib, but some side effects such as nausea and fatigue have been observed.[84] Additionally, patients also can confer resistance to carfilzomib.[87] Research to discover new proteasome inhibitors to aid in the treatment of cancer is ongoing.[87]

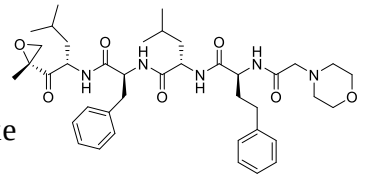

Figure 1.4 Structure of Carfilzomib. Carfilzomib is a second-generation proteasome inhibitor that is used as a chemotherapy agent for multiple forms of hematological malignancies. Unlike bortezomib, it houses an epoxyketone moiety which facilitates irreversible binding of the small molecule to the β5 subunit of the sCP.

As noted above, some cancers also rely on the iCP to clear accumulating proteins, although the exact role of the iCP in cancer remains unclear.[25] iCP expression in cancer cells provides a way to discriminate between normal cells and diseased cells and researchers have begun investigating the iCP as a therapeutic target for cancer. Several small molecule inhibitors of the iCP have been developed as part of an effort to discover new chemotherapy agents. Among them is PR-924 (**Figure 1.5**). This small molecule is an tripeptide housing an epoxyketone.[82] At concentrations lower than 100 nM, PR-924 binds the β5i subunit of the iCP with remarkable specificity, however binding to the β5 subunit of the sCP is observed at concentrations higher than 1 μM.[88] This small molecule has been demonstrated to induce apoptosis of several leukemia and MM cell lines and cells that were resistant to bortezomib.[88,89] Excitingly, mice with MM treated with PR-924 exhibited reduced tumor growth with limited side effects, indicating that targeting the iCP may result in fewer side effects than sCP inhibitors. However, it should be noted that the concentrations of PR-924 required to trigger apoptosis inhibited both the β5i and β5 subunits, indicating that inhibition of the iCP alone may not be sufficient to kill cancer cells.

Another small molecule iCP inhibitor that has shown some efficacy against cancer cells is UK-101, the first known β1i subunit binder (**Figure 1.5**).[90,91] This structure was based off a previously reported iCP inhibitor, dihydroeponemycin. Modeling and molecular dynamic simulations suggest that UK-101 binds the iCP through an interaction of the leucine side chain with a hydrophobic binding pocket within the β1i subunit.[92] This may allow the *tert*-butyldimethyl siyl (TBDMS) group to then be inserted into the active site of the β1i subunit. UK-101 has been tested for its ability to slow proliferation of prostate cancer cells and trigger apoptosis.[50,91] Excitingly, dosage of UK-101 did result in slowed proliferation of iCP-overexpressing prostate cancer cells and not normal cells. All cells tested were equally sensitive to sCP inhibitors, suggesting that the iCP could be a therapeutic target for some prostate cancers. Similar results were obtained when mice with prostate cancer were dosed with UK-101 over several days.[50] Much work is still needed to fully evaluate the potential of the iCP as a therapeutic target for cancer, although initial results are encouraging. New iCP inhibitors are currently being developed in addition to evaluating the use of both an sCP and iCP inhibitor to treat some types of cancer.[93–95]

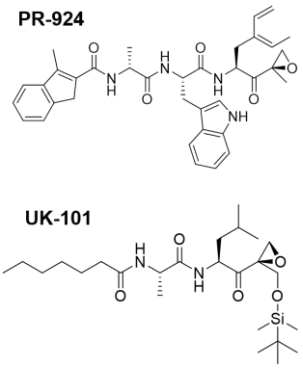

Figure 1.5 Structures of iCP Inhibitors. PR-924 is a potent inhibitor of the β5i subunit o the iCP. UK-101 was the first discovered covalent inhibitor of the β1i subunit of the iCP

1.3.2 Proteasome Stimulators and Neurodegenerative Diseases

Neurodegenerative diseases are often characterized by the buildup of unwanted proteins in the cells of tissues such as the brain.[39,96] In addition to protein accumulation, proteasome activity often declines which eventually leads to cell death.[96,97] Proteasome activity is known to be reduced in diseases such as Parkinson's Disease (PD)[98] and Huntington's Disease (HD).[99] It has been hypothesized that stimulating the proteasome could delay protein accumulation and allow cells to clear proteins that are prone to aggregation. To this end, several small molecule stimulators of the proteasome have been discovered through the efforts of our lab and others. Proteasome stimulators generally fall into two broad categories: (i) detergents, which appear to slightly denature the proteasome and facilitate better substrate entry into the sCP and (ii) stimulators that target a specific subunit of the proteasome and increase its activity.[100]

Among some of the first identify proteasome stimulators is betulinic acid (BA) (**Figure 1.6**).[101] BA is a natural product initially discovered in birch trees and has proven to have anti-HIV and anti-cancer properties which are not related to modulating proteasome activity.[102] BA has been shown to enhance the chymotrypsin-like cleavage activity of the proteasome, indicating that it could be specifically targeting the β5 subunit of the sCP.[101] This was discovered through the use of short peptide fluorogenic substrates that produce a fluorescent signal upon cleavage by the proteasome. In an effort to make more potent stimulators, the group that identified BA synthesized several analogs.[101] Interestingly, none of the analogs further increased proteasome activity and many actually inhibited proteasome activity. The ability of BA to stimulate the proteasome in more biologically relevant situations has subsequently been analyzed.[103] When cleavage of a longer, more complex peptide substrate by the sCP in response to dosage with BA was analyzed by liquid chromatography mass spectrometry (LC/MS), it was discovered that BA did not facilitate increased cleavage of the substrate, indicating that stimulation of the proteasome by BA may only be an artifact of smaller probes.[103] Similarly, BA did not enhance degradation of α-synuclein *in vitro* or *in cellulo* by the proteasome, suggesting further research is required to evaluate BA as a stimulator.

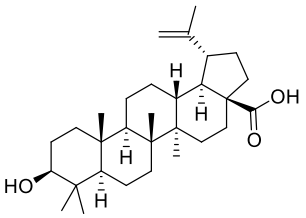

Figure 1.7 Structure of Betulinic Acid. Betulinic acid was one of the first reported proteasome stimulators. Although it has been shown to increase the activity of the β5 subunit, conflicting data suggests it may not stimulate the proteasome in biologically relevant settings

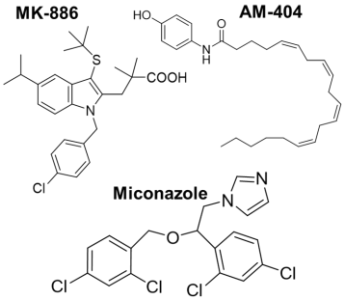

Figure 1.6. MK-886, AM-404, and miconazole have all recently been identified as proteasome stimulators. The mechanism of action for all of these are not fully understood, but it is likely that MK-886 and AM-404 are allosteric stimulators while MO is a gate opener.

Several other stimulators have been discover by our group such as MK-886,[103] AM-404,[103] and miconazole (MO) (**Figure 1.7**).[104] MK-886 and AM-404 were discovered as part of a screen with the National Institutes of Health (NIH) Clinical Collection small molecule library. Not only did these small molecules stimulate purified proteasomes, but also enhanced degradation of α-synuclein *in vitro* and *in cellulo*.[103] The mechanism of stimulation of both MK-886 and AM-404 has not been fully elucidated, but studies suggest they do not act as gate openers, indicating they may allosterically interact with the proteasome to enhance one of its three forms of hydrolysis. MO has also been shown to enhance degradation of α-synuclein *in vitro* and *in cellulo*.[104]

Although great progress had been made in the discovery of small molecule proteasome stimulators, much work remains to be done to determine the therapeutic impact of these small molecules *in vivo* and more complex biological systems. Recently, researchers have also discovered expression of the immunoproteasome in a variety of neurodegenerative diseases such as Huntington's Disease,[105] Alzheimer's Disease,[106] and amyotrophic lateral sclerosis[107]. However, induction of iCP expression and impacts of this on onset and progression of these diseases remains unknown. Therefore, significant knowledge gaps surrounding the iCP as a therapeutic target for neurodegenerative diseases exist and require careful study.

1.4 Methods to Identify Small Molecule Binders of the Proteasome

1.4.1 Activity-Based Screening

Methods to discover small molecule modulators of proteasome activity have, until recently, primarily involved utilizing activity-based assays in which cleavage of a reporter probe by the proteasome is monitored over time in response to dosing with a small molecule. Generally, cleavage of such probes releases a fluorophore that produces a fluorescent signal that can be quantified. The rate of cleavage of the probe is then calculated to determine how a small molecule impacts proteasome activity.[108] Several reporter probes are commercially available, with the succinyl (Suc)-LLVY-AMC probe being the most common (**Figure 1.8**).[109] This probe was initially designed to monitor the activity of calpain I and II, two cysteine proteases. However, this probe more broadly monitors chymotrypsin-like protease activity and since has been used to monitor sCP activity of the proteasome. The 7-amino-4-methylcoumarin (AMC) fluorophore was originally incorporated into such probes because of its high quantum yield, which produces an intense

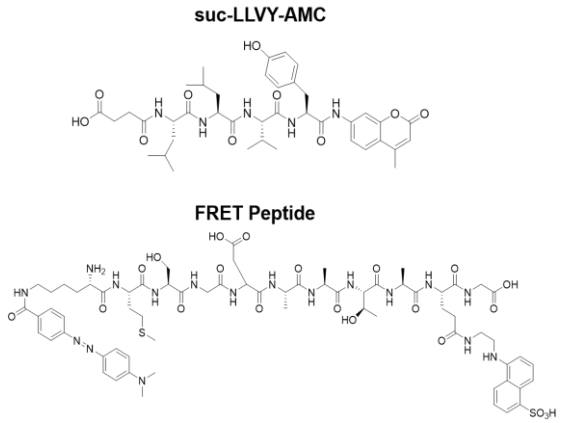

Figure 1.8 Structures of Proteasome Reporter Probes. Suc-LLVY-AMC is a peptide probe is commercially available and used to monitor chymotrypsin-like cleavage by proteases, including the proteasome. Its small size makes detecting proteasome stimulation difficult. The FRET peptide was designed by our lab and offers a longer peptide sequence that separates Edans and Dabcyl, two fluorophores that form a FRET pair. Its larger size allows for more sensitive detection of proteasome stimulation than the suc-LLVY-AMC probe.

fluorescent signal.[108] When the proteasome encounters this probe, it cleaves after the tyrosine residue, which releases the AMC and produces a fluorescent signal.[108] Although this probe is used extensively in the literature, it is not very sensitive to proteasome stimulation. This is partially because of its small size. The four amino acid substrate readily enters the proteasome and is quickly degraded.[110]

In an effort to make probes that are more sensitive to stimulation, our lab has developed several new substrates that are longer than the traditional Suc-LLVY-AMC probe. Among these is a substrate that relies on fluorescence resonance energy transfer (FRET) (**Figure 1.8**).[110] This probe houses two fluorophores, Edans and Dabcyl, separated by eight amino acid residues. When the two fluorophores are in close proximity, the fluorescent signal is quenched. Upon cleavage of the probe by the proteasome, the distance between the fluorophores is increased and produces a measurable fluorescent signal. This probe is also much larger than Suc-LLVY-AMC. As a result, the substrate cannot pass as quickly into the proteasome as Suc-LLVY-AMC and is cleaved more slowly. This lower rate of cleavage allows for more sensitive detection of proteasome stimulation. This probe was utilized to discover MO as a proteasome stimulator.[104]

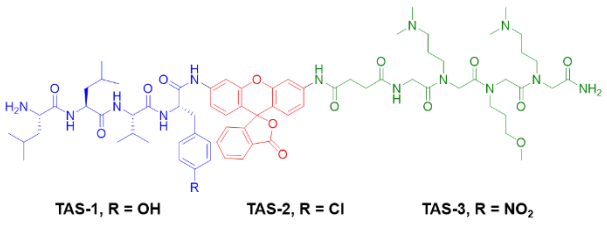

Figure 1.9 Structure of the TAS Probes. The TAS probes consist of a peptide region (blue) that is recognized and cleaved by the proteasome, a rhodamine fluorophore (red), and peptoid region (green) that promotes solubility and cell permeability. Cleavage of the peptide region by the proteasome releases the rhodamine to produce a quantifiable fluorescent signal. This set of probes is also cell permeable which facilitates detecting proteasome stimulation in a variety of cell models.

Along similar lines, newer fluorescent probes have been designed by our lab to not only monitor proteasome stimulation *in vitro* but also in cells. A set of three peptide/peptoid probes, TAS-1, -2, and -3 have been developed to monitor proteasome stimulation (**Figure 1.9**).[111] These probes house a rhodamine fluorophore between a peptide sequence recognized by the proteasome and a peptoid sequence that facilitates cell permeability. Creation of these probes has opened new avenues to monitoring proteasome activity in cells. A similar probe has also been designed to monitor activity of the iCP.[112]

In addition to monitoring the activity of the proteasome biochemically, several fluorescent probes that interact covalently with one of the catalytic subunits of the proteasome have been developed.[83,113,114] Proteasome can be incubated with a small molecule of interest then incubated

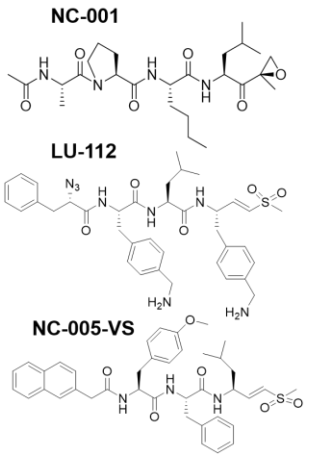

Figure 1.10 Structure of Covalent Catalytic Subunit Binders. NC-001 binds the β1/β1i subunits of the sCP. It covalently binds with these subunits via the epoxyketone moeity. LU-112 and NC-005-VS both contain a vinyl sulfone moeity that facilitaes covalent binding to the β2/β2i and β5/β5i sCP subunits, respectively. These probes can be conjugated to fluorphores and incubated with the proteasome in the presence of a stimulator. Samples are then subjected to SDS-PAGE and changes in fluroescence intensities produced by the labeled probes binding sCP subuntis in response to a small moleucle can reveal which subunit the molecule binds.

with a cocktail of covalent probes. When samples are analyzed by sodium dodecyl sulfate gel electrophoresis (SDS-PAGE), fluorescent intensities corresponding to the probe binding the specific subunit can analyzed. Changes in fluorescence intensities in response to addition of the small molecule can be monitored to determine which subunit the small molecule binds.[113,115] Of the most common probes are NC-001 (β1/β1i specific),[113] LU-112 (β2/β2i specific),[116] and NC-005-VS (β5/β5i specific) (**Figure 1.10**).[117] NC-001 facilitates covalent linkage to the β1/β1i subunit through an epoxyketone moiety. This probe is also cell permeable and shows remarkable specificity, with no inhibition of other proteasome subunits in response to dosing cells with up to 4 μM of NC-001.[118] LU-112 was discovered by a series of structure-activity studies to evaluate the binding pockets of the β2 subunit.[116] Finally, NC-005 was initially discovered with an epoxyketone moiety and was based off of the structure of another known β5 inhibitor, aldehyde1-naptylacetyl(Nac)- 4-methyl-tyrosine(mTyr)-phenylalanine-4-methyl-tyrosinal.[118,119] This probe is known to be cell permeable. Further studies to elucidate the impact of the warhead on the probe's specificity revealed that exchanging the epoxyketone for another warhead known to promote covalent binding to the β5 subunit, a vinyl sulfone,[120] was shown to further increase its specificity to β5 and β5i over other subunits.[121]

Although these probes can be used to monitor the composition of proteasomes in a sample and the ability of a small molecule to bind a particle subunit, careful characterization of the probes' specificity after attaching a fluorophore must be studied. Some groups have reported that adding a fluorophore can alter the specificity of the probe to a particular subunit.[117] Similarly, these probes are used to monitor activity of the catalytic subunits. Targeting the noncatalytic subunits also has potential as a therapeutic intervention in several diseases. Methods to screen for noncatalytic subunit binders are discussed next.

1.4.2 Screening Techniques for Binders to the Noncatalytic Proteasome Subunits

Until recently, research has primarily focused on identifying small molecules that interact with the catalytic subunits of the proteasome. However, this only represents a small fraction of proteasome subunits. It has been demonstrated that the subunits of the RP play critical roles in the rate and types of substrates that are degraded by the proteasome.[6] In fact, many noncatalytic subunits have altered expression in cancer, making them an interesting target in the pursuit of new chemotherapy agents.[10] Screening of proteins with no enzymatic activity such as the noncatalytic proteasome subunits can be difficult, since there is no measurable output that can be monitored in response to a small molecule. In recent years, techniques to screen one-bead-one-compound (OBOC) libraries have emerged as important strategies to screen noncatalytic proteins. OBOCs have revolutionized the speed at which thousands of small molecules can be synthesized.[122] Significant progress remains in creating more efficient methods to screen OBOC libraries, but a few have been developed that have led to the discovery of new small molecule binders to noncatalytic proteasome subunits.

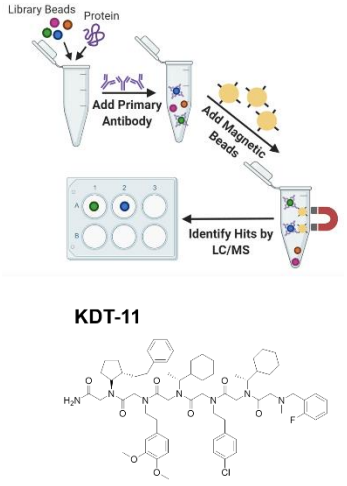

Figure 1.11 Screening Scheme for Magnetic Bead OBOC Lbirary Screening. Beads of the OBOC are incubated with a target protein. A primary antibody against the protein is then added followed by magentic beads conjugate to a secondary antibody. Beads that bound the protein, primary and secondary antibody can then be separeted with a strong magent and the small molecule can be identified by mass spectrometry. KDT-11 was identified as binder to Rpn-13 using this screening method.

Several OBOC screening methods have been developed, including utilizing magnetic beads.[123] Briefly, this method involves incubating OBOC beads with a target protein (**Figure 1.11**). A primary antibody is added to the sample, followed by magnetic beads conjugated to a secondary antibody. Hit beads that successfully bound the target protein, primary antibody, and secondary antibody can be physical separated from nonhits with a strong magnet.[123,124] The identity of the small molecule on-bead is determined by mass spectrometry analysis or DNA sequencing if the library was DNA encoded prior to the screen.[123–125] This method was recently employed to screen a 100,000 peptoid OBOC library against Rpn-13, a noncatalytic proteasome subunit.[126] Six hits were yielded from this screen and derivatives were synthesized and subsequently analyzed with a fluorescence polarization assay in which fluorescently labeled ligands interacted with varying amounts of Rpn-13. This resulted in the discovery of KDT-11 (**Figure 1.11**). Not only does KDT-11 bind Rpn-13 with modest

affinity, it was also shown to kill MM cells at a lower IC_{50} than noncancerous cells.[126] As previously discussed, MM cells rely more heavily on proteasome activity than healthy cells and KDT-11 highlights important implications of the roles of noncatalytic proteasome subunit function in cancer cells.

Thermal shift assays are also beginning to emerge as interesting tools to screen OBOC libraries. This method utilizes fluorescent dyes that bind hydrophobic regions of proteins.[127,128] A target protein is incubated with the dye and a small molecule then the temperature is gradually raised over time (**Figure 1.12**). This causes the protein to denature, exposing hydrophobic regions that are generally internalized to the surrounding environment. The dye binds these regions and produces a fluorescent signal. The temperature at which the fluorescent signal is maximal is the melting temperature of the protein and signifies the protein has completely unfolded. If a small molecule binds the target protein and stabilizes it, the melting temperature shifts. These shifts provide a basis to determine if a small molecule of interest bound a target protein when compared to control samples. This technology was recently used to screen an OBOC library against Rpn-6, a subunit of the RP. TXS-8 was discovered from this screen, a peptoid composed of four amines (**Figure 1.12**). Excitingly, TXS-8 was more toxic towards Burkitt's lymphoma cells than noncancerous cells.[129]

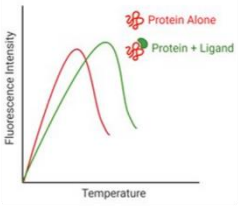

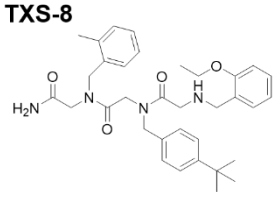

Figure 1.12 Thermal Shift Assay and TXS-8. Thermal shift assays rely a fluroscent dye that binds hydrophobic regions of a protein. When a protein is incubated with the dye and gradually heated, it unfolds to expose the hydropbhic regions that the dye recongizes and binds, which produces a fluroescent signal. Changes in flourescence can be used to determine when the protein has completely unfolded. When a protein is incubated with a small molecule that stabilizes it, the melting temperature increases and this can be detemrined by monitoring the flureoscent signal. TXS-8 was discovered as a binder to Rpn-6 with this method.

Screening methods to identify new proteasome binders have yielded several interesting compounds that either modulate the activity of the catalytic subunits or bind noncatalytic subunits. More attention is now being turned to screening the noncatalytic subunits to further elucidate the impacts of their expression in cancer and other diseases.[129,129–132] While current OBOC screening techniques have facilitated the discovery of these ligands, these methods have several drawbacks. Primarily, binding between the target protein and small molecule must be strong to identify hits[133] and these methods do not allow for hits to be prioritized from the initial screen. This is compounded with the fact that false positives are very common among these techniques, which leads to significant work to validate hits.[133] As a result, new screening

techniques are needed to overcome these limitations and make the discovery of noncatalytic proteasome subunit binders more streamlined. Newer screening methods are currently under development and will be discussed in following chapters.[134,135]

1.5 Conclusions

Since the proteasome plays a critical role in maintaining proteostasis, its function must be tightly regulated by cells.[26] Therefore, it is unsurprising that dysfunction of its activity is implicated in several pathologies associated with aging,[61] neurodegenerative diseases,[100,101,108] and cancer progression.[41,42,77,126] As a result, it has emerged as an important therapeutic target for a variety of diseases. Since many types of cancer cells rely more heavily on proteasome activity than normal cells, they are more sensitive to its inhibition.[41,42] Conversely, aging and neurodegenerative diseases are often characterized by slowing of proteasome activity and a significant body of research has shown that stimulating the proteasome can delay and reverse some of these pathologies.[39,60,96,136] Similarly, the role of the iCP in cancer[56] and neurodegeneration[107,108] are beginning to be studied. As new probes and small molecule binders are developed for the proteasome, its role in these diseases will be even better characterized. Moreover, a deeper understanding of this will facilitate better treatment strategies for diseases that are devastating and pose a significant public health and economic burden.

To this end, significant attention has been turned to developing sets of fluorescent probes that can be used to monitor the activity of the proteasome and the iCP.[83,117,121] These probes have assisted in the discovery of proteasome binders such as bortezomib, which is now FDA approved to treat certain hematological cancers.[44] Newer fluorescent proteasome substrates have also been developed to identify stimulators which could eventually be used to treat aging pathologies and neurodegenerative diseases.[110–112] Although these probes can be used to detect proteasome stimulation, more standardized techniques to evaluate the biological relevance of this in disease still remain as a significant gap between initial discovery and use in the clinic. Methods to monitor degradation of proteins prone to aggregation fused to green fluorescent protein (GFP) have been developed, but can lead to inconsistent results.[103,110,114,137] As a result a suite of new techniques to evaluate small molecule stimulators for biological relevance is required for a full understanding of their therapeutic potential.

Similarly, although the development of OBOC libraries has revolutionized the number and variety of small molecules that can be synthesized, progress lags in the ability to efficiently screen these libraries.[122] This is especially relevant for screening against noncatalytic subunits of the proteasome, which have no known enzymatic function. Tools such as thermal shift and magnetic beads have facilitated the discovery of ligands to RP subunits such as KDT-11[126] and TXS-8[129], but these methods have several drawbacks. Most significantly, hits from the initial screen cannot be prioritized with these methods, making validation cumbersome. Methods in which binding between a target protein and small molecule can be quantified are currently under development, but significant work remains to make these techniques widespread and commercially available.[123,134] Development of more stringent, easier OBOC library screening techniques against proteins with no known function will vastly expedite the process of discovering small molecule binders of the noncatalytic subunits of the proteasome. Research has recently implicated these subunits as having important roles in cancer progression, identifying them as a new target for therapeutic intervention.[126,129] Discovery of new small molecules that can be developed into probes to monitor expression of the noncatalytic subunits of the proteasome will result in a deeper understanding of their role in disease.

Here, we describe several new methods to discover small molecule binders of the proteasome and evaluate their impacts in biologically relevant systems. We first developed a method to screen OBOC libraries against proteins of interest in which hits can be prioritized. We used this method to identify a covalent peptoid ligand to gankyrin, an oncoprotein that has no known catalytic function.[134] Next, we describe an assay to monitor lifespan extension of yeast in response to small molecules that modulate proteasome activity. Finally, we describe stimulators of the iCP and evaluate their impact in cell models.

1.6 References

(1) Lilienbaum, A. Relationship between the Proteasomal System and Autophagy. *Int. J. Biochem. Mol. Biol.* **2013**, *4* (1), 1–26.

(2) Bedford, L.; Paine, S.; Sheppard, P. W.; Mayer, R. J.; Roelofs, J. Assembly, Structure, and Function of the 26S Proteasome. *Trends Cell Biol.* **2010**, *20* (7), 391–401. https://doi.org/10.1016/j.tcb.2010.03.007.

(3) Coux, O.; Tanaka, K.; Goldberg, A. L. Structure and Functions of the 20S and 26S Proteasomes. *Annu. Rev. Biochem.* **1996**, *65*, 801–847. https://doi.org/10.1146/annurev.bi.65.070196.004101.

(4) Kloetzel, P.-M. Ubiquitin and Proteasomes: Antigen Processing by the Proteasome. *Nat. Rev. Mol. Cell Biol.* **2001**, *2* (3), 179–188. https://doi.org/10.1038/35056572.

(5) Huang, X.; Luan, B.; Wu, J.; Shi, Y. An Atomic Structure of the Human 26S Proteasome. *Nat. Struct. Mol. Biol.* **2016**, *23* (9), 778–785. https://doi.org/10.1038/nsmb.3273.

(6) Muli, C. S.; Tian, W.; Trader, D. J. Small-Molecule Inhibitors of the Proteasome's Regulatory Particle. *ChemBioChem* **2019**, *20* (14), 1739–1753. https://doi.org/10.1002/cbic.201900017.

(7) Rabl, J.; Smith, D. M.; Yu, Y.; Chang, S.-C.; Goldberg, A. L.; Cheng, Y. Mechanism of Gate Opening in the 20S Proteasome by the Proteasomal ATPases. *Mol. Cell* **2008**, *30* (3), 360–368. https://doi.org/10.1016/j.molcel.2008.03.004.

(8) Finley, D.; Chen, X.; Walters, K. J. Gates, Channels, and Switches: Elements of the Proteasome Machine. *Trends Biochem. Sci.* **2016**, *41* (1), 77–93. https://doi.org/10.1016/j.tibs.2015.10.009.

(9) Jung, T.; Grune, T. The Proteasome and the Degradation of Oxidized Proteins: Part I—Structure of Proteasomes. *Redox Biol.* **2013**, *1* (1), 178–182. https://doi.org/10.1016/j.redox.2013.01.004.

(10) Thibaudeau, T. A.; Smith, D. M. A Practical Review of Proteasome Pharmacology. *Pharmacol. Rev.* **2019**, *71* (2), 170–197. https://doi.org/10.1124/pr.117.015370.

(11) Liu, W.; Tang, X.; Qi, X.; Fu, X.; Ghimire, S.; Ma, R.; Li, S.; Zhang, N.; Si, H. The Ubiquitin Conjugating Enzyme: An Important Ubiquitin Transfer Platform in Ubiquitin-Proteasome System. *Int. J. Mol. Sci.* **2020**, *21* (8). https://doi.org/10.3390/ijms21082894.

(12) Mehrtash, A. B.; Hochstrasser, M. Ubiquitin-Dependent Protein Degradation at the Endoplasmic Reticulum and Nuclear Envelope. *Semin. Cell Dev. Biol.* **2019**, *93*, 111–124. https://doi.org/10.1016/j.semcdb.2018.09.013.

(13) Thrower, J. S.; Hoffman, L.; Rechsteiner, M.; Pickart, C. M. Recognition of the Polyubiquitin Proteolytic Signal. *EMBO J.* **2000**, *19* (1), 94–102. https://doi.org/10.1093/emboj/19.1.94.

(14) Deveraux, Q.; Ustrell, V.; Pickart, C.; Rechsteiner, M. A 26 S Protease Subunit That Binds Ubiquitin Conjugates. *J. Biol. Chem.* **1994**, *269* (10), 7059–7061.

(15) Jørgensen, J. P.; Lauridsen, A.-M.; Kristensen, P.; Dissing, K.; Johnsen, A. H.; Hendil, K. B.; Hartmann-Petersen, R. Adrm1, a Putative Cell Adhesion Regulating Protein, Is a Novel Proteasome-Associated Factor. *J. Mol. Biol.* **2006**, *360* (5), 1043–1052. https://doi.org/10.1016/j.jmb.2006.06.011.

(16) Prakash, S.; Tian, L.; Ratliff, K. S.; Lehotzky, R. E.; Matouschek, A. An Unstructured Initiation Site Is Required for Efficient Proteasome-Mediated Degradation. *Nat. Struct. Mol. Biol.* **2004**, *11* (9), 830–837. https://doi.org/10.1038/nsmb814.

(17) Choi, J. H.; Lee, W. K.; Han, S. H.; Ha, S.; Ahn, S. M.; Kang, J. S.; Choi, Y. J.; Yun, C.-H. Identification and Characterization of Nonapeptide Targeting a Human B Cell Lymphoma, Raji. *Int. Immunopharmacol.* **2008**, *8* (6), 852–858. https://doi.org/10.1016/j.intimp.2008.01.037.

(18) Jariel-Encontre, I.; Bossis, G.; Piechaczyk, M. Ubiquitin-Independent Degradation of Proteins by the Proteasome. *Biochim. Biophys. Acta BBA - Rev. Cancer* **2008**, *1786* (2), 153–177. https://doi.org/10.1016/j.bbcan.2008.05.004.

(19) Whitby, F. G.; Masters, E. I.; Kramer, L.; Knowlton, J. R.; Yao, Y.; Wang, C. C.; Hill, C. P. Structural Basis for the Activation of 20S Proteasomes by 11S Regulators. *Nature* **2000**, *408* (6808), 115–120. https://doi.org/10.1038/35040607.

(20) Erales, J.; Coffino, P. Ubiquitin-Independent Proteasomal Degradation. *Biochim. Biophys. Acta* **2014**, *1843* (1), 216–221. https://doi.org/10.1016/j.bbamcr.2013.05.008.

(21) Zhang, P.; Park, H.-J.; Zhang, J.; Junn, E.; Andrews, R. J.; Velagapudi, S. P.; Abegg, D.; Vishnu, K.; Costales, M. G.; Childs-Disney, J. L.; Adibekian, A.; Moss, W. N.; Mouradian, M. M.; Disney, M. D. Translation of the Intrinsically Disordered Protein α-Synuclein Is Inhibited by a Small Molecule Targeting Its Structured MRNA. *Proc. Natl. Acad. Sci.* **2020**, *117* (3), 1457–1467. https://doi.org/10.1073/pnas.1905057117.

(22) Witt, S. N.; Flower, T. R. Alpha-Synuclein, Oxidative Stress and Apoptosis from the Perspective of a Yeast Model of Parkinson's Disease. *FEMS Yeast Res.* **2006**, *6* (8), 1107–1116. https://doi.org/10.1111/j.1567-1364.2006.00135.x.

(23) Uversky, V. N. Targeting Intrinsically Disordered Proteins in Neurodegenerative and Protein Dysfunction Diseases: Another Illustration of the D2 Concept. *Expert Rev. Proteomics* **2010**, *7* (4), 543–564. https://doi.org/10.1586/epr.10.36.

(24) Ben-Nissan, G.; Sharon, M. Regulating the 20S Proteasome Ubiquitin-Independent Degradation Pathway. *Biomolecules* **2014**, *4* (3), 862–884. https://doi.org/10.3390/biom4030862.

(25) Zerfas, B. L.; Maresh, M. E.; Trader, D. J. The Immunoproteasome: An Emerging Target in Cancer and Autoimmune and Neurological Disorders. *J. Med. Chem.* **2020**, *63* (5), 1841–1858. https://doi.org/10.1021/acs.jmedchem.9b01226.

(26) Kloetzel, P. M. Antigen Processing by the Proteasome. *Nat. Rev. Mol. Cell Biol.* **2001**, *2* (3), 179–187. https://doi.org/10.1038/35056572.

(27) Kimura, H.; Caturegli, P.; Takahashi, M.; Suzuki, K. New Insights into the Function of the Immunoproteasome in Immune and Nonimmune Cells https://www.hindawi.com/journals/jir/2015/541984/ (accessed Jun 17, 2019). https://doi.org/10.1155/2015/541984.

(28) Basler, M.; Kirk, C. J.; Groettrup, M. The Immunoproteasome in Antigen Processing and Other Immunological Functions. *Curr. Opin. Immunol.* **2013**, *25* (1), 74–80. https://doi.org/10.1016/j.coi.2012.11.004.

(29) Acheson, N. *Fundementals of Molecular Virology*, 2nd ed.; 2011.

(30) Hewitt, E. W. The MHC Class I Antigen Presentation Pathway: Strategies for Viral Immune Evasion. *Immunology* **2003**, *110* (2), 163–169. https://doi.org/10.1046/j.1365-2567.2003.01738.x.

(31) Huang, X.; Seifert, U.; Salzmann, U.; Henklein, P.; Preissner, R.; Henke, W.; Sijts, A. J.; Kloetzel, P.-M.; Dubiel, W. The RTP Site Shared by the HIV-1 Tat Protein and the 11S Regulator Subunit α Is Crucial for Their Effects on Proteasome Function Including Antigen Processing. *J. Mol. Biol.* **2002**, *323* (4), 771–782. https://doi.org/10.1016/S0022-2836(02)00998-1.

(32) Apcher, G. S.; Heink, S.; Zantopf, D.; Kloetzel, P.-M.; Schmid, H.-P.; Mayer, R. J.; Krüger, E. Human Immunodeficiency Virus-1 Tat Protein Interacts with Distinct Proteasomal α and β Subunits. *FEBS Lett.* **2003**, *553* (1), 200–204. https://doi.org/10.1016/S0014-5793(03)01025-1.

(33) Khu, Y.-L.; Tan, Y.-J.; Lim, S. G.; Hong, W.; Goh, P.-Y. Hepatitis C Virus Non-Structural Protein NS3 Interacts with LMP7, a Component of the Immunoproteasome, and Affects Its Proteasome Activity. *Biochem. J.* **2004**, *384* (Pt 2), 401–409. https://doi.org/10.1042/BJ20040858.

(34) Dantuma, N. P.; Heessen, S.; Lindsten, K.; Jellne, M.; Masucci, M. G. Inhibition of Proteasomal Degradation by the Gly-Ala Repeat of Epstein–Barr Virus Is Influenced by the Length of the Repeat and the Strength of the Degradation Signal. *Proc. Natl. Acad. Sci. U. S. A.* **2000**, *97* (15), 8381–8385.

(35) Cui, Z.; Hwang, S. M.; Gomes, A. V. Identification of the Immunoproteasome as a Novel Regulator of Skeletal Muscle Differentiation. *Mol. Cell. Biol.* **2014**, *34* (1), 96–109. https://doi.org/10.1128/MCB.00622-13.

(36) Zu, L.; Bedja, D.; Fox-Talbot, K.; Gabrielson, K. L.; Van Kaer, L.; Becker, L. C.; Cai, Z. P. Evidence for a Role of Immunoproteasomes in Regulating Cardiac Muscle Mass in Diabetic Mice. *J. Mol. Cell. Cardiol.* **2010**, *49* (1), 5–15. https://doi.org/10.1016/j.yjmcc.2010.02.007.

(37) de Verteuil, D. A.; Rouette, A.; Hardy, M.-P.; Lavallée, S.; Trofimov, A.; Gaucher, É.; Perreault, C. Immunoproteasomes Shape the Transcriptome and Regulate the Function of Dendritic Cells. *J. Immunol. Baltim. Md 1950* **2014**, *193* (3), 1121–1132. https://doi.org/10.4049/jimmunol.1400871.

(38) Caudill, C. M.; Jayarapu, K.; Elenich, L.; Monaco, J. J.; Colbert, R. A.; Griffin, T. A. T Cells Lacking Immunoproteasome Subunits MECL-1 and LMP7 Hyperproliferate in Response to Polyclonal Mitogens. *J. Immunol.* **2006**, *176* (7), 4075–4082. https://doi.org/10.4049/jimmunol.176.7.4075.

(39) Zheng, Q.; Huang, T.; Zhang, L.; Zhou, Y.; Luo, H.; Xu, H.; Wang, X. Dysregulation of Ubiquitin-Proteasome System in Neurodegenerative Diseases. *Front. Aging Neurosci.* **2016**, *8*. https://doi.org/10.3389/fnagi.2016.00303.

(40) Coleman, R. A.; Trader, D. J. All About the Core: A Therapeutic Strategy to Prevent Protein Accumulation with Proteasome Core Particle Stimulators. *ACS Pharmacol. Transl. Sci.* **2018**, *1* (2), 140–142. https://doi.org/10.1021/acsptsci.8b00042.

(41) Almond, J. B.; Cohen, G. M. The Proteasome: A Novel Target for Cancer Chemotherapy. *Leukemia* **2002**, *16* (4), 433–443. https://doi.org/10.1038/sj.leu.2402417.

(42) Chen, Y.; Zhang, Y.; Guo, X. Proteasome Dysregulation in Human Cancer: Implications for Clinical Therapies. *Cancer Metastasis Rev.* **2017**, *36* (4), 703–716. https://doi.org/10.1007/s10555-017-9704-y.

(43) Chauhan, D.; Catley, L.; Li, G.; Podar, K.; Hideshima, T.; Velankar, M.; Mitsiades, C.; Mitsiades, N.; Yasui, H.; Letai, A.; Ovaa, H.; Berkers, C.; Nicholson, B.; Chao, T.-H.; Neuteboom, S. T. C.; Richardson, P.; Palladino, M. A.; Anderson, K. C. A Novel Orally Active Proteasome Inhibitor Induces Apoptosis in Multiple Myeloma Cells with Mechanisms Distinct from Bortezomib. *Cancer Cell* **2005**, *8* (5), 407–419. https://doi.org/10.1016/j.ccr.2005.10.013.

(44) Chen, D.; Frezza, M.; Schmitt, S.; Kanwar, J.; Dou, Q. P. Bortezomib as the First Proteasome Inhibitor Anticancer Drug: Current Status and Future Perspectives. *Curr. Cancer Drug Targets* **2011**, *11* (3), 239–253.

(45) Cenci, S.; Mezghrani, A.; Cascio, P.; Bianchi, G.; Cerruti, F.; Fra, A.; Lelouard, H.; Masciarelli, S.; Mattioli, L.; Oliva, L.; Orsi, A.; Pasqualetto, E.; Pierre, P.; Ruffato, E.; Tagliavacca, L.; Sitia, R. Progressively Impaired Proteasomal Capacity during Terminal Plasma Cell Differentiation. *EMBO J.* **2006**, *25* (5), 1104–1113. https://doi.org/10.1038/sj.emboj.7601009.

(46) Rajkumar, S. V.; Kumar, S. Multiple Myeloma: Diagnosis and Treatment. *Mayo Clin. Proc.* **2016**, *91* (1), 101–119. https://doi.org/10.1016/j.mayocp.2015.11.007.

(47) Gandolfi, S.; Laubach, J. P.; Hideshima, T.; Chauhan, D.; Anderson, K. C.; Richardson, P. G. The Proteasome and Proteasome Inhibitors in Multiple Myeloma. *Cancer Metastasis Rev.* **2017**, *36* (4), 561–584. https://doi.org/10.1007/s10555-017-9707-8.

(48) Reece, D. E. Carfilzomib in Multiple Myeloma: Gold, Silver, or Bronze? *Blood* **2012**, *120* (14), 2776–2777. https://doi.org/10.1182/blood-2012-08-446534.

(49) Kuhn, D. J.; Hunsucker, S. A.; Chen, Q.; Voorhees, P. M.; Orlowski, M.; Orlowski, R. Z. Targeted Inhibition of the Immunoproteasome Is a Potent Strategy against Models of Multiple Myeloma That Overcomes Resistance to Conventional Drugs and Nonspecific Proteasome Inhibitors. *Blood* **2009**, *113* (19), 4667–4676. https://doi.org/10.1182/blood-2008-07-171637.

(50) Wehenkel, M.; Ban, J.-O.; Ho, Y.-K.; Carmony, K. C.; Hong, J. T.; Kim, K. B. A Selective Inhibitor of the Immunoproteasome Subunit LMP2 Induces Apoptosis in PC-3 Cells and Suppresses Tumour Growth in Nude Mice. *Br. J. Cancer* **2012**, *107* (1), 53–62. https://doi.org/10.1038/bjc.2012.243.

(51) Rouette, A.; Trofimov, A.; Haberl, D.; Boucher, G.; Lavallée, V.-P.; D'Angelo, G.; Hébert, J.; Sauvageau, G.; Lemieux, S.; Perreault, C. Expression of Immunoproteasome Genes Is Regulated by Cell-Intrinsic and -Extrinsic Factors in Human Cancers. *Sci. Rep.* **2016**, *6*, 34019. https://doi.org/10.1038/srep34019.

(52) Groettrup, M.; Kirk, C. J.; Basler, M. Proteasomes in Immune Cells: More than Peptide Producers? *Nat. Rev. Immunol.* **2010**, *10* (1), 73–78. https://doi.org/10.1038/nri2687.

(53) Mlecnik, B.; Bindea, G.; Kirilovsky, A.; Angell, H. K.; Obenauf, A. C.; Tosolini, M.; Church, S. E.; Maby, P.; Vasaturo, A.; Angelova, M.; Fredriksen, T.; Mauger, S.; Waldner, M.; Berger, A.; Speicher, M. R.; Pagès, F.; Valge-Archer, V.; Galon, J. The Tumor Microenvironment and Immunoscore Are Critical Determinants of Dissemination to Distant Metastasis. *Sci. Transl. Med.* **2016**, *8* (327), 327ra26-327ra26. https://doi.org/10.1126/scitranslmed.aad6352.

(54) Frisan, T.; Levitsky, V.; Masucci, M. G. Variations in Proteasome Subunit Composition and Enzymatic Activity in B-Lymphoma Lines and Normal B Cells. *Int. J. Cancer* **2000**, *88* (6), 881–888. https://doi.org/10.1002/1097-0215(20001215)88:6<881::AID-IJC7>3.0.CO;2-D.

(55) Ebstein, F.; Kloetzel, P.-M.; Krüger, E.; Seifert, U. Emerging Roles of Immunoproteasomes beyond MHC Class I Antigen Processing. *Cell. Mol. Life Sci. CMLS* **2012**, *69* (15), 2543–2558. https://doi.org/10.1007/s00018-012-0938-0.

(56) Barton, L. F.; Cruz, M.; Rangwala, R.; Deepe, G. S.; Monaco, J. J. Regulation of Immunoproteasome Subunit Expression In Vivo Following Pathogenic Fungal Infection. *J. Immunol.* **2002**, *169* (6), 3046–3052. https://doi.org/10.4049/jimmunol.169.6.3046.

(57) Seliger, B.; Maeurer, M. J.; Ferrone, S. Antigen-Processing Machinery Breakdown and Tumor Growth. *Immunol. Today* **2000**, *21* (9), 455–464.

(58) Saez, I.; Vilchez, D. The Mechanistic Links Between Proteasome Activity, Aging and Agerelated Diseases https://www.ingentaconnect.com/content/ben/cg/2014/00000015/00000001/art00006 (accessed Apr 1, 2019).

(59) Kaushik, S.; Cuervo, A. M. Proteostasis and Aging. *Nat. Med.* **2015**, *21* (12), 1406–1415. https://doi.org/10.1038/nm.4001.

(60) Koga, H.; Kaushik, S.; Cuervo, A. M. Protein Homeostasis and Aging: The Importance of Exquisite Quality Control. *Ageing Res. Rev.* **2011**, *10* (2), 205–215. https://doi.org/10.1016/j.arr.2010.02.001.

(61) Janssens, G. E.; Meinema, A. C.; González, J.; Wolters, J. C.; Schmidt, A.; Guryev, V.; Bischoff, R.; Wit, E. C.; Veenhoff, L. M.; Heinemann, M. Protein Biogenesis Machinery Is a Driver of Replicative Aging in Yeast. *eLife* **2015**, *4*, e08527. https://doi.org/10.7554/eLife.08527.

(62) Bulteau, A.-L.; Szweda, L. I.; Friguet, B. Age-Dependent Declines in Proteasome Activity in the Heart. *Arch. Biochem. Biophys.* **2002**, *397* (2), 298–304. https://doi.org/10.1006/abbi.2001.2663.

(63) Kelmer Sacramento, E.; Kirkpatrick, J. M.; Mazzetto, M.; Baumgart, M.; Bartolome, A.; Di Sanzo, S.; Caterino, C.; Sanguanini, M.; Papaevgeniou, N.; Lefaki, M.; Childs, D.; Bagnoli, S.; Terzibasi Tozzini, E.; Di Fraia, D.; Romanov, N.; Sudmant, P. H.; Huber, W.; Chondrogianni, N.; Vendruscolo, M.; Cellerino, A.; Ori, A. Reduced Proteasome Activity in the Aging Brain Results in Ribosome Stoichiometry Loss and Aggregation. *Mol. Syst. Biol.* **2020**, *16* (6). https://doi.org/10.15252/msb.20209596.

(64) Hwang, J. S.; Hwang, J. S.; Chang, I.; Kim, S. Age-Associated Decrease in Proteasome Content and Activities in Human Dermal Fibroblasts: Restoration of Normal Level of Proteasome Subunits Reduces Aging Markers in Fibroblasts From Elderly Persons. *J. Gerontol. Ser. A* **2007**, *62* (5), 490–499. https://doi.org/10.1093/gerona/62.5.490.

(65) Chondrogianni, N.; Petropoulos, I.; Franceschi, C.; Friguet, B.; Gonos, E. S. Fibroblast Cultures from Healthy Centenarians Have an Active Proteasome. *Exp. Gerontol.* **2000**, *35* (6–7), 721–728. https://doi.org/10.1016/s0531-5565(00)00137-6.

(66) Tomaru, U.; Takahashi, S.; Ishizu, A.; Miyatake, Y.; Gohda, A.; Suzuki, S.; Ono, A.; Ohara, J.; Baba, T.; Murata, S.; Tanaka, K.; Kasahara, M. Decreased Proteasomal Activity Causes Age-Related Phenotypes and Promotes the Development of Metabolic Abnormalities. *Am. J. Pathol.* **2012**, *180* (3), 963–972. https://doi.org/10.1016/j.ajpath.2011.11.012.

(67) Schweitzer, A.; Aufderheide, A.; Rudack, T.; Beck, F.; Pfeifer, G.; Plitzko, J. M.; Sakata, E.; Schulten, K.; Förster, F.; Baumeister, W. Structure of the Human 26S Proteasome at a Resolution of 3.9 Å. *Proc. Natl. Acad. Sci.* **2016**, *113* (28), 7816–7821. https://doi.org/10.1073/pnas.1608050113.

(68) Burtner, C. R.; Murakami, C. J.; Kennedy, B. K.; Kaeberlein, M. A Molecular Mechanism of Chronological Aging in Yeast. *Cell Cycle Georget. Tex* **2009**, *8* (8), 1256–1270. https://doi.org/10.4161/cc.8.8.8287.

(69) Kruegel, U.; Robison, B.; Dange, T.; Kahlert, G.; Delaney, J. R.; Kotireddy, S.; Tsuchiya, M.; Tsuchiyama, S.; Murakami, C. J.; Schleit, J.; Sutphin, G.; Carr, D.; Tar, K.; Dittmar, G.; Kaeberlein, M.; Kennedy, B. K.; Schmidt, M. Elevated Proteasome Capacity Extends Replicative Lifespan in Saccharomyces Cerevisiae. *PLOS Genet.* **2011**, *7* (9), e1002253. https://doi.org/10.1371/journal.pgen.1002253.

(70) Carmona-Gutierrez, D.; Zimmermann, A.; Kainz, K.; Pietrocola, F.; Chen, G.; Maglioni, S.; Schiavi, A.; Nah, J.; Mertel, S.; Beuschel, C. B.; Castoldi, F.; Sica, V.; Trausinger, G.; Raml, R.; Sommer, C.; Schroeder, S.; Hofer, S. J.; Bauer, M. A.; Pendl, T.; Tadic, J.; Dammbrueck, C.; Hu, Z.; Ruckenstuhl, C.; Eisenberg, T.; Durand, S.; Bossut, N.; Aprahamian, F.; Abdellatif, M.; Sedej, S.; Enot, D. P.; Wolinski, H.; Dengjel, J.; Kepp, O.; Magnes, C.; Sinner, F.; Pieber, T. R.; Sadoshima, J.; Ventura, N.; Sigrist, S. J.; Kroemer, G.; Madeo, F. The Flavonoid 4,4'-Dimethoxychalcone Promotes Autophagy-Dependent Longevity across Species. *Nat. Commun.* **2019**, *10* (1), 651. https://doi.org/10.1038/s41467-019-08555-w.

(71) Hideshima, T.; Richardson, P.; Chauhan, D.; Palombella, V. J.; Elliott, P. J.; Adams, J.; Anderson, K. C. The Proteasome Inhibitor PS-341 Inhibits Growth, Induces Apoptosis, and Overcomes Drug Resistance in Human Multiple Myeloma Cells. *Cancer Res.* **2001**, *61* (7), 3071–3076.

(72) Kane, R. C.; Bross, P. F.; Farrell, A. T.; Pazdur, R. Velcade®: U.S. FDA Approval for the Treatment of Multiple Myeloma Progressing on Prior Therapy. *The Oncologist* **2003**, *8* (6), 508–513. https://doi.org/10.1634/theoncologist.8-6-508.

(73) Chauhan, D.; Catley, L.; Li, G.; Podar, K.; Hideshima, T.; Velankar, M.; Mitsiades, C.; Mitsiades, N.; Yasui, H.; Letai, A.; Ovaa, H.; Berkers, C.; Nicholson, B.; Chao, T.-H.; Neuteboom, S. T. C.; Richardson, P.; Palladino, M. A.; Anderson, K. C. A Novel Orally Active Proteasome Inhibitor Induces Apoptosis in Multiple Myeloma Cells with Mechanisms Distinct from Bortezomib. *Cancer Cell* **2005**, *8* (5), 407–419. https://doi.org/10.1016/j.ccr.2005.10.013.

(74) Ma, M. H.; Yang, H. H.; Parker, K.; Manyak, S.; Friedman, J. M.; Altamirano, C.; Wu, Z.; Borad, M. J.; Frantzen, M.; Roussos, E.; Neeser, J.; Mikail, A.; Adams, J.; Sjak-Shie, N.; Vescio, R. A.; Berenson, J. R. The Proteasome Inhibitor PS-341 Markedly Enhances Sensitivity of Multiple Myeloma Tumor Cells to Chemotherapeutic Agents. *Clin. Cancer Res. Off. J. Am. Assoc. Cancer Res.* **2003**, *9* (3), 1136–1144.

(75) An, W. G.; Hwang, S. G.; Trepel, J. B.; Blagosklonny, M. V. Protease Inhibitor-Induced Apoptosis: Accumulation of Wt P53, P21WAF1/CIP1, and Induction of Apoptosis Are Independent Markers of Proteasome Inhibition. *Leukemia* **2000**, *14* (7), 1276–1283.

(76) Richardson, P. G.; Sonneveld, P.; Schuster, M. W.; Irwin, D.; Stadtmauer, E. A.; Facon, T.; Harousseau, J.-L.; Ben-Yehuda, D.; Lonial, S.; Goldschmidt, H.; Reece, D.; San-Miguel, J. F.; Bladé, J.; Boccadoro, M.; Cavenagh, J.; Dalton, W. S.; Boral, A. L.; Esseltine, D. L.; Porter, J. B.; Schenkein, D.; Anderson, K. C.; Assessment of Proteasome Inhibition for Extending Remissions (APEX) Investigators. Bortezomib or High-Dose Dexamethasone for Relapsed Multiple Myeloma. *N. Engl. J. Med.* **2005**, *352* (24), 2487–2498. https://doi.org/10.1056/NEJMoa043445.

(77) Dorsey, B. D.; Iqbal, M.; Chatterjee, S.; Menta, E.; Bernardini, R.; Bernareggi, A.; Cassarà, P. G.; D'Arasmo, G.; Ferretti, E.; De Munari, S.; Oliva, A.; Pezzoni, G.; Allievi, C.; Strepponi, I.; Ruggeri, B.; Ator, M. A.; Williams, M.; Mallamo, J. P. Discovery of a Potent, Selective, and Orally Active Proteasome Inhibitor for the Treatment of Cancer. *J. Med. Chem.* **2008**, *51* (4), 1068–1072. https://doi.org/10.1021/jm7010589.

(78) Adams, J.; Behnke, M.; Chen, S.; Cruickshank, A. A.; Dick, L. R.; Grenier, L.; Klunder, J. M.; Ma, Y. T.; Plamondon, L.; Stein, R. L. Potent and Selective Inhibitors of the Proteasome: Dipeptidyl Boronic Acids. *Bioorg. Med. Chem. Lett.* **1998**, *8* (4), 333–338. https://doi.org/10.1016/s0960-894x(98)00029-8.

(79) Kumar, S.; Rajkumar, S. V. Many Facets of Bortezomib Resistance/Susceptibility. *Blood* **2008**, *112* (6), 2177–2178. https://doi.org/10.1182/blood-2008-07-167767.

(80) Lichter, D. I.; Danaee, H.; Pickard, M. D.; Tayber, O.; Sintchak, M.; Shi, H.; Richardson, P. G.; Cavenagh, J.; Bladé, J.; Façon, T.; Niesvizky, R.; Alsina, M.; Dalton, W.; Sonneveld, P.; Lonial, S.; van de Velde, H.; Ricci, D.; Esseltine, D.-L.; Trepicchio, W. L.; Mulligan, G.; Anderson, K. C. Sequence Analysis of β-Subunit Genes of the 20S Proteasome in Patients with Relapsed Multiple Myeloma Treated with Bortezomib or Dexamethasone. *Blood* **2012**, *120* (23), 4513–4516. https://doi.org/10.1182/blood-2012-05-426924.

(81) Lü, S.; Yang, J.; Chen, Z.; Gong, S.; Zhou, H.; Xu, X.; Wang, J. Different Mutants of PSMB5 Confer Varying Bortezomib Resistance in T Lymphoblastic Lymphoma/Leukemia Cells Derived from the Jurkat Cell Line. *Exp. Hematol.* **2009**, *37* (7), 831–837. https://doi.org/10.1016/j.exphem.2009.04.001.

(82) Oerlemans, R.; Franke, N. E.; Assaraf, Y. G.; Cloos, J.; van Zantwijk, I.; Berkers, C. R.; Scheffer, G. L.; Debipersad, K.; Vojtekova, K.; Lemos, C.; van der Heijden, J. W.; Ylstra, B.; Peters, G. J.; Kaspers, G. L.; Dijkmans, B. A. C.; Scheper, R. J.; Jansen, G. Molecular Basis of Bortezomib Resistance: Proteasome Subunit Beta5 (PSMB5) Gene Mutation and Overexpression of PSMB5 Protein. *Blood* **2008**, *112* (6), 2489–2499. https://doi.org/10.1182/blood-2007-08-104950.

(83) Parlati, F.; Lee, S. J.; Aujay, M.; Suzuki, E.; Levitsky, K.; Lorens, J. B.; Micklem, D. R.; Ruurs, P.; Sylvain, C.; Lu, Y.; Shenk, K. D.; Bennett, M. K. Carfilzomib Can Induce Tumor Cell Death through Selective Inhibition of the Chymotrypsin-like Activity of the Proteasome. *Blood* **2009**, *114* (16), 3439–3447. https://doi.org/10.1182/blood-2009-05-223677.

(84) de Bruin, G.; Xin, B. T.; Kraus, M.; van der Stelt, M.; van der Marel, G. A.; Kisselev, A. F.; Driessen, C.; Florea, B. I.; Overkleeft, H. S. A Set of Activity-Based Probes to Visualize Human (Immuno)Proteasome Activities. *Angew. Chem. Int. Ed.* **2016**, *55* (13), 4199–4203. https://doi.org/10.1002/anie.201509092.

(85) Khan, M. L.; Stewart, A. K. Carfilzomib: A Novel Second-Generation Proteasome Inhibitor. *Future Oncol. Lond. Engl.* **2011**, *7* (5), 607–612. https://doi.org/10.2217/fon.11.42.

(86) Groll, M.; Berkers, C. R.; Ploegh, H. L.; Ovaa, H. Crystal Structure of the Boronic Acid-Based Proteasome Inhibitor Bortezomib in Complex with the Yeast 20S Proteasome. *Structure* **2006**, *14* (3), 451–456. https://doi.org/10.1016/j.str.2005.11.019.

(87) Demo, S. D.; Kirk, C. J.; Aujay, M. A.; Buchholz, T. J.; Dajee, M.; Ho, M. N.; Jiang, J.; Laidig, G. J.; Lewis, E. R.; Parlati, F.; Shenk, K. D.; Smyth, M. S.; Sun, C. M.; Vallone, M. K.; Woo, T. M.; Molineaux, C. J.; Bennett, M. K. Antitumor Activity of PR-171, a Novel Irreversible Inhibitor of the Proteasome. *Cancer Res.* **2007**, *67* (13), 6383–6391. https://doi.org/10.1158/0008-5472.CAN-06-4086.

(88) Lee, M. J.; Bhattarai, D.; Yoo, J.; Miller, Z.; Park, J. E.; Lee, S.; Lee, W.; Driscoll, J. J.; Kim, K. B. Development of Novel Epoxyketone-Based Proteasome Inhibitors as a Strategy To Overcome Cancer Resistance to Carfilzomib and Bortezomib. *J. Med. Chem.* **2019**, *62* (9), 4444–4455. https://doi.org/10.1021/acs.jmedchem.8b01943.

(89) Niewerth, D.; Jansen, G.; Assaraf, Y. G.; Zweegman, S.; Kaspers, G. J. L.; Cloos, J. Molecular Basis of Resistance to Proteasome Inhibitors in Hematological Malignancies. *Drug Resist. Updat.* **2015**, *18*, 18–35. https://doi.org/10.1016/j.drup.2014.12.001.

(90) Singh, A. V.; Bandi, M.; Aujay, M. A.; Kirk, C. J.; Hark, D. E.; Raje, N.; Chauhan, D.; Anderson, K. C. PR-924, a Selective Inhibitor of the Immunoproteasome Subunit LMP-7, Blocks Multiple Myeloma Cell Growth Both in Vitro and in Vivo. *Br. J. Haematol.* **2011**, *152* (2), 155–163. https://doi.org/10.1111/j.1365-2141.2010.08491.x.

(91) Kim, K. B.; Myung, J.; Sin, N.; Crews, C. M. Proteasome Inhibition by the Natural Products Epoxomicin and Dihydroeponemycin: Insights into Specificity and Potency. *Bioorg. Med. Chem. Lett.* **1999**, *9* (23), 3335–3340.

(92) Ho, Y. K. (Abby); Bargagna-Mohan, P.; Wehenkel, M.; Mohan, R.; Kim, K.-B. LMP2-Specific Inhibitors: Chemical Genetic Tools for Proteasome Biology. *Chem. Biol.* **2007**, *14* (4), 419–430. https://doi.org/10.1016/j.chembiol.2007.03.008.

(93) Lei, B.; Abdul Hameed, M. D. M.; Hamza, A.; Wehenkel, M.; Muzyka, J. L.; Yao, X.-J.; Kim, K.-B.; Zhan, C.-G. Molecular Basis of the Selectivity of the Immunoproteasome Catalytic Subunit LMP2-Specific Inhibitor Revealed by Molecular Modeling and Dynamics Simulations. *J. Phys. Chem. B* **2010**, *114* (38), 12333–12339. https://doi.org/10.1021/jp1058098.

(94) Klein, M.; Busch, M.; Esdar, C.; Friese-Hamim, M.; Krier, M.; Musil, D.; Rohdich, F.; Sanderson, M.; Walter, G.; Schadt, O.; Zanelli, U.; Ma, J. Abstract LB-054: Discovery and Profiling of M3258, a Potent and Selective LMP7 Inhibitor Demonstrating High Efficacy in Multiple Myeloma Models. *Cancer Res.* **2019**, *79* (13 Supplement), LB-054-LB-054. https://doi.org/10.1158/1538-7445.AM2019-LB-054.

(95) Sanderson, M.; Busch, M.; Esdar, C.; Friese-Hamim, M.; Krier, M.; Ma, J.; Musil, D.; Rohdich, F.; Sloot, W.; Walter, G.; Zanelli, U.; Schadt, O.; Klein, M. Abstract DDT02-01: First-Time Disclosure of M3258: A Selective Inhibitor of the Immunoproteasome Subunit LMP7 with Potential for Improved Therapeutic Utility in Multiple Myeloma Compared to Pan-Proteasome Inhibitors. *Cancer Res.* **2019**, *79* (13 Supplement), DDT02-01-DDT02-01. https://doi.org/10.1158/1538-7445.AM2019-DDT02-01.

(96) Downey-Kopyscinski, S.; Daily, E. W.; Gautier, M.; Bhatt, A.; Florea, B. I.; Mitsiades, C. S.; Richardson, P. G.; Driessen, C.; Overkleeft, H. S.; Kisselev, A. F. An Inhibitor of Proteasome B2 Sites Sensitizes Myeloma Cells to Immunoproteasome Inhibitors. *Blood Adv.* **2018**, *2* (19), 2443–2451. https://doi.org/10.1182/bloodadvances.2018016360.

(97) Thibaudeau, T. A.; Anderson, R. T.; Smith, D. M. A Common Mechanism of Proteasome Impairment by Neurodegenerative Disease-Associated Oligomers. *Nat. Commun.* **2018**, *9* (1), 1–14. https://doi.org/10.1038/s41467-018-03509-0.

(98) Rubinsztein, D. C. The Roles of Intracellular Protein-Degradation Pathways in Neurodegeneration. *Nature* **2006**, *443* (7113), 780–786. https://doi.org/10.1038/nature05291.

(99) McNaught, K. S. P.; Jenner, P. Proteasomal Function Is Impaired in Substantia Nigra in Parkinson's Disease. *Neurosci. Lett.* **2001**, *297* (3), 191–194. https://doi.org/10.1016/S0304-3940(00)01701-8.

(100) Dasgupta, S.; Fishman, M. A.; Mahallati, H.; Castro, L. M.; Tashima, A. K.; Ferro, E. S.; Fricker, L. D. Reduced Levels of Proteasome Products in a Mouse Striatal Cell Model of Huntington's Disease. *PLOS ONE* **2015**, *10* (12), e0145333. https://doi.org/10.1371/journal.pone.0145333.

(101) Njomen, E.; Tepe, J. J. Proteasome Activation as a New Therapeutic Approach To Target Proteotoxic Disorders. *J. Med. Chem.* **2019**, *62* (14), 6469–6481. https://doi.org/10.1021/acs.jmedchem.9b00101.

(102) Huang, L.; Ho, P.; Chen, C.-H. Activation and Inhibition of the Proteasome by Betulinic Acid and Its Derivatives. *FEBS Lett.* **2007**, *581* (25), 4955–4959. https://doi.org/10.1016/j.febslet.2007.09.031.

(103) Ríos, J. L.; Máñez, S. New Pharmacological Opportunities for Betulinic Acid. *Planta Med.* **2018**, *84* (1), 8–19. https://doi.org/10.1055/s-0043-123472.

(104) Trader, D. J.; Simanski, S.; Dickson, P.; Kodadek, T. Establishment of a Suite of Assays That Support the Discovery of Proteasome Stimulators. *Biochim. Biophys. Acta* **2017**, *1861* (4), 892–899. https://doi.org/10.1016/j.bbagen.2017.01.003.

(105) Coleman, R. A.; Mohallem, R.; Aryal, U. K.; Trader, D. J. Protein Degradation Profile Reveals Dynamic Nature of 20S Proteasome Small Molecule Stimulation. *RSC Chem. Biol.* **2021**. https://doi.org/10.1039/D0CB00191K.

(106) Díaz-Hernández, M.; Hernández, F.; Martín-Aparicio, E.; Gómez-Ramos, P.; Morán, M. A.; Castaño, J. G.; Ferrer, I.; Avila, J.; Lucas, J. J. Neuronal Induction of the Immunoproteasome in Huntington's Disease. *J. Neurosci. Off. J. Soc. Neurosci.* **2003**, *23* (37), 11653–11661.

(107) Orre, M.; Kamphuis, W.; Dooves, S.; Kooijman, L.; Chan, E. T.; Kirk, C. J.; Dimayuga Smith, V.; Koot, S.; Mamber, C.; Jansen, A. H.; Ovaa, H.; Hol, E. M. Reactive Glia Show Increased Immunoproteasome Activity in Alzheimer's Disease. *Brain J. Neurol.* **2013**, *136* (Pt 5), 1415–1431. https://doi.org/10.1093/brain/awt083.

(108) Cheroni, C.; Peviani, M.; Cascio, P.; Debiasi, S.; Monti, C.; Bendotti, C. Accumulation of Human SOD1 and Ubiquitinated Deposits in the Spinal Cord of SOD1G93A Mice during Motor Neuron Disease Progression Correlates with a Decrease of Proteasome. *Neurobiol. Dis.* **2005**, *18* (3), 509–522. https://doi.org/10.1016/j.nbd.2004.12.007.

(109) Kisselev, A. F.; Goldberg, A. L. Monitoring Activity and Inhibition of 26S Proteasomes with Fluorogenic Peptide Substrates. In *Methods in Enzymology*; Elsevier, 2005; Vol. 398, pp 364–378. https://doi.org/10.1016/S0076-6879(05)98030-0.

(110) Sasaki, T.; Kikuchi, T.; Yumoto, N.; Yoshimura, N.; Murachi, T. Comparative Specificity and Kinetic Studies on Porcine Calpain I and Calpain II with Naturally Occurring Peptides and Synthetic Fluorogenic Substrates. *J. Biol. Chem.* **1984**, *259* (20), 12489–12494.

(111) Coleman, R. A.; Trader, D. J. Development and Application of a Sensitive Peptide Reporter to Discover 20S Proteasome Stimulators. *ACS Comb. Sci.* **2018**, *20* (5), 269–276. https://doi.org/10.1021/acscombsci.7b00193.

(112) Zerfas, B. L.; Coleman, R. A.; Salazar-Chaparro, A. F.; Macatangay, N. J.; Trader, D. J. Fluorescent Probes with Unnatural Amino Acids to Monitor Proteasome Activity in Real-Time. *ACS Chem. Biol.* **2020**, *15* (9), 2588–2596. https://doi.org/10.1021/acschembio.0c00634.

(113) Zerfas, B. L.; Trader, D. J. Monitoring the Immunoproteasome in Live Cells Using an Activity-Based Peptide–Peptoid Hybrid Probe. *J. Am. Chem. Soc.* **2019**, *141* (13), 5252–5260. https://doi.org/10.1021/jacs.8b12873.

(114) de Bruin, G.; Xin, B.-T.; Florea, B. I.; Overkleeft, H. S. Proteasome Subunit Selective Activity-Based Probes Report on Proteasome Core Particle Composition in a Native Polyacrylamide Gel Electrophoresis Fluorescence-Resonance Energy Transfer Assay. *J. Am. Chem. Soc.* **2016**, *138* (31), 9874–9880. https://doi.org/10.1021/jacs.6b04207.

(115) Maresh, M. E.; Salazar-Chaparro, A. F.; Trader, D. J. Methods for the Discovery of Small Molecules to Monitor and Perturb the Activity of the Human Proteasome. *Future Med. Chem.* **2020**. https://doi.org/10.4155/fmc-2020-0288.

(116) Sekar, R. B.; Periasamy, A. Fluorescence Resonance Energy Transfer (FRET) Microscopy Imaging of Live Cell Protein Localizations. *J. Cell Biol.* **2003**, *160* (5), 629–633. https://doi.org/10.1083/jcb.200210140.

(117) Geurink, P. P.; van der Linden, W. A.; Mirabella, A. C.; Gallastegui, N.; de Bruin, G.; Blom, A. E. M.; Voges, M. J.; Mock, E. D.; Florea, B. I.; van der Marel, G. A.; Driessen, C.; van der Stelt, M.; Groll, M.; Overkleeft, H. S.; Kisselev, A. F. Incorporation of Non-Natural Amino Acids Improves Cell Permeability and Potency of Specific Inhibitors of Proteasome Trypsin-like Sites. *J. Med. Chem.* **2013**, *56* (3), 1262–1275. https://doi.org/10.1021/jm3016987.

(118) Verdoes, M.; Florea, B. I.; Menendez-Benito, V.; Maynard, C. J.; Witte, M. D.; van der Linden, W. A.; van den Nieuwendijk, A. M. C. H.; Hofmann, T.; Berkers, C. R.; van Leeuwen, F. W. B.; Groothuis, T. A.; Leeuwenburgh, M. A.; Ovaa, H.; Neefjes, J. J.; Filippov, D. V.; van der Marel, G. A.; Dantuma, N. P.; Overkleeft, H. S. A Fluorescent Broad-Spectrum Proteasome Inhibitor for Labeling Proteasomes In Vitro and In Vivo. *Chem. Biol.* **2006**, *13* (11), 1217–1226. https://doi.org/10.1016/j.chembiol.2006.09.013.

(119) Britton, M.; Lucas, M. M.; Downey, S. L.; Screen, M.; Pletnev, A. A.; Verdoes, M.; Tokhunts, R. A.; Amir, O.; Goddard, A. L.; Pelphrey, P. M.; Wright, D. L.; Overkleeft, H. S.; Kisselev, A. F. Selective Inhibitor of Proteasome's Caspase-like Sites Sensitizes Cells to Specific Inhibition of Chymotrypsin-like Sites. *Chem. Biol.* **2009**, *16* (12), 1278–1289. https://doi.org/10.1016/j.chembiol.2009.11.015.

(120) Momose, I.; Umezawa, Y.; Hirosawa, S.; Iinuma, H.; Ikeda, D. Structure-Based Design of Derivatives of Tyropeptin A as the Potent and Selective Inhibitors of Mammalian 20S Proteasome. *Bioorg. Med. Chem. Lett.* **2005**, *15* (7), 1867–1871. https://doi.org/10.1016/j.bmcl.2005.02.013.

(121) Bogyo, M.; McMaster, J. S.; Gaczynska, M.; Tortorella, D.; Goldberg, A. L.; Ploegh, H. Covalent Modification of the Active Site Threonine of Proteasomal β Subunits and the Escherichia Coli Homolog HslV by a New Class of Inhibitors. *Proc. Natl. Acad. Sci.* **1997**, *94* (13), 6629–6634. https://doi.org/10.1073/pnas.94.13.6629.

(122) Verdoes, M.; Willems, L. I.; Linden, W. A. van der; Duivenvoorden, B. A.; Marel, G. A. van der; Florea, B. I.; Kisselev, A. F.; Overkleeft, H. S. A Panel of Subunit-Selective Activity-Based Proteasome Probes. *Org. Biomol. Chem.* **2010**, *8* (12), 2719–2727. https://doi.org/10.1039/C001036G.

(123) Lam, K. S.; Lebl, M.; Krchňák, V. The "One-Bead-One-Compound" Combinatorial Library Method. *Chem. Rev.* **1997**, *97* (2), 411–448. https://doi.org/10.1021/cr9600114.

(124) Pei, D. On-Bead Library Screening Made Easier. *Chem. Biol.* **2010**, *17* (1), 3–4. https://doi.org/10.1016/j.chembiol.2010.01.003.

(125) Mendes, K.; Ndungu, J. M.; Clark, L. F.; Kodadek, T. Optimization of the Magnetic Recovery of Hits from One-Bead–One-Compound Library Screens. *ACS Comb. Sci.* **2015**, *17* (9), 506–517. https://doi.org/10.1021/acscombsci.5b00090.

(126) MacConnell, A. B.; McEnaney, P. J.; Cavett, V. J.; Paegel, B. M. DNA-Encoded Solid-Phase Synthesis: Encoding Language Design and Complex Oligomer Library Synthesis. *ACS Comb. Sci.* **2015**, *17* (9), 518–534. https://doi.org/10.1021/acscombsci.5b00106.

(127) Trader, D. J.; Simanski, S.; Kodadek, T. A Reversible and Highly Selective Inhibitor of the Proteasomal Ubiquitin Receptor Rpn13 Is Toxic To Multiple Myeloma Cells. *J. Am. Chem. Soc.* **2015**, *137* (19), 6312. https://doi.org/10.1021/jacs.5b02069.

(128) Huynh, K.; Partch, C. L. Analysis of Protein Stability and Ligand Interactions by Thermal Shift Assay. *Curr. Protoc. Protein Sci.* **2015**, *79*, 28.9.1-14. https://doi.org/10.1002/0471140864.ps2809s79.

(129) Ng, Y. Z.; Baldera-Aguayo, P. A.; Cornish, V. W. Fluorescence Polarization Assay for Small Molecule Screening of FK506 Biosynthesized in 96-Well Microtiter Plates. *Biochemistry* **2017**, *56* (40), 5260–5268. https://doi.org/10.1021/acs.biochem.7b00602.

(130) Tian, W.; Trader, D. J. Discovery of a Small Molecule Probe of Rpn-6, an Essential Subunit of the 26S Proteasome. *ACS Chem. Biol.* **2020**, *15* (2), 554–561. https://doi.org/10.1021/acschembio.9b01019.

(131) Anchoori, R. K.; Karanam, B.; Peng, S.; Wang, J. W.; Jiang, R.; Tanno, T.; Orlowski, R. Z.; Matsui, W.; Zhao, M.; Rudek, M. A.; Hung, C.; Chen, X.; Walters, K. J.; Roden, R. B. S. A Bis-Benzylidine Piperidone Targeting Proteasome Ubiquitin Receptor RPN13/ADRM1 as a Therapy for Cancer. *Cancer Cell* **2013**, *24* (6), 791–805. https://doi.org/10.1016/j.ccr.2013.11.001.

(132) Anchoori, R. K.; Jiang, R.; Peng, S.; Soong, R.; Algethami, A.; Rudek, M. A.; Anders, N.; Hung, C.-F.; Chen, X.; Lu, X.; Kayode, O.; Dyba, M.; Walters, K. J.; Roden, R. B. S. Covalent Rpn13-Binding Inhibitors for the Treatment of Ovarian Cancer. *ACS Omega* **2018**, *3* (9), 11917–11929. https://doi.org/10.1021/acsomega.8b01479.

(133) Song, Y.; Park, P. M. C.; Wu, L.; Ray, A.; Picaud, S.; Li, D.; Wimalasena, V. K.; Du, T.; Filippakopoulos, P.; Anderson, K. C.; Qi, J.; Chauhan, D. Development and Preclinical Validation of a Novel Covalent Ubiquitin Receptor Rpn13 Degrader in Multiple Myeloma. *Leukemia* **2019**, *33* (11), 2685–2694. https://doi.org/10.1038/s41375-019-0467-z.

(134) Lian, W.; Upadhyaya, P.; Rhodes, C. A.; Liu, Y.; Pei, D. Screening Bicyclic Peptide Libraries for Protein–Protein Interaction Inhibitors: Discovery of a Tumor Necrosis Factor-α Antagonist. *J. Am. Chem. Soc.* **2013**, *135* (32), 11990–11995. https://doi.org/10.1021/ja405106u.

(135) Maresh, M. E.; Trader, D. J. Development of a Method To Prioritize Protein–Ligand Pairs on Beads Using Protein Conjugated to a Near-IR Dye. *ACS Comb. Sci.* **2019**, *21* (3), 223–228. https://doi.org/10.1021/acscombsci.8b00165.

(136) Doran, T. M.; Gao, Y.; Mendes, K.; Dean, S.; Simanski, S.; Kodadek, T. Utility of Redundant Combinatorial Libraries in Distinguishing High and Low Quality Screening Hits. *ACS Comb. Sci.* **2014**, *16* (6), 259–270. https://doi.org/10.1021/co500030f.

(137) Nguyen, N. N.; Rana, A.; Goldman, C.; Moore, R.; Tai, J.; Hong, Y.; Shen, J.; Walker, D. W.; Hur, J. H. Proteasome B5 Subunit Overexpression Improves Proteostasis during Aging and Extends Lifespan in Drosophila Melanogaster. *Sci. Rep.* **2019**, *9* (1), 1–12. https://doi.org/10.1038/s41598-019-39508-4.

(138) Jones, C. L.; Njomen, E.; Sjögren, B.; Dexheimer, T. S.; Tepe, J. J. Small Molecule Enhancement of 20S Proteasome Activity Targets Intrinsically Disordered Proteins. *ACS Chem. Biol.* **2017**, *12* (9), 2240–2247. https://doi.org/10.1021/acschembio.7b00489.

CHAPTER 2. DEVELOPMENT OF A NIR-BASED OBOC SCREENING METHOD

*Reproduced in part with permission from Maresh, M.E.; Trader, D.J. Development of a Method To Prioritize Protein-Ligand Pairs on Beads Using Protein Conjugated to Near-IR Dye. *ACS Comb. Sci.* **2019,** *21* (3), 223-228.

2.1 Introduction

Although creation of one-bead-one-compound (OBOC) libraries has revolutionized the speed at which thousands of small molecules can be synthesized, progress falls short in the ability to screen these libraries against target proteins that have no known enzymatic function.[1] In these instances, libraries can be screened by monitoring a protein's melting temperature in response to dosage with a small molecule[2–4] or by using a combination of primary and secondary antibodies conjugated to magnetic beads.[5] While these methods have been used to discover small molecule binders to target proteins, they have several drawbacks. First, binding between the target protein and small molecule must be strong enough to withstand various wash steps. Depending on the application of the small molecule post-screen, a weaker binding ligand might be desired. Secondly, hits from the initial screen cannot be readily prioritized. As a result, validation of hits can be tedious and time consuming. Therefore, developing novel OBOC library screening techniques in which protein-ligand pairs could be prioritized would expedite the hit identification process and reduce the number of hits that require validation.

Attention has been turned to developing more quantitative OBOC library screening methods. Some of these methods entail printing small molecules on glass slides, then adding a target protein and antibody cocktail. This method requires specialized, expensive equipment and is limited in the diversity of small molecules that can be screened.[6–8] More recently, incorporation of fluorescent dyes to detect binding between a ligand and protein has resulted in OBOC library screening techniques that are quantitative while not limiting chemical diversity of the library. Such methods often involve labeling a target protein with a fluorophore and incubating it with OBOC library beads. Binding is then visualized with confocal microscopy.[9–11] Other techniques utilize quantum dots conjugated to streptavidin to screen OBOC libraries.[12] This technique requires labeling a target protein with biotin prior to screening. The protein is then incubated with library

beads and quantum dots conjugated to streptavidin bind the labeled protein that has bound the small molecule on-bead. Fluorescent signal produced by the quantum dot can be visualized with fluorescence microscopy and hit beads can be identified. While these methods overcome some of the challenges posed by techniques utilizing magnetic beads, they also have drawbacks. Most commonly, the fluorophores utilized to visualize binding between a target protein and small molecule often overlap with autofluorescence produced by the protein or resin. This can make data deconvolution difficult and cumbersome.

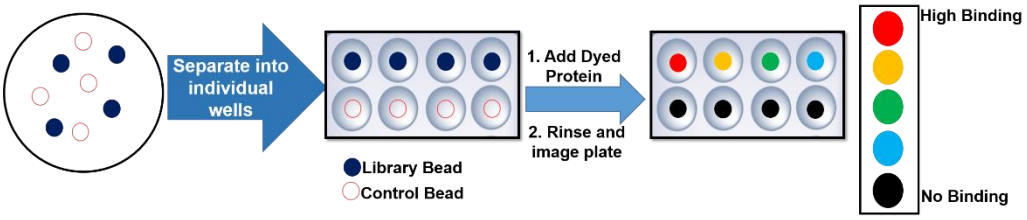

Figure 2.1 General Screening Scheme. Our screening method involves labeling a target protein with a NIR-emitting fluorophore. Beads of an OBOC or beads conjugated to a control small molecule are then individually separated into the wells of a black 96-well plate with a clear bottom. The labeled protein is then added to the wells. After binding between the protein and bead, the plate is rinsed to remove excess protein and imaged for NIR fluorescence. Fluorescence intensities that result from the labeled protein binding the small molecule on-bead can be quantified and provide a basis to rank hits.

To overcome this obstacle, some research groups have focused on incorporating fluorophores that emit at longer wavelengths into their screening methods.[13] Since protein and bead autofluorescence generally do not occur at these wavelengths, data obtained from screens are easier to evaluate. In an effort to build upon these methods and create an OBOC library screening method in which protein-ligand pairs can be prioritized, we have recently develop screening technique in which a target protein is conjugated to a near-infrared range (NIR) fluorophore.[14] Briefly, a target protein is labeled with a NIR fluorophore and beads of an OBOC are individually separated into a black 96-well plate with a clear bottom (**Figure 2.1**). Beads are blocked with protein blocking buffer to limit nonspecific binding. The labeled protein is then diluted in blocking buffer and added to the wells. After incubation, beads are rinsed, and the plate is imaged for NIR fluorescence. The fluorescence intensities that result from the labeled protein binding the small molecule on-bead can be quantified and provide a basis to rank hits. Since this method does not rely on the function of the protein being measured, both catalytic and non-catalytic proteins can be screened for potential binders.

2.2 Results and Discussion

2.2.1 Establishing Assay Design and Screening Conditions with NIR-Labeled Streptavidin and Biotin On-Bead

To establish screening conditions to detect NIR-labeled proteins to small molecules on-bead, we wanted to utilize a high affinity protein-ligand pair. Binding between streptavidin and biotin is among the strongest noncovalent interactions and as a result, was selected as a model protein-ligand system. Streptavidin was first labeled with a NIR fluorophore, IRDye 800CW, conjugated to a *N*-hydroxysuccinimide (NHS) ester moiety. NHS esters react with primary amines, and by controlling the pH of the protein solution, attachment of the dye to the N-terminus is possible.[15,16] NIR fluorophores are sensitive and produce a strong fluorescent signal. As a result, only one or two fluorophores must be attached to the protein to detect a signal.[17] The number of dye molecules attached to the protein can be controlled by adjusting the amount of dye added to the protein solution. The dye-to-protein ratio of labeled streptavidin was determined to be 2-to-1. The labeled streptavidin was aliquoted at -20 ˚C and thawed before use.

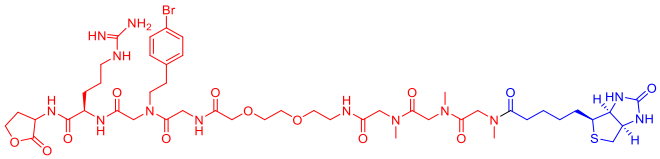

Figure 2.2 Linker Structure Conjugated to Biotin. The linker (red) was synthesized on the resin to provide space between the bead and small molecule and to assist in identifying ligands by MALDI-TOF analysis after a screen against an OBOC library. The methionine residue is cleaved by cyanogen bromide so the small molecule can be removed from the bead. The arginine provides the necessary charge for ionization during MALDI-TOF analysis. The bromine produces a unique isotope pattern so fragments produced during MALDI-TOF can be readily identified as part of the small molecule. Biotin (blue) was conjugated to the linker.

Next, a linker structure was synthesized on TentaGel resin, followed by conjugation of biotin (**Figure 2.2**). The linker provides physical space between the bead and the small molecule to prevent nonspecific interactions between the protein and bead. This structure also contains an arginine residue that provides the necessary charge for ionization to identify a small molecule synthesized on the bead during an OBOC library screen against a target protein by matrix assist laser desorption ionization- time of flight (MALDI-TOF). The linker also houses a methionine residue so the small molecule can be cleaved from the resin with a cyanogen bromide cocktail.[18] Finally, the bromine in the linker was added to produce a unique isotope pattern in which there is a 1:1 ratio of the M:M+2. Therefore, any structure containing a bromine will produce two peaks following this mass pattern, simplifying identification of structures by MALDI-TOF.

This would allow us to readily differentiate between fragments produced by a small molecule during MALDI-TOF and background signal. The linker and biotin were both attached to the resin by standard solid phase synthesis. A small amount of product was cleaved from the resin and checked by liquid chromatography mass spectrometry (LC/MS) to ensure successful addition of the linker and biotin. Importantly, before the resin was used in the assay, it was swollen in phosphate-buffered saline (PBS) to prevent the beads from collapsing when exposed to aqueous solvents. TentaGel resin was selected for this purpose because, unlike other resins, it is structurally sound in aqueous environments.

The first challenge we faced was establishing blocking conditions such that nonspecific interactions between the resin, well plate, and protein were minimal. We found that adding the labeled protein diluted in PBS led to significant background signal because of the protein nonspecifically binding to the well plate (**Figure 2.3**). However, background signal was essentially eliminated when blocking buffer was added to the wells and the labeled protein was diluted in blocking buffer. As a result, wells and beads were first blocked with protein blocking buffer and the labeled protein was diluted in blocking buffer in all the remaining experiments.

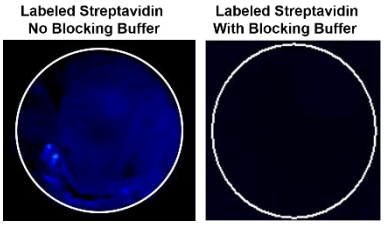

Figure 2.3 Establishing Proper Blocking Conditions for the OBOC Screening Method. A two-step method that involves blocking both the beads and well and diluting the labeled protein in blocking buffer eliminates background signal. When NIR-labeled streptavidin diluted in PBS was added directly to the well without blocking, signal resulting from the protein nonspecifically interacting with the plate was observed. However, when the plate was first blocked with protein blocking buffer and the protein was diluted in blocking buffer, background signal is eliminated. The white circles indicate the outline of an individual well.

With the blocking conditions established, we next turned our attention to evaluating if binding between NIR-labeled streptavidin and biotin on-bead could be observed. Beads conjugated to biotin were separated into the wells of a 96-well plate. NIR-labeled streptavidin was then diluted in blocking buffer and varying amounts (ranging from 1.25 ng to 0.005 ng) were added to the wells. The protein incubated with the resin overnight. The following day, the protein solution was removed by pipetting, and the beads were rinsed with PBS to remove excess protein. The plate was then imaged for NIR fluorescence with a LI-COR Odyssey CLx imaging system. It is important to note that the average diameter of the resin was 90 µm, so the resolution of the instrument was set to 81 µm to facilitate visualization of individual beads. Similarly, the instrument was set to medium imaging quality. Excitingly, the beads produced a fluorescent signal, indicating that streptavidin had bound biotin.

Moreover, differences in fluorescence intensities corresponding to the amount of labeled protein added to the wells was readily visualized when zooming in on individual beads (**Figure 2.4A**). The fluorescence intensities were quantified and graphed, further revealing that higher fluorescence intensities correlated to higher amounts of protein bound to biotin on-bead in the well (**Figure 2.4B**). Fluorescence produced by adding 1.25 ng of protein almost saturated the detector, as represented by the bright red color of the bead. Fluorescence could reliably be detected with as little as 0.01 ng of protein added to the well, indicating that this assay could potentially be very sensitive to detecting relatively strong binding affinity between a protein and a ligand.

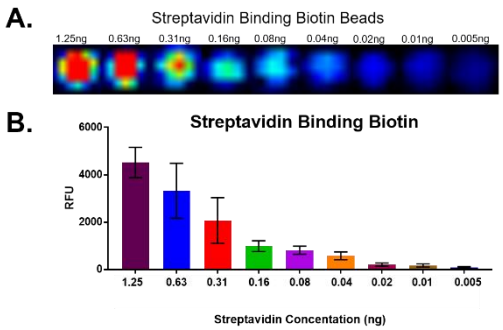

Figure 2.4 Detecting Binding of Varying Amounts of NIR-Labeled Streptavidin to Biotin On-Bead. Individual beads decorated with biotin were separated into the wells of a black 96-well plate with a clear bottom. The beads were blocked with protein blocking buffer. Then, NIR-labeled streptavidin was diluted in blocking buffer and varying amounts were added to the wells. After overnight incubation, the protein solution was removed, and beads were rinsed with PBS. The beads were resuspended in PBS and imaged for NIR fluorescence. (A) Individual beads were visualized by zooming in on the well. Clear differences in the fluorescence intensities were obvious and correlated to the amount of protein added to each well. (B) Fluorescence intensities of each bead were quantified and graphed, further revealing that higher fluorescence intensities resulted from more protein added to the wells.

Since binding between streptavidin and biotin is very strong, we next sought to determine if binding could be observed with a ligand that had lower affinity to streptavidin.[19] We selected desthiobiotin as a new ligand, which still binds to streptavidin, but has a weaker K_D than biotin. Desthiobiotin was synthesized on a similar linker structure using standard solid phase synthesis (**Figure 2.5**). The product was cleaved from a small amount of resin and analyzed by LC/MS to ensure the desired sequence was correctly conjugated to the resin. Beads were swollen in PBS then individually separated into the wells of a 96-well plate. Beads were blocked with protein blocking buffer, then NIR-labeled streptavidin was diluted in blocking buffer, and varying amounts of the protein was added to each well. After overnight incubation, the protein solution was removed, beads were rinsed with PBS, and then the plate was imaged on a LI-COR Odyssey CLx imaging

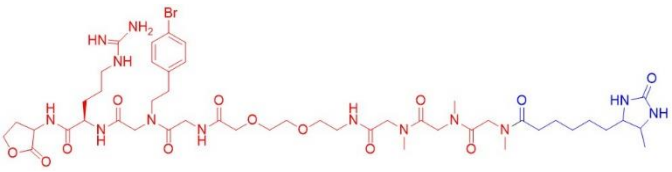

Figure 2.5 Desthiobiotin Conjugated to the Linker. Desthiobiotin (blue) was conjugated to TentaGel resin with the same linker structure used for experiments with biotin (red). Desthiobiotin has a lower affinity for streptavidin than biotin. We sought to determine if binding between NIR-labeled streptavidin and desthiobiotin could be observed with our screening method.

system. Fluorescence intensities that resulted from the labeled streptavidin binding desthiobiotin were visualized by zooming in on individual beads (**Figure 2.6A**). The fluorescence intensities were quantified and graphed (**Figure 2.6B**). Similar to biotin, differences in fluorescence intensities were clear and correlated to the amount of protein added to the well. Large amounts of protein resulted in higher fluorescence intensities, while lower amounts of protein resulted in weaker fluorescent signals. The limit of detection was similar to that observed with biotin, where binding could be reliably detected with as little as 0.01 ng of protein added to the well. Importantly, fluorescence intensities were generally lower for each amount of labeled streptavidin added to the well than the corresponding amount binding biotin. This further showed that differences in binding affinities between ligands and a target protein could be detected with this screening method.

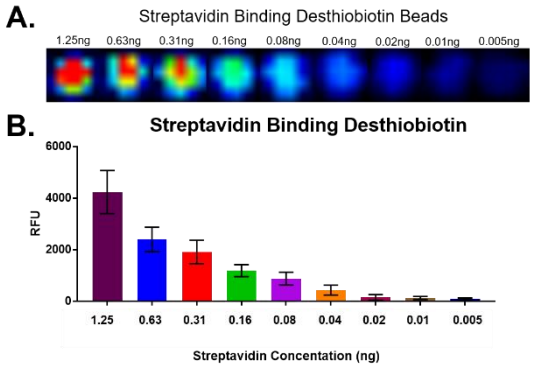

Figure 2.6 Detecting Binding of Varying Amounts of NIR-Labeled Streptavidin to Desthiobiotin On-Bead. Individual beads decorated with desthiobiotin were separated into the wells of a black 96-well plate with a clear bottom. The beads were blocked with protein blocking buffer. Then, NIR-labeled streptavidin was diluted in blocking buffer and varying amounts were added to the wells. After overnight incubation, the protein solution was removed, and beads were rinsed with PBS. The beads were resuspended in PBS and imaged for NIR fluorescence. (A) Individual beads were visualized by zooming in on the well. Clear differences in the fluorescence intensities were observed and correlated to the amount of protein added to each well. (B) Fluorescence intensities of each bead were quantified and graphed, further revealing that higher fluorescence intensities resulted from more protein added to the wells.

As a control to ensure binding of the labeled protein to the biotin and desthiobiotin resin was not the result of nonspecific interactions, 1.25 ng of labeled streptavidin was incubated with resin conjugated to the FLAG peptide. Since streptavidin is not known to interact with the FLAG peptide, we expected to find almost no fluorescence from the FLAG beads incubated with the labeled streptavidin. After incubation, the plate was rinsed, and the beads were analyzed for fluorescence. Fluorescence intensities were quantified and graphed and plotted with the values from labeled streptavidin binding with biotin and desthiobiotin (**Figure 2.7**). As expected, almost no binding between the FLAG peptide and labeled streptavidin was observed, indicating that the fluorescent signals are not the result of nonspecific binding between the labeled protein and the resin.

We demonstrated successful optimization of our screening assay using NIR-labeled streptavidin and two ligands, biotin and desthiobiotin. Varying concentrations of the labeled protein incubated with beads conjugated to one of the ligands. Clear differences in fluorescence intensities were observed. Higher fluorescence intensities correlated to larger amounts of protein added to the well. Likewise, differences in the intensities produced by the labeled protein binding biotin and desthiobiotin were observed. This suggested that differences in binding affinities between ligands and a protein could be detected with our screening method. Importantly, we showed that fluorescence intensities are dependent on the protein recognizing and binding the ligand, as almost no fluorescence was observed with labeled streptavidin incubating with a ligand (the FLAG peptide) that is not known to bind streptavidin.

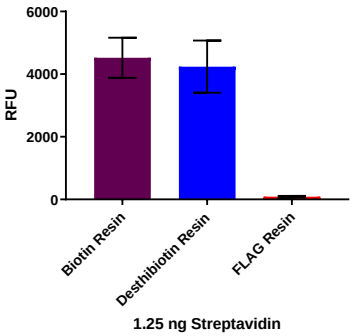

Figure 2.7 Binding of NIR-Labeled Streptavidin to the FLAG Peptide On-Bead. As a control to ensure that fluorescence intensities observed in our other experiments were not the result of nonspecific interactions between the labeled protein and bead, 1.25 ng of labeled streptavidin was incubated with beads conjugated to the FLAG peptide. This peptide should not be recognized by streptavidin. Fluorescence intensities that resulted from the labeled protein binding the peptide were quantified and graphed to compare to the signals produced by incubation 1.25 ng of labeled streptavidin with biotin and desthiobiotin. Almost no signal was observed with the FLAG peptide, indicating that nonspecific interactions were not responsible for the fluorescent signals

2.2.2 Monitoring Binding of NIR-Labeled Carbonic Anhydrase to Ligands of Varying Affinity

Although streptavidin binding to biotin and desthiobiotin served as a good model to optimize the conditions for our screening assay, binding between the protein and these ligands is among the strongest noncovalent interactions. As a result, we sought to test a protein with ligands that have more realistic binding affinities that could be detected in a screen against a target protein. We selected the carbonic anhydrase protein and three ligands with varying affinities, carboxybenzylsulfonamide (CBS), glycylleucine-CBS (GL-CBS), and aspartic acid-CBS (D-CBS).[20] Purified carbonic anhydrase was purchased

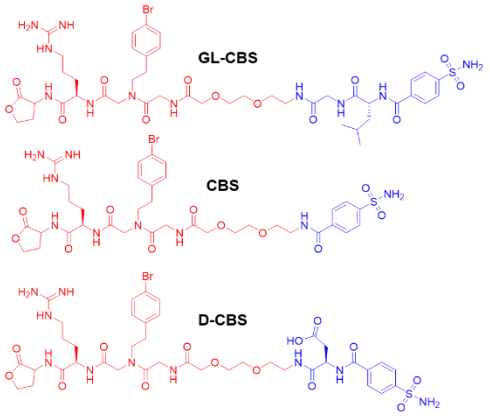

Figure 2.8 Structures of GL-CBS, CBS, and D-CBS. Each ligand (blue) was conjugated to TentaGel resin with the attached linker (red). GL-CBS has the highest affinity to carbonic anhydrase with a K_D of 120 nM. CBS has an affinity of 1.6 µM and D-CBS has an affinity of 4.6 µM.

and labeled with the NIR fluorophore. The resulting dye-to protein-ratio was calculated to be 1.8-to-1. The selected ligands had K_D's of 120 nM (GL-CBS), 1.6 µM (CBS), and 4.7 µM (D-CBS). Each ligand was conjugated to resin decorated with a linker structure similar to that used to screen streptavidin against biotin and desthiobiotin using standard solid phase synthesis (**Figure 2.8**). The mass of each ligand was confirmed by cleaving the product from a small amount of resin and subjecting it to LC/MS analysis. The resin was swollen in PBS prior to use.

Beads decorated with one of the three ligands were individually separated into the wells of a black 96-well plate with a clear bottom. The beads were then blocked with a protein blocking buffer. NIR-labeled carbonic anhydrase was diluted in blocking buffer, and varying amounts of protein ranging from 8.8 ng to 0.1 ng was added to the wells. After overnight incubation, the wells were rinsed with PBS to remove excess protein solution and the plate was imaged for NIR fluorescence (**Figure 2.9A**). We expected to observe similar results to streptavidin and biotin, such that higher fluorescence intensities would result when more labeled protein was added to the wells and lower fluorescence intensities would result when less labeled protein was added. In addition, we expected higher overall fluorescence intensities from the protein binding GL-CBS, as it has the highest affinity. Conversely, we expected lower fluorescence intensities resulting from the same amount of protein binding both the CBS and D-CBS ligand. This would suggest that the fluorescence intensities were dependent

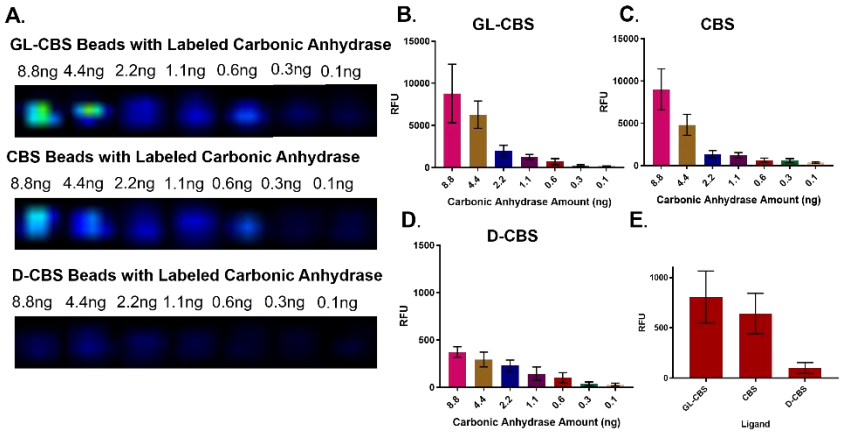

Figure 2.9 Detecting Binding of NIR-Labeled Carbonic Anhydrase with Ligands of Varying Affinity. (A) Resin decorated with GL-CBS, CBS, or D-CBS was split into the wells of a 96-well plate and blocked with protein blocking buffer. NIR-labeled carbonic anhydrase was then diluted in blocking buffer and varying amounts were added to the wells. After overnight incubation, the protein solution was removed, and the beads were rinsed with PBS. The plate was imaged for fluorescence and zoomed in pictures of individual beads were observed. Clear differences in fluorescence were observed. GL-CBS produced the highest fluorescence intensities at each amount of protein tested while D-CBS produced the lowest. (B-D) The fluorescence intensities resulting the labeled protein binding each ligand was quantified and graphed. This further demonstrated that the binding affinities correlated to the fluorescence intensities, with the GL-CBS ligand producing higher fluorescence intensities than the CBS and D-CBS ligand. (E) The fluorescent signal that resulted from 0.6 ng of carbonic anhydrase binding each ligand were compared. It is apparent that the GL-CBS ligand produced the highest fluorescence intensity, as it has the highest affinity to the protein. Likewise, D-CBS produced the lowest fluorescence intensity and had the lowest affinity to the protein.

on the affinity of the ligand to the protein. The resulting fluorescence intensities were quantified for each ligand and graphed (**Figure 2.9B-D**). Excitingly, not only did we observe differences in fluorescence intensities that correlated with the amount of protein added to the well, but clear differences in intensities resulting from the same amount of protein binding one of the three ligands was evident. When comparing the signal produced from each ligand after adding 0.6 ng of labeled carbonic anhydrase, the difference in the binding affinity for each ligand was obvious, especially when comparing signal from the GL-CBS and D-CBS ligand (**Figure 2.9E**). Since differences in fluorescence intensities correlated to the affinity of the ligands, with the highest affinity ligand producing the highest fluorescence intensities and lowest affinity ligand producing the lowest intensities, we concluded that this screening method could be used to detect ligands of varying affinity to a protein of interest.

As a control, labeled carbonic anhydrase incubated with resin conjugated to the FLAG peptide. No interaction is known for this protein-ligand combination, so we expected to see very little fluorescence. The final amount of protein added to the well was 17 ng. The fluorescence intensities were then quantified and compared to wells in which 17 ng of labeled protein was added to GL-CBS resin. As expected, almost no fluorescence was detected in response to adding labeled carbonic anhydrase to the wells containing the FLAG peptide (**Figure 2.10**). This suggested that binding between the labeled protein and the ligand was not the result of nonspecific binding.

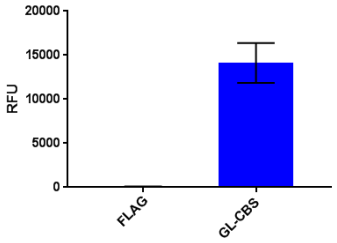

Figure 2.10 Binding of NIR-Labeled Carbonic Anhydrase to the FLAG Peptide on Resin. 17 ng of labeled carbonic anhydrase incubated with beads conjugated to the FLAG peptide or GL-CBS. After overnight incubation, the protein solution was removed, and the beads were rinsed with PBS. The plate was imaged for fluorescence and the resulting fluorescence intensities were quantified and graphed. Almost no binding of the labeled protein to the FLAG resin was detected.

We initially wanted to test binding of carbonic anhydrase to the ligands of varying affinity to ensure that we could monitor binding of protein-ligand pairs with weaker affinities than biotin and streptavidin. We chose carbonic anhydrase because it had three ligands with varying affinities, GL-CBS, CBS, and D-CBS. When varying amounts of labeled protein incubated with beads conjugated to one of the three ligands, clear differences in fluorescence intensities were observed. Not only did fluorescence intensities correlate with the amount of protein added to the well, but more importantly, differences in the fluorescence resulting from the same amount of protein binding each ligand were apparent. In general, binding of the protein to GL-CBS produced the

highest fluorescence intensities of all the ligands and D-CBS resulted in the lowest fluorescence intensities. Almost no binding of carbonic anhydrase to the FLAG peptide was detected, indicating that fluorescence is not the result of nonspecific binding between the protein and the ligand. This data indicated that differences in binding affinities between a protein and ligand correlate to the fluorescence intensity and can be detected with our screening method.

2.2.3 Screening NIR-Labeled Gankyrin Against a Covalent OBOC Library

After optimizing our assay conditions with fluorescently labeled streptavidin and biotin on resin and determining binding of ligands of varying affinity to carbonic anhydrase could be detected with our new screening method, we next wanted to screen a protein of interest against an OBOC library. Since we wanted to highlight the applicability of our assay to screen proteins with no known enzymatic function, we selected gankyrin as our target protein. Gankyrin is an oncoprotein that is overexpressed in a variety of cancers including liver,[21] breast,[22,23] and colorectal.[24,25] In normal cells, gankyrin is known to interact with the S6 ATPase subunit of the 19S regulatory particle of the proteasome.[26,27] When gankyrin is overexpressed, it forms protein-protein interactions with the E3 ligase MDM2 which promotes ubiquitination and subsequent degradation of p53, a key cell cycle-regulating protein.[28] Overexpression of gankyrin also leads to increased degradation of retinoblastoma protein, another protein that is critical in cell cycle regulation.[29] Since these interactions drive cell cycle dysregulation and cancer progression, some research groups have turned their attention to better characterizing gankyrin and evaluating it as a therapeutic target for some cancers. This has led to the discovery of a small molecule binder of gankyrin.[30] p53 stabilization was observed when cells transfected with gankyrin were dosed with this small molecule, highlighting gankyrin's potential as a therapeutic target. In an effort to discover more small molecule binders of gankyrin that could potentially be developed into probes to

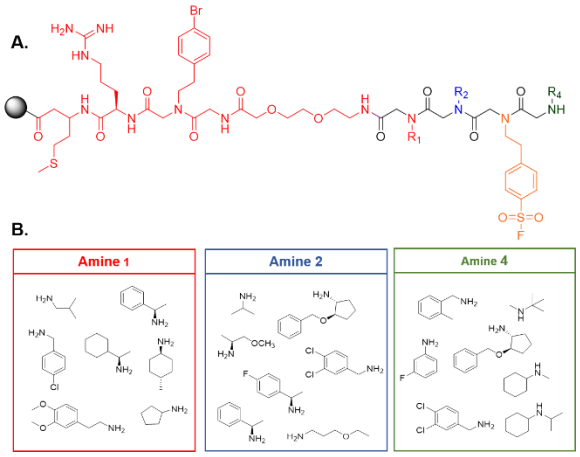

Figure 2.11 OBOC Library Design. (A) Scaffold of the OBOC library including the linker (red) and all amine positions. (B) Amines were selected randomly for positions one, two and four. Position three only housed one amine, 4-(2-aminoethyl)benzensulfonyl fluoride, which facilitates covalent binding to serine and threonine amino acid residues via a sulfonyl fluoride moiety.

monitor its expression and activity, we screened an OBOC library against gankyrin.[31]

Our 343-member peptoid OBOC library consisted of four positions with one of seven amines. We selected to screen a peptoid library over a peptide library because peptoids are more resistant to cleavage by proteases in the cell.[32] Since we hoped to eventually use hits from this screen for in-cell applications, peptoids were selected over peptides. A linker structure similar to that used in the carbonic anhydrase experiments was first synthesized on the resin (**Figure 2.11A**). This linker would allow us to identify the peptoids on hit beads after the screen by MALDI-TOF. The library was synthesized using the split and pool method and standard solid phase synthesis. Positions one, two, and four consisted of randomly selected amines (**Figure 2.11B**). Position three was only composed of one amine that housed a sulfonyl fluoride moiety that facilitates covalent binding to amino acid residues such as threonine and serine.[33] Analysis of gankyrin's amino acid sequence revealed it has several serine and threonine residues that could covalently interact with the peptoids on-bead.

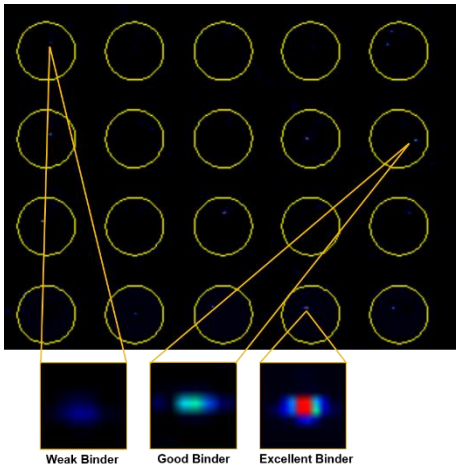

Figure 2.12 OBOC Library Design. (A) Scaffold of the OBOC library including the linker (red) and all amine positions. (B) Amines were selected randomly for positions one, two and four. Position three only housed one amine, 4-(2-aminoethyl)benzensulfonyl fluoride, which facilitates covalent binding to serine and threonine amino acid residues via a sulfonyl fluoride moiety.

Gankyrin was purified through bacterial expression as described in the Materials and Methods section. The protein was then labeled with the NIR-emitting fluorophore. The protein solution was aliquoted and stored at -20 ˚C until use. Beads were swollen in PBS and then individually separated into the wells of a black 96-well plate with a clear bottom. Beads were blocked with protein blocking buffer. NIR-labeled gankyrin was diluted in blocking buffer, and 0.6 ng was added to each well. Protein incubated with the beads overnight, and then the beads were rinsed with PBS. The plate was imaged for NIR fluorescence with a LI-COR Odyssey CLx imaging system (**Figure 2.12**).[31] The resolution was set to 81 µm to facilitate better visualization of the beads which were an average of 90 µm. Fluorescence intensities that resulted from the labeled gankyrin binding the small molecules on-bead were analyzed by viewing zoomed-in images of the bead (**Figure 2.12**). Clear differences in fluorescence intensities were observed. Some beads displayed very high fluorescence, indicating that a large amount of protein had bound the small molecule. Conversely,

some beads produced very little fluorescence, suggesting that gankyrin was unable to significantly bind the small molecule.

Two screens of 424 beads against gankyrin were performed. Since our library consist of 343 members, we screened 424 beads, which accounts for a 23% overage to ensure statistically that the entire library would be covered in the screens. The fluorescence intensities that resulted from the labeled protein binding the small molecules on-bead were quantified and ranked. The top 5% of fluorescence intensities from each screen were selected as our initial hits, which produced a total of 42 hits per screen. The structures of the hits from each screen were identified by MALDI-TOF analysis (**Appendix A**). When comparing the hit structures between both screens, we noted that several structures overlapped, with similar amines in similar positions. Since these amines appeared in multiple structures, we reasoned that they were likely important for binding to gankyrin. A total of 10 overlapping structures were selected for further investigation and validation.

2.2.4 Validation of Hits from the OBOC Screen

After identifying 10 structures as our initial hits, we next sought to validate their binding to gankyrin. Since the interaction between the ligands and gankyrin is covalent, we reasoned that it could withstand SDS-PAGE analysis and used an in-gel fluorescence assay to confirm binding of the fluorescently labeled ligands to gankyrin. Samples were then subjected to SDS-PAGE analysis, and the gel was imaged for fluorescence. To do this, we synthesized the ligands on a linker with a monomethoxytrityl (MMT)-protected cysteine residue where fluorescein could be attached via a maleimide group. After synthesis of each of the ten ligands was complete, the MMT group was removed, and fluorescein was conjugated to the linker to fluorescently label the ligands (**Figure 2.13A**).[31] Importantly, a negative control was also synthesized which was composed of amines that were present in the initial screen but were not observed in any of the hit structures (**Figure 2.13A**). This control still contained the sulfonyl fluoride moiety, therefore some binding of the negative control to gankyrin was anticipated. All fluorescent peptoids were purified by high performance liquid chromatography (HPLC), and purity was determined by LC/MS analysis (**Appendix B**). Fractions containing pure product were lyophilized and stored at -20 ˚C protected from light until use.

Gankyrin was purified as described in the Materials and Methods section and was stored at 4 ˚C for up to three days before use. Fluorescently labeled ligands and the negative control were

diluted in dimethyl sulfoxide (DMSO) such that the final concentration in the samples would range from 20 to 0.1 µM. Then, the ligands incubated with purified gankyrin. After incubation, the reaction was quenched by adding laemmli buffer and heating. Samples were subjected to SDS-PAGE and imaged for fluorescence. We anticipated that the ligands would bind gankyrin and result in a fluorescent band in the gel. Moreover, validated hits would produce higher fluorescence intensities at each concentration tested when compared to the negative control. This would suggest that the amines that composed each ligand were important to binding gankyrin, not only the sulfonyl fluoride moiety. Fluorescence intensities from the bands that resulted from the labeled ligands covalently binding gankyrin were quantified and graphed (**Appendix C**).

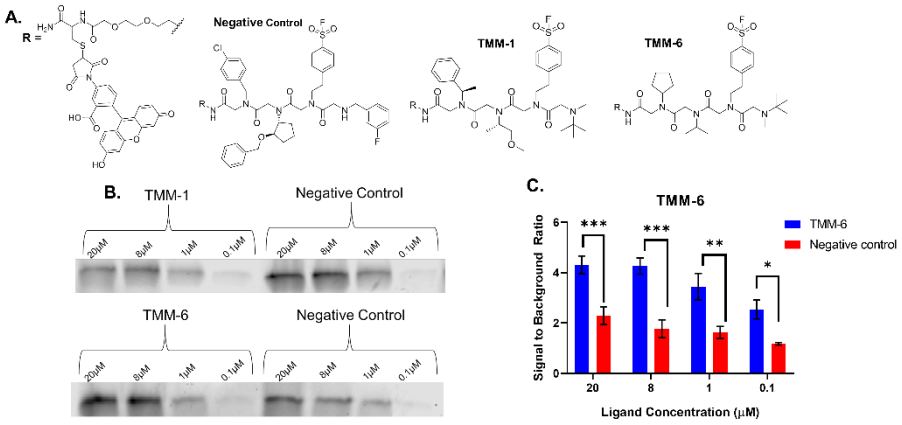

Figure 2.13 Validating Hits from Screening Gankyrin Against an OBOC. (A) Structures of the linker conjugated to fluorescein, the negative control ligand, and two example structures of ligands being validated. (B) Varying concentrations of the fluorescently labeled ligands or the negative control incubated with 500 ng of purified gankyrin. The samples were then subjected to SDS-PAGE, and the gels were imaged for fluorescence. TMM-1 did not validate because it produced less intense bands than the negative control. TMM-6, however, did validate because the fluorescence intensities at each concentration tested were higher than the negative control. (C) This experiment was repeated in experimental triplicate. As a control, one sample containing only DMSO was used run on each gel so the data could be normalized. The fluorescent signal for each gel was normalized to the DMSO control and the resulting number from each run at each concentration were compiled and graphed. This revealed that TMM-6 produced statistically significantly higher fluorescence intensities at each concentration tested than the negative control, confirming it as a true hit. * $p < 0.05$, ** $p < 0.01$, *** $p < 0.001$

Most of our hits did not validate, such as TMM-1, because they did not produce fluorescence intensities that were higher than those produced by the negative control (**Figure 2.13B**). However, one hit, TMM-6, did produce higher fluorescence intensities than the negative control (**Figure 2.13B**). Initially, this assay was performed in singlet with all then ligands. We repeated the assay in experimental triplicate with TMM-6 to ensure our initial result was valid. As a control, one sample of gankyrin that was DMSO-dosed was included during each replicate. Fluorescent signal from the bands corresponding to gankyrin bound to TMM-6 were normalized by dividing all values by the intensity produced by the DMSO lane. The values that resulted from

each trial at each concentration were compiled and graphed (**Figure 2.13C**). This revealed that TMM-6 produced statistically significant higher fluorescence intensities than the negative control at every concentration tested, rendering it a valid hit.

We next wanted to be certain that the fluorescein tag was not responsible for the binding of TMM-6 to gankyrin. A nonfluorescent version of TMM-6 was synthesized to perform a competition experiment. Either fluorescently labeled or unlabeled TMM-6 incubated with purified gankyrin. After one hour, the other ligand was added and incubated for an additional hour. Samples were then quenched with laemmli buffer and heating and analyzed by SDS-PAGE. We expected that addition of the nonfluorescent ligand followed by the fluorescent ligand would result in lower fluorescence intensities because the unlabeled ligand would bind most of the gankyrin the sample and prevent binding of fluorescently labeled TMM-6. Conversely, we expected high fluorescence intensities to result from the addition of the fluorescent ligand first. The gel was imaged for fluorescence, and the fluorescence intensities of the resulting bands were quantified (**Figure 2.14**).[31] We observed significantly lower signal from the samples in which the nonfluorescent TMM-6 was added first. This indicated that the fluorescein tag was not responsible for binding of the ligand to gankyrin.

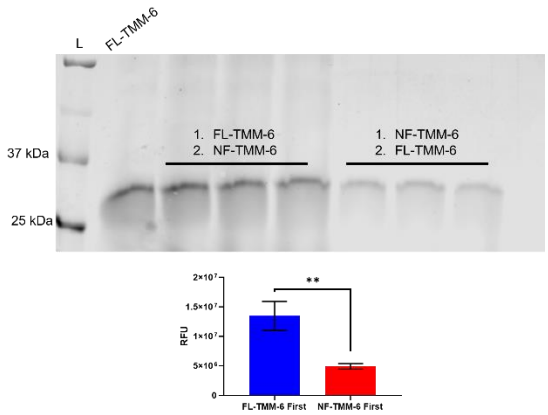

Figure 2.14 Competition of Fluorescent and Nonfluorescent TMM-6 Binding Gankyrin. A competition experiment in which either fluorescent (FL-TMM-6) or nonfluorescent TMM-6 (NF-TMM-6) was first added to purified gankyrin followed by addition of the other ligand was performed to ensure the fluorescein tag was not responsible for binding of the peptoid to the protein. As a control, one sample incubated with only FL-TMM-6. After subjecting the samples to SDS-PAGE, the fluorescent signal was quantitated and graphed. This revealed addition of NF-TMM-6 first resulted in significantly lower fluorescence intensities than adding the fluorescent TMM-6 first. This suggests that the fluorescein tag is not responsible for binding of the ligand to the protein.

We next sought to ensure that binding between TMM-6 and gankyrin was the result of covalent linkage of the ligand to the protein and no other nonspecific interactions. To do this, we synthesized a noncovalent version of TMM-6 in which the 4-(2-aminoethyl)benzensulfonyl fluoride was exchanged for 2-phenylethylamine. This amine is very similar in structure but does not possess the sulfonyl fluoride and should therefore not covalently bind to gankyrin. The noncovalent ligand was synthesized on the fluorescein linker. Next, covalent or noncovalent TMM-6 was incubated with purified gankyrin at concentrations ranging from 20-0.1 µM and

subjected to SDS-PAGE (**Figure 2.15**).[31] We expected that the complex of noncovalent TMM-6 and gankyrin would fall apart in the gel during SDS-PAGE and result in very low fluorescence intensities. Conversely, we expected to see bands with high fluorescence intensities result from samples that were incubated with the covalent TMM-6 since its interaction with gankyrin should withstand SDS-PAGE. The experiment was conducted in triplicate, and the resulting bands from each concentration were quantified/normalized to the signal produced by a control that consisted of only DMSO-dosed gankyrin. The data was then graphed and revealed that incubation of gankyrin with the noncovalent TMM-6 resulted in statistically significant lower fluorescence intensities than incubation with the covalent ligand (**Figure 2.15**). This indicates that covalent attachment of the ligand to the protein is responsible for binding that can withstand SDS-PAGE, and binding is not the result of nonspecific interactions.

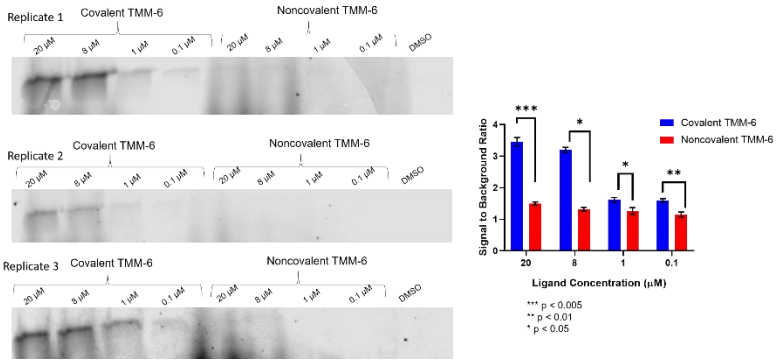

Figure 2.15 Binding of Covalent and Noncovalent TMM-6 to Gankyrin. A fluorescent noncovalent version of TMM-6 was synthesized by exchanging the 4-(2-aminoethyl)benzensulfonyl fluoride for 2-phenylethylamine. Varying concentrations of covalent or noncovalent TMM-6 incubated with 500 ng of purified gankyrin and was then subjected to SDS-PAGE (left). The experiment was conducted in triplicate. The resulting fluorescence intensities were quantified and normalized to a control consisting of only DMSO-treated gankyrin. The resulting data was combined for each concentration to produce a triplicate and graphed (right). This revealed that incubation of noncovalent TMM-6 with gankyrin resulted in statistically significantly lower fluorescence intensities than incubation with the covalent ligand. This suggests that covalent binding between the ligand and the target is required to visualize by SDS-PAGE and the resulting fluorescent bands are not the result of nonspecific interactions between the ligand and protein.

Because the sulfonyl fluoride on TMM-6 nonspecifically interacts with serine and threonine amino acid residues, we sought to determine the specificity of the ligand to gankyrin. To do this, we conducted a pulldown experiment in human embryonic kidney (HEK) 293T cell lysate was spiked with purified gankyrin. Gankyrin was added to the lysate at a final concentration of 1% of the total protein amount. Then, fluorescently labeled TMM-6 or the negative control used in our in-gel validation experiments was added to the samples such that the final concentration was 8 µM. After incubation, laemmli buffer was added to the samples and they were subjected to SDS-PAGE. The gel was then imaged for fluorescence. We expected to find bands varying in molecular weight and fluorescence intensity, as some nonspecific binding of TMM-6 to other proteins via the

sulfonyl fluoride moiety would occur. However, we expected to find one strong fluorescent band corresponding to the molecular weight of gankyrin. Imaging of the gel revealed two intense fluorescent bands (**Figure 2.16A**).[31] These bands were present in the lysate dosed with TMM-6 but not to the same extent as the lysate dosed with the negative control. These bands were excised from the gel by cutting with a clean razor blade and placed in a clean tube. The gel was rescanned to ensure the bands were fully excised. The resulting gel pieces were sent to the Purdue Proteomics Facility for protein identification. Excitingly, gankyrin was revealed to be the most abundant protein in both bands. Not only did proteomics analysis show moderate sequence coverage of gankyrin, but both bands had high MS/MS counts of 43 and 45, respectively (**Figure 2.16B**). Other fluorescent bands were observed in both the TMM-6 and negative control dosed lysate, indicating that there is some nonspecific binding of TMM-6 to other proteins. However, the most intense fluorescent bands were composed primarily of gankyrin, indicating that TMM-6 has moderate specificity. It is not known why two bands were observed that were composed of gankyrin since purified gankyrin was added directly to the lysate. It is possible that band A, which has a higher molecular weight than band B, was modified by other enzymes in the lysate.

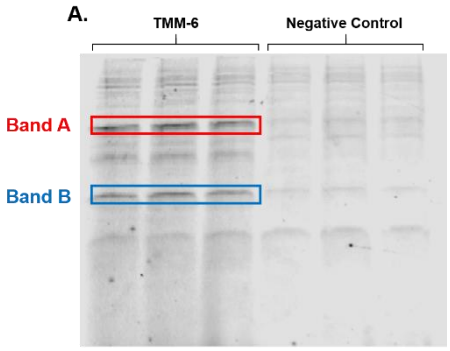

B.

	Band A	Band B
Gankyrin Sequence Coverage	60.6%	49.6%
MS/MS Count	43	45

Figure 2.16 Pulldown of Gankyrin in Spiked HEK 293T Cell Lysate. HEK 293T cells were lysed, and 500 ng of purified gankyrin was added to the samples. The final gankyrin concentration was 1% of the total protein amount. Fluorescent TMM-6 or negative control was added to the samples at a final concentration of 8 µM. (A) Samples were then subjected to SDS-PAGE and the gel was imaged for fluorescence. Several fluorescent bands were observed; however, two intense bands were most obvious (Band A and Band B). These bands were excised for proteomics analysis. (B) Proteomics analysis revealed that both bands were composed primarily of gankyrin. Modest sequence coverage of 60.6% (Band A) and 49.6% (Band B). Additionally, high MS/MS counts of 43 and 45 were found as well. Other fluorescent bands were observed, indicating some nonspecific binding to TMM-6, but this peptoid binds gankyrin with moderate specificity.

To our knowledge, TMM-6 is the first reported covalent binder of gankyrin. Further work is needed to understand its implications in cancer cell lines that are known to overexpress gankyrin. Similarly, TMM-6 could be developed into a probe to monitor expression of gankyrin during cancer onset and progression by attachment of a fluorophore like the experiments performed in the validation of ligands binding pure gankyrin. TMM-6 bound gankyrin with moderate specificity in a pulldown in which HEK 293T cell lysate was spiked with purified protein, suggesting that off-

target binding could be limited. TMM-6 could emerge as an important tool to better understand the implications of gankyrin in cancer and evaluate it as a therapeutic target for some cancers.

2.2.5 Establishing Conditions to Detected a FLAG Antibody Binding the FLAG Peptide Conjugated to Resin

After successfully establishing screening conditions for a protein target against an OBOC library, we next turned our attention to the possibility of detecting antibodies with this assay. Several autoimmune disorders are characterized by overexpression of antibodies that lead to attack on the body's own tissues.[34,35] Sensitive detection of these antibodies could facilitate better diagnosis of autoimmune disorders. Similarly, screening these antibodies for new small molecule binders could lead to the development of a better understanding of the impacts of antibody production during autoimmunity and better therapies to treat these diseases. Screening samples for antibodies relevant for diagnostic purposes are often limited to the use of microarrays, in which the chemical diversity of ligands is significantly restrained to what can be conjugated to a glass slide or well plate.[36] As a result, there remains a need for better tools to screen antibodies against a wide variety of ligands. This will facilitate a deeper understanding of autoimmunity.

We hypothesized that our OBOC screening method could be adapted to detect and screen antibodies of interest. Individual beads of an OBOC library or ligand known to interact with a target antibody conjugated to resin could be split into the wells of a 96-well plate and blocked. Next, a pure antibody of interest, or a sample containing a target antibody, such as blood serum, could be added to the wells and incubate with the small molecule on-bead. After incubation, the beads could be rinsed and a fluorescently labeled secondary antibody could then be added to detect the presence of the target antibody. After washing the plate to remove excess secondary antibody, the plate could then be imaged for fluorescence and fluorescence intensities could be quantified. If an antibody were screened, hits could then be ranked to expedite the validation process. Similarly, if we sought to detect the presence of an antibody in a sample, a fluorescent signal would signify that the target antibody is present. This could expedite the process of diagnosing autoimmune disorders.

To establish conditions to screen antibodies against an OBOC library, we wanted to choose an antibody-ligand combination that was well characterized. The FLAG peptide is commonly used

to tag proteins of interest during purification and represented an ideal ligand for the optimization of our assay. The FLAG antibody is commercially available and served as our target antibody. We first synthesized the FLAG peptide on TentaGel resin conjugated to the linker structure used for our OBOC library screen against gankyrin (**Figure 2.17**). Since the long-term goal of this method is to screen antibodies against OBOC libraries, it is important to include the linker that will facilitate identification of the ligands post-screen. As a control, a scrambled version of the FLAG peptide was also synthesized. We hypothesized that the FLAG antibody would be unable to recognize the scrambled sequence and should therefore not bind, providing a negative control for our optimization experiments (**Figure 2.17**). The linker and peptides were synthesized with standard solid phase peptide synthesis, and the identity was confirmed by LC/MS prior to use. The resin was swollen in PBS prior to use.

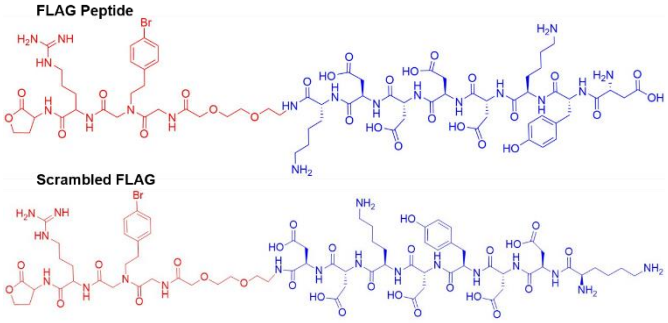

Figure 2.17 Structures of the FLAG and Scrambled FLAG Sequence. A linker (red) and the FLAG or scrambled FLAG peptide (blue) were synthesized on TentaGel resin. The FLAG peptide served as our model ligand for detection of the FLAG antibody in a protein solution. The scrambled FLAG peptide served as a negative control, as it should not be recognized by the antibody.

FLAG beads or scrambled FLAG beads were individually separated into the wells of a 96-well plate and blocked with protein blocking buffer. Next, a FLAG antibody was diluted in blocking buffer and varying amounts ranging from 12.5-0.1 ng were added to the wells. After overnight incubation, the antibody solution was removed, and the beads were washed with PBS. A fluorescently labeled secondary antibody was diluted in blocking buffer and 50 ng was added to the wells. The excess antibody was removed, the beads were rinsed with PBS and the plate was imaged for NIR fluorescence. Zoomed in pictures of the beads were examined (**Figure 2.18A**). The fluorescence intensities that resulted from the fluorescently labeled secondary antibody binding the primary antibody attached to the FLAG peptide on resin were quantified and graphed (**Figure 2.18B**). It was apparent that the fluorescent signal increased with increasing amounts of primary antibody. Addition of 12.5 ng and 6.3 ng nearly saturated the detector. Importantly, even when as little as 0.1 ng of primary antibody was added to the well (average signal of 68 RFU), the signal was still six times higher than background signal produced by incubating the antibodies in wells that did not contain beads (average signal of 10 RFU). Almost no binding of the primary

antibody to the scrambled FLAG peptide was observed after addition of the secondary antibody, suggesting nonspecific binding of the primary antibody to the resin was not responsible for the fluorescent signal (**Figure 2.18B**).

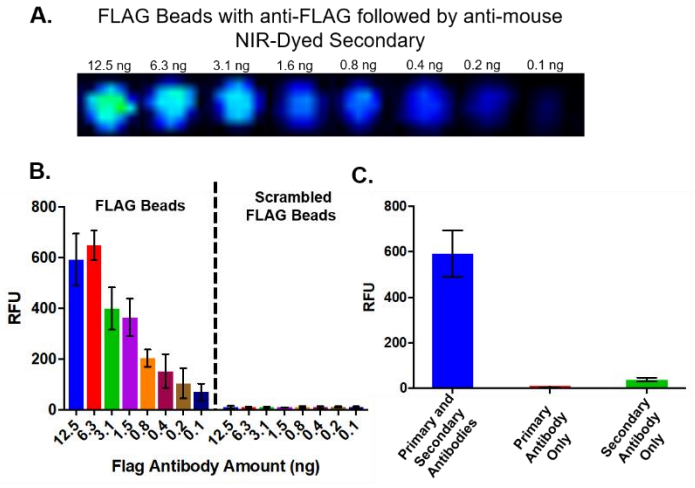

Figure 2.18 Detection of a FLAG Antibody Binding the FLAG Peptide on Resin with a Fluorescently Labeled Secondary Antibody. Resin conjugated to the FLAG and scrambled FLAG peptide were separated into a 96-well plate and varying amounts of a FLAG antibody were added to the wells. A fixed amount of fluorescently labeled secondary antibody was then added. The beads were rinsed and plate was imaged for NIR fluorescence. (A) Individual beads were visualized. Addition of more primary antibody to the well resulted in higher fluorescence intensities, indicating that more FLAG antibody had bound the bead. (B) The fluorescence intensities produced by FLAG and scrambled FLAG resin were graphed. This further confirmed that adding more primary antibody to the FLAG resin resulted in higher fluorescence intensities. Importantly, no binding of the FLAG antibody to the scrambled FLAG resin was observed. This indicated that the fluorescent signal was dependent on the primary antibody recognizing and binding the sequence on resin. (C) As a control, 12.5 ng of primary antibody or a fixed amount of fluorescently labeled secondary antibody were individually incubated with FLAG resin. Very little fluorescent signal was observed from either antibody incubating with the beads, suggesting that nonspecific interactions between the antibodies and the resin were not responsible for the observed fluorescent signal.

To further evaluate the extent of nonspecific binding of both the primary and secondary antibody to the bead, FLAG resin was incubated with each antibody independently, the plate was imaged for fluorescence, and the fluorescence intensities were quantified (**Figure 2.18C**). Essentially no signal was produced as result of incubating the primary FLAG antibody with the resin. Similarly, very little signal was produced from incubating the fluorescently labeled secondary antibody with the FLAG resin. This further suggested that the fluorescent signal resulted from a combination of the primary and secondary antibody. Moreover, fluorescent signal also depends on the primary antibody recognizing the sequence on-bead, as the almost no fluorescent signal was observed after incubating scrambled FLAG beads with the antibodies.

2.3 Conclusions

Although the development of OBOC libraries has made the process of synthesizing thousands of small molecules streamline and cost effective, progress lags in the ability to screen these libraries against target proteins. Common screening techniques are not quantitative and

require strong binding between the biological target and small molecule.[13,14,37] This makes the process of validating hits lengthy and cumbersome. Some research groups have turned attention to developing more quantitative OBOC screening methods that utilize fluorophores. These methods generally involve conjugating a fluorophore to a protein before or after it has bound ligands of the OBOC library.[9–11] Beads can then be visualized with a confocal microscope. While these methods do provide more quantitative screening options for OBOC libraries, the fluorophores used in these techniques often overlap with autofluorescence produced by the bead or the protein, making data deconvolution difficult. As a result, there is a new interest in the use of NIR fluorophores, as they emit at wavelengths longer than those associated with autofluorescence.

In an effort to build upon currently available quantitative screening techniques and create a screening method that is amendable to a wide variety of proteins, we developed an OBOC screening method that entails labeling a target protein with a NIR-emitting fluorophore. The labeled protein is then incubated with beads of an OBOC library. The beads are rinsed, and the plate is imaged for fluorescence. Fluorescence intensities that result from the labeled protein binding the ligands on-bead can be quantified and provide a basis to rank hits. Since this method does not rely on the function of the protein being known for screening, the types of proteins that can be screened are vast. Similarly, because the fluorophore is conjugated to the N-terminus of the protein via a NHS ester moiety, it can readily be attached to many types of proteins.

We optimized conditions for this screening method by synthesizing biotin and desthiobiotin on resin and monitored binding of NIR-labeled streptavidin. We found that addition of more streptavidin led to higher fluorescent signals. In general, fluorescence intensities that resulted from streptavidin binding biotin were higher than those produced by the protein binding desthiobiotin. Since the affinity of streptavidin to biotin is higher than its affinity to desthiobitoin, this suggested that our method could be used to detect differences in binding affinities of a protein to a ligand. Additionally, we screened NIR-labeled carbonic anhydrase against three ligands with varying affinities: GL-CBS , CBS, and D-CBS. These affinities ranged from 120 nM to 4.7 µM and are much more realistic to the types of affinities that would be detected in a screen. Excitingly, clear differences in the fluorescence intensities that resulted from the labeled protein binding each ligand were observed, with the highest affinity ligand (GL-CBS) producing the highest fluorescence intensities. From this, we concluded that this assay could readily detect differences

in binding affinities of a ligand to a target protein and that fluorescence output correlated to binding affinity.

We then screened a 343-member OBOC library that contained a covalent amine against our protein of interest, gankyrin. We selected gankyrin as a target because it has no known enzymatic function and its overexpression drives progression of some cancers.[28,29] This yielded ten hits that were validated with an in-gel fluorescence assay. One hit validated, TMM-6, and demonstrated modest specificity to gankyrin in a pulldown experiment in which HEK 293T cell lysate was spiked with the purified protein. To the best of our knowledge, TMM-6 is the first reported covalent binder of gankyrin. This screen demonstrates the first successful use of our OBOC screening technique to identify ligands to a protein with no enzymatic function. We are hopeful that in the future, TMM-6 could be developed into a probe to monitor gankyrin expression in cancer onset and progression. This will improve understanding of gankyrin as a therapeutic target for some forms of cancer. The impacts of TMM-6 on degradation of p53 and retinoblastoma protein, two cell cycle-regulating proteins that are degraded as a result of gankyrin overexpression, are still being elucidated.

Finally, we established conditions to detect and screen antibodies with our OBOC screening method. Many autoimmune disorders are characterized by overexpression of antibodies. Screening these antibodies for small molecule binders could lead to the development of probes to monitor autoimmune disorder progression. The framework for a screen against a target antibody was created using the FLAG peptide and a FLAG antibody. When varying amounts of the FLAG antibody were incubated with beads conjugated to the FLAG peptide followed by a fixed concentration of fluorescently labeled secondary antibody, clear differences in fluorescence were observed. Higher fluorescence intensities were produced by adding more primary antibody to the well, indicating that fluorescence correlated with the amount of antibody present. Importantly, almost no signal was observed when the antibody was incubated with a scrambled FLAG sequence. As little as 0.1 ng of antibody could be detected with our assay, which rivals the sensitivity of commercially available ELISA assays. From this, we concluded that this assay could be used to screen antibodies implicated in autoimmune disorders for new ligands. Similarly, in the future, this technology could be expanded into a diagnostic tool. A ligand to a target antibody could be synthesized on-bead. Then, samples such as blood serum could be incubated with the bead. If a fluorescent signal results from the addition of a labeled secondary antibody, this could provide

evidence that an antibody is present in the sample and assist doctors in diagnosing autoimmune disorders.

2.4 Materials and Methods

2.4.1 General Materials and Methods

All peptides were synthesized on TentaGel resin using solid-phase peptide synthesis and reactions were carried out in fritted syringes (purchased from Henke Sass Wolfe). 90μm TentaGel S NH2 resin was purchased from Rapp Polymere. Fmoc-protected natural amino acids were purchased from Novabiochem. HBTU was purchased from Oakwood Chemical and HOBt Hydrate was purchased from Creosalus. N,N-Dimethylformamide (DMF) and Dichloromethane (DCM) were purchased from Fisher Scientific. N,N-Diisopropylethylamine (DIPEA) was purchased from Fisher Scientific. Piperdine was purchased from Sigma Aldrich. Biotin was purchased from Thermo Fisher Scientific and desthiobiotin was purchased from Sigma Aldrich. Streptavidin was purchased from Sigma Aldrich. After synthesis was complete, peptides were cleaved from resin using cyanogen bromide purchased from Sigma Aldrich and identities were confirmed using an Agilent single quadrupole LC/MS system. Assays were visualized on a LI-COR Odyssey® CLx imaging System.

A gankyrin plasmid for bacterial expression was purchased from Addgene and used for expression and purification of the protein (Cat. Number 31332). Plasmid DNA was extracted with a mini-prep kit purchased from Qiagen. DNA was introduced to Rosetta (DE3) Competent cells purchased from Invitrogen. Bacteria was cultured in Luria-Bertani (LB) broth purchased from Fisher Scientific supplemented with ampicillin and chloramphenicol purchased from GoldBio and Fisher Scientific, respectively. Protein was captured with HisPur™ Ni-NTA resin and eluted with imidazole both purchased from Fisher Scientific. Gankyrin was labeled with a NIR-emitting Fluorophore with an IRDye® 800CW NHS Ester Kit purchased from LI-COR (Cat. Number 928-38042). NIR-labeled protein was aliquoted and stored a -20 ˚C and only thawed immediately before use. Labeled protein was diluted in Intercept (PBS) Blocking Buffer purchased from LI-COR for screening.

Screening was conducted in black 96-well plates with a clear bottom purchased from Fisher Scientific (Cat. Number 265301). After OBOC library beads were individually separated into the

wells of the plate, they were blocked with StartBlock™ (PBS) blocking buffer purchased from ThermoFisher Scientific. Fluorescence intensities were quantified using ImagesStudio software from LI-COR. Hit peptoids were cleaved from the resin using cyanogen bromide that was purchased from Sigma-Aldrich. Identity of the hit peptoid was determined with a Sciex 4800 MALDI TOF/TOF instrument.

HEK 293T cells were maintained in Dulbecco's Modified Eagle Medium purchased from Corning. Cells were lysed with MPER purchased from Fisher Scientific. Gels from SDS-PAGE for cell culture studies and the in-gel fluorescence studies were imaged on a Sapphire Biomolecular Imager from Azure. Fluorescence intensities were quantified using ImageStudio software from LI-COR.

2.4.2 Synthesis of Ligands on Resin and Establishing Screening Conditions

2.4.2.1 Linker Synthesis

100 mg of 90 µm TentaGel S NH2 resin was swollen in DMF for 1 hour followed by DCM for 1 hour. The terminal fmoc was removed by adding 2 mL of a 20% piperdine solution in DMF to the resin and allowing it to agitate for 20 minutes at room temperature. A Kaiser test was performed to ensure successful removal of the fmoc and the resin was rinsed three times with DMF followed by three times with DCM. HBTU (4.5 equiv.), HOBt (4.4 equiv.), and Fmoc-methionine-OH (5 equiv.) were premixed in 600 µL of DMF. After dissolving, 10 equiv. of DIPEA was added and the solution was added to the resin. This coupled to the resin for 30 minutes at 37 ˚C with agitation. The solution was drained, and the resin was rinsed with DMF and DCM. A Kaiser test was performed, producing a negative result to indicate full coupling of the amino acid to the resin. Fmoc was removed by adding 2 mL of a 20% piperdine solution to the resin and allowing it to agitate for 20 minutes at room temperature then the resin was rinsed with DMF followed by DCM. A Kaiser test was performed and produced a positive result, indicating removal of the fmoc. Next, the same equivalences of HBTU, HOBt were weighed followed by Fmoc-Arg(pbf)-OH (5 equiv). These components were dissolved in 600 µL of DMF, then 10 equiv. of DIPEA was added. This solution was added to the resin and allowed to couple for 30 minutes at 37 ˚C with agitation. The solution was drained, the resin was rinsed with DMF and DCM, and a Kaiser test was performed to ensure successful coupling. The fmoc was removed by adding 2 mL of 20% piperdine in DMF

to the resin and agitating for 20 minutes at room temperature. A Kaiser test was performed, and the resin was rinsed with anhydrous DMF. A 2 M BAA and 1 M DIC solution were prepared in anhydrous DMF. Equal amounts were mixed until a precipitate was formed. This was then added to the resin and agitated for 20 minutes at 37 ˚C. While the resin was activating, a 1 M stock of bromophenethylamine was prepared by diluting the amine in anhydrous DMF. The BAA/DIC mixture was drained and the resin was washed to remove the precipitate. The 1 M stock of bromophenethylamine was added to the resin and coupled for 1 hour at 37 ˚C. The solution was then drained and a chloranil test was performed to detect the presence of a primary amine. The same equivalence of HBTU and HOBt as listed above were weighed followed by Fmoc-gly-OH (5 equiv.) and dissolved in 600 µL of DMF. After the solids were dissolved, 10 equiv. of DIPEA was added to the solution and this was added to the resin. The amino acid residue coupled for 30 minutes at 37 ˚C. the solution was drained, the resin was rinsed with DMF and DCM, and a Kaiser test was performed to ensure the reside had successfully coupled. Fmoc was removed by adding 2 mL of a 20% piperdine solution in DMF to the resin and letting it agitate for 20 minutes at room temperature. A Kaiser test was then performed to ensure the fmoc removal was complete. The same equivalence of HBTU and HOBt as listed above were weighed followed by 5 equiv. of N-[(9H-Fluoren-9-ylmethoxy)-carbonyl]-L-propargylglycine. For biotin and desthiobiotin conjugation, three sacrosines were added after the N-[(9H-Fluoren-9-ylmethoxy)-carbonyl]-L-propargylglycine (**Figure 2.19**). This was dissolved in 600 µL of DMF followed by 10 equiv. of DIPEA. The solution was added to the

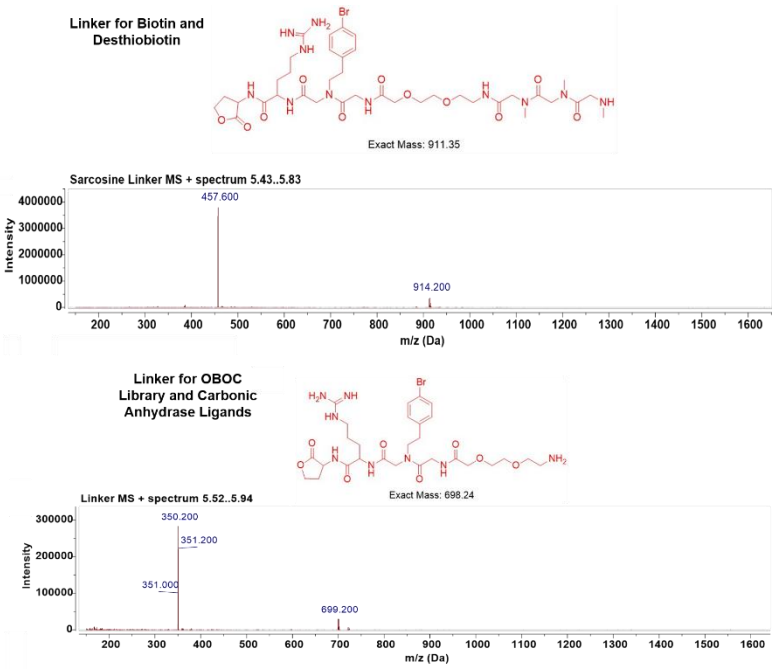

Figure 2.19 LC/MS Traces for the Linkers to Establish the Screening Method and OBOC Library. The linker structures shown above were synthesized on 90 µm TentaGel resin. After synthesis, a test cleavage was performed. LC/MS traces for each linker are shown above.

resin and allowed to couple for 30 minutes at 37 ˚C with agitation. The solution was drained and the resin was rinsed with DMF followed by DCM and a Kaiser test was performed.

A small clump of resin was transferred to a 1.5 mL eppitbue and the synthesized linker was cleaved from the resin by adding 1 mL of a 95% TFA, 2.5% DCM, and 2.5% Triisopropylsilane (TIPS) solution. This agitated for 1 hour at room temperature. The TFA was blown off with argon gas, then the cleaved product was resuspended in a 50/50 mixture of ultrapure water and acetonitrile (ACN) substituted with 0.1% formic acid (FA). The dissolved product was run on LC/MS to ensure the linker structure had been properly synthesized (**Figure 2.19**). The resin was stored at 4 ˚C until use with the terminal fmoc still attached. Right before the ligands were synthesized, the fmoc was removed by adding 2 mL of a 20% piperdine solution to the resin and allowing it to agitate for 20 minutes at room temperature. The resin was then rinsed with DMF followed by DCM and a Kaiser test was performed to ensure successful deprotection.

2.4.2.2 Conjugating Biotin to Resin

To assess the ability of the assay to detect protein-ligand interactions, biotin was attached to resin containing the linker sequence shown above. After confirmation that the linker was properly synthesized on the resin by LC/MS, 100 mg of resin was deprotected by the addition of 2 mL of 20% piperdine in DMF. The deprotection was carried out for 20 minutes at room temperature with agitation. The piperdine solution was drained and the resin was washed three times with 1 mL of DMF followed by three times with 1 mL of DCM. A Kaiser test was performed to ensure successful deprotection of the resin. Next, 5 eq. of biotin, 4.5 eq. of HBTU, 4.5 eq. of HOBt, and 10 eq. of DIPEA was dissolved in 600 µL of DMF and added to the resin. The biotin was allowed to couple to the resin for 30 minutes at room 37 ℃ with agitation. After 30 minutes, the biotin had crashed out of solution. The resin was washed three times with 2 mL DMF followed by three times with 2 mL of DCM to remove solid biotin. The coupling was repeated using 2.5 equivalents of HBTU and HOBt, 10 equivalents of DIPEA, and 3 equivalents of biotin was dissolved in 1 mL of DMF to improve solubility. The mixture was added to the resin and coupled for 30 minutes at 37 °C with agitation. The biotin solution was drained, and the resin was washed three times with 2 mL of DMF followed by three washes with 2 mL of DCM. A Kaiser test was performed to ensure successful coupling of biotin to the resin.

After the biotin coupling, the protecting groups were removed from amino acid residues by the addition of 1 mL of a 95% TFA, 5% DCM, and 5% TIPS solution. The resin was agitated for 1 hour at room temperature with the TFA solution. Then, the solution was drained, and the resin was washed three times with 2 mL DCM. To cleave the peptide, a small clump of resin was placed in a 1.5 mL eppitube and suspended in 70 µL of a 50 mg/mL solution of cyanogen bromide dissolved in 5:4:1 ACN: glacial acetic acid (GAA): water. The peptide was allowed to cleave overnight at room temperature with agitation. The following morning, the cyanogen bromide solution was evaporated using a SpeedVac and the cleaved peptide was dissolved in 60 µL of a solution of 50:50 ACN: water with 0.1% formic acid (FA). 25 µL of this solution was injected onto an Agilent single quadrupole LC/MS system to determine the identity of the cleaved peptide (**Figure 2.20**).

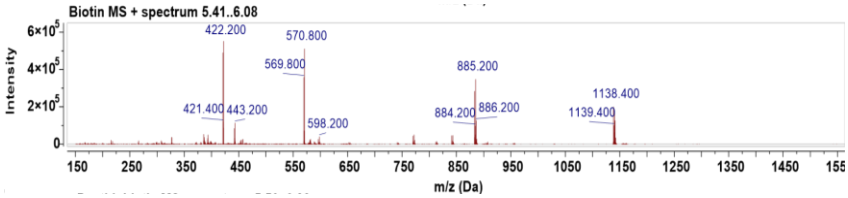

Figure 2.20 LC/MS Trace of Biotin Conjugated to the Linker. The structure of biotin conjugated to the linker can be seen in Figure 2.2. The expected molecular weight was 1137.43 g/mol. The (M+2H)/2 mass is seen at 570 m/z. The M+H mass is also seen at 1138 m/z.

Next, desthiobiotin was synthesized on the linker containing sacrosine. After confirmation by LC/MS that the linker was properly synthesized on the resin, Fmoc was removed from the final residue of 100 mg of resin by the addition of 2 mL of 20% piperdine in DMF. The deprotection took place for 20 minutes at room temperature with agitation. The piperdine was then drained, and the resin was washed three times with 1 mL of DMF followed by three washes with 1 mL DCM. A Kaiser test was performed to ensure successful deprotection. Next, the desthiobiotin was coupled to the resin by dissolving 5 eq. of desthiobiotin, 4.5 eq. of HBTU, 4.5 eq. of HOBt, and 10 eq. of DIPEA in 600 µL DMF. The solution was added to the resin and the coupling was allowed to go for 30 minutes at 37 °C with agitation. The desthiobiotin solution was then drained and the resin was washed three times with 1 mL DMF followed by three washes with 1 mL DCM. A Kaiser test was performed to ensure successful coupling.

After coupling desthiobiotin to the linker, protecting groups were removed from the amino acid residues by adding 1 mL of a 95% TFA, 5% DCM, and 5% TIPS solution to the resin. The resin agitated with the TFA solution for 1 hour at room temperature. The TFA solution was then drained, and the resin was washed three times with 2 mL of DCM. The peptide was then cleaved by adding 70 µL of a 50 mg/mL solution of cyanogen bromide dissolved in 5:4:1 ACN: GAA: water. The cleavage took place overnight at room temperature with agitation. The following morning, the cyanogen bromide solution was evaporated by using a SpeedVac and the cleaved product was resuspended in 60 µL of a 50:50 ACN: water solution with 0.1% FA. 25 µL of the dissolved product was then injected into an Agilent single quadrupole LC/MS system (**Figure 2.21**).

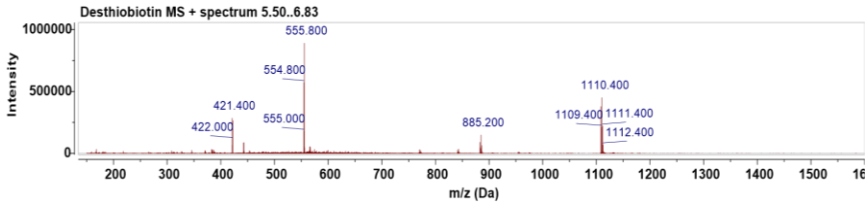

Figure 2.21 LC/MS Trace of Desthiobtion Conjugated to the Linker. The structure of desthiobiotin conjugated to the linker can be seen in Figure 2.5. The expected mass was 1107.47. the (M+3H)/3 mass can be seen at 554 m/z.

2.4.2.3 Labeling Purified Streptavidin and Carbonic Anhydrase with a NIR Fluorophore

To determine the ability of the assay to detect protein-ligand interactions, streptavidin was purchased from Sigma Aldrich and labeled with an IRDye® 800CW Protein Labeling Kit-High Molecular Weight, purchased from LI-COR (Cat. 928-38040). Streptavidin was labeled exactly following the manufacturer's protocol. Briefly, 1 mg of streptavidin was dissolved in 1 mL of phosphate-buffered saline (PBS). The pH of the protein solution was raised to 8.5 by adding 100 µL 1 M potassium phosphate, pH 9.0. One vial of near infrared dye was thawed and dissolved in 25 µL of ultra-pure water. The proper amount of dye was calculated using the manufacturer's instructions and was added to the protein solution. The dye was allowed to react with the protein for 2 hours at 4 °C, protected from light. After 2 hours, free dye was removed by passing the labeled protein through a Pierce® ZebaTM Desalting Column that was washed three times with 2.5 mL of PBS before the protein was added. After the free dye was removed, the protein concentration was measured using a NanoDrop One system purchased from Thermo Scientific. The absorbance at 780 nm was also measured using a nanodrop one system. The fluorophore to protein ratio was calculated following the directions provided in the manufacturer's protocol. The final fluorophore to protein ratio for streptavidin was 2:1.

Carbonic Anhydrase was purchased from Sigma Aldrich and labeled with an IRDye® 800CW Protein Labeling Kit-High Molecular Weight, purchased from LI-COR (Cat. 928-38040). Carbonic anhydrase was labeled exactly following the manufacturer's instructions. Briefly, 1 mg of protein was weighed and dissolved in 1 mL of PBS. The pH of the protein solution was adjusted to 8.5 by adding 100 µL of 1 M potassium phosphate, pH 9.0. Then, one vial of infrared dye was thawed and dissolved in 25 µL of ultra-pure water. Using the manufacturer's protocol, the correct amount of dye was calculated and added to the protein solution. The dye was allowed to react with the protein for 2 hours at 4 ˚C, protected from light. To remove excess dye, the protein solution was passed through a Pierce® ZebaTM Desalting Colum that was washed 3 times with 2.5 mL of PBS prior to use. After removal of extra dye, the protein concentration was measured by using a NanoDrop One system purchased form Thermo Scientific. The absorbance of the protein labeled with the NIR fluorophore was measured also measured at 780 nm. Using the manufacturer's protocol, the dye to protein ratio of the carbonic anhydrase was calculated to be 1.8.

2.4.2.4 Determining Lowest Detectable Binding of NIR-Labeled Streptavidin to Biotin On-Bead

Streptavidin purchased from Sigma Aldrich was dyed with a NIR-emitting fluorophore following the described protocol. Prior to the beginning of the experiment, TentaGel resin with either biotin or desthiobiotin was swollen in PBS by adding 750 µL of DMF and 250 µL of PBS to the resin and allowing it to agitate for 20 minutes at room temperature. The resin was then checked for clumping and the solution was drained. The amount of PBS added to the DMF was gradually increased and the process was repeated until the resin agitated in 1 mL of PBS. The day of the experiment, beads conjugated with biotin or desthiobiotin were split into the wells of a black 96-well plate with a clear bottom such that there was one bead per well. Next, the resin was blocked with 50 µL of StartingBlockTM (PBS) Blocking Buffer purchased from Thermo Scientific (Cat. 37538) for 30 minutes at room temperature with agitation. While the resin was blocking a 1,000 ng/µL frozen stock of dyed streptavidin was thawed and 1 µL was added to 499 µL of Odyssey® Blocking buffer PBS purchased from LI-COR (Cat. 92740000) to create a solution that had a concentration of 2 ng/µL. Next, 12.5 µL of the 2 ng/µL stock solution was added to 987.5 µL of Odyssey® Blocking buffer PBS purchased from LI-COR (Cat. 92740000) to achieve a stock concentration of 0.025 ng/µL. This stock solution was then serially diluted such that the lowest

concentration of streptavidin was 0.0001 ng/µL. After blocking was complete, 50 µL of each dyed streptavidin concentration was added to wells containing biotin and desthiobiotin in quadruplicate. The highest protein concentration in the well was 1.25 ng and the lowest protein concentration in the well was 0.005 ng. The resin was allowed to incubate with the protein overnight at 4 ˚C with agitation, protected from light.

The following morning, the protein was removed, and the resin was washed once with 50µL of PBS. The beads were resuspended in 50 µL of fresh PBS and imaged on a LI-COR Odyssey® CLx imaging system. As a control, 1.25 ng of dyed streptavidin was allowed to incubate with four beads conjugated to the FLAG peptide and four beads conjugated to the scrambled FLAG peptide. ImageStudio software from LI-COR was used to quantify fluorescence intensities produced by the dyed streptavidin protein binding the biotin and desthiobiotin-conjugated resin. The fluorescence intensity of an empty well was set to 0.0 to normalize the intensities of the other wells. This experiment was repeated twice, with each protein concentration being added in quadruplicate, then the fluorescence intensities for each concentration of dyed streptavidin were pooled. The highest and lowest fluorescence intensities were removed, and the data was graphed. Occasionally, a bead was lost during the washing process. Wells in which a bead was missing were not quantified.

2.4.2.5 Conjugating CBS, D-CBS, and GL-CBS Carbonic Anhydrase Ligands to Resin

To test the ability of our assay to detect protein-ligand binding with a K_D in the low micromolar range, we synthesized substrates of varying affinity to carbonic anhydrase. After conformation by LC/MS that the linker was properly synthesized on the resin, the Fmoc on the final residues was removed from 15 mg of resin by the addition of 2 mL of 20% piperdine in DMF. The solution was allowed to agitate with the resin for 20 minutes at room temperature and a Kaiser test was performed to ensure the deprotection was complete. The resin was then washed three times with 2 mL of DMF followed by 2 mL of DCM. For The CBS ligand, carboxybenzylsulfonamide was coupled to the resin by dissolving 6 mg of carboxybenzylsulfonamide (50 mM final concentration), 6.6 µL of EDC-HCL (50 mM final concentration) and 0.4 mg of HOAt (5 mM final concentration) in 600 µL of DCM. About 50 µL of methanol was added to facilitate dissolving of the CBS.

For GL-CBS, a glycine and leucine residue were coupled prior to the carboxybenzylsulfonamide. After confirmation by LC/MS that the linker was properly synthesized

on the resin, the Fmoc on the final residue was removed from 15 mg of the resin by the addition of 2 mL of 20% piperdine in DMF. The resin was allowed to agitate with the piperdine for 20 minutes at room temperature then a Kaiser test was used to ensure deprotection was complete. Next, Fmoc-Gly-OH was coupled to the linker by dissolving 5 eq. of Fmoc-Gly-OH, 4.5 eq. of HBTU, 4.5 eq. of HOBt and 10 eq. of DIPEA in 600 µL of DMF. The solution was added to the resin and allowed to couple for 30 minutes at room temperature with agitation, the resin was washed with DMF and DCM, then a Kaiser test was performed to ensure complete coupling. Then, the resin was deprotected with 2 mL of 20% piperdine in DMF, which agitated for 20 minutes at room temperature. After conformation by Kaiser test that the Fmoc was removed, Fmoc-Leu-OH was coupled by dissolving 5 eq. of Fmoc-Leu-OH, 4.5 eq. of HBTU, 4.5 eq. of HOBt and 10 eq. of DIPEA in 600 µL of DMF. The solution was allowed to incubate with the resin for 30 minutes at room temperature with agitation. A Kaiser test was performed to ensure the coupling was complete. The resin was then washed three times with 2 mL of DMF followed by 2 mL of DCM. CBS was coupled as described above.

For D-CBS, an aspartic acid residue was coupled prior to the addition of the carboxybenzylsulfonamide. After confirmation by LC/MS that the linker was properly synthesized, the Fmoc on the final residue was removed from 15 mg of resin by allowing the resin to incubate with 2 mL of a 20% piperdine solution in DMF for 20 minutes at room temperature. A Kaiser test was performed to ensure the deprotection was complete. Next, Fmoc-Asp(OtBu)-OH was coupled to the linker by dissolving 5 eq. of Fmoc-Asp(OtBu)-OH, 4.5 eq. of HBTU, 4.5 eq. of HOBt, and 10 eq. of DIPEA in 600 µL of DMF. The solution was added to the resin and allowed to couple for 30 minutes at room temperature with agitation. The resin was then washed three times with 2 mL of DMF followed by 2 mL of DCM. A Kaiser test was performed to ensure the coupling was complete and the last residue was deprotected by adding 2 mL of a 20% piperdine solution in DMF and allowing incubation for 20 minutes at room temperature. A Kaiser test was performed to ensure successful deprotection. The carboxybenzylsulfonamide was coupled as described above.

The protecting groups on the linker were removed by incubating the resin with a 95% TFA, 5% DCM, and 5% TIPS solution for 1 hour at room temperature. The solution was then drained, and the resin was washed several times with DCM to remove excess reagents. Then, a small clump of resin was placed in the well of a chemical resistant 96-well plate and the product was cleaved by adding 70 µL of a 50 mg/mL cyanogen bromide solution dissolved in 5:4:1 ACN: GAA: water. The cleavage took place overnight at room temperature. The following morning, the cyanogen bromide solution was removed with a SpeedVac and the product was dissolved in 60 µL of a 50:50 ACN: water solution with 0.1% FA. 25 µL of this solution was then injected onto an Agilent single quadruple LC/MS system (**Figure 2.22**).

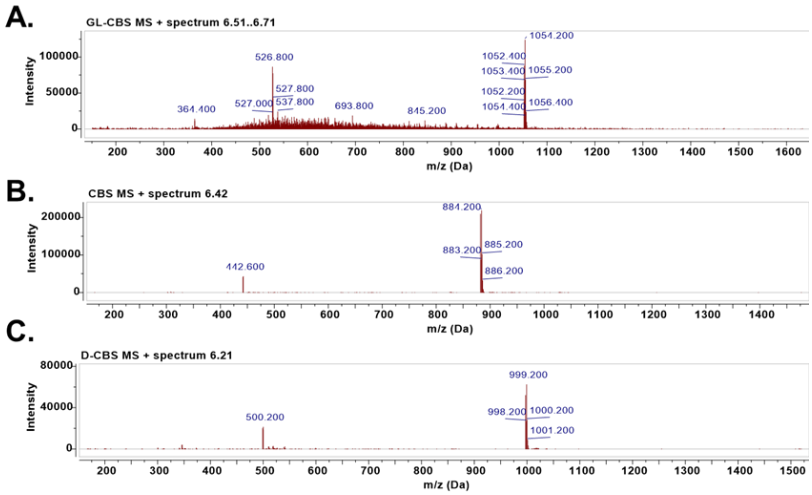

Figure 2.22 LC/MS Traces of GL-CBS, CBS, and D-CBS on the Linker. The structure of ligands conjugated to the linker can be seen in Figure 2.8. (A) LC/MS trace for GL-CBS. The expected mass is 1051.34. (B) LC/MS trace for CBS. The expected mass is 881.24. (C) LC/MS trace for D-CBS. The expected mass was 996.26

2.4.2.6 Determining Differences in Fluorescence Intensities Produced by Adding NIR-Labeled Carbonic Anhydrase to Beads Conjugated to Each Ligand

To determine the ability of our assay to detect protein-ligand binding with affinities in the low micromolar range, we screened several substrates with labeled carbonic anhydrase. First, TentaGel resin conjugated with GL-CBS, CBS, and D-CBS was swollen in PBS by adding 250 µL of PBS and 750 µL of DMF to the resin. The resin was allowed to agitate with this solution for 20 minutes. The solution was then drained, and the amount of PBS was gradually increased until the resin was swollen in 1 mL of PBS. The day of the experiment, GL-CBS, CBS, and D-CBS beads were split into the wells of a black 96-well plate with a clear bottom such that there was one bead per well. As a negative control, FLAG resin was split into 8 wells. The beads were then blocked with 50 µL of StartingBlockTM (PBS) Blocking Buffer for 30 minutes at room temperature with agitation. During this time, a stock of 0.0044 mg/mL of labeled carbonic

anhydrase was serially diluted in Odyssey® Blocking buffer PBS such that the highest concentration in the well would be 282 ng and the lowest concentration would be 0.1 ng. After blocking was complete, blocking buffer was removed from the resin and 50 µL of each protein concentration was added to the wells containing GL-CBS, CBS, and D-CBS resin in quadruplicate. Binding was allowed to take place overnight at 4 ˚C with agitation, protected from light. The following morning, the protein was removed, and the beads were washed once with 50 µL of PBS. The beads were resuspended in 50 µL of PBS and imaged on a LI-COR Odyssey® CLx imaging system. Wells containing FLAG resin beads incubated with 17 ng of carbonic anhydrase to ensure there was no nonspecific binding and fluorescence intensities of these wells was quantitated.

ImageStudio software from LI-COR was used to quantify fluorescence intensities produced by the labeled carbonic anhydrase protein binding the GL-CBS, CBS, and D-CBS-conjugated resin. The fluorescence intensity of an empty well was set to 0.0 to normalize the intensities of the other wells. This experiment was repeated twice, with each protein concentration being added in quadruplicate, then the fluorescence intensities for each concentration of dyed carbonic anhydrase were pooled. Fluorescence Intensities that were above or below one standard deviation of the mean were removed. Occasionally, a bead was lost during the washing process. Wells in which a bead was missing were not included.

2.4.3 Screening of Gankyrin Against an OBOC Library

2.4.3.1 Covalent OBOC Library Synthesis

100 mg of linker resin synthesized as described above was swollen in DMF for 30 minutes followed by DCM for 30 minutes. The terminal fmoc was removed as described above. The resin was washed once with anhydrous DMF then a 2 M stock of BAA and a 1 M stock of DIC in anhydrous DMF was prepared. Equal amounts of the solutions were mixed until a precipitate formed and this was added to the resin. The resin activated for 15 minutes at 37 ˚C with agitation. During this time, 0.5 M stocks of the seven amines listed in **Figure 2.11** at position 1 were prepared by diluting the amines in anhydrous DMF. The activating solution was drained from the resin and the resin was rinsed with anhydrous DMF then split roughly equally between seven syringes. One of the diluted amines was added to each syringe and coupled for 1 hour at 37 ˚C with agitation. The amine solutions were then drained, and the resin was rinsed three times with anhydrous DMF.

A chloranil test was performed for each syringe to ensure successful coupling of each amine. The resin was then pooled back into one syringe and activated using the premixed 2 M BAA and 1 M DIC solution as described above. Resin was then roughly equally separated into seven syringes and 0.5 M stocks of the amines listed for position 2 in **Figure 2.11** were added. Amines coupled for 1 hour at 37 ˚C with agitation. The solutions were then drained, and the resin was washed 3 times with anhydrous DMF. A chloranil test was performed for each syringe, then the resin was pooled back together. The resin was activated with the 2 M BAA and 1 M DIC solutions as described above. After activation, however, the resin was not split into separate syringes, as the same amine was going to be coupled for all the structures in the 3rd position. 4-(2-aminoethyl)benzensulfonyl fluoride hydrochloride was weighed such that dissolving in 500 µL of anhydrous DMF would produce a 0.5 M stock. After dissolving the amine, DIPEA was added to a final concentration of 0.5 M to quench the hydrochloride. This was then added to the resin and allowed to couple for 1 hour at 37 ˚C with agitation. The amine was then removed, resin was washed three times with anhydrous DMF and a chloranil test was performed. The resin was then activated with the 2 M BAA and 1 M DIC as described above. The resin was then roughly equally split between 7 syringes and 0.5 M stocks of amines listed at position four in **Figure 2.11** were added to one of the syringes. This incubated for 1 hour at 37 ˚C with agitation. The solution was drained, the resin was washed three times with anhydrous DMF, and a chloranil test was performed for each syringe. Resin was then combined into one syringe and the pbf protecting group on the arginine in the linker was removed by adding 1 mL of a 95% TFA, 2.5% TIPS, and 2.5% DCM solution. This agitated for 1 hour at room temperature. The solution was drained and the resin was washed 3 times with DMF followed by 3 times with DCM. The resin was stored at 4 ˚C until use.

2.4.3.2 Purification and Labeling of Gankyrin with a NIR Fluorophore

A His-tagged gankyrin plasmid resistant to ampicillin was purchased from AddGene. An 8 mL starter culture was prepared by scrapping bacteria from the agar stab and inoculating it in LB broth with 0.1 mg/mL of ampicillin. The culture grew overnight at 37 ℃. The following morning the plasmid DNA was extracted with a mini-prep kit following the manufacturer's protocol. Rosetta (DE3) competent cells were transformed with the plasmid DNA following the manufacturer's protocol. Competent bacteria were streaked on a LB agar plate supplemented with ampicillin and allowed to grow overnight at 37 ℃. The next day, single bacterial colonies were

inoculated into 8 mL of LB broth supplemented with ampicillin and chloramphenicol and allowed to grow overnight at 37 ℃. Glycerol stocks of the transformed bacteria were prepared by diluting 100 µL of the bacteria stock in 100 µL of a sterile 50% glycerol solution. Glycerol stocks were stored at -80 ℃.

To purify gankyrin, 20 µL of the glycerol stock was inoculated into 8 mL of LB broth supplemented with ampicillin and chloramphenicol and grew overnight at 37 ℃ with agitation. 1 L of LB broth was sterilized by autoclaving and once the media had cooled, 100 mg of ampicillin was added to the broth. The entire 8 mL starter culture was then added to the broth and agitated at 37 ℃. Bacteria grew until and OD_{600} of 0.6-0.8 was reached. Isopropyl β-D-1-thiogalactopyranoside (IPTG) was dissolved in PBS such that the final concentration in the 1 L flask would be 1 mM. Protein production was induced with IPTG for 2.5 hours at 37 ℃. Then, bacteria were pelleted by centrifuging at 4,700 xg for 15 minutes. Media was poured off and bacteria were resuspended in 40 mL of lysis buffer (50 mM Tris-HCl (pH 8.0), 300 mM NaCl, 0.1% triton-X 100, 1 mM EDTA supplemented with 0.25 mg/mL lysozyme and 1 mM phenylmethylsulfonyl fluoride (PMSF). Bacteria was transferred to a 50 mL falcon tube and ultrasonicated at 30% amplitude for 1 minute with 3 seconds on and 2 seconds off. Ultrasonication was carried out at 4 ℃ and the falcon tube was placed in ice. Lysate was clarified by pelleting at 14,000 xg for 40 minutes at 4 ℃ in a prechilled centrifuge.

Supernatant was collected in a new tube. Gankyrin was purified by allowing the lysate to incubate with 200 µL of HisPur™ NI-NTA resin for 40 minutes at room temperature with gentle agitation. Lysate was then drained and the resin was washed three times with 10 mL of PBS to remove protein that was bound nonspecifically. 10 mM, 50 mM, 150 mM, 350 mM, and 600 mM solutions of imidazole were prepared by dissolving imidazole in PBS. Two 1 mL imidazole fractions of each concentration were added to the resin and collected in 1.5 mL eppitubes starting with the 10 mM concentration. 42 µL from each fraction was mixed with 8 µL of 4X Laemmli buffer and samples were heated for 5 minutes at 95 ℃. Samples were run on SDS-PAGE and the gel was stained with Coomassie (**Figure 2.23A**). Fractions containing only pure gankyrin (protein

near 24 kDa) were compiled and added to a dialysis bag. The pure protein dialyzed in PBS overnight at 4 ℃. A western blot was conducted using an anti-HIS antibody (Novus Biologicals) the first time the protein was purified (**Figure 2.23B**). The following day, the pure protein was collected and protein concentration was determined by measuring absorbance at 280 nm with a Nanodrop one system. Protein was then concentrated to 1 mg/mL by placing the protein solution in a 5,000 MWCO amicon protein concentrator and centrifuging at 4,000 xg at 4 ℃.

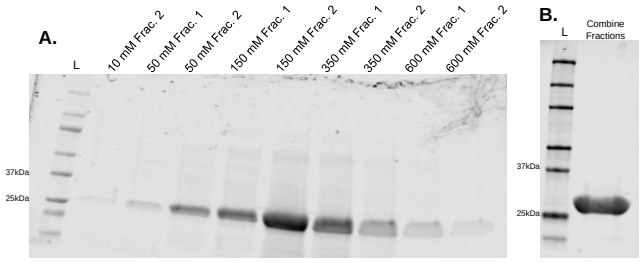

Figure 2.23 Purification of His-Tagged Gankyrin for Screening. (A) Coomassie stain of fractions eluted from the resin with an imidazole gradient. (B) Fractions containing pure gankyrin were combine and dialyzed in PBS. Protein was then concentrated, and a western blot was performed with an anti-His antibody.

1 mg of gankyrin was labeled with the NIR fluorophore using an IRDye® 800CW NHS Ester Kit purchased from LI-COR following the manufacturer's protocol. Briefly, the pH of the protein solution was raised to 8.5 by adding 1 M potassium phosphate buffer, pH 9.0. This ensured the NHS ester moiety on the dye only bound the N-terminus of the protein. Next, a vial of 800CW dye was dissolved in 25 µL of ultrapure water. The correct amount of dye was calculated using the manufacturer's protocol and was added to the gankyrin solution. The dye incubated with the gankyrin for 2 hours at 4 ℃. Excess dye was removed by passing the solution through a desalting column. The absorbance at 780 and 280 nm of the solution was measured with a NanoDrop One system and used to calculate the dye to protein ratio using the manufacturer's protocol. The dye to protein ratio was determined to be 0.7. The protein was aliquoted and stored at -20 °C. Protein was thawed and used immediately before use.

2.4.3.3 Screen of Gankyrin Against the OBOC Library

Beads of the OBOC were stored at 4 ˚C until use. Prior to screening beads were conditioned in PBS. Beads were first swollen in DMF for 20 minutes. The solution was drained at replaced with a 75% DMF, 25% PBS solution for 30 minutes. This was drained and replaced with a 50% DMF 50% PBS solution and agitated for 30 minutes. Beads were check after an increase in the percentage of PBS to ensure there was no clumping. If the beads did clump, the amount of PBS was reduced, and beads were agitated until clumps no longer formed prior to increasing the amount of PBS. The solution was drained and replaced with a 25% DMF, 75% PBS solution that agitated

for 30 minutes. Finally, beads were swollen in 100% PBS for 30 minutes. Beads were stored dry at 4 ˚C after the initial transfer to PBS. Beads were allowed to swell in 100% PBS for 20 minutes after each removal from the refrigerator to ensure they would not collapse during screening.

Beads were individually split into the wells of a black 96-well plate with a clear bottom by adding 1 mL of PBS to the syringe with the library and cutting the tip off of a 200 µL micropipette tip and looking at the well plate under a microscope. 50 µL of PBS was added to each well of the plate. About 20 µL of the library in PBS was pipetted with the cut micropipette tip and added to one well of the plate. Then, about 4 µL of beads from the first well were transferred to the second well. Individual beads in the second well were then transferred to the wells of the plate. PBS was then removed from the wells by careful pipetting. 50 µL of blocking buffer purchased from ThermoFisher (see general methods for full name) was added to each well. Beads blocked for 30 minutes at room temperature with gentle agitation. The blocking buffer was then removed by pipetting.

An aliquot of NIR-labeled gankyrin was removed from the freezer immediately before use and diluted in Intercept Blocking buffer (PBS) from LI-COR. 50 µL of the protein diluted in blocking buffer was added to each well. The final amount of labeled gankyrin per well was 0.6 ng. The plate was covered with a lid and wrapped in tin foil. The beads incubated with the labeled protein overnight at 4 ˚C with gentle agitation. The following day the protein solution was removed and wells were washed with 50 µL of PBS. Beads were then resuspended in 50 µL of PBS and imaged on an Odyssey CLx imaging system from LI-COR. Importantly, the resolution of the scan was set to 84 µm to accommodate visualizing the 90 µm beads. Fluorescence intensities of individual beads that resulted from the labeled protein binding the small molecule were quantified using ImageStudio software from LI-COR. Fluorescence intensities were normalized to the intensity of a well containing no bead to accommodate for background fluorescence. Two screens of 424 beads were performed. The top 5% fluorescence intensities from each screen were considered initial hits. Hits were then identified as follows.

2.4.3.4 Identification of Hits from the Gankyrin Screen

After selecting the top 5% of fluorescence intensities as hits, beads in the corresponding wells were removed from the screening plate and placed into a chemical resistant plate by pipetting. Since the binding between the protein and small molecule is covalent, the protein was first removed

by agitating beads in increasingly organic solvent to unfold the protein and promote disassociation with bead. First, beads were washed three times with 50 µL of ultrapure water. Beads were agitated for 10 minutes during each wash. Next, beads were washed three times for 10 minutes in a solution of 50/50 ultrapure water and DMF. Next, beads were washed three times for 10 minutes with DMF. Beads were then washed three times for 10 minutes with DCM. Finally, the beads were agitated overnight with 50 µL of DCM at room temperature. The plate was tightly wrapped with tin foil to prevent evaporation. The next day, the DCM was removed. The small molecule on the bead was cleaved with a 50 mg/mL solution of cyanogen bromide dissolved in a 5:4:1 ACN: Glacial Acetic Acid (GAA):Water. 50 µL of this cocktail was added to each well. The plate was wrapped in tin foil to prevent evaporation and agitated overnight in a chemical hood. The following morning, the plate was speed vacced to dry the cleaved product. The product was re-dissolved in 7 µL of a 50/50 ACN/Ultrapure water solution with 0.1% TFA. 1.3 µL of this was spotted with 0.7 µL of MALDI matrix solution. Hits were subjected to MALDI-TOF analysis. The unique isotope provided by the bromine in the linker structure facilitated identification of amines from the hit structures from other fragments associated with left over protein or other sample contaminates. Several hit structures were identified from each independent screen. The structures between the two screens were combine and peptoids that exhibited similarity in the amines at various positions were further pursued for validation. This produced 10 structures between the two screens that were further validated for binding to gankyrin with an in-gel fluorescence assay. Sample structures from both screens and the resulting overlapping structures from combining both screens can be seen in **Appendix A**.

2.4.3.5 Validation of Hits Using an In-Gel Fluorescence Assay

2.4.3.5.1 Synthesis of Ligands for the Validation Experiments

50 mg of resin containing the linker shown in **Figure 2.13A** was swollen in DMF for 30 minutes followed by DCM for 30 minutes. The fmoc was removed from the mini-peg by adding 1 mL of 20% piperdine in DMF to the syringe and agitating it for 20 minutes. A Kaiser test was performed to ensure successful deprotection. The resin was washed with anhydrous DMF. Next, a 2 M BAA and 1 M DIC solution was prepared and equal volumes were mixed until a white precipitate formed and the solution was added to the resin. This incubated for 15 minutes at 37 ˚C.

500 µL of a 0.5 M solution of the first amine of each structure was prepared by diluting it in anhydrous DMF. The activating solution was removed and the resin was rinsed once with anhydrous DMF and the amine solution was added to the syringe. The amine coupled for 1 hour at 37 ˚C. The resin was then washed with anhydrous DMF and a chloranil test was performed to ensure successful coupling. This procedure was repeated for all four positions. For the 4-(2-aminoethyl)benzensulfonyl fluoride hydrochloride, 1.5 equivalence of the solid was weighed and dissolved in 250 µL of anhydrous DMF. DIPEA was added to a final concentration of 0.5 M. This was added then added to the syringe and coupled for 1 hour at 37 ˚C.

After all the amines were coupled, the MMT protecting group was removed from the cysteine on the linker to conjugate fluorescein. 1 mL of a 2% TFA solution in DCM was added to the syringe and agitated or 5 minutes. The solution was drained and replaced until it no longer turned yellow. Then, the pH of the resin was neutralized by washing with a 10% DIPEA solution in DCM three times for 5 minutes. 1.5 equivalence of N-(5-Fluoresceinyl)-maleinimide was weighed and dissolved in 250 µL of DMF. This was then added to the syringe and coupled for 1 hour. The solution was drained and the resin was washed 3 times with DMF followed by 3 washes with DCM. The resin was stored at 4 ˚C until purification. The peptoid was cleaved from the resin by adding a 95% TFA, 2.5% TIPS, 2.5% DCM solution to the resin and agitating it for 2 hours at room temperature. The cleaved produce was collected in a clean 15 mL Falcon tube and the resin was rinse twice with 1 mL of DCM. The TFA was blown off with argon. The cleaved product was resuspended in 200 µL of a 50/50 ACN/ultrapure water solution with 0.1% TFA. The product was then purified by RP-HPLC and the purity was checked by LC/MS as shown in **Appendix B**. After purification, HPLC fractions containing the pure product were combine and rotovapped to remove residual ACN. The product was then frozen and lyophilized. The resulting powder was stored at -20 ˚C protected from light until use.

2.4.3.5.2 In-Gel Fluorescence Validation of Ligands

Gankyrin was purified as described above. Immediately prior to the start of the experiment, fluorescently labeled negative control or the test ligand were removed from the freezer and a small amount of powder was scrapped from the vial and placed in a 0.6 mL tube. Ligands were dissolved in 6 µL of DMSO then diluted 1:100 in PBS. The concentration of the ligands were determined by measuring absorption at 494 nm and Beer's Law. Stocks of each ligand were prepared such that

the final concentrations in the samples would be 20, 8, 1, or 0.1 µM by diluting the ligands in DMSO. Purified gankyrin was concentrated to a 10.2 ng/µL stock. 49 µL of the protein was added to 0.6 mL eppitubes. Next, 1 µL of the negative control or test ligands at each concentration were added to one sample of protein. As a control, one sample was also dosed with 1 µL of DMSO. The final protein amount was 500 ng per sample. Samples were vortexed to mix then incubated at 4 ˚C for three hours with gentle rotation, protected from light. During incubation, 12.5% resolving SDS-PAGE gels were prepared with a 4.5% stacking gel. The reaction between the ligands and the protein was quenched by adding 20 µL of 4X Laemmli buffer and heating at 95 ˚C for about five minutes. Samples were then run on SDS-PAGE in chambers protected from light. The gel was run at 120 V for about 1.5 hours to prevent streaking of the excess ligand in the gel. Gels were run until all Laemmli dye was run off the bottom. The gels were then washed three times with ultrapure water.

Gels were imaged on an Azure Sapphire Biomolecular Imager (**Figure 2.24A**). The intensity of the fluorescing bands resulting from the labeled ligands binding the purified gankyrin were quantified using ImageStudio software from LI-COR. The intensities of the negative control band and test ligands were compared. Quantification of the fluorescence intensities of the bands produced by TMM-1 and TMM-6 shown in **Figure 2.13** are provided as well (**Figure 2.24B**).

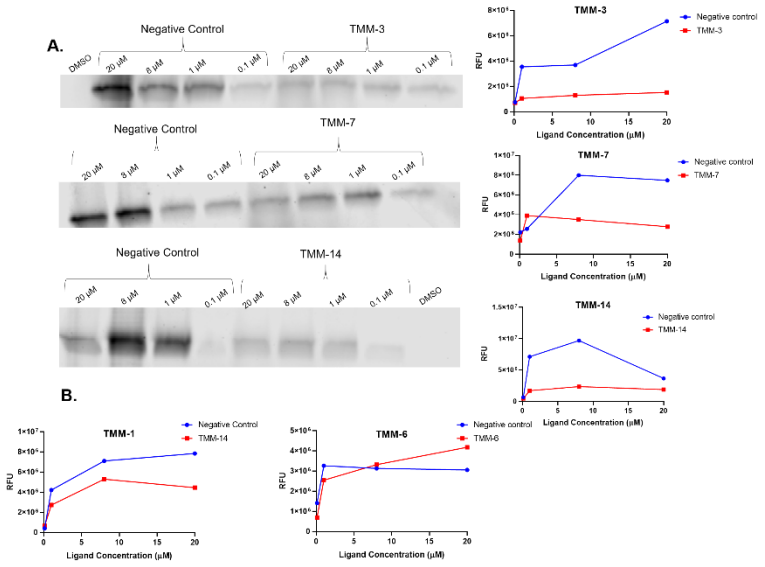

Figure 2.24 In-Gel Fluorescence Validation of Ligands. (A) Examples of gels obtained during the in-gel fluorescence validation experiment. The fluorescence intensities of the bands shown in the gels on the left were quantified to produce the graphs on right. (B) Quantification of the gels provided in Figure 2.13. Since TMM-6 appeared to produce higher fluorescence intensities at some of the concentrations compared to the negative control, this was repeated in experimental triplicate.

2.4.3.6 Pulldown of Gankyrin in Spiked Cell Lysate Samples with TMM-6

To determine if TMM-6 could recognize and bind gankyrin in more complex protein mixtures and evaluate the specificity of TMM-6, we conducted a binding experiment in which fluorescently labeled ligand incubated with HEK 293T cell lysate spiked with purified gankyrin. Fluorescently labeled TMM-6 and the negative control were synthesized as described above and purified by RP-HPLC. After checking purity by LC/MS, the lyophilized product was stored at -20 ˚C until use. Gankyrin was purified as described above the day before the experiment. HEK 293T cells were maintained in DMEM supplemented with 10% FBS at 37 ˚C with 5% CO2.

The day of the experiment, HEK 293T cells were pelleted at 1,000 x g for 5 minutes. Cells were washed once with 500 µL of PBS. Cells were then lysed with 300 µL of MPER following the manufacturer's instructions. Briefly, cells gently rotated with MPER for 10 minutes at room temperature. Lysate was clarified by centrifuging at 14,500 xg for 15 minutes at 4 ˚C in a prechilled centrifuge. Supernatant was transferred to a new 1.5 mL eppitube and the protein concentration was determined by measuring absorbance at 280 nm with a NanoDrop One system. Purified gankyrin was concentrated such that the final concentration in each sample would be 500 ng. Lysate was diluted in PBS and 46.3 µL of lysate was added to 0.6 mL tubes. The final lysate amount in each sample was 50,000 ng. Next, 2.7 µL of gankyrin was added to each tube, making the final amount of gankyrin in each sample 500 ng, or 1% of the total protein concentration. Fluorescently labeled TMM-6 and negative control was scrapped from the vial and dissolved 6 µL of DMSO. This was diluted 1:100 in PBS and the concentration of the stock was determined by measuring absorbance at 494 nm and using Beer's Law.

400 µM stocks of each ligand were prepared by further dilution in DMSO. 1 µL of either TMM-6 or the negative control was added to the tubes containing HEK 293T cell lysate spiked with gankyrin. The samples incubated for 3 hours at 4 ˚C protected from light with gentle rotation. After incubation, the reaction was quenched by adding 20 µL of 4X Laemmli buffer and heating samples at 95 ˚C for 5 minutes. 50 µL of each sample was subjected to SDS-PAGE using a freshly made gel as described above. The gel was run at 120 V for about 90 minutes, until the loading buffer ran off the bottom. The gel was then washed 3 times with ultrapure water and imaged on a Sapphire Biomolecular Imager from Azure. Two bands produced the highest fluorescence intensities after incubating with TMM-6. These were excised from the gel by cutting with a clean

razor blade and placed in clean 1.5 mL eppitubes. The gel was then rescanned to ensure the entire band had been successfully cut from the gel.

The gel fragments were submitted to the Purdue Proteomics Facility and the most abundant protein in each band was determined to be gankyrin. Since purified gankyrin was added to the samples, it is unclear why it produced two bands differing in molecular weights in the spiked HEK 293T lysate samples. It is possible that one band represents gankyrin that has been modified by other enzymes in the lysate, resulting in a different molecular weight. Notably, there were other fluorescent bands in the TMM-6 sample, indicating that this ligand may bind other proteins. However, none of the bands fluoresced to the same extent as the bands identified as gankyrin, indicating that this interaction is the most prominent in the lysate. Binding of the negative control to protein in the spiked lysate produced only a few bands, indicating that is does not bind many proteins to a significant extent.

2.4.4 Establishing Conditions for Screening Antibodies

2.4.4.1 Conjugating the FLAG Peptide to Resin

After confirmation by LC/MS that the linker sequence was successfully synthesized on the resin, the last Fmoc deprotection was carried out with 2 mL of 20% piperdine in DMF for 20 minutes at room temperature with agitation. The FLAG peptide was then synthesized continuing off the linker following the exact same peptide coupling procedure described above. Briefly, 5 eq. of Fmoc-Lys(Boc)-OH, 4.5 eq. of HBTU, 4.5 eq. of HOBt, and 10 eq. of DIPEA was dissolved in 600 µL DMF and added to the resin. The coupling was allowed to proceed for 30 minutes at 37 °C with agitation. The amino acid solution was drained, and the resin was washed three times with 1 mL of DMF and three times with 1 mL of DCM. A Kaiser test was performed to ensure successful coupling of the amino acid. The fmoc was removed with 2 mL of 20% piperdine in DMF for 20 minutes at room temperature with agitation. Piperdine was drained, resin was washed, and a Kaiser test was performed to ensure successful deprotection. This process was repeated for each amino acid residue in the FLAG sequence.

After the final Fmoc deprotection, protecting groups were removed by adding 1 mL of a 95% TFA, 5% DCM, and 5% TIPS solution to the resin and allowing it to incubate for 1 hour at room temperature with agitation. The solution was drained, and the resin was washed three times with 1 mL DCM. A small clump of resin was removed and placed in a 1.5 mL eppitube. The peptide was cleaved by adding 70 µL of a 50 mg/mL solution of cyanogen bromide dissolved in 5:4:1 ACN: GAA: water and allowing the resin to incubate overnight at room temperature with agitation. The following morning, the cyanogen bromide solution was evaporated using a SpeedVac and the cleaved peptide was dissolved in 60 µL of 50:50 ACN: water solution with 0.1% FA. 25 µL of the dissolved peptide was injected onto an Agilent single quadrupole LC/MS system (**Figure 2.25**).

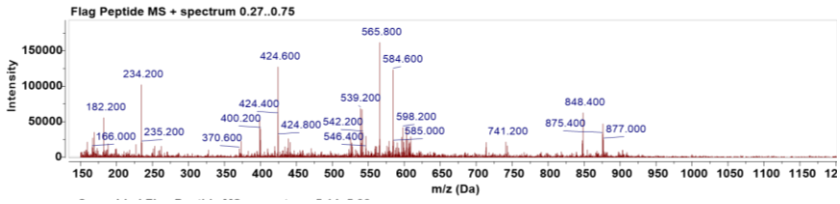

Figure 2.25 LC/MS Trace of the Linker and FLAG Peptide. The structure of the FLAG peptide and linker can be seen in Figure 2.12. The expected mass is 1692.63 g/mol. The (M+3H)/3 mass is seen at 565 m/z.

2.4.4.2 Conjugating the Scrambled FLAG Peptide to Resin

To evaluate whether the interaction between the FLAG antibody and resin loaded with the FLAG peptide was specific, the sequence of the FLAG peptide was scrambled and synthesized on resin containing the linker. Priority was given to separating the aspartic acid residues. The scrambled FLAG peptide was synthesized following the same protocol as described above. Briefly, 25 mg of resin containing the linker was deprotected with 2 mL of 20% piperdine in DMF for 20 minutes at room temperature with agitation. The piperdine was then drained and the resin was washed three times with 1 mL of DMF followed by three washes with 1 mL of DCM. A Kaiser test was performed to ensure the fmoc deprotection was complete. The scrambled FLAG peptide sequence was synthesized directly off the linker by dissolving 4.5 eq. of HBTU, 4.5 eq. of HOBt, 10 eq. of DIPEA, and 5 eq. of Fmoc-Asp(OtBu)-OH (5 eq.) in 600 µL of DMF. The solution was added to the resin and the residue was allowed to couple for 30 minutes at 37 °C with agitation. The solution was drained, and the resin was washed three times with 1 mL of DMF and three times with 1 mL of DCM. A Kaiser test was performed to ensure the coupling was complete. Next, fmoc was removed from the newly coupled residue by adding 2 mL of 20% piperdine in DMF to the

resin. The resin was deprotected for 20 minutes at room temperature with agitation. The piperdine was drained and the resin was washed three times with 1 mL of DMF followed by three washed with 1 mL of DCM. This process was repeated for each amino acid residue in the scrambled FLAG sequence.

After the final Fmoc deprotection, protecting groups were removed from the peptide by the addition of 1 mL of a solution of 95% TFA, 5% DCM, and 5% TIPS to the resin. The resin incubated with the solution for 1 hour at room temperature with agitation. The TFA solution was drained, and the resin was washed three times with 2 mL of DCM. Next, a small clump of resin was placed in a 1.5 mL eppitube and the scrambled FLAG peptide was cleaved from the resin by the addition of 70 µL of a 50 mg/mL solution of cyanogen bromide dissolved in 5:4:1 ACN: GAA: water. The peptide cleavage went overnight at room temperature with agitation. The following morning, the cyanogen bromide solution was evaporated with a SpeedVac. The cleaved peptide was dissolved in 60 µL of a 50:50 ACN: water solution with 0.1% FA. 25 µL of this solution was then injected into an Agilent single quadrupole LC/MS system to confirm the identity of the peptide (**Figure 2.26**).

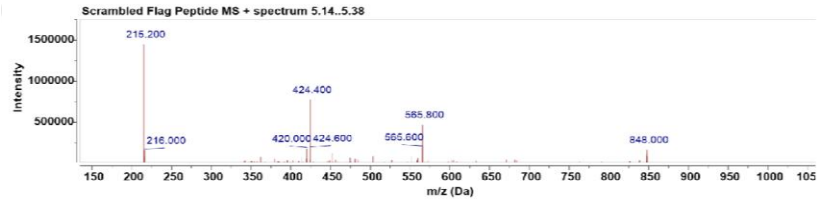

Figure 2.26 LC/MS Trace of the Linker and Scrambled FLAG Peptide. The structure of the scrambled FLAG peptide and linker can be seen in Figure 2.12. The expected mass is 1692.63 g/mol. The (M+2H)/2 mass is seen at 848. The (M+3H)/3 mass is seen at 565 m/z.

2.4.4.3 Detecting a FLAG Antibody Binding the FLAG Peptide On-Bead

FLAG antibody purchased from Novus Biologicals (Cat. NBP2-37823) was used with FLAG resin and scrambled FLAG resin. Prior to the experiment, resin with the FLAG or scrambled FLAG peptide was swollen in PBS by adding 250 µL of PBS to 750 µL of DMF. This solution was added to the resin and allowed to shake for 20 minutes at room temperature. The resin was then checked to ensure no clumps had formed, and the solution was drained. The amount of PBS added to the DMF was gradually increased until the resin was agitated in 1 mL of PBS. On the day of the experiment, FLAG resin and scrambled FLAG resin were split into the wells of a black 96-well plate with a clear bottom such that there was one bead per well. The resin was then blocked with 50 µL of StartingBlockTM (PBS) Blocking Buffer for 30 minutes at room temperature with

agitation. During this time, anti-FLAG antibody was thawed and diluted to 0.25 ng/µL in Odyssey® Blocking Buffer (PBS). The antibody was then serially diluted in the blocking buffer such that the lowest stock solution was 0.002 ng/µL. After blocking, 50 µL of each antibody concentration was added to wells containing FLAG and scrambled FLAG beads in quadruplicate. As a control, both the primary and secondary antibody were allowed to incubate with the FLAG resin to ensure there was no intrinsic fluorescence or nonspecific binding. The controls were prepared the same way as described above. The fluorescence intensity for each control was quantitated and graphed. The highest primary antibody concentration in the well was 12.5 ng and the lowest concentration was 0.1 ng. The beads were allowed to bind the antibody overnight at 4 ˚C with agitation.

The following morning, the primary antibody was removed, and the resin was washed once with 50 µL of PBS. A secondary mouse antibody conjugated with IRDye 800CW, a fluorophore that fluoresces at 795 nm, was used to bind the FLAG antibody and image the resin (LI-COR, Cat. 925-32210). The secondary antibody was diluted 1:10,000 in in Odyssey® Blocking Buffer (PBS). 50 µL of the diluted secondary antibody was added to every well containing resin. The final secondary antibody amount in the wells was 50 ng. The secondary antibody was allowed to incubate with the resin for 40 minutes at room temperature with agitation, protected from light. The secondary antibody was then removed, and the resin was washed once with 50 µL of PBS. The resin was resuspended in 50 µL of fresh PBS and imaged on a LI-COR Odyssey® CLx imaging system. ImageStudio software from LI-COR was used to quantify the fluorescence intensity produced by the secondary antibody. Fluorescence intensity was normalized to an empty well such that the fluorescence intensity of the empty well was 0.0. The experiment was repeated twice, once in triplicate and once in quadruplicate, and the fluorescence intensities for each antibody concentration were pooled. The highest and lowest fluorescence intensities were removed from each antibody concentration and the remaining data was graphed. Occasionally, a resin bead was lost from a well during the washing process. Wells were beads were missing were not quantitated.

2.5 References

(1) Lam, K. S.; Lebl, M.; Krchňák, V. The “One-Bead-One-Compound” Combinatorial Library Method. *Chem. Rev.* **1997**, *97* (2), 411–448. https://doi.org/10.1021/cr9600114.

(2) Martinez Molina, D.; Nordlund, P. The Cellular Thermal Shift Assay: A Novel Biophysical Assay for In Situ Drug Target Engagement and Mechanistic Biomarker Studies. *Annu. Rev. Pharmacol. Toxicol.* **2016**, *56*, 141–161. https://doi.org/10.1146/annurev-pharmtox-010715-103715.

(3) Huynh, K.; Partch, C. L. Analysis of Protein Stability and Ligand Interactions by Thermal Shift Assay. *Curr. Protoc. Protein Sci.* **2015**, *79*, 28.9.1-14. https://doi.org/10.1002/0471140864.ps2809s79.

(4) Lo, M.-C.; Aulabaugh, A.; Jin, G.; Cowling, R.; Bard, J.; Malamas, M.; Ellestad, G. Evaluation of Fluorescence-Based Thermal Shift Assays for Hit Identification in Drug Discovery. *Anal. Biochem.* **2004**, *332* (1), 153–159. https://doi.org/10.1016/j.ab.2004.04.031.

(5) Trader, D. J.; Simanski, S.; Kodadek, T. A Reversible and Highly Selective Inhibitor of the Proteasomal Ubiquitin Receptor Rpn13 Is Toxic To Multiple Myeloma Cells. *J. Am. Chem. Soc.* **2015**, *137* (19), 6312. https://doi.org/10.1021/jacs.5b02069.

(6) Hergenrother, P. J.; Depew, K. M.; Schreiber, S. L. Small-Molecule Microarrays: Covalent Attachment and Screening of Alcohol-Containing Small Molecules on Glass Slides. *J. Am. Chem. Soc.* **2000**, *122* (32), 7849–7850. https://doi.org/10.1021/ja0014032.

(7) MacBeath, G.; Koehler, A. N.; Schreiber, S. L. Printing Small Molecules as Microarrays and Detecting Protein−Ligand Interactions En Masse. *J. Am. Chem. Soc.* **1999**, *121* (34), 7967–7968. https://doi.org/10.1021/ja991083q.

(8) Koehler, A. N.; Shamji, A. F.; Schreiber, S. L. Discovery of an Inhibitor of a Transcription Factor Using Small Molecule Microarrays and Diversity-Oriented Synthesis. *J. Am. Chem. Soc.* **2003**, *125* (28), 8420–8421. https://doi.org/10.1021/ja0352698.

(9) Heusermann, W.; Ludin, B.; Pham, N. T.; Auer, M.; Weidemann, T.; Hintersteiner, M. A Wide-Field Fluorescence Microscope Extension for Ultrafast Screening of One-Bead One-Compound Libraries Using a Spectral Image Subtraction Approach. *ACS Comb. Sci.* **2016**, *18* (5), 209–219. https://doi.org/10.1021/acscombsci.5b00175.

(10) Hintersteiner, M.; Auer, M. A Two-Channel Detection Method for Autofluorescence Correction and Efficient on-Bead Screening of One-Bead One-Compound Combinatorial Libraries Using the COPAS Fluorescence Activated Bead Sorting System. *Methods Appl. Fluoresc.* **2013**, *1* (1), 017001. https://doi.org/10.1088/2050-6120/1/1/017001.

(11) Hintersteiner, M.; Kimmerlin, T.; Kalthoff, F.; Stoeckli, M.; Garavel, G.; Seifert, J.-M.; Meisner, N.-C.; Uhl, V.; Buehler, C.; Weidemann, T.; Auer, M. Single Bead Labeling Method for Combining Confocal Fluorescence On-Bead Screening and Solution Validation of Tagged One-Bead One-Compound Libraries. *Chem. Biol.* **2009**, *16* (7), 724–735. https://doi.org/10.1016/j.chembiol.2009.06.011.

(12) Olivos, H. J.; Bachhawat-Sikder, K.; Kodadek, T. Quantum Dots As A Visual Aid For Screening Bead-Bound Combinatorial Libraries. *ChemBioChem* **2003**, *4* (11), 1242–1245. https://doi.org/https://doi.org/10.1002/cbic.200300712.

(13) Mendes, K.; Ndungu, J. M.; Clark, L. F.; Kodadek, T. Optimization of the Magnetic Recovery of Hits from One-Bead–One-Compound Library Screens. *ACS Comb. Sci.* **2015**, *17* (9), 506–517. https://doi.org/10.1021/acscombsci.5b00090.

(14) Maresh, M. E.; Trader, D. J. Development of a Method To Prioritize Protein–Ligand Pairs on Beads Using Protein Conjugated to a Near-IR Dye. *ACS Comb. Sci.* **2019**, *21* (3), 223–228. https://doi.org/10.1021/acscombsci.8b00165.

(15) Brinkley, M. A Brief Survey of Methods for Preparing Protein Conjugates with Dyes, Haptens and Crosslinking Reagents. *Bioconjug. Chem.* **1992**, *3* (1), 2–13. https://doi.org/10.1021/bc00013a001.

(16) Roberts, M. J.; Bentley, M. D.; Harris, J. M. Chemistry for Peptide and Protein PEGylation. *Adv. Drug Deliv. Rev.* **2002**, *54* (4), 459–476. https://doi.org/10.1016/s0169-409x(02)00022-4.

(17) Pansare, V. J.; Hejazi, S.; Faenza, W. J.; Prud'homme, R. K. Review of Long-Wavelength Optical and NIR Imaging Materials: Contrast Agents, Fluorophores, and Multifunctional Nano Carriers. *Chem. Mater.* **2012**, *24* (5), 812–827. https://doi.org/10.1021/cm2028367.

(18) Gross, E.; Witkop, B. Nonenzymatic Cleavage of Peptide Bonds: The Methionine Residues in Bovine Pancreatic Ribonuclease. *J. Biol. Chem.* **1962**, *237*, 1856–1860.

(19) Hirsch, J. D.; Eslamizar, L.; Filanoski, B. J.; Malekzadeh, N.; Haugland, R. P.; Beechem, J. M.; Haugland, R. P. Easily Reversible Desthiobiotin Binding to Streptavidin, Avidin, and Other Biotin-Binding Proteins: Uses for Protein Labeling, Detection, and Isolation. *Anal. Biochem.* **2002**, *308* (2), 343–357. https://doi.org/10.1016/S0003-2697(02)00201-4.

(20) Denton, K. E.; Krusemark, C. J. Crosslinking of DNA-Linked Ligands to Target Proteins for Enrichment from DNA-Encoded Libraries. *MedChemComm* **2016**, *7* (10), 2020–2027. https://doi.org/10.1039/C6MD00288A.

(21) Zamani, P.; Riahi, M. M.; Momtazi-Borojeni, A. A.; Jamialahmadi, K. Gankyrin: A Novel Promising Therapeutic Target for Hepatocellular Carcinoma. *Artif. Cells Nanomedicine Biotechnol.* **2017**, *0* (0), 1–13. https://doi.org/10.1080/21691401.2017.1388250.

(22) Kim, Y. H.; Kim, J.-H.; Choi, Y. W.; Lim, S. K.; Yim, H.; Kang, S. Y.; Chung, Y. S.; Lee, G.-Y.; Park, T. J. Gankyrin Is Frequently Overexpressed in Breast Cancer and Is Associated with ErbB2 Expression. *Exp. Mol. Pathol.* **2013**, *94* (2), 360–365. https://doi.org/10.1016/j.yexmp.2012.12.002.

(23) Zhen, C.; Chen, L.; Zhao, Q.; Liang, B.; Gu, Y.-X.; Bai, Z.-F.; Wang, K.; Xu, X.; Han, Q. –.; Fang, D. –.; Wang, S. –.; Zhou, T.; Xia, Q.; Gong, W.-L.; Wang, N.; Li, H.-Y.; Jin, B.-F.; Man, J. –. Gankyrin Promotes Breast Cancer Cell Metastasis by Regulating Rac1 Activity. *Oncogene* **2013**, *32* (29), 3452–3460. https://doi.org/10.1038/onc.2012.356.

(24) Bai, Z.; Tai, Y.; Li, W.; Zhen, C.; Gu, W.; Jian, Z.; Wang, Q.; Lin, J. E.; Zhao, Q.; Gong, W.; Liang, B.; Wang, C.; Zhou, T. Gankyrin Activates IL-8 to Promote Hepatic Metastasis of Colorectal Cancer. *Cancer Res.* **2013**, *73* (14), 4548–4558. https://doi.org/10.1158/0008-5472.CAN-12-4586.

(25) Tang, S.; Yang, G.; Meng, Y.; Du, R.; Li, X.; Fan, R.; Zhao, L.; Bi, Q.; Jin, J.; Gao, L.; Zhang, L.; Li, H.; Fan, M.; Wang, Y.; Wu, K.; Liu, J.; Fan, D. Overexpression of a Novel Gene Gankyrin Correlates with the Malignant Phenotype of Colorectal Cancer. *Cancer Biol. Ther.* **2010**, *9* (2), 88–95. https://doi.org/10.4161/cbt.9.2.10283.

(26) Nakamura, Y.; Nakano, K.; Umehara, T.; Kimura, M.; Hayashizaki, Y.; Tanaka, A.; Horikoshi, M.; Padmanabhan, B.; Yokoyama, S. Structure of the Oncoprotein Gankyrin in Complex with S6 ATPase of the 26S Proteasome. *Struct. Lond. Engl. 1993* **2007**, *15* (2), 179–189. https://doi.org/10.1016/j.str.2006.11.015.

(27) Dawson, S.; Apcher, S.; Mee, M.; Higashitsuji, H.; Baker, R.; Uhle, S.; Dubiel, W.; Fujita, J.; Mayer, R. J. Gankyrin Is an Ankyrin-Repeat Oncoprotein That Interacts with CDK4 Kinase and the S6 ATPase of the 26 S Proteasome. *J. Biol. Chem.* **2002**, *277* (13), 10893–10902. https://doi.org/10.1074/jbc.M107313200.

(28) Higashitsuji, H.; Higashitsuji, H.; Itoh, K.; Sakurai, T.; Nagao, T.; Sumitomo, H.; Masuda, T.; Dawson, S.; Shimada, Y.; Mayer, R. J.; Fujita, J. The Oncoprotein Gankyrin Binds to MDM2/HDM2, Enhancing Ubiquitylation and Degradation of P53. *Cancer Cell* **2005**, *8* (1), 75–87. https://doi.org/10.1016/j.ccr.2005.06.006.

(29) Higashitsuji, H.; Itoh, K.; Nagao, T.; Dawson, S.; Nonoguchi, K.; Kido, T.; Mayer, R. J.; Arii, S.; Fujita, J. Reduced Stability of Retinoblastoma Protein by Gankyrin, an Oncogenic Ankyrin-Repeat Protein Overexpressed in Hepatomas. *Nat. Med.* **2000**, *6* (1), 96–99. https://doi.org/10.1038/71600.

(30) Chattopadhyay, A.; O'Connor, C. J.; Zhang, F.; Galvagnion, C.; Galloway, W. R. J. D.; Tan, Y. S.; Stokes, J. E.; Rahman, T.; Verma, C.; Spring, D. R.; Itzhaki, L. S. Discovery of a Small-Molecule Binder of the Oncoprotein Gankyrin That Modulates Gankyrin Activity in the Cell. *Sci. Rep.* **2016**, *6*, 23732. https://doi.org/10.1038/srep23732.

(31) Maresh, M. E.; Zerfas, B. L.; Wuthrich, B. S.; Trader, D. J. Identification of a Covalent Binder to the Oncoprotein Gankyrin Using a NIR-Based OBOC Screening Method. *RSC Adv.* **2021**, *11* (21), 12794–12801. https://doi.org/10.1039/D0RA10976B.

(32) Culf, A. S.; Ouellette, R. J. Solid-Phase Synthesis of N-Substituted Glycine Oligomers (A-Peptoids) and Derivatives. *Molecules* **2010**, *15* (8), 5282–5335. https://doi.org/10.3390/molecules15085282.

(33) Narayanan, A.; Jones, L. H. Sulfonyl Fluorides as Privileged Warheads in Chemical Biology. *Chem. Sci.* **2015**, *6* (5), 2650–2659. https://doi.org/10.1039/c5sc00408j.

(34) Graus, F.; Saiz, A.; Dalmau, J. Antibodies and Neuronal Autoimmune Disorders of the CNS. *J. Neurol.* **2010**, *257* (4), 509–517. https://doi.org/10.1007/s00415-009-5431-9.

(35) Nakamura, H.; Usa, T.; Motomura, M.; Ichikawa, T.; Nakao, K.; Kawasaki, E.; Tanaka, M.; Ishikawa, K.; Eguchi, K. Prevalence of Interrelated Autoantibodies in Thyroid Diseases and Autoimmune Disorders. *J. Endocrinol. Invest.* **2008**, *31* (10), 861–865. https://doi.org/10.1007/BF03346432.

(36) Conrad, K.; Roggenbuck, D.; Reinhold, D.; Sack, U. Autoantibody Diagnostics in Clinical Practice. *Autoimmun. Rev.* **2012**, *11* (3), 207–211. https://doi.org/10.1016/j.autrev.2011.05.014.

(37) Maresh, M. E.; Salazar-Chaparro, A. F.; Trader, D. J. Methods for the Discovery of Small Molecules to Monitor and Perturb the Activity of the Human Proteasome. *Future Med. Chem.* **2020**. https://doi.org/10.4155/fmc-2020-0288.

CHAPTER 3. EVALUATING PROTEASOME STIMULATORS BY MONITORING YEAST LIFESPAN

3.1 Introduction

Aging and its related pathologies pose a significant global health and economic burden, as humans are living longer. Currently, there are no specific medical interventions to slow or reverse the signs of aging, making the discovery of new therapeutics critical to improving the quality of life of an aging population. Aging is driven by several changes in cellular processes.[1] This includes decline in the autophagy pathway and protein clearance by the proteasome.[2,3] This is further exacerbated by dysregulation of the transcriptome and proteome, which leads to accumulation of unwanted proteins in the cell.[4] Protein accumulation in regions of the brain and spinal cord can lead to the onset of neurodegenerative diseases.[5,6] The link between decline of protein clearance pathways and aging has warranted investigation of the proteasome as a therapeutic target for aging.

Recent studies have demonstrated that the naked mole rat, one of the longest-lived mammals, exhibits increased proteasome activity compared to other rodents of similar size.[7] Although the rodents studied showed similar amounts of protein damage, naked mole rats had lower amounts of ubiquitinated proteins in various tissues than other rodents. This suggests that increased proteasome activity facilitates better clearance of proteins, including those that are damaged, and results in a longer lifespan. Conversely, studies with transgenic mice knocked down for proteasome subunit expression exhibited earlier onset of aging and shorter lifespans than normal mice.[8] This phenomenon also extends to humans. Decline in proteasome activity has been observed in several aged human tissues including the brain,[9] heart,[10] and fibroblasts.[11] Interestingly, fibroblasts harvested from centenarians demonstrated increased proteasome activity compared to other aged individuals.[12] Not only was proteasome activity higher in centenarian tissues, but was also similar to that of fibroblasts taken from younger humans.

Currently, there are few tools that can be used to monitor proteasome activity and aging together, slowing efforts to evaluate the proteasome as a therapeutic target. Yeast have emerged as an important tool to study aging.[13] The lifespan of the budding yeast, *Saccharomyces cerevisiae*, can be monitored in several ways. One of which is through monitoring replicative lifespan (RLS), where the ability of a single yeast cell to produce daughter cells is observed over time.[4,14] As yeast age, they begin to produce fewer offspring cells. The ability of yeast to continue to produce

daughters in response to treatment with different compounds is sometimes used to evaluate the impact of small molecules on aging. The chronological lifespan (CLS) of yeast can also be measured.[15] CLS is monitored by determining how many days nondividing yeast survive in response to a treatment (**Figure 3.1**).

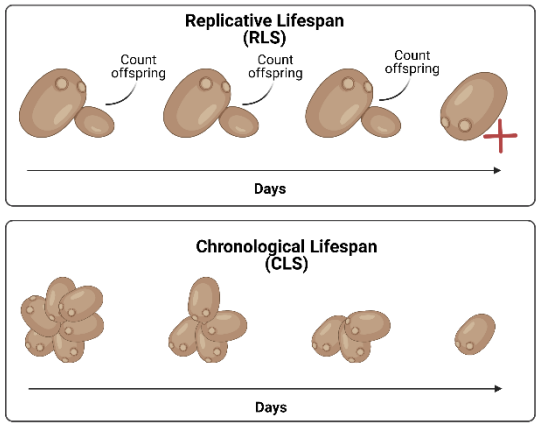

Figure 3.1 Monitoring the Lifespan of Yeast. Yeast lifespan can be evaluated by monitoring the replicative lifespan (RLS) or chronological lifespan (CLS). RLS is studied by counting the number of daughter cells a single mother is able to produce. As the mother cell ages, it is no longer able to produce offspring. CLS is studied by allowing yeast to reach a stationary growth phase and monitoring the number of days the culture can survive in media or sterile water.

While both methods are frequently used to study changes in yeast lifespan, they come with several drawbacks. Monitoring RLS requires careful technical work in which single daughter cells are removed from single mother cells and counted over many days until the mother cell no longer produces offspring.[16,17] This is very labor intensive and requires extreme attention to detail. CLS assays generally involve allowing yeast to reach a nondividing state known as senescence. Outgrowth on agar plates can then be monitored over several weeks. However, this is not amenable to high throughput applications in which longevity is measured in response to dosage with several small molecules.

Both RLS and CLS have been used to study yeast lifespan in response to changes in proteasome activity.[18,19] Since gene expression of yeast can be readily altered using genetic techniques, they are an ideal organism for manipulating proteasome expression and activity. Recently, it was demonstrated that knocking down expression of proteasome subunits in yeast resulted in shortened RLS.[19] Conversely, increased expression of proteasome subunits extended the RLS of the yeast. Increased expression correlated with higher activity of the proteasome, suggesting that its activity directly relates to yeast longevity. Several strains of yeast that are knocked down for proteasome subunit expression are commercially available. Among them is the *rpn4Δ* BY4741 strain. This strain of *S. cerevisiae* is knocked down for the RPN4 transcription factor, which controls expression of proteasome subunits.[19,20] Reduced expression of these genes results in fewer proteasomes, which leads to reduced proteasome activity compared to the wildtype (WT) BY4741 strain.

Thus far, research to elucidate the implications of proteasome activity on yeast lifespan have been limited to genetic manipulation of proteasome expression. However, full characterization of the proteasome as a therapeutic target for aging will rely on the ability to alter the lifespan of an organism in response to dosage with a small molecule proteasome stimulator. The impacts of small molecules that promote autophagy on the CLS of yeast have recently been studied. In fact, the flavonoid 4,4'-dimethoxychalcone (DMC) has been discovered as an autophagy promoting small molecule and was shown to increase the CLS of yeast (**Figure 3.2**).[21] This suggests that manipulation of protein clearance pathways could prevent or delay the onset of aging.

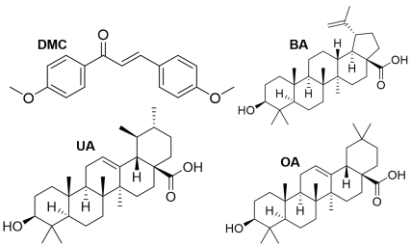

Figure 3.2 Structures of BA, UA, and OA. BA and UA have previously been demonstrated to enhance the activity of the proteasome. We sought to determine if both of these small molecules, and another one of similar structure, OA, could extend the CLS of yeast with reduced proteasome capacity.

Several small molecule stimulators of the proteasome have been identified by our research group and others. Among them are betulinic acid (BA) and ursolic acid (UA) (**Figure 3.2**).[22,23] We sought to determine if the CLS of both WT and *rpn4Δ* yeast could be extended in response to dosage with BA, UA, and another related compound, oleanolic acid (OA) (**Figure 3.2**). This not only required confirmation of proteasome stimulation with a suite of biochemical assays, but also optimization of a CLS assay in which data could be obtained in the short period of one week, compared to over a month with traditional methods.

3.2 Results and Discussion

3.2.1 Identification of Proteasome Stimulators Through an Activity-Based Assay

We first sought to confirm that UA, BA, and OA stimulated the proteasome. Unfortunately, purified yeast proteasome is not commercially available. As a result, we utilized a biochemical assay in which purified human 20S was dosed with each compound and a reporter probe. The human and yeast proteasome share remarkable structural similarity, indicating that the effects of the stimulators may be similar between the two forms.[24] Purified human 20S was dosed with 10 μM of BA, UA, or OA. To ensure that DMC, the compound that would be used as a positive

control, did not stimulate the proteasome samples were also dosed with 10 µM of this compound. As a negative control, samples were dosed with 25 µM of bortezomib (BTZ), a known proteasome inhibitor.[25] Stimulation was monitored with a reporter probe that has recently been developed by our lab, TAS-1 (**Figure 3.3**).[26] This is hybrid probe contains a rhodamine fluorophore housed between a peptide and peptoid region. The peptide region is recognized and cleaved by the proteasome. This releases the rhodamine/peptoid to produce a fluorescent signal. The peptoid region makes the probe more water soluble and cell permeable. We selected this probe to monitor stimulation over other commercially available probes because it is larger, making it a more challenging substrate for the proteasome and less easily cleaved.[26,27] Therefore, TAS-1 is more sensitive to detecting stimulation than other probes that are cleaved quickly by the proteasome.

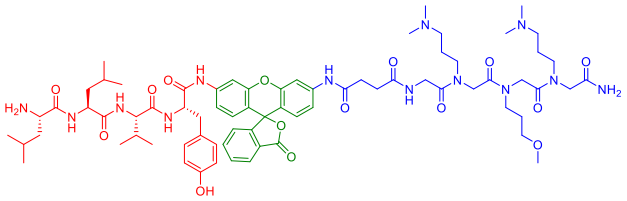

Figure 3.3 Structure of the TAS-1 Reporter Probe. TAS-1 is a peptide/peptoid hybrid probe. The peptide region (red) is recognized and cleaved by the proteasome. This releases the rhodamine (green) which produces a quantifiable fluorescent signal. The peptoid region (blue) facilitates cell permeability and makes the probe more soluble.

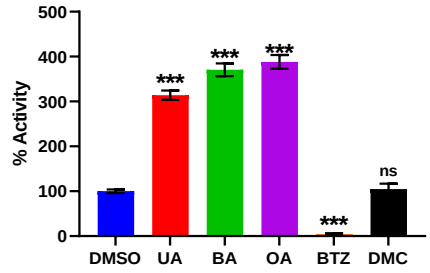

Figure 3.4 UA and Its Derivatives Stimulate Human 20S Proteasomes. Purified human 20S was dosed with 10 µM of UA, BA, OA, or DMSO. As a control, samples were also dosed with 25 µM BTZ or DMSO. TAS-1 was added to a final concentration of 10 µM and fluorescence was monitored over an hour. Slopes from the resulting lines produced by cleavage of the probe by the proteasome were calculated. This was normalized to the DMSO control in which activity was set to 100% for these samples. The resulting data was graphed as a bar graph as shown above. UA, BA, and OA all significantly stimulated the proteasome. As expected, BTZ significantly inhibited proteasome activity. DMC did not alter proteasome activity. * $p < 0.05$, ** $p < 0.01$. *** $p < 0.001$

Purified proteasome was dosed with each compound and 10 µM of TAS-1. Fluorescence was measured over the course of one hour. The slopes of the resulting lines were calculated and normalized to proteasome samples dosed with dimethyl sulfoxide (DMSO). The resulting data was graphed as a bar graph, revealing that all the compounds tested significantly increased proteasome activity (**Figure 3.4**). The extent of stimulation was similar among all the compounds tested. As expected, dosage with BTZ resulted in a significant reduction in proteasome activity. Importantly, DMC did not alter proteasome activity. This was expected, as DMC is known to promote autophagy and should not impact proteasome activity.[21] Since DMC did not alter proteasome activity, we concluded this could be used as a positive control for CLS experiments.

Next, we wanted to confirm that there was a difference in the activity of proteasomes in WT and *rpn4Δ* yeast lysate. Since the *rpn4Δ* strain is knocked down for the RPN4 transcription factor which controls expression of proteasome subunits, this strain should exhibit lower proteasome activity than its counterpart WT strain.[20] To test this, lysate from both strains of yeast were dosed with a commercially available reporter probe, Suc-LLVY-amino-4-methylcoumarin (AMC). Since Suc-LLVY-AMC is well established in the literature and is readily cleaved by the proteasome, we hypothesized it would sensitive to the reduced proteasome activity in the *rpn4Δ* lysate. This probe houses the peptide sequence L-L-V-Y which is recognized and cleaved by the proteasome. Cleavage of the peptide release the AMC fluorophore which produces a quantifiable signal. Lysate from both strains were dosed with 20 µM of the reporter probe and fluorescence was monitored over one hour. The change in RFU per minute was calculated from the resulting lines. Slopes were normalized to the WT strain and graphed (**Figure 3.5**). Strikingly, we observed about a 40% reduction in proteasome activity of the *rpn4Δ* strain compared to the WT strain. This suggests that reduced expression of proteasome subunits correlates to reduced proteasome activity. Further, this validated that both strains could be used to monitor changes in lifespan extension in response to dosage with proteasome stimulators.

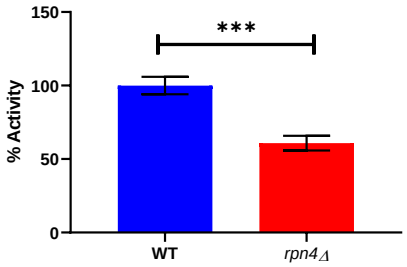

Figure 3.5 Lysate from *rpn4Δ* Yeast Display Reduced Proteasome Activity Compared to WT Lysate. Lysate of both *rpn4Δ* and WT yeast were dosed with 20 µM of suc-LLY-AMC, a reporter probe. Fluorescence was monitored over one hour and the slopes of the resulting lines were calculated. Data was normalized to the WT strain and graphed as shown above. The *rpn4Δ* lysate showed significantly reduced proteasome activity compared to the WT lysate. This was expected, as the *rpn4Δ* strain produces fewer proteasome subunits than the WT strain.

With these results, we next turned our attention to determining if dosage with proteasome stimulators could extend the CLS of yeast. This would provide evidence that the proteasome could be a viable therapeutic target to delay the onset of aging.

3.2.2 Optimization of a Chronological Lifespan Assay with Yeast with Reduced Proteasome Activity

We began our studies of lifespan extension in response to dosage with proteasome stimulators by utilizing an isogenic strain of BY4741 yeast devoid of eight drug resistance-associated genes (*Δ8*).[28] This work was completed in collaboration with the Hazbun lab. We

selected the *Δ8* strain because yeast are equipped with transporters that can expel drugs. Additionally, the cell wall of yeast can make passage of small molecules into the cytosol difficult. We wanted to develop lifespan extension assays with a yeast strain in which a small molecule could readily enter and would not be rapidly exported. We sought to monitor the CLS of this strain, which refers to the ability of the yeast to survive after reaching a nondividing state.[15] To do this, we dosed cultures of yeast with proteasome stimulators and incubated in media with aeration. Every seven days, samples of the *Δ8* yeast were diluted in sterile water and spotted on agar plates. Outgrowth on the plates was monitored at each dilution to determine if any of the proteasome stimulators tested resulted in CLS extension. This was characterized by better outgrowth of the yeast at higher dilutions over time. We selected three proteasome stimulators previously identified by our lab, Vitamin E succinate (VE),[23] UA,[23] and MK886.[29] *Δ8* yeast were dosed with two concentrations of each compound, 200 µM or 20 µM.

We found that the *Δ8* strain had a relatively long lifespan and took almost 40 days to produce measurable results. However, results from dosage with different proteasome stimulators revealed that both MK886 and UA enhanced CLS compared to the DMSO control (**Figure 3.6**). This is evidenced by better outgrowth of 1:1,000 and 1:10,000 diluted samples compared to the same dilutions of the DMSO-dosed samples after 39 days of growth. Since UA extended lifespan to a similar extent as MK886 but could be dosed at 20 µM instead of 200 µM, we selected it for further study.

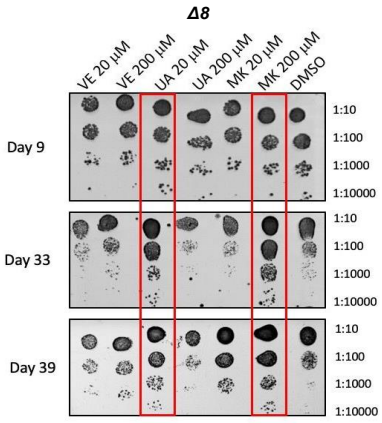

Figure 3.6 VE and UA Extend *Δ8* Yeast Lifespan. *Δ8* yeast were dosed with the indicated proteasome stimulates at a final concentration of 200 µM or 20 µM. Every seven days, samples were diluted in sterile water (right) and spotted on agar plates. Outgrowth was monitored over several weeks. Dosage of 200 µM MK886 or 20 µM UA extended CLS, as evidenced by the increased outgrowth of more dilute samples compared to the DMSO control after 39 days.

Since results took about 40 days to obtain, we sought to alter the CLS assay conditions to make it more amendable to high-throughput applications. It has been well established that several factors of the growth media impact the lifespan of yeast, including amino acid composition, glucose concentration, and nitrogen concentration.[31] We performed a series of CLS assays using three base medias that differed in amino acid composition (SD, SC, and CSM). Each media was supplemented with a combination of low, high, or normal concentration of glucose and nitrogen source. We initially conducted the *Δ8* CLS experiment with

SD media supplemented with normal glucose and nitrogen concentrations. Therefore, we wanted to compare the other media conditions to the initial media to determine if lifespan could be shortened. The assay was further altered by scaling down from culture tubes to a deep well 96-well plate. The deep wells facilitated proper agitation of the yeast while still maintaining aeration. Additionally, more compounds can be tested in a 96-well plate format than culture tubes, which are used in a traditional assay. Since we wanted to use both the WT and *rpn4Δ* yeast strain for experimentation with our small molecule proteasome stimulators, both strains were grown in one of the fifteen media conditions. Every day, a sample from each media was diluted in sterile water and spotted on agar plates. Outgrowth was monitored each day to determine the impacts of the altered media conditions on yeast CLS (**Figure 3.7**).

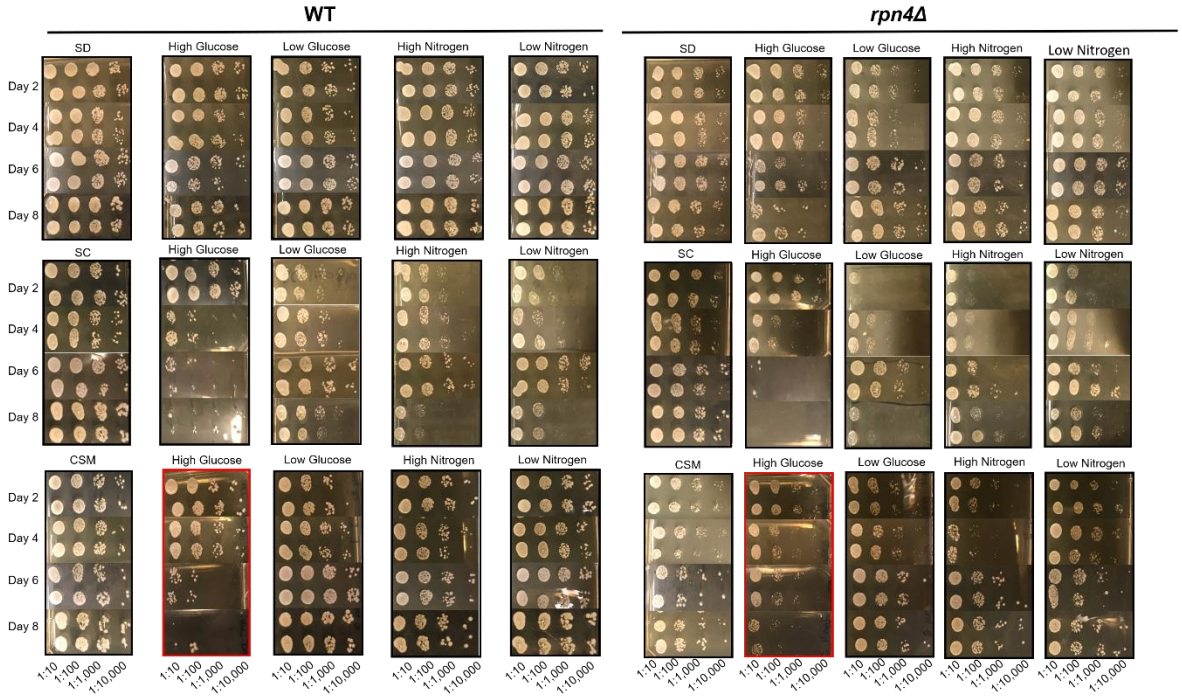

Figure 3.7 Media Conditions Alter CLS of WT and *rpn4Δ* Yeast. Three base medias that differed in amino acid composition, SD, SC, and CSM were supplemented with a low, normal, or high amount of glucose or nitrogen source. Every combination was tested, resulting in 15 media conditions. Both strains of yeast were grown in each media in duplicate in a deep well 96-well plate. Everyday samples of yeast were diluted in sterile water and spotted on an agar plate. Outgrowth was monitored over eight days. Clear differences in CLS were observed in response to growing yeast in the different media conditions. One condition, CSM supplemented with a high glucose concentration and normal nitrogen concentration, reduced WT yeast lifespan to just six days (highlighted in red). Similarly, the *rpn4Δ* strain also exhibited a lifespan around 6 days. Shortening of lifespan from 39 days to just 6 would facilitate faster data acquisition.

We observed clear differences in the ability of both WT and *rpn4Δ* yeast to grow in the various media conditions. Some media conditions resulted in outgrowth that was similar to our original media, SD supplemented with normal glucose and nitrogen concentrations, such as SC with normal glucose and nitrogen concentrations. This was reflected by similar extents of outgrowth after six days. Since the CLS of yeast was not reduced in response to these medias, they were not selected for further investigation. Conversely, some medias resulted in CLS that was too short, such as SC supplemented with high glucose. Since the WT yeast died after only two days, we hypothesized that this media would not produce consistent results and lifespan could not be accurately studied. However, one media, CSM supplemented with high glucose and normal nitrogen concentration, shortened WT lifespan to just six days (highlighted in red). Similarly, *rpn4Δ* CLS was around six days. This was thirty-four days shorter than the lifespan observed in our initial media. This result was somewhat unsurprising, as high glucose concentration has been previously demonstrated to shorten CLS because of possible superoxide generation.[30,32] We believed that reliable data involving lifespan extension after six days could be obtained and this media was used in further experiments.

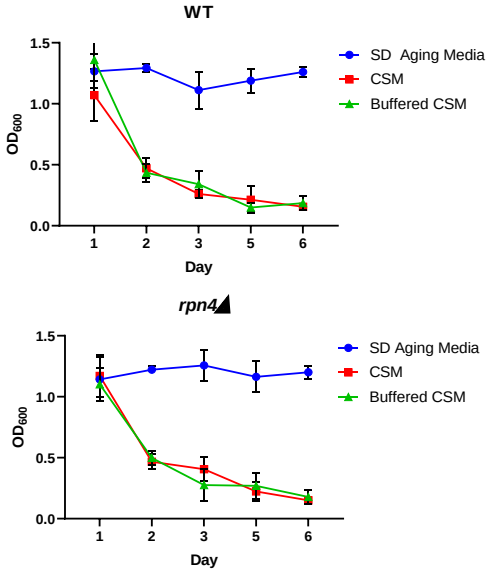

Figure 3.8 Buffered Media Does Not Impact CLS of WT and *rpn4Δ* Yeast in CSM Media. To determine if acidification of the media was responsible for reduced CLS of the yeast, we grew the WT and *rpn4Δ* yeast in SD aging media which is buffered with citric acid, buffered, and unbuffered CSM media. The SD media was used in our initial CLS experiments with the *Δ8* strain. Every day, samples of yeast were diluted in growth media and the OD_{600} was measured after 16 hours of growth. This data was graphed and revealed that the buffered CSM performed almost identically to the unbuffered media. This suggests that acidification of the media was not responsible for reduction in CLS.

Yeast produce acetic acid which results in media acidification and subsequent death. We wanted to ensure that the shortened CLS observed from our optimized media was not the result of acidification. To test this, we performed a CLS assay with WT and *rpn4Δ* yeast that grew in CSM media or CSM media that was buffered with citric acid. Outgrowth of the yeast was compared to our original SD aging that was also buffered with citric acid. Every day, samples were diluted in Yeast Extract-Peptone-Dextrose (YPD) media, grew for sixteen hours, then the OD_{600} was measured. The resulting OD_{600} values were graphed to determine trends in CLS of both strains

(**Figure 3.8**). We found that both buffered and unbuffered CSM media performed almost exactly the same. The OD_{600} of the yeast for both strains decreased at a similar rate. When compared to the buffered SD aging media that was used in the study with the *Δ8* strain, the CLS was, as expected, shortened, since the OD_{600} remained almost the same after eight days in the SD media. Considering that buffering did not appear to contribute the CLS of either yeast strain, we continued to use CSM media with high glucose concentration and normal nitrogen concentration that was not buffered (referred to as aging media from here on).

3.2.3 Elucidating the Impacts of Proteasome Stimulators on Yeast Lifespan

After establishing CLS assay conditions that expedited the data acquisition process, we next wanted to establish our controls for dosing yeast with proteasome stimulators. As a positive control, we used DMC, the small molecule discussed above that has been demonstrated to extend CLS by promoting autophagy.[21] We selected BTZ as our negative control, as it is a well-established proteasome inhibitor.[25,33,34] WT and *rpn4Δ* yeast were grown on agar plates for four days to allow them to enter a senescent state. Then, single colonies were inoculated in YPD broth and grew overnight at 30 ˚C. The following day, the OD_{600} was measured, yeast were pelleted, then resuspended in aging media and added to the wells of a deep well 96-well plate. Samples were dosed in triplicate with either DMSO, 200 µM DMC, or 200 µM BTZ. The final concentration of DMSO in all the wells was 0.2%. Every day, samples of yeast were diluted in sterile water and spotted on agar plates. Outgrowth was compared each day to determine if these compounds influenced CLS of either strain (**Figure 3.9**). We expected to find that dosage with DMC would result in extension of CLS of the yeast and this would be reflected

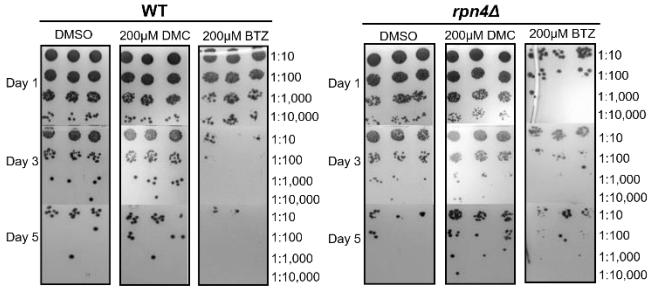

Figure 3.9 Establishing Controls for the CLS Assay. WT and *rpn4Δ* yeast reached a senescent state and were then diluted in aging media. Yeast were dosed with DMSO, or 200 µM DMC or BTZ. Everyday samples of yeast were diluted in sterile water and spotted on agar plates. Outgrowth in response to dosage with one of the small molecules was monitored over six days. Since DMC promotes autophagy and has been previously shown to extend CLS, we expected to find that dosage with this small molecule would result in better outgrowth at high dilutions of yeast compared to the DMSO control. Conversely, we expected to see reduced outgrowth in response to dosage with BTZ compared to the DMSO control. We found that DMC did appear to slightly extend the lifespan of the *rpn4Δ* yeast, but this effect was not as profound in the WT strain. This could because the WT strain has fully functional protein clearance pathways. BTZ successfully reduced outgrowth of both strains, suggesting that inhibiting proteasome activity reduces CLS of both strains.

by better outgrowth of more dilute samples compared to the DMSO control. Conversely, we expected to find that CLS would shorten in response to dosage with BTZ. This would be observed by less outgrowth of the more dilute yeast compared to the DMSO control. Analysis of the outgrowth after six days revealed that DMC extended lifespan of the *rpn4Δ* yeast, while BTZ shortened lifespan. Interestingly, BTZ shortened the lifespan of the WT yeast, but the impacts of DMC were not as profound as the *rpn4Δ* strain. Since the WT strain is not compromised in protein clearance, it is possible that the DMC will not impact this strain to the same extent as the *rpn4Δ* that has reduced proteasome activity.

After establishing our positive and negative controls, we next wanted to determine the optimal concentration of UA for monitoring lifespan extension. Unlike the *Δ8* strain, the WT and *rpn4Δ* strains have fully functional drug transporters, meaning small molecules could be expelled by the yeast. As a result, we tested several concentrations of UA to determine which elicited the best effect on CLS. We expected to find that dosage with higher concentrations of UA would result in greater CLS extension. WT and *rpn4Δ* yeast were grown on agar plates and allowed to reach a nondividing state. Then, single colonies were inoculated in YPD broth and grew overnight. Yeast were diluted in aging media and added to the wells of a deep well 96-well plate. Samples were dosed with 200 µM of DMC and concentrations of UA varying from 5-50 µM. Every day, samples of yeast were diluted in sterile water and spotted on agar plates to monitor outgrowth (**Figure 3.10**). We expected to find that dosage with higher concentrations of UA would result in better extension of CLS. Surprisingly, we found that none of

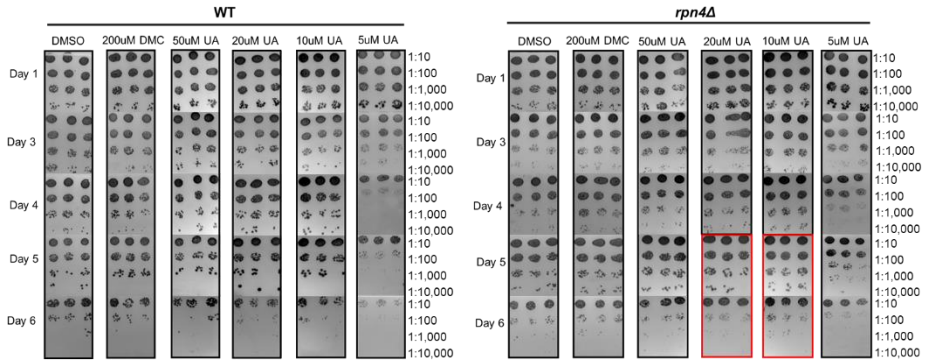

Figure 3.10 Outgrowth of WT and *rpn4Δ* Yeast In Response to Varying Concentrations of UA. WT and *rpn4Δ* yeast reached a nondividing state, diluted in aging media, then dosed with 200 µM of DMC as a control, or varying concentrations of UA in replicates of five. Every day, samples were diluted in sterile water and spotted on agar plates. Outgrowth was monitored over six days and compared to the DMSO control. None of the UA concentrations seemed to impact CLS of WT yeast, as evidenced by similar amounts of outgrowth observed at all dilutions compared to the DMSO control. Dosage of 20 µM and 10 µM of UA (red) slightly extended the CLS of the *rpn4Δ* yeast. This is reflected by better outgrowth of the diluted yeast compared to the DMSO control. It is possible UA did not extend WT CLS because this strain exhibits normal proteasome activity.

the concentrations tested appeared to extend the lifespan of the WT yeast. This is reflected by the similar amounts of outgrowth at each dilution of yeast after six days. However, dosage with 20 µM and 10 µM of UA seemed to slightly extend the lifespan of the *rpn4Δ* strain. This was demonstrated by better outgrowth of more diluted yeast dosed with UA than the DMSO control (highlighted in red). It is unclear why UA did not extend the lifespan of the WT yeast. Since this strain exhibits full expression of the proteasome compared to the *rpn4Δ* strain and thus does not have compromised proteasome activity, it is possible that impairment of proteasome activity is necessary for the stimulators to extend CLS. Similarly, the number of proteasomes in the WT strain is larger than the *rpn4Δ* strain and this may lower the drug to target ratio, making the impacts of UA more minute.

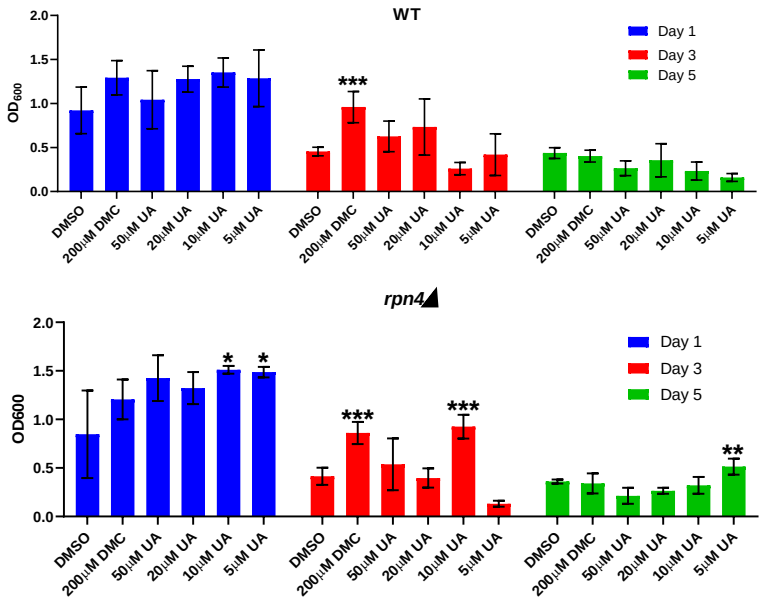

Figure 3.11 Monitoring the OD_{600} of Yeast in Response to Dosage with UA. The OD_{600} of the same samples used for the spot assay was measured for the WT and *rpn4Δ* strain. Samples were diluted in growth media and added to the wells of a sterile 96-well plate. After 18 hours of growth, the OD_{600} was measured for each well. This data correlated with the results observed from the spot assay experiment. DMC was the only small molecule that significantly extended the growth rate of the WT yeast. However, dosage with both UA and DMC significantly increased the growth rate of the *rpn4Δ* yeast on day 3. This suggested that 10 µM was the optimal concentration to monitor lifespan extension.

Since the impacts on CLS seemed slight for the *rpn4Δ* strain, we confirmed this result by monitoring the OD_{600} of each sample by diluting yeast in YPD media in a sterile 96-well plate. Cultures grew for 18 hours, then the OD_{600} was measured and graphed (**Figure 3.11**). Since OD_{600} reflects the growth of the yeast, we expected to find that dosage with UA would result in higher a OD_{600}, indicating better outgrowth. These results correlated with the observations from the spot assay. Dosage with DMC was the only condition that appeared to extend the lifespan of the WT yeast. This was reflected by a significantly higher OD_{600} than the DMSO sample on day three. Similarly, both dosage with DMC and 10 µM of UA significantly increased the OD_{600} of the *rpn4Δ* yeast on day one and three. Excitingly, the enhancement of the OD_{600} was similar to that from

dosage with 200 µM of DMC. None of the other concentrations of UA tested produced a significant result on day three. Although dosage with 5 µM of UA appeared to significantly enhance the growth of the *rpn4Δ* yeast on day five, the low OD_{600} observed for all samples suggested that the yeast were dead, and this result is not reliable.

With the optimal concentration of UA established and observing that UA resulted in only slight CLS extension from the spot assay, we next sought to determine if dosage with the other derivatives of UA, BA and OA, could extend CLS to a greater extent. WT and *rpn4Δ* yeast grew on agar plates until reaching a senescent state. Single colonies were then inoculated in growth media and grew overnight. The following day, yeast were diluted in aging media and dispensed in the wells of a deep well 96-well plate. Samples were dosed with 10 µM of UA, BA, or OA in replicates of three. As additional controls, samples were also dosed with DMSO, 200 µM DMC, or 200 µM BTZ. Every day, samples of yeast were diluted in sterile water and spotted on agar plates. Outgrowth was monitored over six days and compared to the DMSO-dosed samples (**Figure 3.12**). According to our biochemical data obtained with purified human proteasome, all three derivatives stimulated the proteasome to a similar extent, although OA exhibited slightly higher proteasome activity than UA and BA. Therefore, we expected to find that lifespan would be extended to a similar extent with dosage of each small molecule. None of the stimulators appeared to extend lifespan of the WT strain, which was consistent to our previous results. DMC also did not appear to significantly extend CLS of the WT strain. As expected, BTZ reduced WT lifespan to just four days. Excitingly, both UA and BA appeared to extend the lifespan of the *rpn4Δ* yeast (highlighted in red). This was evidenced by better outgrowth of more dilute samples compared to the DMSO

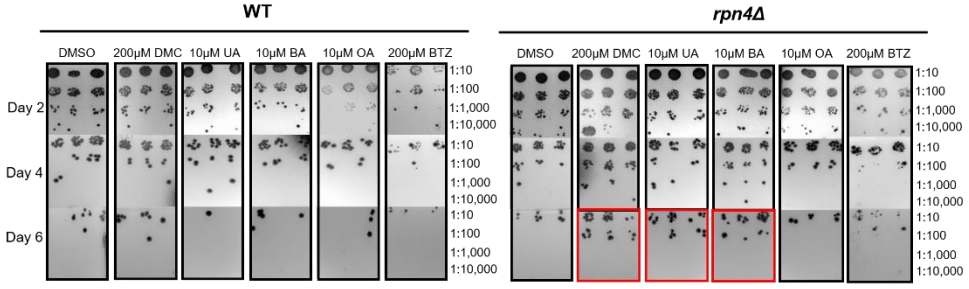

Figure 3.12 UA and BA Extend the CLS of *rpn4Δ* Yeast. WT and *rpn4Δ* yeast were dosed with 10 µM of UA, BA, or OA after reaching a nondividing state. As additional controls, samples were also dosed with 200 µM of DMC or BTZ or DMSO. Every day, samples were diluted in sterile waster and spotted on agar plates. Outgrowth was monitored over six days. The CLS of WT yeast did not appear to extend in response to dosing with any of the compounds, including DMC, which was consistent with previous observations. However, BTZ reduced the lifespan of the WT yeast to just four days. However, dosage of the *rpn4Δ* yeast with UA and BA successfully increased CLS. This is evidenced by the better outgrowth of more dilute yeast compared to the DMSO control (highlighted in red). Outgrowth was similar to that produced by dosing with 200 µM DMC. BTZ reduced lifespan of the *rpn4Δ* to four days.

control. Lifespan was extended to a similar extent as dosage with 200 µM of DMC. Although OA resulted in the highest amount of proteasome stimulation in our biochemical assay, it did not appear to impact the lifespan of the *rpn4Δ* strain. Although it is unclear why OA did not extend the CLS of the yeast, it is possible that this small molecule interacts with other cellular pathways that did not influence the biochemical data. Taken together with the *in vitro* assay with purified human proteasome, these results suggested that the proteasome could be a viable therapeutic target to delay on the onset of aging.

3.2.4 Proteasome Stimulators Enhance Degradation of YFP-Fused α-synuclein in Yeast Lysate

Since none of the compounds appeared to extend lifespan to a greater extent than UA, we moved forward with UA to determine if dosage with this compound could facilitate better degradation of aggregate-prone proteins by the proteasome. Among several proteins known to aggregate is α-synuclein, a protein that is key in the progression of Parkinson's Disease (PD).[5,35] Aggregates of α-synuclein are extremely difficult for the proteasome to clear and buildup eventually leads to cell death. Since proteasome activity is known to slow during aging, it is unsurprising that onset of neurodegenerative diseases such as PD happens later in life. Aggregate formation of α-synuclein is further exacerbated by reduction in

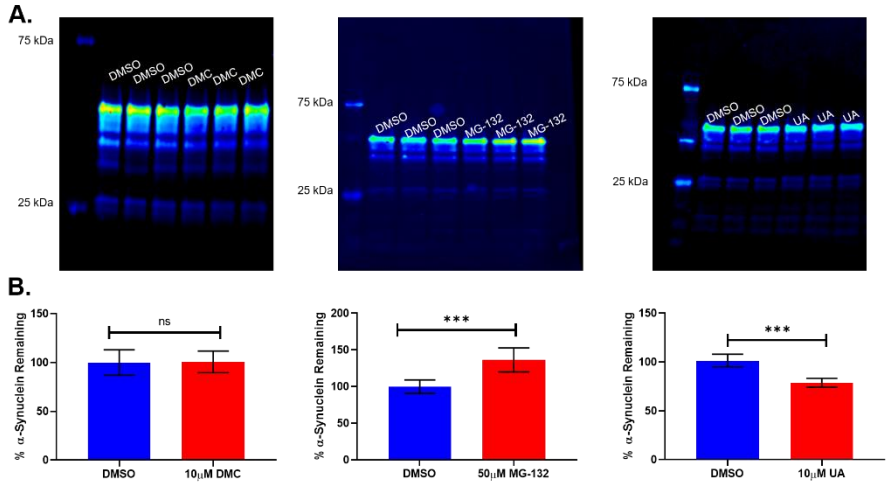

Figure 3.13 UA Facilitates Degradation of YFP-α-Synuclein. Lysate from yeast induced to express YFP-α-synuclein was dosed with 10 µM UA or DMC, or 50 µM MG-132. (A) After dosing, western blots were performed with an antibody that recognizes YFP to determine the amount of α-synuclein remaining in the lysate (B) The experiment was conducted in experimental and technical triplicate. Fluorescence intensities were quantified for each protein band. Signal was normalized to the DMSO control for each independent run, then the data was compiled as graphed. DMC did not significantly impact α-synuclein levels. However, dosage with MG-132 resulted in significant accumulation of α-synuclein. Excitingly, dosage with UA resulted in significant reduction of α-synuclein compared to the DMSO control, suggesting that proteasome stimulator can facilitate better degradation of aggregate-prone proteins.

proteasome activity. We sought to determine if dosage with a proteasome stimulator could assist the proteasome in clearing α-synuclein aggregation.

To test this, we utilized strain of yeast that can be induced to express high levels of α-synuclein fused to Yellow Fluorescent Protein (YFP) at a genomically integrated loci.[36] Importantly, α-synuclein is not natively expressed in yeast, but previous studies suggest that expression of α-synuclein in yeast is relevant to that expressed in human models.[36] Further, aggregates of α-synuclein that are formed in yeast models are detectable.

Yeast were induced to express YFP-α-synuclein and samples were lysed. Lysate samples were dosed with 10 µM of UA or DMC, or DMSO. As an additional control, samples were also dosed with MG-132, a well-established proteasome inhibitor.[37] Lysate incubated with each compound for four hours. Then, protein concentration was normalized. Samples were then subjected to SDS-PAGE, transferred to a membrane for western blot analysis, and blotted with an antibody that recognizes YFP. After staining with a fluorescently labeled secondary antibody, blots were imaged to determine the amount of α-synuclein remaining in the sample (**Figure 3.13A**). The fluorescence intensities for each band were quantified and graphed (**Figure 3.13B**). We expected to find that dosage of the YFP-α-synuclein expressing yeast lysate with UA would result in a significant decrease in remaining α-synuclein, as the small molecule should stimulate the proteasomes in the lysate and facilitate degradation of the protein. Conversely, we expected that dosage with MG-132 would inhibit proteasomes in the lysate and lead to an accumulation of α-synuclein. Excitingly, we found that dosage with UA resulted in a significant decrease α-synuclein levels compared to the DMSO control. This suggested that the small molecule proteasome stimulator facilitates degradation of this aggregate-prone protein. As anticipated, dosage with MG-132 resulted in significant accumulation of α-synuclein, showing that inhibiting

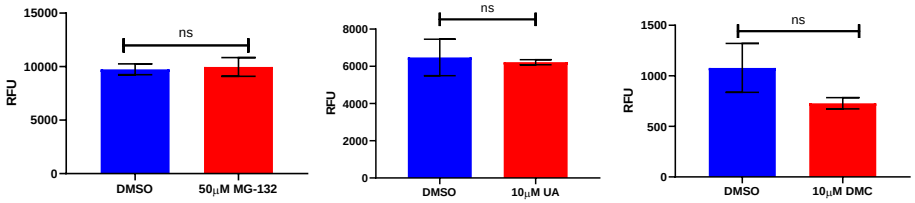

Figure 3.14 Levels of G6PDH Are Not Significantly Impacted by Dosage with Proteasome Stimulators. The western blots stained with the YFP were also stained with an antibody for the housekeeping protein, G6PDH. Levels of the loading control were similar between the DMSO samples and samples dosed with MG-132 and UA. This suggests that no significant degradation or accumulation of this protein resulted from dosed with the proteasome stimulator or inhibitor, respectively. Levels of G6DPH were lower in the DMC dosed lysate than the negative control, all though this was not statistically significant.

proteasome activity leads to buildup of the protein. Dosage with DMC did not significantly alter α-levels. This is unsurprising, as DMC is known to promote autophagy.[21] Autophagy can still occur in the absence of cells, but it is likely that it is not fully functional in this type of system, explaining why no decrease in α-synuclein was observed.[38]

As a loading control, we also blotted the membranes for a housekeeping protein, Glucose-6-phosphate 1-dehydrogenase (G6DPH). Fluorescence intensities of the resulting bands were quantified and graphed (**Figure 3.14**). Dosage of lysate with UA and MG-132 did not result in significant degradation of the loading control. This suggested that chemical stimulation could prove to be a viable strategy to prevent accumulation of unwanted proteins and modulation of proteasome activity does not result in enhanced degradation of all proteins. This has also been previously established.[39] A slight, but not significant, decrease in G6DPH levels was observed in response to dosing with DMC.

3.3 Conclusions

Aging poses a significant public health threat and economic burden as a large portion of the world's population enters later stages of life. One of the hallmarks of aging onset and progression is a decline in protein clearance pathways, including the ubiquitin-proteasome system.[2,3] As proteasome activity declines, unwanted proteins buildup, which can result in cell death. This is further amplified by dysregulation of the transcriptome and proteome, making proper function of the proteasome critical to cell survival. Reduced proteasome activity has been shown in several aged human tissues such as fibroblasts,[11] heart,[10] and brain.[9] Conversely, proteasome activity in centenarians has been demonstrated to be higher than other aged humans and similar to that of younger populations.[12] Long-lived rodents are also known to have increased proteasome activity and decreased buildup of ubiquitinated proteins compared to other rodents of similar size.[7] All of this evidence strongly suggests that there is link between proteasome activity and the onset of aging, warranting thorough investigation of the proteasome as a therapeutic target to delay aging and its associated pathologies. Specifically, elucidating the impacts of small molecule proteasome stimulators on aging pathologies will lead to a better understanding of its onset.

Monitoring cellular changes that take place during aging processes in humans can be difficult, as subjects must be studied over several years. However, model organisms such as yeast have emerged as important tools to study the impacts of aging.[13] Genetic manipulation of genes

encoding for proteasome subunits in yeast have revealed that knocking down proteasome activity significantly shortens their lifespan.[19] Likewise, stabilizing proteasome activity leads to significant lifespan extension. Although these genetic studies have provided critical information to understanding proteasome expression and aging, research surrounding the ability of proteasome stimulators to enhance lifespan is limited. Recently, DMC, a small molecule that enhances autophagy, was shown to increase the lifespan of yeast.[21] This suggests that small molecules that target protein clearance pathways show potential to be developed into therapeutics to delay aging. We sought to determine if proteasome stimulators could elicit a similar extension in lifespan as demonstrated by DMC. To do this, we optimized assays to monitor the CLS of yeast knocked down for proteasome expression.

Our lab and others have identified several proteasome stimulators, including UA and BA.[22,23] We demonstrated that UA, BA, and a related molecule, OA, significantly elevate purified human proteasome activity using a reporter probe recently developed by our lab.[26] We next turned our attention to elucidating the impacts of these stimulators on yeast CLS. We first tested a suite of stimulators for CLS extension with a strain of yeast knocked down for drug efflux pumps, as it is difficult for small molecules to cross the cell wall and be retained.[20] While our initial data revealed some lifespan extension, the assay required over one month of data collection before results were measurable. As a result, we sought to optimize the CLS assay conditions to make it more amenable to high-throughput applications. Alterations in the amino acid composition, glucose, and nitrogen source concentration successfully reduced the assay to just six days. Similarly, the assay was scaled down to a deep well 96-well plate format, greatly increasing the number of small molecules that could be evaluated at one time.

With the new assay conditions optimized, we next established our positive and negative controls. We utilized two BY4741 yeast strains, WT and *rpn4Δ*. The *rpn4Δ* strain is knocked down for proteasome subunit expression, and we demonstrated that this reduced expression is correlated with reduced activity.[20] Both strains were dosed with DMC, the positive control small molecule that enhances autophagy, or BTZ, a proteasome inhibitor.[21,34] Excitingly, CLS extension was observed in response to dosing with DMC and shortened in response to BTZ treatment. From this, we concluded that our optimized assay could be used to detect changes in CLS. Since the extent of proteasome stimulation was very similar among UA and all its derivatives according to the data obtained with our biochemical assay with purified human proteasomes, we utilized UA to establish

the proper dosage concentration to evaluate the impacts of proteasome stimulation on CLS extension. We found that 10 μM resulted in better outgrowth of diluted yeast on agar plates compared to DMSO-dosed control yeast and higher OD_{600}'s after several days. CLS extension was similar to that of the DMC-dosed yeast.

WT and *rpn4Δ* yeast were dosed with UA, BA, OA, DMC, and BTZ. None of the compounds appeared to extend the CLS of WT yeast. This result is not surprising, as these yeast are not compromised for proteasome activity and have more proteasomes in the cell than the *rpn4Δ* strain. However, lifespan extension was detected in the *rpn4Δ* strain in response to dosing with UA and BA. OA did not appear to extend *rpn4Δ* CLS, despite producing significant simulation of human proteasomes. It is possible that OA interferes with other pathways in yeast which prevents CLS extension. Excitingly, lifespan extension that resulted from UA ad BA was similar to that of the DMC-dosed control. Importantly, DMC was added to a final concentration of 200 μM, while UA and BA were added to a final concentration of 10 μM. The extent of lifespan extension was similar among all samples, even though UA and BA were added at a much lower concentration. This suggests that the proteasome could be a viable target to delay the onset of aging.

Since neurodegenerative diseases are characterized by protein buildup and often onset during later stages of life, we next sought to determine if chemical stimulation of the proteasome could facilitate better degradation of aggregate-prone proteins.[1,5] We utilized a strain of yeast that can be induced to express YFP-fused α-synuclein to monitor its degradation in response to chemical stimulation of the proteasome.[36] Lysate from the yeast were dosed with UA, DMC, or MG-132, a known proteasome inhibitor.[37] The amount of α-synuclein remaining in the lysate was determined by western blot analysis and blotting for YFP. We observed a significant decrease in the amount of YFP-fused α-synuclein in response to dosing with UA, which suggested that stimulating the proteasome could facilitate clearance of aggregate-prone proteins. Similarly, a significant increase in α-synuclein levels was observed in response to dosing with MG-132. No significant change in α-synuclein levels was seen in response to dosage with DMC. It is possible that autophagy does not work efficiently in lysate, but this warrants further investigation. Importantly, levels of the housekeeping protein, G6PDH were not significantly altered in response to dosing with UA or MG-132. This suggested that specific proteins are more impacted by modulating proteasome activity and stimulation of the proteasome does not result in enhanced degradation of all proteins.

It should be noted that changes in CLS were minute in response to UA and its derivatives. This could suggest that UA is not potent enough in yeast to cause large extensions in lifespan. Although the specific simulators tested here did not result in extreme CLS extension, the presented optimized CLS assay could be readily used to evaluate other proteasome stimulators. Currently, there are very few techniques to consistently monitor changes in lifespan and aging onset. Therefore, the assays presented here represent a streamline approach to monitor the impacts of small molecule proteasome stimulators on lifespan. In the future, more potent proteasome stimulators should be tested using our new CLS method, as this will further characterize the proteasome as a therapeutic target for aging.

3.4 Materials and Methods

3.4.1 General Materials and Methods

Wildtype (WT) BY4741 and *rpn4Δ* BY4741 yeast strains were purchased from Dharmacon. The α-synuclein expression strain was previously described and has the α-synuclein gene fused to Yellow Fluorescent Protein (YFP) under control of the galactose promoter at the URA3 locus (W303 pGAL-α-Synuclein-YFP::URA3).[36] The yeast strain with increased drug sensitivity had deletions of eight drug resistance and transport-associated genes (*Δ8*).[28]

Components for the yeast media including complete supplement mixture (CSM) amino acid mixture, synthetic complete (SC) amino acid mixture and yeast nitrogen base (YNB) were purchased from Sunrise Science Products. SD aging media amino acid mix was made as previously described.[40] Glucose, ammonium sulfate, and yeast extract were purchased from Fisher Scientific. The following compounds were purchased from Fisher Scientific: ursolic acid (UA), oleanolic acid (OA), betulinic acid (BA), bortezomib (BTZ), and vitamin E succinate. 4'4-Dimethoxychalcone (DMC) was purchased from ChemImpex. The proteasome stimulator MK886 was purchased from Tocris Bioscience. Chronological lifespan experiments were conducted in sterile deep well 96-well plates purchased from VWR. Plates were covered with sterile gas exchange membranes purchased from VWR. Solid black 96-well plates were used for the biochemical assays to monitor proteasome activity and were purchased from Fisher Scientific. MG-132 used in the α-synuclein degradation assays was purchased from Enzo Life Sciences. All compounds were diluted in molecular biology grade dimethyl sulfoxide (DMSO) (Fisher

Scientific). Purified human 20S proteasome used in the biochemical assays was purchased from Boston Biochem.

Yeast stocks were stored in 25% glycerol at -80 ˚C. To recover yeast from the stock, a small amount of yeast was streaked on prewarmed yeast-peptone-dextrose (YPD) plate. Colonies were allowed to grow for two to four days at 30˚C, depending on the experiment. For liquid culture, a single colony from the agar plate was inoculated in 8 mL of liquid YPD media with a sterile inoculating loop and allowed to grow overnight at 30 ˚C with agitation. Yeast were then pelleted for the biochemical assay or further diluted in various media after 4 days for the chronological lifespan (CLS) assay.

3.4.2 Media Preparation

YPD media was prepared by dissolving 10 g of YNB and 20 g of peptone in 900 mL of water. The volume of the solution was adjusted to 1 L with water and then autoclaved. Sterile filtered glucose was supplemented to 2% directly before use.

YPD agar media plates were prepared by adding 20 g of bacto agar to the ingredients used to prepare the YPD media described above. The solution was the autoclaved and gently mixed as it cooled to prevent solidification of the agar. Just prior to pouring the plates, a glucose solution that had been previously filter sterilized was added to the solution such that the final glucose concentration was 2%. Media was poured into sterile single well omni plates (Fisher Scientific) such that the bottom of the plate was completely covered. This was performed in a laminar flow hood. Plates were allowed to solidify for one hour, then were turned upside down to prevent condensation from settling on the plates. Plates were dried in the laminar flow hood overnight, then placed in a plastic bag, sealed, and stored at 4 ˚C until use. Right before use, plates were prewarmed by placing them in a 30 ˚C incubator for 30 minutes.

SD aging media used in the *Δ8* strain CLS experiments was prepared by first dissolving 4.6 g of sodium phosphate dibasic and 1.73 g of citric acid in 450 mL of water. The pH was adjusted to 6.0 by adding 6 M HCl. Subsequently, 0.87 g of aging media amino acid powder, 10 g of glucose, 0.85 g of yeast nitrogen base, and 2.5 g of ammonium sulfate were added. The final volume was adjusted to 500 mL with water. This media was then filter sterilized and supplemented to 2% glucose. CSM aging media with high glucose was prepared by dissolving 1.71 g/L of yeast nitrogen base (Sunrise Science Products) in water and autoclaving. While the liquid was still hot,

0.79 g/L of CSM (Sunrise Science Products) was added and the solution was swirled to mix. Directly before use, a sterile filtered ammonium sulfate solution (nitrogen source) was added to a final concentration of 0.5%. Similarly, a previously sterile filtered solution of glucose was added to a final concentration of 10%.

Induction media for expression of α-synuclein-YFP was prepared by first dissolving 1.7 g of yeast nitrogen base and 5 g of ammonium sulfate in 1 L of water. The solution was autoclaved, and 1.5 g of synthetic complete amino acid mixture was added immediately after autoclaving and stirred until it fully dissolved. Media was supplemented with 2% raffinose and 2% galactose.

3.4.3 Monitoring Purified Human Proteasome Activity in Response to Dosing with UA, BA, OA, DMC, and BTZ

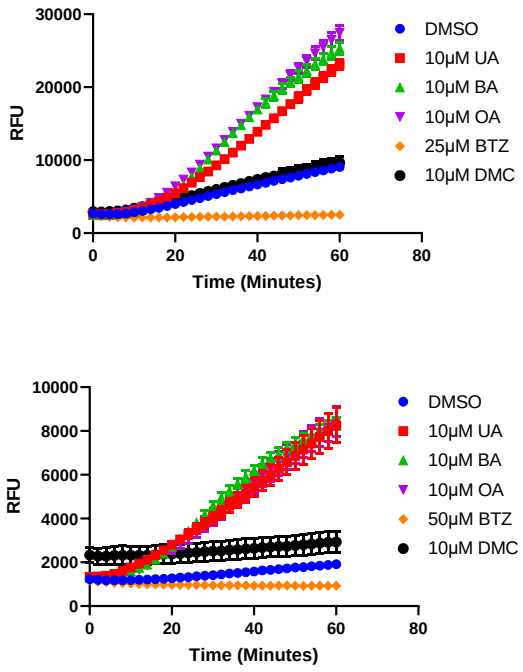

Figure 3.15 Lines Resulting from Cleavage of the TAS-1 Probe by the Proteasome. 50 nM of purified human 20S proteasome was dosed with 10 μM of UA, BA, OA, and DMC. As a control, samples were dosed with 50 μM or 25 μM BTZ or DMSO. The final concentration of TAS-1 was 10 μM. Fluorescence that resulted from cleavage of the reporter probe by the proteasome was monitored every two minutes for one hour and graphed as shown above. Each graph represents one replicate of the experiment. Each line represents three data points.

The day of the experiment, a 20 mM TAS-1 stock was thawed and diluted to a final concentration of 11.4 μM in 50 mM Tris-HCl pH 7.4. Importantly, the tris buffer was made fresh every two days. 1 mg of UA, BA, OA, DMC, and BTZ was weighed. 20 mM stocks of UA, DMC, and BTZ were prepared by dissolving the solids in DMSO. Because of solubility issues, 10 mM stocks of BA and OA were prepared by dissolving the solid in DMSO. 500 μM stocks of UA, BA, and OA were prepared by further diluting the 20 mM or 10 mM stocks in DMSO. A 2.5 mM stock of BTZ was prepared by diluting the 20 mM stock in DMSO. 198 μL of the 11.4 μM TAS-1 solution was added to 0.6 mL eppitubes. 4.5 μL of each compound was added to one tube of TAS-1 solution. Samples were thoroughly vortexed to mix. As a control, 4.5 μL of DMSO was diluted in 198 μL of TAS-1 solution. A black 96-well plate was placed on ice and 45 μL of the TAS-1 solution with the compounds was added to the wells in replicates of

three. The edge wells of the plate were not used. 125 µL of a 50 nM stock of purified human 20S proteasome was prepared by diluting a 2,000 nM stock in tris buffer. This was pipetted up and down several times to mix. 5 µL of proteasome was added to all the wells as quickly as possible. The plate was struck gently on the edges to mix then briefly spun in a plate centrifuge. The final concentration of UA, BA, OA, and DMC was 10 µM. The final BTZ concentration was 50 µM. The final TAS-1 concentration was 10 µM. The final proteasome concentration was 5 nM. The final volume in the well was 50 µL. Fluorescence was read every two minutes for one hour on a plate reader prewarmed to 30 ˚C. This experiment was performed in experimental duplicate and technical triplicate. One run was performed with a final BTZ concentration of 50 µM and one run was performed with a final BTZ concentration of 25 µM.

Data was collected from the plate reader and plotted with GraphPad Prism 9 software (**Figure 3.15**). Slopes from the lines resulting from graphing fluorescence versus time were calculated to determine the rate of cleavage of the probe by the proteasome. The resulting slopes were normalized to the DMSO control dosed samples by taking the average of the DMSO slopes and dividing all other slopes by the average. This number was multiplied by 100 and graphed as a bar graph, as shown in Figure 3.3. Significance was calculated with an unpaired T-test between the DMSO sample and each compound.

3.4.4 Monitoring Proteasome Activity in Lysate of WT and *rpn4Δ* Yeast

Two days prior to the experiment, frozen stocks of WT or *rpn4Δ* yeast were plated on YPD agar plates and incubated at 30 ˚C. Single colonies were inoculated into 8 mL of YPD broth and allowed to grow overnight at 30 ˚C. The following day, yeast were pelleted at 1,000 xg for 5 minutes and media was decanted. Yeast were resuspended in 300 µL of ice-cold lysis buffer (10 mM Tris-HCl, 150 mM NaCl, and 0.5 mM EDTA with no protease inhibitor). About 300 µL of 0.5 mm glass beads were added to each sample. Samples were vortexed at max speed for 25 seconds followed by incubation on ice for 25 seconds. This was repeated a total of seven times. Lysate was clarified by centrifuging at 13,000 rpm for 10 minutes in a centrifuge prechilled to 4 ˚C. Supernatant was transferred to a new tube and protein concentration was determined with a BCA assay. A 40 µM stock of the reporter probe, suc-LLVY-AMC was prepared by diluting a 20 mM stock in tris buffer (see recipe in the above section). 25 µL of the reporter probe solution was added to the wells of a black 96-well plate that was placed on ice. 2 ng/µL stocks of WT and *rpn4Δ*

lysate were prepared by diluting the lysate in tris buffer. 25 µL of this was then added to the wells in replicates of three as fast as possible. The final amount of lysate in each sample was 50 ng. The final concentration of the reporter probe was 20 µM. The plate was gently struck on each side to facilitate mixing of the probe solution with the lysate. The plate was then briefly spun in a plate centrifuge. Fluorescence that resulted from the reporter probe being cleaved by the proteasomes in the lysate was measured every 2 minutes for 40 minutes on a plate reader that was prewarmed to 30 ˚C. The experiment was repeated in experimental triplicate and technical triplicate.

The resulting data was graphed as fluorescence versus time with GraphPad Prism 9 software to visualize cleavage of the probe over time for each trial (**Figure 3.16**). Slopes of the resulting graphed lines were calculated to determine rate of probe cleavage by proteasomes in the samples. For each run, the slope was normalized to the WT strain by calculating the average rate of change of the WT strain then dividing all remaining slopes by this value. Data was combined for each of the three trials and graphed as bar graph as displayed in Figure 3.4. Statistical significance was calculated with an unpaired T-test. This revealed that proteasome activity in the *rpn4Δ* strain was significantly lower than the WT strain.

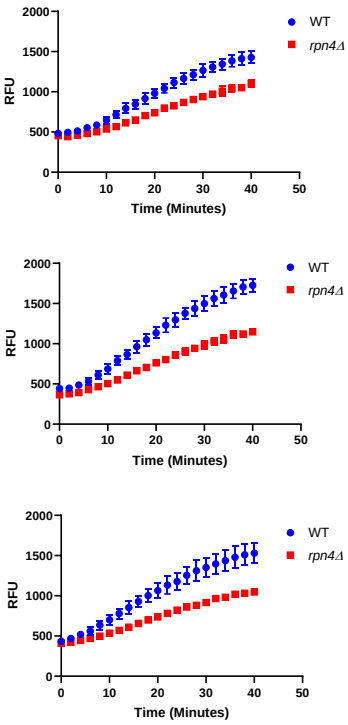

Figure 3.16 Lines Resulting from Dosing WT and *rpn4Δ* Yeast Lysate with a Proteasome Reporter Probe. 50 ng of lysate from the WT and *rpn4Δ* strain was dosed with 20 µM of suc-LLVY-AMC in replicates of three. Fluorescence was monitored every 2 minutes for 40 minutes. This was performed in experimental triplicate and graphed. Each graph represents one trial of the experiment. The slopes of the lines shown were calculated, normalized to the WT strain, and graphed as a bar graph as shown in Figure 3.5.

3.4.5 CLS Assay using Various Proteasome Stimulators with *Δ8* BY4741 Yeast

Several proteasome stimulators from our previous studies, including vitamin E succinate, MK886, and UA were tested for their ability to prolong the lifespan of *Δ8* yeast with a CLS assay. The *Δ8* strain of yeast was selected for initial study because of its increased permeability and intracellular retention of compounds. Other strains of yeast with the full complement of drug transporters and pleiotropic drug resistance genes expel compounds more efficiently, making it difficult to establish the impact of a small molecule on lifespan. This strain served as an

initial point of study to ensure small molecules were more likely to produce a measurable effect. Two days prior to the experiment, a frozen stock of *Δ8* yeast was plated on a YPD agar plate and allowed to grow at 30 ˚C. A single colony was inoculated in YPD liquid media and allowed to incubate overnight at 30 ˚C with agitation. Next, vitamin E succinate, MK886, and UA were weighed and dissolved in DMSO to create a stock concentration of 2 mM and 20 mM. Yeast cultures were diluted in 125 mL of buffered SD aging media such that the final OD_{600} was 0.01. 5 mL of diluted culture was distributed to sterilized culture tubes. 50 µL of each compound at each concentration was added to tubes in duplicate such that the final concentration of test compound in each tube were 20 µM or 200 µM. As a control, two cultures were dosed with 50 µL of DMSO.

Cultures were then allowed to grow to saturation at 30 ˚C for 3 days with agitation. Starting from day 3, yeast cultures were sampled and serially diluted with sterilized deionized water in a 96-well plate. On day 3, 20 µL of each yeast sample was diluted in 180 µL of sterile water to produce a 1:10 dilution in a sterile clear flat-bottom 96-well plate. 30 µL of the 1:10 diluted sample was then further diluted in 270 µL of sterile water to produce a dilution of 1:100. This was repeated two more times with each dilution to achieve final dilutions of 1:10, 1:100, 1:1,000, and 1:10,000. 3 µL of each sample at each dilution were spotted on YPD agar plates and allowed to grow at 30 ˚C for 2 days before the plate image was acquired (Figure 3.5). This was repeated every seven days for 21 days. Then the frequency of spotting plates was increased to every three days until excess death of yeast. The results from this experiment revealed that 200 µM MK886 and 20 µM UA were both capable of prolonging yeast lifespan as evidenced by the enhanced outgrowth at higher dilutions compared to the DMSO-dosed control yeast after 39 days of growth. We proceeded our further studies with UA since it produced the desired effect at a lower concentration than MK886.

3.4.6 Establishing Optimal Media for the Chronological Lifespan Assay

Because the CLS assay required extended incubation of 40 days to produce results, we investigated if altered media conditions would allow this assay to be conducted in a more timely and high-throughput manner. We tested several modified synthetic complete medias differing in amino acid composition (SD, CSM, and SC) and varying glucose and nitrogen source concentrations. Each synthetic complete media was tested with three different glucose concentrations, low (0.2%), normal (2%) or high (10%) and three different ammonium sulfate

concentrations, low (0.05%), normal (0.5%) or high (1%). Media was prepared by dissolving yeast nitrogen base (YNB) in distilled water, then autoclaving. Each concentration level of ammonium sulfate and glucose concentrations was combined with three amino acid mixtures, producing a total of 15 combinations.

Four days prior to the experiment, WT or *rpn4Δ* glycerol stocks that were stored at -80˚C were streaked on YPD agar plates by scrapping a small amount of yeast from the frozen stock with a flamed inoculating loops and spreading the product on an agar plate. Then, individual colonies were inoculated in 8 mL of liquid YPD media with a sterile inoculating loop and allowed to shake overnight at 30 ˚C. The following morning, the OD_{600} of each strain sample was determined with a NanoDrop One system and diluted in 1,500 µL of each of the 15 media types. 500 µL of each sample was added to the wells of a sterile deep well 96-well plate in duplicate. This produced a total of 60 samples, 30 WT samples and 30 *rpn4Δ* samples. The outer edge wells of the 96-well plate were filled with 500 µL of sterile water to prevent excessive evaporation of the samples. The plate was sealed with a sterile gas exchange membrane. A lid was then placed on the plate and secured with medical tape. The plate was then placed in a plastic container with wet paper towels and a lid was attached. The plate was allowed to incubate at 30 ˚C with agitation for 8 days.

Yeast samples removed from the stock plate and diluted 1:10, 1:100, 1:1,000, and 1:10,00 in sterile water. Samples of each dilution were spotted on YPD agar plates and plates were incubated at 30 ˚C prior to imaging. Outgrowth of each media type was compared over 8 days for the WT and the *rpn4Δ* strain. Clear differences in the ability of the yeast to grow in varying media conditions were observable. Neither the WT nor *rpn4Δ* strain apparently differed in their viability after 8 days in the SD aging media. The other two medias, however, had appreciable effects on yeast viability from day 2. We reasoned that media resulting in low viability after only two days would not produce reliable results. The *rpn4Δ* strain appeared to have increased sensitivity compared to WT at low glucose conditions consistent with a recent report that investigated replicative lifespan.[41] However, we found that the low glucose conditions were susceptible to regrowth phenomena which is attributed to release of nutrients from dying cells.[13] Instead, we opted to use the CSM media with high glucose, which will now be referred to as “aging media”, as this appeared to decrease viability of both the WT and the *rpn4Δ* strains more consistently after 6 days. This media was used for the remaining CLS experiments.

It has been previously established that as yeast age, they release acetic acid into the surrounding media, and this may contribute to shortening of lifespan of yeast in unbuffered medias. To test the effects of buffering on the lifespan of both yeast strains in CSM media, we conducted a CLS experiment in which the outgrowth of yeast in citric acid-buffered and unbuffered media was compared to SD media, which contained citric acid as a buffer. If prolonged lifespan was observed in the buffered CSM media, this would indicate that acetic acid released by the yeast was responsible for shortening the lifespan. Media was prepared as described above, except citric acid was added to a final concentration of 0.34% weight by volume (this was consistent with the amount of citric acid added to the SD aging media). Yeast were streaked on a YPD agar plate and grew for four days at 30 ˚C. Then, single colonies were inoculated in 8 mL of YPD liquid media and allowed to grow overnight at 30 ˚C with agitation. The following day, the OD_{600} of both samples was determined with a NanoDrop One system and yeast were diluted in either SD media, buffered aging media, or unbuffered aging media such that the final OD_{600} was 0.2. 500 µL of yeast diluted in each media type was added to wells of a sterile deep well 96-well plate in replicates of five. Every day, 20 µL of each sample was diluted to 1:100 and 30 µL was added to YPD media in a sterile clear, flat bottom 96-well plate and allowed to grow for 16 hours at 30 ˚C with agitation. The OD_{600} of each sample was measured with a Tecan Infinite F200 Pro plate reader system. Values were then graphed and compared over six days.

3.4.7 Monitoring CLS of WT and *rpn4Δ* Yeast Dosed with DMC and BTZ

With the new CLS conditions and media established, we next sought to establish that our positive control DMC, and negative control, BTZ, were sound for further use. We monitored the CLS of WT and *rpn4Δ* yeast in response to dosing with 200 µM DMC or BTZ in replicates of five. The final DMSO concentration was 0.2%. As a control, DMSO was added to five wells of both yeast strains to 0.2%. Edge wells were filled with 500 µL of sterile water to prevent excess evaporation of the sample. A gas exchange membrane was placed on the plate and a lid was secured to the plate with medical tape. The plate was placed in a plastic container with wet paper towels. The plate was agitated at 30 ˚C. Every day for 6 days, 20 µL of each sample was removed from the stock plate and diluted to 1:10, 1:100, 1:1,000, and 1:10,000. Samples from these dilutions were spotted onto YPD plates and allowed to grow. To quantitate yeast viability, a liquid outgrowth experiment was performed where 30 µL of the 1:100 dilution of yeast was added to 270

µL of YPD media in a sterile 96-well plate. A lid was placed on the plate and sealed with parafilm and agitated at 30 ˚C for 18 hours. The OD_{600} of each well was then read on a Tecan Infinite200 Pro plate reader system. This data was compiled and graphed. Values beyond one standard deviation from the mean were designated as outliers and excluded, unless this resulted in less than three values being graphed. In this case, all values were kept. The data was graphed to compare outgrowth of yeast dosed with each compound compared to the DMSO control (**Figure 3.17**). Interestingly, DMC did not appear to greatly impact the OD_{600} of the WT yeast. BTZ, however, was successful in lowering the OD_{600} at day one, indicating decreased viability in response to dosage with this compound. DMC increased the OD_{600} of the *rpn4Δ* strain, indicating that lifespan extension occurred at day 2 and 3. BTZ also successfully prevented growth of the *rpn4Δ* strain on day 1.

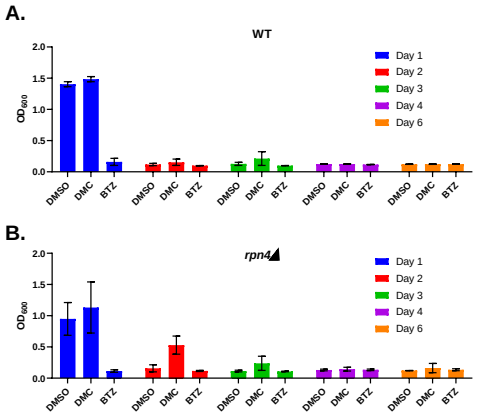

Figure 3.17 Monitoring the OD_{600} of WT and *rpn4Δ* Yeast Dosed with DMC and BTZ. To establish our positive and negative controls, WT or *rpn4Δ* yeast were dosed with DMSO, 200 µM DMC or BTZ. Yeast were diluted every day and spotted on agar plates. Yeast were further diluted in YPD media in a sterile clear 96-well plate and allowed to grow 18 hours. The OD_{600} of each well was measured on a plate reader. This was repeated every day and the data was graphed as shown above. This data, combined with the spot assay, reveals that dosing with DMC extended lifespan of the yeast, as evidenced by higher OD_{600} during the first few days of the assay in the *rpn4Δ* strain. Likewise, BTZ successfully inhibited lifespan, as shown by the lower OD_{600} during the first few days of the experiment. The OD_{600} was similar for all samples on day 6, indicating the excess yeast had died.

3.4.8 Optimizing Proteasome Stimulator Concentrations to Monitor Lifespan Extension

After establishing the positive and negative controls, we then dosed WT and *rpn4Δ* yeast with varying concentrations of UA. We had initially selected 10 µM for monitoring proteasome activity with human proteasome, but it can be difficult for compounds to cross the cell membrane or be retained intracellularly, so we investigated if a higher dosage of UA was necessary to observe an effect on yeast lifespan. WT or *rpn4Δ* strains were tested in replicates of five. A final OD_{600} of 0.1 was dispensed to each well and UA concentrations of 50, 20, 10, or 5 µM, and a DMC concentration of 200 µM were tested. Yeast were allowed to grow at 30 ˚C with agitation and reached saturation the next day. Every day, 20 µL of each sample was removed from the plate and diluted 1:10 in sterile water in a sterile 96-well plate. Outgrowth was compared day to day and to the DMSO control to determine which dosage of UA extended lifespan. Interestingly, none of the

concentrations of UA seemed to significantly extend the lifespan of the WT yeast, as evidenced by similar amounts of outgrowth of each dilution after six days. However, at 20 µM and 10 µM UA appeared to extend the lifespan of the *rpn4Δ* yeast. Since lifespan extension was of similar extent between the two dosages, we proceeded with 10 µM for further study. To further monitor outgrowth, a 1:100 dilution of the aged culture was added to YPD media in a clear, flat bottom 96-well plate and allowed to agitate at 30 ˚C for 18 hours. The OD_{600} of each sample was read on a Tecan Infinite200 Pro plate reader system and the data was compiled. Values that were outside one standard deviation of the mean were excluded, assuming this resulted in at least three values per sample and graphed.

3.4.9 Evaluating CLS Extension of Yeast with Reduced Proteasome Activity in Response to Dosage with Proteasome Stimulators

With the CLS assay and concentration of UA to monitor CLS established, we next turned our attention to elucidating the impact of the derivatives of UA on CLS. Four days prior to the start of the experiment, WT and *rpn4Δ* yeast were plated on YPD agar plates and incubated at 30 ˚C. Single colonies were then inoculated in 8 mL of YPD broth and agitated overnight at 30 ˚C. The OD_{600} of each strain was determined using a NanoDrop One system. Yeast were pelleted at 1,000 xg for 5 minutes. Yeast were resuspended in CSM media supplemented with 10% glucose and 0.5% nitrogen source. 250 µL of yeast was added to the wells of a sterile deep well 96-well plate. Edge wells were excluded and filled with 500 µL of water to prevent evaporation of the samples. UA, BA, and OA were dissolved in DMSO to create 5 mM stock. DMSO stocks of BTZ and DMC were prepared at a concentration of 100 mM. 11 µL of each compound was diluted in the aging media used to dilute the yeast. 250 µL of each compound was added to 5 wells with WT yeast and 5 wells with *rpn4Δ* yeast. The final UA, BA, and OA concentration was 10 µM. 5 wells for each strain were dosed with DMSO at a final concentration of 0.2%. The final BTZ and DMC concentration was 200 µM. The starting OD_{600} of the yeast in each well was 0.2. The plate was sealed with a gas exchange membrane and a plastic lid was secured with medical tape. The plate was placed inside a plastic container with wet paper towels to prevent sample evaporation. The container agitated at 30 ˚C.

Every day, 20 µL of yeast was removed from each sample and diluted in 280 µL of sterile water. 30 µL of this was further diluted in 270 µL of sterile water. This was repeated two more

times to create final dilutions of 1:10, 1:100, 1:1,000, and 1:10,000. 3 µL of each dilution was plated on pre-warmed YPD agar plates. Yeast grew for 2 days at 30 ˚C and the plates were imaged. Outgrowth was monitored by comparing growth of yeast at each dilution over six days.

3.4.10 Monitoring Degradation of YFP-Fused α-Synuclein in Yeast Lysate

Finally, to elucidate the ability of UA to promote the proteasome's ability to clear proteins with a propensity to aggregate, we selected a strain of yeast that expresses YFP-fused α-synuclein. α-synuclein has previously been shown to aggregate in brain cells of people with Parkinson's Disease. To determine the impact of UA on yeast expressing α-synuclein, lysate from yeast was dosed with DMC, UA, or MG-132. Two days prior the experiment yeast was plated on a YPD agar plate and incubated at 30 ˚C. Single colonies were then inoculated in 8 mL of YPD media and grew overnight at 30 ˚C with agitation. The next day, the OD_{600} was determined with NanoDrop One system and yeast were pelleted at 1,000 xg for 5 minutes such that resuspension in 20 mL of induction media (SC media with 2% galactose and 2% raffinose) would produce an OD_{600} of 0.2. The culture was incubated in induction media at 30 ˚C with agitation for six hours. The 20 mL culture was pelleted at 1,000 xg for 5 minutes. The pellet was then resuspended in 50 µL of ice-cold lysis buffer and 50 µL of 0.5 mm glass beads were added to each sample. Samples were vortexed at max speed for 25 seconds followed by incubation on ice for 25 seconds and this was repeated seven times. Lysate was clarified by centrifuging at 13,000 rpm for 10 minutes at 4 ˚C in a prechilled centrifuge. Lysate was then transferred to a new 1.5 mL eppitube. Protein concentration was determined by BCA and 650 µL of a 0.75 µg/µL lysate stocks were prepared by diluting lysate in PBS. 100 µL of lysate was added to six wells of a clear, flat bottom 96-well plate to achieve a final lysate amount of 75 µg per well. 1 µL of DMSO, DMC, UA, or MG-132 was added to wells in triplicate to make a final DMSO concentration of 1%, 10 µM DMC or UA, and 50 µM of MG-132.

The plate was sealed with parafilm to prevent evaporation of the samples and the plate was incubated at 30 ˚C for 4 hours. Protein concentration was then rechecked with a NanoDrop One system and normalized with PBS if necessary (dosage with MG-132 resulted in a slight accumulation of protein, as it inhibits proteasomal degradation of proteins). 11 µL of each sample was mixed with 4 µL of 4X Laemmli buffer (Alfa Aesar) and heated for five minutes. Precast 15-well Mini-PROTEAN TGX Gels 4-15% (BIO-RAD) were prepared and the whole 15 µL sample

was loaded on the gel. Gels were washed three times with water, then protein was transferred to a nitrocellulose membrane with a TurboBlot system (BIO-RAD). Membranes were washed three times with water, then blocked with 5% milk in PBS for 40 minutes at room temperature. An anti-GFP antibody (Novus Biologics) with the ability to also detect YFP was diluted 1:1,000 in protein blocking buffer (LI-COR) and 5 mL was added to the membranes. The blots were incubated at 4 ˚C overnight with gentle agitation. The following morning, the antibody was collected, blots were washed three times with PBS, and an anti-rabbit 800CW antibody (LI-COR) was diluted 1:10,000 in protein blocking buffer (LI-COR) and 5 mL was added to each blot. The secondary antibody incubated with the blots for 40 minutes at room temperature with gentle agitation, protected from light. The antibody was then collected, and the blots were washed three times with PBS, then imaged on a LI-COR CLx Odyssey imaging system.

The fluorescence intensities of bands corresponding to the YFP-fused α-synuclein (about 41 kDa) were quantified with ImageStudio software (LI-COR) and graphed as bar graphs. These graphs were produced by combining data from experimental and technical triplicate (9 values in total). DMSO bands were considered to show 100% of α-synuclein and values for treatment with DMC, UA, or MG-132 were divided by the mean fluorescence of the DMSO bands to produce the amount of α-synuclein remaining in each sample compared to the DMSO control and this was graphed. As a control, the membranes were reblotted for the house keeping protein, G6PDH with a molecular weight around 57 kDa. Blots were re-blocked with 5% milk in PBS for 40 minutes at room temperature with gentle agitation. Then, an anti-G6PDH antibody (Abcam) was diluted 1:1,000 in protein blocking buffer (LI-COR) and 5 mL was added to the blots. This incubated overnight at 4 ˚C with gentle agitation. The following day, the antibody was collected, and the blots were washed three times with PBS. Next, an anti-rabbit 680RD antibody (LI-COR) was diluted 1:10,000 in protein blocking buffer (LI-COR) and 5 mL was added to the blots. This was allowed to incubate at room temperature for 40 minutes with gentle agitation, protected from light. The antibody was then collected, and the blots were washed three times with PBS, then imaged on a LI-COR CLx Odyssey system. Bands corresponding to the fluorescence intensities of the loading control were quantified and graphed, revealing no statistically significant differences. Although not statistically significant, DMC treatment appeared to potentially decrease the level of G6PDH. MG-132 and UA dosage did not reveal any difference, suggesting only certain proteins are being preferentially targeted for proteasomal degradation under the conditions of this experiment.

3.5 References

(1) Saez, I.; Vilchez, D. The Mechanistic Links Between Proteasome Activity, Aging and Age-Related Diseases. *Curr. Genomics* **2014**, *15* (1), 38–51. https://doi.org/10.2174/1389202915011403061133 44.

(2) Koga, H.; Kaushik, S.; Cuervo, A. M. Protein Homeostasis and Aging: The Importance of Exquisite Quality Control. *Ageing Res. Rev.* **2011**, *10* (2), 205–215. https://doi.org/10.1016/j.arr.2010.02.001.

(3) Kaushik, S.; Cuervo, A. M. Proteostasis and Aging. *Nat. Med.* **2015**, *21* (12), 1406–1415. https://doi.org/10.1038/nm.4001.

(4) Janssens, G. E.; Meinema, A. C.; González, J.; Wolters, J. C.; Schmidt, A.; Guryev, V.; Bischoff, R.; Wit, E. C.; Veenhoff, L. M.; Heinemann, M. Protein Biogenesis Machinery Is a Driver of Replicative Aging in Yeast. *eLife* **2015**, *4*, e08527. https://doi.org/10.7554/eLife.08527.

(5) Zheng, Q.; Huang, T.; Zhang, L.; Zhou, Y.; Luo, H.; Xu, H.; Wang, X. Dysregulation of Ubiquitin-Proteasome System in Neurodegenerative Diseases. *Front. Aging Neurosci.* **2016**, *8*. https://doi.org/10.3389/fnagi.2016.00303.

(6) Saez, I.; Vilchez, D. The Mechanistic Links Between Proteasome Activity, Aging and Agerelated Diseases https://www.ingentaconnect.com/content/ben/cg/2014/00000015/00000001/art00006 (accessed Apr 1, 2019).

(7) Pérez, V. I.; Buffenstein, R.; Masamsetti, V.; Leonard, S.; Salmon, A. B.; Mele, J.; Andziak, B.; Yang, T.; Edrey, Y.; Friguet, B.; Ward, W.; Richardson, A.; Chaudhuri, A. Protein Stability and Resistance to Oxidative Stress Are Determinants of Longevity in the Longest-Living Rodent, the Naked Mole-Rat. *Proc. Natl. Acad. Sci.* **2009**, *106* (9), 3059–3064. https://doi.org/10.1073/pnas.0809620106.

(8) Tomaru, U.; Takahashi, S.; Ishizu, A.; Miyatake, Y.; Gohda, A.; Suzuki, S.; Ono, A.; Ohara, J.; Baba, T.; Murata, S.; Tanaka, K.; Kasahara, M. Decreased Proteasomal Activity Causes Age-Related Phenotypes and Promotes the Development of Metabolic Abnormalities. *Am. J. Pathol.* **2012**, *180* (3), 963–972. https://doi.org/10.1016/j.ajpath.2011.11.012.

(9) Kelmer Sacramento, E.; Kirkpatrick, J. M.; Mazzetto, M.; Baumgart, M.; Bartolome, A.; Di Sanzo, S.; Caterino, C.; Sanguanini, M.; Papaevgeniou, N.; Lefaki, M.; Childs, D.; Bagnoli, S.; Terzibasi Tozzini, E.; Di Fraia, D.; Romanov, N.; Sudmant, P. H.; Huber, W.; Chondrogianni, N.; Vendruscolo, M.; Cellerino, A.; Ori, A. Reduced Proteasome Activity in the Aging Brain Results in Ribosome Stoichiometry Loss and Aggregation. *Mol. Syst. Biol.* **2020**, *16* (6). https://doi.org/10.15252/msb.20209596.

(10) Bulteau, A.-L.; Szweda, L. I.; Friguet, B. Age-Dependent Declines in Proteasome Activity in the Heart. *Arch. Biochem. Biophys.* **2002**, *397* (2), 298–304. https://doi.org/10.1006/abbi.2001.2663.

(11) Hwang, J. S.; Hwang, J. S.; Chang, I.; Kim, S. Age-Associated Decrease in Proteasome Content and Activities in Human Dermal Fibroblasts: Restoration of Normal Level of Proteasome Subunits Reduces Aging Markers in Fibroblasts From Elderly Persons. *J. Gerontol. Ser. A* **2007**, *62* (5), 490–499. https://doi.org/10.1093/gerona/62.5.490.

(12) Chondrogianni, N.; Petropoulos, I.; Franceschi, C.; Friguet, B.; Gonos, E. S. Fibroblast Cultures from Healthy Centenarians Have an Active Proteasome. *Exp. Gerontol.* **2000**, *35* (6–7), 721–728. https://doi.org/10.1016/s0531-5565(00)00137-6.

(13) Mirisola, M. G.; Braun, R. J.; Petranovic, D. Approaches to Study Yeast Cell Aging and Death. *FEMS Yeast Res.* **2014**, *14* (1), 109–118. https://doi.org/10.1111/1567-1364.12112.

(14) Polymenis, M.; Kennedy, B. K. Chronological and Replicative Lifespan in Yeast. *Cell Cycle* **2012**, *11* (19), 3531–3531. https://doi.org/10.4161/cc.22041.

(15) Fabrizio, P.; Longo, V. D. The Chronological Life Span of Saccharomyces Cerevisiae. In *Biological Aging: Methods and Protocols*; Tollefsbol, T. O., Ed.; Methods in Molecular Biology™; Humana Press: Totowa, NJ, 2007; pp 89–95. https://doi.org/10.1007/978-1-59745-361-5_8.

(16) Steffen, K. K.; Kennedy, B. K.; Kaeberlein, M. Measuring Replicative Life Span in the Budding Yeast. *JoVE J. Vis. Exp.* **2009**, No. 28, e1209. https://doi.org/10.3791/1209.

(17) Sutphin, G. L.; Delaney, J. R.; Kaeberlein, M. Replicative Life Span Analysis in Budding Yeast. In *Yeast Genetics: Methods and Protocols*; Smith, J. S., Burke, D. J., Eds.; Methods in Molecular Biology; Springer: New York, NY, 2014; pp 341–357. https://doi.org/10.1007/978-1-4939-1363-3_20.

(18) da Cunha, F. M.; Demasi, M.; Kowaltowski, A. J. Aging and Calorie Restriction Modulate Yeast Redox State, Oxidized Protein Removal, and the Ubiquitin–Proteasome System. *Free Radic. Biol. Med.* **2011**, *51* (3), 664–670. https://doi.org/10.1016/j.freeradbiomed.2011.05.035.

(19) Kruegel, U.; Robison, B.; Dange, T.; Kahlert, G.; Delaney, J. R.; Kotireddy, S.; Tsuchiya, M.; Tsuchiyama, S.; Murakami, C. J.; Schleit, J.; Sutphin, G.; Carr, D.; Tar, K.; Dittmar, G.; Kaeberlein, M.; Kennedy, B. K.; Schmidt, M. Elevated Proteasome Capacity Extends Replicative Lifespan in Saccharomyces Cerevisiae. *PLOS Genet.* **2011**, *7* (9), e1002253. https://doi.org/10.1371/journal.pgen.1002253.

(20) Wang, X.; Xu, H.; Ju, D.; Xie, Y. Disruption of Rpn4-Induced Proteasome Expression in Saccharomyces Cerevisiae Reduces Cell Viability Under Stressed Conditions. *Genetics* **2008**, *180* (4), 1945–1953. https://doi.org/10.1534/genetics.108.094524.

(21) Carmona-Gutierrez, D.; Zimmermann, A.; Kainz, K.; Pietrocola, F.; Chen, G.; Maglioni, S.; Schiavi, A.; Nah, J.; Mertel, S.; Beuschel, C. B.; Castoldi, F.; Sica, V.; Trausinger, G.; Raml, R.; Sommer, C.; Schroeder, S.; Hofer, S. J.; Bauer, M. A.; Pendl, T.; Tadic, J.; Dammbrueck, C.; Hu, Z.; Ruckenstuhl, C.; Eisenberg, T.; Durand, S.; Bossut, N.; Aprahamian, F.; Abdellatif, M.; Sedej, S.; Enot, D. P.; Wolinski, H.; Dengjel, J.; Kepp, O.; Magnes, C.; Sinner, F.; Pieber, T. R.; Sadoshima, J.; Ventura, N.; Sigrist, S. J.; Kroemer, G.; Madeo, F. The Flavonoid 4,4'-Dimethoxychalcone Promotes Autophagy-Dependent Longevity across Species. *Nat. Commun.* **2019**, *10* (1), 651. https://doi.org/10.1038/s41467-019-08555-w.

(22) Huang, L.; Ho, P.; Chen, C.-H. Activation and Inhibition of the Proteasome by Betulinic Acid and Its Derivatives. *FEBS Lett.* **2007**, *581* (25), 4955–4959. https://doi.org/10.1016/j.febslet.2007.09.031.

(23) Coleman, R. A.; Trader, D. J. Development and Application of a Sensitive Peptide Reporter to Discover 20S Proteasome Stimulators. *ACS Comb. Sci.* **2018**, *20* (5), 269–276. https://doi.org/10.1021/acscombsci.7b00193.

(24) Schweitzer, A.; Aufderheide, A.; Rudack, T.; Beck, F.; Pfeifer, G.; Plitzko, J. M.; Sakata, E.; Schulten, K.; Förster, F.; Baumeister, W. Structure of the Human 26S Proteasome at a Resolution of 3.9 Å. *Proc. Natl. Acad. Sci.* **2016**, *113* (28), 7816–7821. https://doi.org/10.1073/pnas.1608050113.

(25) Paramore, A.; Frantz, S. Bortezomib. *Nat. Rev. Drug Discov.* **2003**, *2* (8), 611–612. https://doi.org/10.1038/nrd1159.

(26) Zerfas, B. L.; Coleman, R. A.; Chaparro, A. S.; Macatangay, N. J.; Trader, D. Fluorescent Probes with Unnatural Amino Acids to Monitor Proteasome Activity in Real-Time. **2020**. https://doi.org/10.26434/chemrxiv.12043101.v1.

(27) Maresh, M. E.; Salazar-Chaparro, A. F.; Trader, D. J. Methods for the Discovery of Small Molecules to Monitor and Perturb the Activity of the Human Proteasome. *Future Med. Chem.* **2020**. https://doi.org/10.4155/fmc-2020-0288.

(28) Hoepfner, D.; Helliwell, S. B.; Sadlish, H.; Schuierer, S.; Filipuzzi, I.; Brachat, S.; Bhullar, B.; Plikat, U.; Abraham, Y.; Altorfer, M.; Aust, T.; Baeriswyl, L.; Cerino, R.; Chang, L.; Estoppey, D.; Eichenberger, J.; Frederiksen, M.; Hartmann, N.; Hohendahl, A.; Knapp, B.; Krastel, P.; Melin, N.; Nigsch, F.; Oakeley, E. J.; Petitjean, V.; Petersen, F.; Riedl, R.; Schmitt, E. K.; Staedtler, F.; Studer, C.; Tallarico, J. A.; Wetzel, S.; Fishman, M. C.; Porter, J. A.; Movva, N. R. High-Resolution Chemical Dissection of a Model Eukaryote Reveals Targets, Pathways and Gene Functions. *Microbiol. Res.* **2014**, *169* (2–3), 107–120. https://doi.org/10.1016/j.micres.2013.11.004.

(29) Trader, D. J.; Simanski, S.; Dickson, P.; Kodadek, T. Establishment of a Suite of Assays That Support the Discovery of Proteasome Stimulators. *Biochim. Biophys. Acta* **2017**, *1861* (4), 892–899. https://doi.org/10.1016/j.bbagen.2017.01.003.

(30) Jr, S. D.; Ch, M.; Cr, C.; Ra, W.; JL 4th, H. Gene-Nutrient Interaction Markedly Influences Yeast Chronological Lifespan. *Exp. Gerontol.* **2016**, *86*, 113–123. https://doi.org/10.1016/j.exger.2016.04.012.

(31) Santos, J.; Leitão-Correia, F.; Sousa, M. J.; Leão, C. Nitrogen and Carbon Source Balance Determines Longevity, Independently of Fermentative or Respiratory Metabolism in the Yeast Saccharomyces Cerevisiae. *Oncotarget* **2016**, *7* (17), 23033–23042. https://doi.org/10.18632/oncotarget.8656.

(32) Longo, V. D.; Shadel, G. S.; Kaeberlein, M.; Kennedy, B. Replicative and Chronological Aging in Saccharomyces Cerevisiae. *Cell Metab.* **2012**, *16* (1), 18–31. https://doi.org/10.1016/j.cmet.2012.06.002.

(33) Chauhan, D.; Catley, L.; Li, G.; Podar, K.; Hideshima, T.; Velankar, M.; Mitsiades, C.; Mitsiades, N.; Yasui, H.; Letai, A.; Ovaa, H.; Berkers, C.; Nicholson, B.; Chao, T.-H.; Neuteboom, S. T. C.; Richardson, P.; Palladino, M. A.; Anderson, K. C. A Novel Orally Active Proteasome Inhibitor Induces Apoptosis in Multiple Myeloma Cells with Mechanisms Distinct from Bortezomib. *Cancer Cell* **2005**, *8* (5), 407–419. https://doi.org/10.1016/j.ccr.2005.10.013.

(34) Chen, D.; Frezza, M.; Schmitt, S.; Kanwar, J.; Dou, Q. P. Bortezomib as the First Proteasome Inhibitor Anticancer Drug: Current Status and Future Perspectives. *Curr. Cancer Drug Targets* **2011**, *11* (3), 239–253.

(35) McNaught, K. S. P.; Jenner, P. Proteasomal Function Is Impaired in Substantia Nigra in Parkinson's Disease. *Neurosci. Lett.* **2001**, *297* (3), 191–194. https://doi.org/10.1016/S0304-3940(00)01701-8.

(36) Tsai, C.; Aslam, K.; Drendel, H. M.; Asiago, J. M.; Goode, K. M.; Paul, L. N.; Rochet, J.-C.; Hazbun, T. R. Hsp31 Is a Stress Response Chaperone That Intervenes in the Protein Misfolding Process. *J. Biol. Chem.* **2015**, *290* (41), 24816–24834. https://doi.org/10.1074/jbc.M115.678367.

(37) Crawford, L. J. A.; Walker, B.; Ovaa, H.; Chauhan, D.; Anderson, K. C.; Morris, T. C. M.; Irvine, A. E. Comparative Selectivity and Specificity of the Proteasome Inhibitors BzLLLCOCHO, PS-341, and MG-132. *Cancer Res.* **2006**, *66* (12), 6379–6386. https://doi.org/10.1158/0008-5472.CAN-06-0605.

(38) Moparthi, S. B.; Wollert, T. Reconstruction of Destruction - in Vitro Reconstitution Methods in Autophagy Research. *J. Cell Sci.* **2018**, *132* (4). https://doi.org/10.1242/jcs.223792.

(39) Coleman, R. A.; Paschoal Sobreira, T. J.; Aryal, U.; Trader, D. Protein Degradation Profile Reveals Dynamic Nature of 20S CP Small Molecule Stimulation. **2020**. https://doi.org/10.26434/chemrxiv.12180402.v1.

(40) Murakami, C. J.; Wall, V.; Basisty, N.; Kaeberlein, M. Composition and Acidification of the Culture Medium Influences Chronological Aging Similarly in Vineyard and Laboratory Yeast. *PLOS ONE* **2011**, *6* (9), e24530. https://doi.org/10.1371/journal.pone.0024530.

(41) Zou, K.; Rouskin, S.; Dervishi, K.; McCormick, M. A.; Sasikumar, A.; Deng, C.; Chen, Z.; Kaeberlein, M.; Brem, R. B.; Polymenis, M.; Kennedy, B. K.; Weissman, J. S.; Zheng, J.; Ouyang, Q.; Li, H. Life Span Extension by Glucose Restriction Is Abrogated by Methionine Supplementation: Cross-Talk between Glucose and Methionine and Implication of Methionine as a Key Regulator of Life Span. *Sci. Adv.* **2020**, *6* (32), eaba1306. https://doi.org/10.1126/sciadv.aba1306.

CHAPTER 4. DISCOVERY OF IMMUNOPROTEASOME STIMULATORS

4.1 Introduction

Cells undergo several changes in response to inflammatory conditions in order to trigger an immune response against invading pathogens, such as viruses, and warn neighboring cells of tissue damage.[1] Upon interaction with the cytokine interferon gamma (IFN-γ) cells begin to produce new catalytic subunits of the proteasome, β1i, β2i, and β5i.[2] These subunits are incorporated into newly synthesized proteasomes to form the immunoproteasome (iCP) (**Figure 4.1**). The cleavage specificities of these catalytic subunits differ slightly from their sCP counterparts, resulting in a proteasome that is more efficient at generating peptides with hydrophobic C-termini.[3] These peptides are compatible with major histocompatibility complexes type I (MHC-I).[2] The iCP is capable of degrading both cellular proteins and pathogenic proteins into antigenic peptides. Peptide-loaded MHC-I complexes are transported to the cell surface and displayed to immune cells which survey the loaded peptides to detect abnormalities.[4,5] If a peptide:MHC-I complex is recognized by a cytotoxic T-cell, the immune cell takes action to kill the infected cell, preventing propagation of a virus.[6,7] T-cells force the infected cell to undergo apoptosis by either injecting a cocktail of proteases such as granzyme B into the cell or by activating the caspase cascade. Once activated by a virally infected cell, a cytotoxic T-cell can kill multiple cells infected with the same virus.

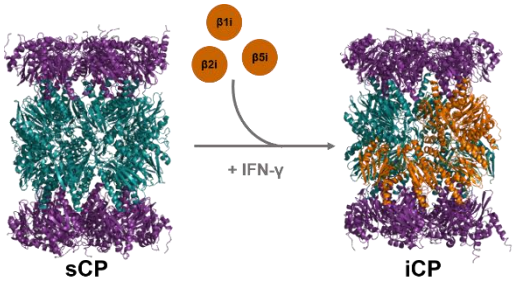

Figure 4.1 Structure of the iCP. Upon stimulation by cytokines such as IFN-γ, three new catalytic subunits are expressed, β1i, β2i, and β5i. These are incorporated into newly synthesized proteasomes to form the iCP.

Because of its important role in antigen presentation via MHC-I expression, the iCP is endogenously expressed in several immune cell types, particularly antigen presenting cells such as dendritic cells.[4,8–10] In addition to the iCP's role in generating antigenic peptides, recent research has also suggested its expression plays an important role in the differentiation of certain immune cell types. Particularly, knockdown of iCP subunit expression in dendritic cells has shown to cause significant changes in the amount of transcription factors such as IRF3, IRF7, STAT1, STAT3, and STAT6.[11] All of these transcription factors are critical for triggering an immune response and

cell division, suggesting the iCP plays an additional role beyond generating antigenic peptides in dendritic cells. Similarly, T-cells from mice knocked down for iCP expression were shown to hyper proliferate in response to mitogenic stimulation compared to mice with normal iCP expression.[11] This suggests that the iCP could be important in regulating mitotic division of certain cell types.

Since viral infection leads to the production of cytokines, including IFN-γ, infected cells often produce the iCP.[1,12] This results in an increase in the number of antigenic peptides in the cell and a subsequent increase in MHC-I expression on the outside of the cell. As a result, immune cells are better able to recognize virally infected cells and clear them to control an infection. As successful infection relies on the virus evading the immune system, several viruses have developed counter measures to reduce MHC-I expression on the outside of the cell.[1] Several viruses, including Human Immunodeficiency virus (HIV),[13–15] Hepatitis C,[16] and Epstein-Barr virus[17] are all known to deploy proteins that inhibit the activity of the iCP. This reduces the number of antigenic peptides and leads to a reduction in MHC-I expression on the outside of the infected cell. As a result, circulating T-cells do not detect the infection and the virus propagates. It should be noted that viruses must maintain a delicate balance of MHC-I expression reduction, as too drastic of a reduction will trigger the immune system to kill the abnormal cell.[18,19]

In addition to its role in aiding with antigen presentation during viral infection, recent research suggests the iCP is expressed in other disease states such as cancer.[20] Cancer cells often rely more heavily on proteasome activity than normal cells to clear protein buildup that results from abnormal levels of transcription and translation.[21,22] Some cancers are marked by increased expression of the iCP such as some forms of breast,[23] prostate,[24] and multiple myeloma (MM).[25] Although the exact implications of iCP expression in these cancers remains unclear, attention has been turned to the iCP as a novel target for therapeutic intervention. As most healthy cells do not express the iCP, it could be used to discriminate between normal and cancerous cells. Additionally, great success in the treatment of cancers such as MM with agents that inhibit the standard proteasome suggest that the iCP could also prove to be an important target for inhibition by small molecules.[26] Currently, several iCP specific inhibitors are under development and research to elucidate their impacts on cancer cells is ongoing.[27–29]

More recently, iCP expression has been detected in a variety of autoimmune disorders[30] and neurodegenerative diseases.[31] Autoimmune diseases are generally characterized by a dysregulated immune response in which immune cells attack normal body tissues. This results in a wide array of symptoms and chronic inflammation. Release of cytokines due to inflammation such as IFN-γ can trigger expression of the iCP in tissues in which it would not normally be expressed.[32] iCP expression has been detected in tissues implicated in autoimmune disorders such as multiple sclerosis[33] and type 1 diabetes.[34] Similarly, expression of the iCP has been detected in brain tissue of patients with neurodegenerative disorders such as Alzheimer's[35] and Huntington's disease.[31] One of the hallmarks of neurodegenerative disease progression is the slowdown of proteasome activity and subsequent buildup of unwanted proteins in the cell.[36] Similar to some autoimmune diseases, tissues in the brain can become inflamed as cellular damage from protein buildup progresses and are exposed to a plethora of cytokines, including IFN-γ. This triggers expression of the iCP in these tissues. The implications of iCP expression in both autoimmune disorders and neurodegenerative diseases remain to be fully understood, but modulation of its activity could represent a novel strategy to treat some forms of these diseases.

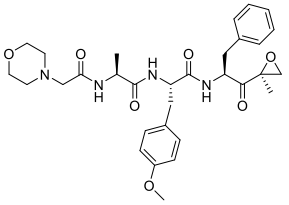

Figure 4.2 Structure of ONX-0914. ONX-0914 was among the first iCP selective probes discovered. It specifically binds the β5i subunit with 20-fold specificity over the β5 subunit. It is commercially available and commonly used to modulate iCP activity.

Since iCP activity has been implicated in a suite of biological processes such as antigen presentation during viral infections, certain cancers, autoimmune disorders, and neurodegenerative diseases, attention has been turned to modulating its activity. In the case of cancer, autoimmune disorders, and neurodegenerative disorders, in which increased iCP activity is thought to exacerbate these conditions, reduction of its activity could result in therapeutic benefit. Several small molecule inhibitors have resulted from research to fully characterize the implications of iCP expression in these diseases. Among these inhibitors is ONX-0914, an epoxyketone that shows 20-fold selectivity for the β5i subunit compared to the β5 subunit of the sCP (**Figure 4.2**).[34] Dosage of ONX-0914 in mouse models of rheumatoid arthritis resulted in reduction in disease progression, indicating that inhibition of the iCP's activity could represent a new strategy to treat some autoimmune disorders.[34]

Although work is underway to determine the impacts of iCP inhibition in disease models characterized by aberrant iCP expression, progress lags in elucidating the biological impacts of iCP stimulation. The well-established link between viral inhibition of the iCP and decreased MHC-

I expression suggests that the iCP could function as a target for therapeutic intervention against certain viral infections. This could be particularly useful for chronic infections such as HIV, where infected cells continuously evade the immune system.[37,38] Latently HIV-infected cells can remain dormant for several years and represent a significant challenge in the development of a cure for HIV, as they cannot be readily targeted by the immune system for elimination. It is possible that stimulating iCP activity with a small molecule could rescue its inhibition by certain viruses. This could then lead to an increase in the pool of antigenic peptides in the infected cell and subsequent increased expression of MHC-I:peptide complexes on the outside of the cell. Restoring MHC-I expression on the cell surface would allow circulating T-cells to recognize infected cells and clear them. Here, we describe the impacts of ursolic acid (UA) on iCP activity *in vitro* and in cells induced to express the iCP.

4.2 Results and Discussion

4.2.1 Identification of Ursolic Acid and its Derivatives as Immunoproteasome Stimulators

UA has previously been reported as a stimulator of the 20S.[39] Similarly, we extensively studied the impacts of UA and structurally similar derivatives, betulinic acid (BA), and oleanolic acid (OA) on the chronological lifespan of yeast with reduced proteasome activity in Chapter 3. After dosage of purified human 20S with 10 µM of UA, BA, or OA, a significant increase in activity was observed (**Figure 4.3**). We next wanted to determine if UA could also stimulate the iCP. Our lab has recently developed a probe, called TBZ-1, that can specifically detect iCP activity in a variety of biochemical assays and in live-cells (**Figure 4.4**).[40] Like the TAS-1 probe, TBZ-1 is a peptide/peptoid hybrid probe that contains a rhodamine moiety.

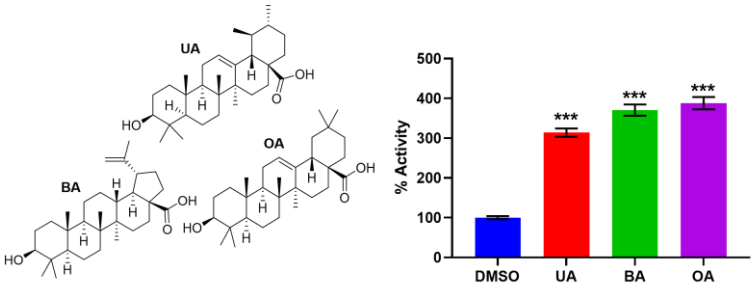

Figure 4.3 UA and Its Derivatives Significantly Increase sCP Activity. Purified human 20S proteasome was dosed with 10 µM of UA, BA, or OA. TAS-1, an sCP reporter probe, was then added to the samples and cleavage of the probe by the sCP was monitored over one hour. Rate of cleavage of the probe was calculated for each compound and normalized to samples dosed with DMSO. This revealed that UA, BA, and OA all significantly increase sCP activity. * $p < 0.05$, ** $p < 0.01$, *** $p < 0.001$

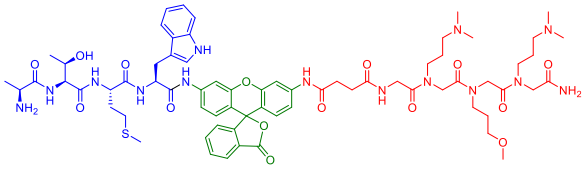

Figure 4.4 Structure of TBZ-1. TBZ-1 is a reporter probe that is cleaved by the iCP. The peptide region (blue) is specifically recognized by the iCP and cleaved. This releases the rhodamine (green) to produce a fluorescent signal. The peptoid region (red) makes the probe cell permeable and more soluble.

The peptide sequence is recognized by the iCP and cleaved, which releases the rhodamine-peptoid to produce a fluorescent signal. The peptoid region makes TBZ-1 more soluble and cell permeable. To evaluate the impacts of UA on iCP activity, we dosed purified iCP with varying concentrations of UA and with TBZ-1. Changes in fluorescence intensity were monitored over one hour and compared to samples dosed with DMSO (**Figure 4.5**). We observed a dose-dependent increase in iCP activity, with dosage of 50 µM UA resulting in a 500% increase in activity compared to DMSO control samples.

After demonstrating that UA stimulates the iCP, we next sought to determine if BA and OA were also iCP stimulators. Purified iCP was dosed with 25 µM, 5 µM, or 0.5 µM of each compound and cleavage of TBZ-1 was monitored over one hour. Our previous results indicated that UA and its derivatives stimulate the sCP to a similar extent, so we anticipated to see an analogous result with iCP stimulation. Dosage of the iCP with varying concentrations of each compound confirmed this hypothesis; UA and all its derivatives stimulated the iCP to a similar extent, suggesting that other derivatives have similar potency (**Figure 4.6**).

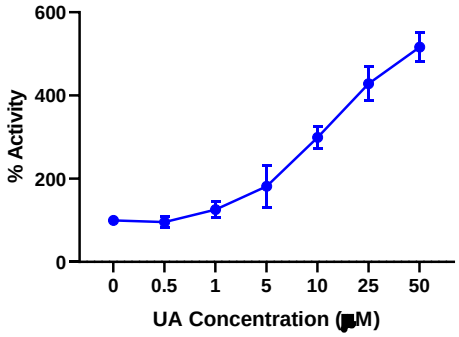

Figure 4.5 UA Stimulates the iCP in a Dose-Dependent Manner. 5 nM of purified iCP was dosed with varying concentrations of UA. TBZ-1 was added to a final concentration of 15 µM and fluorescence was monitored over one hour. Slopes that resulted from the iCP cleaving the probe over time were calculated and normalized to DMSO-dosed samples. This revealed that UA stimulates the iCP in a dose-dependent manner.

Thus far, no stimulators of the iCP have been reported and the iCP largely remains as an underexplored target for therapeutic intervention. We previously established that UA and its derivatives significantly stimulate the sCP. Here, we demonstrated that this also extends to the iCP. With these stimulators in hand, we next turned our attention to elucidating the impacts of UA dosage in cells induced to express the iCP.

4.2.2 Monitoring iCP Activity in Cells Induced to Express the iCP

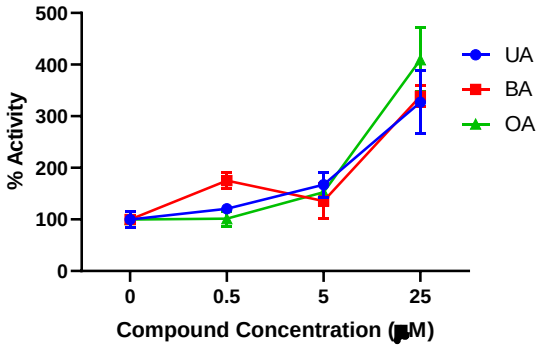

Figure 4.6 UA and Its Derivatives Stimulate the iCP. 5 nM of purified iCP was dosed with varying concentrations of UA, BA, and OA. TBZ-1 was added to a final concentration of 15 μM and fluorescence was monitored over one hour. Slopes that resulted from cleavage of the prober over time were calculated for each compound and normalized to control samples dosed with DMSO. UA and all its derivatives stimulate the iCP.

After determining that UA and its derivatives stimulated purified iCP, we next wanted to determine if UA could stimulate the iCP in cells. As previously discussed, most cells do not endogenously express the iCP. However, IFN-γ can trigger its expression in a variety of cell types. To begin this study, we first needed to establish conditions to induce iCP expression and select a suitable cell line. Cell lines such as BT-20 (breast carcinoma), and MRC-5 (lung fibroblasts) were dosed with varying amounts of IFN-γ for three days. iCP expression was determined by western blot analysis of cell lysates in which expression of β5i was compared to β5 expression. We expected to find that the amount of β5i present in the lysate would increase with increasing amounts of IFN-γ. This should have correlated with a decrease in the amount of β5 present in the lysate. Western blot analysis revealed that all cell lines could be induced to express the iCP, as evidenced by the presence of a band when blotting with a β5i antibody (**Figure 4.7**). As expected, dosage with higher amounts of IFN-γ resulted in increased expression of the β5i subunit, indicating the iCP was expressed in the cells.

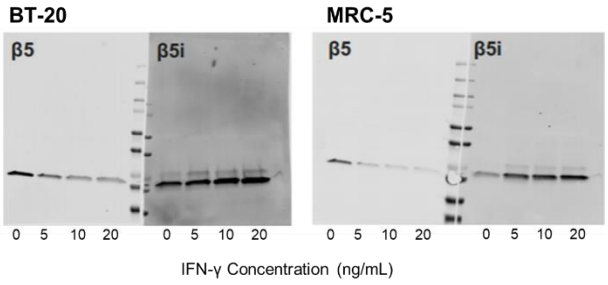

Figure 4.7 Cells Dosed with IFN-γ Express the iCP. BT-20, and MRC-5 cells were dosed with varying amount of IFN-γ for three days and western blots were performed with a β5 and β5i antibody to monitor expression of the sCP and iCP, respectively. Bot cell lines showed an increase in iCP expression, as evidenced by the presence of a band after blotting for β5i. This was met with a correlating decrease in the intensity of the β5 band. MRC-5 was selected as a suitable cell line for further experimentation because the β5 band intensity decreased most significantly at every IFN-γ amount tested compared to the BT-20 cells. This indicated that these cells are expressing mostly iCP and not a mixture of the sCP and iCP. **Data collected by Christine Muli*

Although all the tested cell lines resulted in expression of the iCP, the amount of sCP remaining after IFN-γ treatment varied. The BT-20 cells still expressed the β5 subunit after dosage of up to 20 ng/mL of IFN-γ. This indicated that the sCP was still being expressed.

Since we had demonstrated that UA stimulated both the sCP and iCP, we sought to select a cell line that predominantly expressed the iCP over the sCP. Dosage with as little as 5 ng/mL of IFN-γ in the MRC-5 cells resulted in the largest decrease in β5 expression and subsequent increase in β5i expression of the cell lines tested. Since these cells appeared to express the iCP to a greater extent than the sCP, we selected MRC-5 as our cell line for further studies.

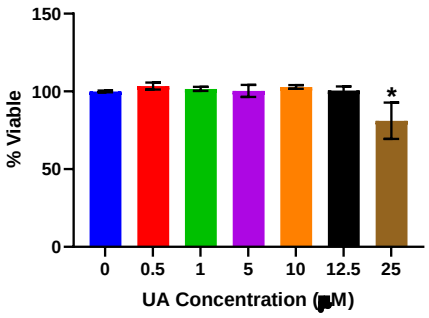

Figure 4.8 Viability of iCP-Expressing MRC-5 Cells After Dosage with UA. MRC-5 cells were inducted to express the iCP by dosing with 5 ng/mL of IFN-γ for 2 days. Cells were then dosed with varying concentrations of UA for 2 hours. A Cell Titer Glo assay was performed to determine viability of the cells after dosing. Luminescent signal was normalized to cells dosed with DMSO (0 μM). Only dosage with 25 μM of UA resulted in significant cell death.

After establishing a suitable cell line for iCP expression, we next sought to determine if dosage of iCP-expressing cells with UA would result in iCP stimulation. MRC-5 cells were dosed with 5 ng/mL of IFN-γ for two days then dosed with varying concentrations of UA for two hours. A viability assay was performed to determine the extent of cytotoxicity (**Figure 4.8**). This revealed that only dosage with 25 μM of UA resulted in significant cell death. However, all other concentrations tested were not cytotoxic to the cells. As a result, 10 μM was selected as an initial concentration for monitoring changes in iCP activity.

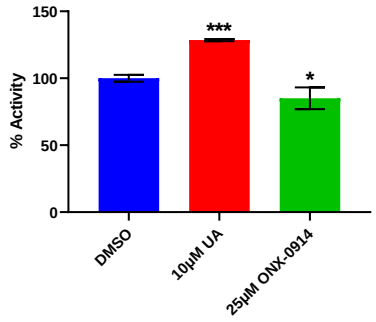

Figure 4.9 UA Stimulates the iCP in Cells. MRC-5 cells were induced to express the iCP and 5,000 cells were seeded in the wells of a 96-well plate. Cells were dosed with 10 μM of UA, DMSO, or 25 μM ONX-0914 for 2 hours. Cells were washed and dosed with 31 μM of TBZ-1. Fluorescence was monitored for 1.5 hours. Slopes of the resulting lines were calculated and values above or below one standard deviation were removed for each sample. Slopes were normalized to the DMSO control and graphed as shown. This revealed that dosage with UA stimulated the iCP. Importantly, dosage with 25 μM ONX-0914, an iCP inhibitor, significantly reduced activity.

To determine the extent of iCP stimulation in cells, we utilized the TBZ-1 probe, as it is cell permeable.[40] Although our western blot analysis showed that the sCP was still expressed in these cells after dosage with IFN-γ, the iCP expression represented the vast majority of proteasomes present in the cells. Similarly, TBZ-1 is more selective toward the iCP than the sCP, suggesting that signal produced by its cleavage in cells primarily resulted from iCP activity. MRC-5 cells were induced to express the iCP by dosing with 5 ng/mL of IFN-γ for two days. Cells were then dosed with 10 μM of UA. After incubating for two hours, cells were dosed with 31 μM of TBZ-1 and fluorescence

was monitored over one and a half hours. The lines that resulted from the probe being cleaved over time were graphed and the resulting slopes were calculated. The slopes were normalized to DMSO-dosed cells and analyzed (**Figure 4.9**).

Dosage with 10 μM UA resulted in a significant increase in iCP activity, which indicated that UA stimulated the iCP both *in vitro* and in cell models. Importantly, a significant decrease in iCP activity was observed in response to dosing cells with 25 μM of ONX-0914, a known iCP inhibitor. Previous viability studies with iCP-expressing MRC-5 cells dosed with ONX-0914 suggested that this concentration is nontoxic (See Materials and Methods section for viability data).

The results of this study indicated that UA stimulates the iCP in a cell model. While significant research remains to be performed to fully characterize UA as an iCP stimulator, this initial study suggested that it could be an interesting small molecule to develop into a tool to monitor the impacts of an increase iCP activity on MHC-I expression.

4.3 Conclusion

The iCP has emerged as an interesting therapeutic target because it is generally only expressed under inflammatory conditions such as a viral infection.[40] Recently, iCP expression has also been implicated in a variety of diseases such as hematological cancers,[20] autoimmune disorders,[30] and neurodegenerative diseases.[35] Since the iCP is not typically highly expressed in healthy counterpart tissues of these diseases, it represents a method to discriminate between normal and abnormal cells. Modulation of iCP activity through the use of small molecules could represent a novel method to treat these diseases, some of which currently only have therapies that treat symptoms and not the underlying cause of disease. In particular, inhibition of activity could prevent the onset and progression of some autoimmune disorders, as they are characterized by overexpression of autoantibodies that target the body's own tissues. Reduction of iCP activity in inflamed tissues could reduce the pool of antigenic peptides, leading to a decrease in MHC-I expression. Reduced MHC-I expression could prevent autoantibodies from recognizing these tissues and prevent progression of some autoimmune disorders. As a result, studies to evaluate the iCP as a therapeutic target are underway.

While inhibition of iCP activity could be useful to treat diseases such as autoimmune disorders and certain neurodegenerative diseases, stimulation of the iCP could prove to be a useful strategy to treat chronic viral infections. Viruses such as Hepatitis B[16] and HIV[14] are known to cause

chronic infection. To evade the immune system, these viruses deploy proteins that directly interact with the iCP and slow its activity. It is believed that this reduces the pool of antigenic peptides, which partially contributes to a decrease in MHC-I expression and subsequent immune system evasion. We hypothesize that iCP inhibition by these viral proteins could be rescued with a small molecule stimulator. This could potentially restore MHC-I expression and trigger an immune response.

Thus far, no iCP stimulators have been reported, making elucidation of the iCP as a potential target for viral infection difficult. We have successfully demonstrated that UA stimulates not only purified iCP, but also iCP in live cells. We monitored iCP activity with TBZ-1, a reporter probe that is specifically recognized by the iCP.[40] A dose-dependent increase in purified iCP activity was observed in response to dosing with UA. Dosage with two structurally similar derivatives, BA and OA produced a similar result, although the extent of iCP stimulation was very similar among the three compounds. Toxicity studies in MRC-5 cells induced to express the iCP suggested that UA is relatively well tolerated, as cells were still viable after dosing with up to 12.5 µM for two hours. Excitingly, dosage of 10 µM of UA in iCP-expressing cells resulted in significant stimulation of the iCP. Although significant progress still needs to be made to fully characterize UA as a small molecule iCP stimulator, the preliminary results described here suggest that it could be further developed into a tool to study the iCP as a therapeutic target in viral infections.

Further work is needed to fully understand the impacts of UA on iCP activity and how this modulates expression MHC-I. We are currently focusing efforts into understanding if stimulation of the iCP can result in increased MHC-I expression. We hypothesize stimulating the iCP will result in an increase in the pool of antigenic peptides that are compatible with MHC-I and this could facilitate increased expression at the cell surface.

4.4 Materials and Methods

4.4.1 General Materials and Methods

UA, BA, and OA were purchased from Fisher Scientific. ONX-0914 was purchased from MedChemExpress. Purified iCP and sCP were purchased from Boston Biochem. All biochemical assays were performed in black 96-well plates purchased from Fisher Scientific. 50 mM Tris-HCl pH 7.4 buffer was prepared fresh every two days with Tris-HCl purchased from Fisher Scientific.

Reagents and the description of TBZ-1 synthesis were described previously.[40] MRC-5 cells were purchased from ATCC and were maintained in Eagle's Minimum Essential Medium (EMEM) supplemented with 10% fetal bovine serum (FBS) purchased from Corning. Cell viability assays were conducted in sterile white 96-well tissue culture plates purchased from corning. Cell Titer Glo reagent purchased from Promega was used for cell viability studies exactly following the manufacturer's protocol. All iCP activity assays conducted in cells were performed in sterile black 96-well tissue culture plates purchased from Fisher Scientific. IFN-γ used to induce iCP expression was purchased from BioLegend.

4.4.2 Monitoring Immunoproteasome Activity with a Biochemical Assay

To determine if UA stimulated the iCP, we performed a biochemical assay in which purified iCP was incubated with varying amount of UA. 1 mg of UA was dissolved in DMSO to make a 20 mM stock. This was further diluted in DMSO to make stocks such that the final concentration in the well would be 50, 25, 10, 5, 1, or 0.5 µM. A 20 mM frozen stock of TBZ-1 was thawed and diluted in 50 mM Tris-HCl pH 7.4 (tris buffer) to produce a 17 µM stock. 154 µL of the diluted TBZ-1 was added to 0.6 mL conical tubes incubating on ice. 3.5 µL of each UA concentration was added to one of the tubes containing TBZ-1 and vortexed to mix. As a control, 3.5 µL of DMSO was added to a stock of TBZ-1 to make master stocks. 45 µL of the master stocks was added to wells of black 96-well plate on ice in replicates of three. 44 µL of 17 µM TBZ-1 was added the three wells followed by 6 µL of tris buffer as a control to monitor background fluorescence. 107.5 µL of a 50 nM stock of iCP was prepared by diluting a 3 µM stock in tris buffer. 5 µL of iCP was added to the wells as quickly as possible. The plate was gently struck with the hand on all sides to facilitate mixing and was briefly spun in a plate centrifuge. Fluorescence was monitored every 2 min for 1.5 hour with a TecanInfinite200 Pro plate reader that was preheated to 37 ˚C. The final volume in the well was 50 µL. The final TBZ-1 concentration was 15 µM. The final DMSO concentration in the well was 2%.

Data collected from the plate reader was graphed with GraphPad Prism 9 software to produce a graph to view fluorescence vs. time (**Figure 4.10**). The resulting slopes of each line were calculated and normalized to the DMSO control by taking the average of the slopes from the DMSO samples and dividing all slopes by that number. The resulting normalized slopes were graphed as shown in Figure 4.5. This was conducted in experimental duplicate and technical

triplicate for UA curves. The exact same procedure was conducted to determine iCP stimulation with BA and OA. This was conducted in experimental singlet and technical triplicate.

4.4.3 Induction of iCP Expression in MRC-5 Cells

MRC-5 cells were maintained in EMEM supplemented with 10% FBS at 37 ˚C with 5% CO_2. Two days prior to the start of an experiment, cells were dosed with 5 ng/mL of IFN-γ by adding a 10 ng/µL stock to the cells. The following day, cells were trypsinized and counted. The desired number of cells were resuspended in media and 5 ng/mL of IFN-γ was added to the suspension. Cells were then seeded in a new plate and adhered overnight. Experiments were performed the next day.

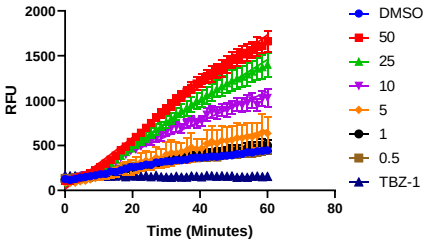

Figure 4.10 Raw Data of Purified iCP Stimulation by UA. Purified iCP was dosed with varying concentrations of UA. TBZ-1 was added to each well at a final concentration of 15 µM. As a control, wells containing only TBZ-1 with no iCP were included to monitor background fluorescence. Samples were also dosed with DMSO as a control. Fluorescence intensity was measured over 1 hour and graphed to visualize fluorescence vs. time. The slopes of each line were calculated, normalized to the DMSO-dosed wells, and graphed as shown in Figure 4.5.

4.4.4 Determining Viability of iCP-Expressing MRC-5 Cells Dosed with UA and ONX-0914

After determining that UA stimulated purified iCP, we next wanted to determine its toxicity in MRC-5 cells expressing the iCP. 2 days prior to the experiment. Cells were dosed with 5 ng/mL of IFN-γ by adding a 10 ng/µL stock to the flask. The following day, cells were trypsinized and counted. 500,000 cells were resuspended in 2.5 mL of media and 5 ng/mL of IFN-γ was added to the suspension. 100 µL of cells were added to the wells of sterile white 96-well plate (20,000 cells per well) and adhered overnight. The following day, 1 mg of UA was weighed and dissolved in DMSO to produce a 20 mM stock. Stock solutions were prepared such that the final concentration in the well would range from 0.5 µM to 25 µM by diluting the 20 mM stock in DMSO. 3.5 µL of each concentration or DMSO was diluted in 31.5 µL of media. 10 µL was added to the wells in replicates of 3. Cells were dosed for 2 hours with each concentration.

The plate was then removed from the incubator and equilibrated to room temperature for 30 minutes. A frozen aliquot of Cell Titer Glo was thawed. 100 µL of Cell Titer Glo was added to each well. The plate was agitated on an orbital shaker for 5 minutes at room temperature to facilitate lysis of the cells. The plate was then placed on the bench top for 10 minutes protected from light to allow the luminescent signal to stabilize. Luminescence was read on a Synergy Neo2

plate reader system with the gain set to 100. Signal was normalized to the DMSO-dosed cells by taking the average of those wells and dividing the remaining signals by this average. This was then graphed with GraphPad Prism 9 software to determine the viability of the cells as displayed in Figure 4.8.

A similar experiment was performed for determining the cytotoxicity of ONX-0914. 20,000 iCP-expressing MRC-5 cells were seeded in the wells of a sterile black 96-well plate and adhered overnight. The following day, a frozen 20 mM stock of ONX-0914 was thawed and diluted in DMSO such that the final concentration in the well would range from 50 µM to 0.5 µM. 3.5 µL of each concentration was diluted in 31.5 µL of media and 10 µL was added to each well in replicates of 3. The final volume in each well was 110 µL. The final DMSO concentration was 1% per well. Cells dosed for 2 hours, then the plate was allowed to equilibrate to room temperature. 100 µL of Cell Titer Glo was added to each well and the plate was agitated for 5 minutes on an orbital shaker. The plate was then incubated, protected from light, at room temperature for 10 minutes to allow the luminescent signal to stabilize. Luminescence was measured with a Synergy Neo2 plate reader system with the gain set to 100. Data was analyzed exactly as described above. This revealed that ONX-0914 is not cytotoxic with dosage up to 50 µM (**Figure 4.11**)

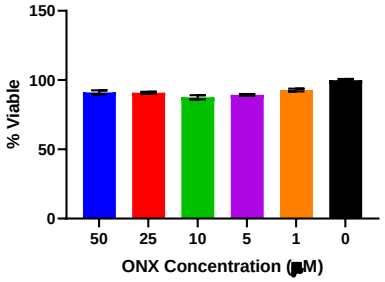

Figure 4.11 Evaluating Cytotoxicity of ONX-0914 in iCP-Expressing MRC-5 Cells. 20,000 iCP-expressing MRC-5 cells were seeded in a black 96-well plate. 3 wells were dosed with varying concentration of ONX-0914 for 2 hours. Cell Titer Glo was then added to each well and luminescence was measured. The signal was normalized to DMSO-dosed wells by dividing the signal from each well by the average of the wells dosed with DMSO and graphed as shown above. ONX-0914 is not toxic to cells with dosage as high as 50 µM.

4.4.5 Activity-Based Assay to Monitor iCP Activity in Cells in Response to Dosage with UA

After establishing that UA stimulates purified iCP, we next turned our attention to evaluating its impacts on iCP activity in cells. MRC-5 cells were induced to produce the iCP as discussed above. After one day of dosing with IFN-γ, cells were tyrpsinized and counted. 150,000 cells were resuspended in 3 mL of media and 1.5 µL of a 10 ng/mL IFN-γ stock was added to the cells. 100 µL of cells was added to the wells of a sterile black 96-well plate (5,000 cells per well) and cells adhered overnight. The following day, 1 mg of UA was weighed and dissolved in DMSO to make a 20 mM stock. A frozen aliquot of 20 mM ONX-0914 solution was thawed. A 1,100 µM

stock of UA and 2.75 mM stock of ONX-0914 was prepared by diluting the 20 mM stocks in DMSO. 6 µL of each compound or DMSO was diluted in 54 µL of media. 10 µL was added to wells in replicates of 5. The final UA concentration in each well was 10 µM. The final ONX-0914 concentration was 25 µM. The final DMSO concentration was 1%. The final volume in the well was 110 µL. Cells were dosed for 2 hours.

Media was then aspirated, and the cells were washed 3X with 100 µL of sterile PBS. A 2 mM stock of UA was prepared by diluting the 20 mM stock in DMSO. A 2.5 mM stock of ONX-0914 was prepared. A frozen aliquot of 20 mM TBZ-1 was thawed and a 6.2 mM stock was prepared by diluting it in DMSO. 1.4 µL of each compound or DMSO was diluted in 272.2 µL of Krebs-Ringer buffer (KRBH) followed by 1.4 µL of the TBZ-1 solution. Samples were vortexed to mix. 50 µL of each master stock was added to the cells in replicates of 5. The final UA concentration was 10 µM. The final ONX-0914 concentration was 25 µM. The final TBZ-1 concentration was 31 µM. The final DMSO concentration was 1%. The final volume in each well was 50 µL. Fluorescence intensity was measured every 2 minutes for 1.5 hour on a TecanInfinite200 Pro plate reader preheated to 37 ˚C.

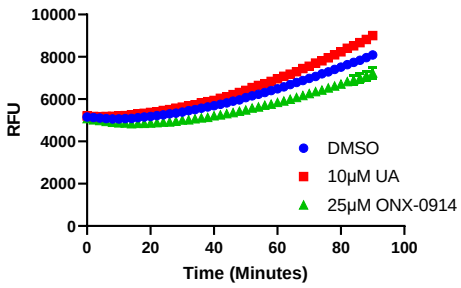

Figure 4.12 Monitoring iCP Activity in MRC-5 Cells. MRC-5 cells were induced to express the iCP and 5,000 cells were seeded in a black 96-well plate. Cells were dosed with DMSO, 10 µM UA, or 25 µM ONX-0914 for 2 hours. Cells were then washed with PBS and dosed with 31 µM of TBZ-1. Fluorescence was read every 2 minutes for 1.5 hours. The resulting lines were graphed as shown above. A lag time is seen during the first 30 minutes of monitoring fluorescence. This was removed and the resulting slopes were calculated and normalized to the DMSO-dosed cells as described. The slopes were displayed as bar graphs as shown in Figure 4.9.

Data was collected and graphed with GraphPad Prism 9 software to visualize fluorescence vs. time (**Figure 4.12**). The first 30 minutes of the data was removed, as there is a lag period between adding the probe and subsequent cleavage. Slopes that resulted from the probe being cleaved over time were calculated. Slopes that were +/- one standard deviation from the mean were excluded. At least three data points remained for each sample. The slopes were then normalized by calculating the average of the DMSO slopes and dividing all data by that number. Slopes were then graphed as bar graphs as shown in Figure 4.9. The experiment was conducted in experimental triplicate and technical quintuplicate.

4.5 References

(1) Acheson, N. *Fundementals of Molecular Virology*, 2nd ed.; 2011.

(2) Kloetzel, P.-M. Ubiquitin and Proteasomes: Antigen Processing by the Proteasome. *Nat. Rev. Mol. Cell Biol.* 2001, *2* (3), 179–188. https://doi.org/10.1038/35056572.

(3) Kimura, H.; Caturegli, P.; Takahashi, M.; Suzuki, K. New Insights into the Function of the Immunoproteasome in Immune and Nonimmune Cells https://www.hindawi.com/journals/jir/2015/541984/ (accessed Jun 17, 2019). https://doi.org/10.1155/2015/541984.

(4) Zerfas, B. L.; Maresh, M. E.; Trader, D. J. The Immunoproteasome: An Emerging Target in Cancer and Autoimmune and Neurological Disorders. *J. Med. Chem.* 2020, *63* (5), 1841–1858. https://doi.org/10.1021/acs.jmedchem.9b01226.

(5) Basler, M.; Groettrup, M. Immunoproteasome-Specific Inhibitors and Their Application. *Methods Mol. Biol. Clifton NJ* 2012, *832*, 391–401. https://doi.org/10.1007/978-1-61779-474-2_27.

(6) Wieczorek, M.; Abualrous, E. T.; Sticht, J.; Álvaro-Benito, M.; Stolzenberg, S.; Noé, F.; Freund, C. Major Histocompatibility Complex (MHC) Class I and MHC Class II Proteins: Conformational Plasticity in Antigen Presentation. *Front. Immunol.* 2017, *8*, 292. https://doi.org/10.3389/fimmu.2017.00292.

(7) Alberts, B.; Johnson, A.; Lewis, J.; Raff, M.; Roberts, K.; Walter, P. T Cells and MHC Proteins. *Mol. Biol. Cell 4th Ed.* 2002.

(8) Tanaka, K. Role of Proteasomes Modified by Interferon-Gamma in Antigen Processing. *J. Leukoc. Biol.* 1994, *56* (5), 571–575. https://doi.org/10.1002/jlb.56.5.571.

(9) Eskandari, S. K.; Seelen, M. a. J.; Lin, G.; Azzi, J. R. The Immunoproteasome: An Old Player with a Novel and Emerging Role in Alloimmunity. *Am. J. Transplant. Off. J. Am. Soc. Transplant. Am. Soc. Transpl. Surg.* 2017, *17* (12), 3033–3039. https://doi.org/10.1111/ajt.14435.

(10) Groettrup, M.; Kirk, C. J.; Basler, M. Proteasomes in Immune Cells: More than Peptide Producers? *Nat. Rev. Immunol.* 2010, *10* (1), 73–78. https://doi.org/10.1038/nri2687.

(11) de Verteuil, D. A.; Rouette, A.; Hardy, M.-P.; Lavallée, S.; Trofimov, A.; Gaucher, É.; Perreault, C. Immunoproteasomes Shape the Transcriptome and Regulate the Function of Dendritic Cells. *J. Immunol. Baltim. Md 1950* 2014, *193* (3), 1121–1132. https://doi.org/10.4049/jimmunol.1400871.

(12) Kloetzel, P. M. Antigen Processing by the Proteasome. *Nat. Rev. Mol. Cell Biol.* 2001, *2* (3), 179–187. https://doi.org/10.1038/35056572.

(13) Apcher, G. S.; Heink, S.; Zantopf, D.; Kloetzel, P.-M.; Schmid, H.-P.; Mayer, R. J.; Krüger, E. Human Immunodeficiency Virus-1 Tat Protein Interacts with Distinct Proteasomal α and β Subunits. *FEBS Lett.* 2003, *553* (1), 200–204. https://doi.org/10.1016/S0014-5793(03)01025-1.

(14) Seeger, M.; Ferrell, K.; Frank, R.; Dubiel, W. HIV-1 Tat Inhibits the 20 S Proteasome and Its 11 S Regulator-Mediated Activation. *J. Biol. Chem.* 1997, *272* (13), 8145–8148. https://doi.org/10.1074/jbc.272.13.8145.

(15) Huang, X.; Seifert, U.; Salzmann, U.; Henklein, P.; Preissner, R.; Henke, W.; Sijts, A. J.; Kloetzel, P.-M.; Dubiel, W. The RTP Site Shared by the HIV-1 Tat Protein and the 11S Regulator Subunit α Is Crucial for Their Effects on Proteasome Function Including Antigen Processing. *J. Mol. Biol.* 2002, *323* (4), 771–782. https://doi.org/10.1016/S0022-2836(02)00998-1.

(16) Khu, Y.-L.; Tan, Y.-J.; Lim, S. G.; Hong, W.; Goh, P.-Y. Hepatitis C Virus Non-Structural Protein NS3 Interacts with LMP7, a Component of the Immunoproteasome, and Affects Its Proteasome Activity. *Biochem. J.* 2004, *384* (Pt 2), 401–409. https://doi.org/10.1042/BJ20040858.

(17) Dantuma, N. P.; Heessen, S.; Lindsten, K.; Jellne, M.; Masucci, M. G. Inhibition of Proteasomal Degradation by the Gly-Ala Repeat of Epstein–Barr Virus Is Influenced by the Length of the Repeat and the Strength of the Degradation Signal. *Proc. Natl. Acad. Sci. U. S. A.* 2000, *97* (15), 8381–8385.

(18) Paul, S.; Lal, G. The Molecular Mechanism of Natural Killer Cells Function and Its Importance in Cancer Immunotherapy. *Front. Immunol.* 2017, *8*. https://doi.org/10.3389/fimmu.2017.01124.

(19) Halenius, A.; Gerke, C.; Hengel, H. Classical and Non-Classical MHC I Molecule Manipulation by Human Cytomegalovirus: So Many Targets—but How Many Arrows in the Quiver? *Cell. Mol. Immunol.* 2015, *12* (2), 139–153. https://doi.org/10.1038/cmi.2014.105.

(20) Kuhn, D. J.; Orlowski, R. Z. The Immunoproteasome as a Target in Hematologic Malignancies. *Semin. Hematol.* 2012, *49* (3), 258–262. https://doi.org/10.1053/j.seminhematol.2012.04.003.

(21) Almond, J. B.; Cohen, G. M. The Proteasome: A Novel Target for Cancer Chemotherapy. *Leukemia* 2002, *16* (4), 433–443. https://doi.org/10.1038/sj.leu.2402417.

(22) Arlt, A.; Bauer, I.; Schafmayer, C.; Tepel, J.; Müerköster, S. S.; Brosch, M.; Röder, C.; Kalthoff, H.; Hampe, J.; Moyer, M. P.; Fölsch, U. R.; Schäfer, H. Increased Proteasome Subunit Protein Expression and Proteasome Activity in Colon Cancer Relate to an Enhanced Activation of Nuclear Factor E2-Related Factor 2 (Nrf2). *Oncogene* 2009, *28* (45), 3983–3996. https://doi.org/10.1038/onc.2009.264.

(23) Lee, M.; Song, I. H.; Heo, S.-H.; Kim, Y.-A.; Park, I. A.; Bang, W. S.; Park, H. S.; Gong, G.; Lee, H. J. Expression of Immunoproteasome Subunit LMP7 in Breast Cancer and Its Association with Immune-Related Markers. *Cancer Res. Treat. Off. J. Korean Cancer Assoc.* 2019, *51* (1), 80–89. https://doi.org/10.4143/crt.2017.500.

(24) Wehenkel, M.; Ban, J.-O.; Ho, Y.-K.; Carmony, K. C.; Hong, J. T.; Kim, K. B. A Selective Inhibitor of the Immunoproteasome Subunit LMP2 Induces Apoptosis in PC-3 Cells and Suppresses Tumour Growth in Nude Mice. *Br. J. Cancer* 2012, *107* (1), 53–62. https://doi.org/10.1038/bjc.2012.243.

(25) Kuhn, D. J.; Hunsucker, S. A.; Chen, Q.; Voorhees, P. M.; Orlowski, M.; Orlowski, R. Z. Targeted Inhibition of the Immunoproteasome Is a Potent Strategy against Models of Multiple Myeloma That Overcomes Resistance to Conventional Drugs and Nonspecific Proteasome Inhibitors. *Blood* 2009, *113* (19), 4667–4676. https://doi.org/10.1182/blood-2008-07-171637.

(26) Chen, D.; Frezza, M.; Schmitt, S.; Kanwar, J.; Dou, Q. P. Bortezomib as the First Proteasome Inhibitor Anticancer Drug: Current Status and Future Perspectives. *Curr. Cancer Drug Targets* 2011, *11* (3), 239–253.

(27) Parlati, F.; Lee, S. J.; Aujay, M.; Suzuki, E.; Levitsky, K.; Lorens, J. B.; Micklem, D. R.; Ruurs, P.; Sylvain, C.; Lu, Y.; Shenk, K. D.; Bennett, M. K. Carfilzomib Can Induce Tumor Cell Death through Selective Inhibition of the Chymotrypsin-like Activity of the Proteasome. *Blood* 2009, *114* (16), 3439–3447. https://doi.org/10.1182/blood-2009-05-223677.

(28) Niewerth, D.; Jansen, G.; Assaraf, Y. G.; Zweegman, S.; Kaspers, G. J. L.; Cloos, J. Molecular Basis of Resistance to Proteasome Inhibitors in Hematological Malignancies. *Drug Resist. Updat.* 2015, *18*, 18–35. https://doi.org/10.1016/j.drup.2014.12.001.

(29) Ho, Y. K. (Abby); Bargagna-Mohan, P.; Wehenkel, M.; Mohan, R.; Kim, K.-B. LMP2-Specific Inhibitors: Chemical Genetic Tools for Proteasome Biology. *Chem. Biol.* 2007, *14* (4), 419–430. https://doi.org/10.1016/j.chembiol.2007.03.008.

(30) Basler, M.; Mundt, S.; Bitzer, A.; Schmidt, C.; Groettrup, M. The Immunoproteasome: A Novel Drug Target for Autoimmune Diseases. *Clin. Exp. Rheumatol.* 2015, *33* (4 Suppl 92), S74-79.

(31) Díaz-Hernández, M.; Martín-Aparicio, E.; Avila, J.; Hernández, F.; Lucas, J. J. Enhaced Induction of the Immunoproteasome by Interferon Gamma in Neurons Expressing Mutant Huntingtin. *Neurotox. Res.* 2004, *6* (6), 463–468. https://doi.org/10.1007/BF03033282.

(32) Johnson, H. W. B.; Lowe, E.; Anderl, J. L.; Fan, A.; Muchamuel, T.; Bowers, S.; Moebius, D. C.; Kirk, C.; McMinn, D. L. Required Immunoproteasome Subunit Inhibition Profile for Anti-Inflammatory Efficacy and Clinical Candidate KZR-616 ((2 S,3 R)- N-((S)-3-(Cyclopent-1-En-1-Yl)-1-((R)-2-Methyloxiran-2-Yl)-1-Oxopropan-2-Yl)-3-Hydroxy-3-(4-Methoxyphenyl)-2-((S)-2-(2-Morpholinoacetamido)Propanamido)Propenamide). *J. Med. Chem.* 2018, *61* (24), 11127–11143. https://doi.org/10.1021/acs.jmedchem.8b01201.

(33) Mishto, M.; Bellavista, E.; Ligorio, C.; Textoris-Taube, K.; Santoro, A.; Giordano, M.; D'Alfonso, S.; Listì, F.; Nacmias, B.; Cellini, E.; Leone, M.; Grimaldi, L. M. E.; Fenoglio, C.; Esposito, F.; Martinelli-Boneschi, F.; Galimberti, D.; Scarpini, E.; Seifert, U.; Amato, M. P.; Caruso, C.; Foschini, M. P.; Kloetzel, P. M.; Franceschi, C. Immunoproteasome LMP2 60HH Variant Alters MBP Epitope Generation and Reduces the Risk to Develop Multiple Sclerosis in Italian Female Population. *PloS One* 2010, *5* (2), e9287. https://doi.org/10.1371/journal.pone.0009287.

(34) Muchamuel, T.; Basler, M.; Aujay, M. A.; Suzuki, E.; Kalim, K. W.; Lauer, C.; Sylvain, C.; Ring, E. R.; Shields, J.; Jiang, J.; Shwonek, P.; Parlati, F.; Demo, S. D.; Bennett, M. K.; Kirk, C. J.; Groettrup, M. A Selective Inhibitor of the Immunoproteasome Subunit LMP7 Blocks Cytokine Production and Attenuates Progression of Experimental Arthritis. *Nat. Med.* 2009, *15* (7), 781–787. https://doi.org/10.1038/nm.1978.

(35) Mishto, M.; Bellavista, E.; Santoro, A.; Stolzing, A.; Ligorio, C.; Nacmias, B.; Spazzafumo, L.; Chiappelli, M.; Licastro, F.; Sorbi, S.; Pession, A.; Ohm, T.; Grune, T.; Franceschi, C. Immunoproteasome and LMP2 Polymorphism in Aged and Alzheimer's Disease Brains. *Neurobiol. Aging* 2006, *27* (1), 54–66. https://doi.org/10.1016/j.neurobiolaging.2004.12.004.

(36) Jansen, A. H. P.; Reits, E. A. J.; Hol, E. M. The Ubiquitin Proteasome System in Glia and Its Role in Neurodegenerative Diseases. *Front. Mol. Neurosci.* 2014, *7*, 73. https://doi.org/10.3389/fnmol.2014.00073.

(37) Deeks, S. G.; Overbaugh, J.; Phillips, A.; Buchbinder, S. HIV Infection. *Nat. Rev. Dis. Primer* 2015, *1*, 15035. https://doi.org/10.1038/nrdp.2015.35.

(38) Chavez, L.; Calvanese, V.; Verdin, E. HIV Latency Is Established Directly and Early in Both Resting and Activated Primary CD4 T Cells. *PLOS Pathog.* 2015, *11* (6), e1004955. https://doi.org/10.1371/journal.ppat.1004955.

(39) Coleman, R. A.; Trader, D. J. Development and Application of a Sensitive Peptide Reporter to Discover 20S Proteasome Stimulators. *ACS Comb. Sci.* 2018, *20* (5), 269–276. https://doi.org/10.1021/acscombsci.7b00193.

(40) Zerfas, B. L.; Trader, D. J. Monitoring the Immunoproteasome in Live Cells Using an Activity-Based Peptide–Peptoid Hybrid Probe. *J. Am. Chem. Soc.* 2019, *141* (13), 5252–5260. https://doi.org/10.1021/jacs.8b12873.

CHAPTER 5. CONCLUSIONS AND FUTURE DIRECTIONS

5.1 General Conclusions

The proteasome is responsible for the majority of cellular protein degradation, making its activity critical to cell viability.[1] Dysregulation of all three isoforms of the proteasome: the 26S, 20S, and iCP is implicated a variety of disease states such as cancer,[2,3] aging,[4–6] and neurodegeneration.[7–9] The link between alterations in proteasome activity and the onset and progression of these diseases has warranted significant investigation of the proteasome as a therapeutic target. This has led to the development of several small molecules that bind the proteasome and modulate its activity. In particular, great success in treating certain forms of cancers with proteasome inhibitors has been demonstrated.[3,10] While inhibition of proteasome activity has shown to be a novel strategy to treat certain forms of cancer, attention is also being turned to elucidating the benefit of proteasome stimulation.

Thus far, most small molecule binders of the proteasome target the 20S proteasome, such as bortezomib and carfilzomib.[11,12] Both of these interact with catalytic subunits of the proteasome and prevent them from cleaving incoming protein substrates. However, the noncatalytic subunits of the 19S regulatory particle also significantly contribute to the activity of the 26S and may be of therapeutic interest.[13] The Rpn-6 subunit facilitates linkage of the 19S to the 20S.[14] Disruption of this subunit could result in altered 26S activity, as attachment of the 19S to the 20S could be altered by a small molecule binder. Similarly, the Rpn-13 subunit is responsible for recognizing ubiquitin tags on proteins marked for degradation by the 26S.[15,16] Disruption of this subunit could prevent it from recognizing proteins tagged for degradation and alter 26S activity. While these 19S subunits and others are attractive targets to modulate 26S activity, very few small molecule binders to these subunits have been discovered. This is partially due to the difficulty of screening these subunits.

Screening proteins with noncatalytic functions is difficult, as several screening methods rely on measuring the functional output of a protein in response to binding a small molecule. Many screening techniques utilize one-bead-one-compound (OBOC) libraries in which thousands of small molecules can be synthesized simultaneously.[17] Noncatalytic proteins can be screened against OBOC libraries through the use of magnetic beads in which a combination of primary antibodies and magnetic beads conjugated to secondary antibodies are used to physically separate

hits from nonhits. While this method has been successfully used to screen a variety of proteins, hits cannot be readily prioritized. This results in lengthy validation experiments to determine the top binders to a target protein. Our lab and others have begun to investigate the use of fluorophores to make screening methods more quantitative.[18–20]

In this work, we successfully developed a screening method in which a protein of interest is labeled with a near-infrared range (NIR) fluorophore. The protein is incubated with beads of an OBOC library individually separated into a well plate, which eliminates the need to cleave the small molecule from the bead prior to the screen. Beads are rinsed to removed excess protein and the plate is imaged for fluorescence. Fluorescence intensities that result from the labeled protein binding the small molecule can be quantified and provide a basis to rank hits. We evaluated this screening method by incubating beads conjugated to ligands of varying affinity to the carbonic anhydrase protein labeled with a NIR fluorophore.[19] Clear differences in the fluorescence intensities that resulted from the labeled protein binding a high and low affinity ligand were observed. From this we concluded that our screening technique could be used to quickly distinguish between good binders and excellent binders in a screen against a target protein. Since this method does not rely on the catalytic activity of a biological target, the types of proteins that could be screened are vast.

We next sought to use this screening method to identify a covalent binder to the oncoprotein gankyrin. In healthy cells, gankyrin is a chaperone of the 19S regulatory particle.[21] However, its overexpression in some cancers allows it to form novel protein-protein interactions. This results in enhanced degradation of two cell cycle regulating proteins, p53 and retinoblastoma protein.[22–24] Degradation of these proteins disrupts check points in the cell cycle and allows cancer cells to undergo uncontrolled proliferation. Since aberrant expression of gankyrin facilitates cell cycle dysregulation, we selected it as our target to screen against an OBOC library. Similarly, gankyrin was also an attractive target because it has no known enzymatic function.

Gankyrin was screened against a 343-member covalent peptoid library.[25] We selected a covalent library because we sought to generate a binder of gankyrin that could eventually be developed into a probe to monitor gankyrin's expression and activity in cells. Covalent linkage of the ligand to gankyrin would facilitate better moderation of its expression in cells, as the ligand would not readily disassociate from the protein. Gankyrin was labeled with a NIR fluorophore and two screens against the OBOC were performed. Fluorescence intensities that resulted from the

labeled gankyrin binding the beads were quantified and the top 5% of fluorescence intensities from both screens were considered our initial hits. When comparing hit structures between the two screens, we noted that ten structures had similar amines in the similar positions. We concluded that these were likely important for binding to gankyrin and selected these ten structures for validation. Validation was performed by an in-gel fluorescence assay, which produced one validated hit, TMM-6. We further demonstrated that TMM-6 primarily binds gankyrin in spiked HEK 293T cell lysate.

Based on our results from the OBOC screen against gankyrin, we concluded that our screening method can be used to rapidly identify high quality binders to target proteins. Not only did we successfully demonstrate that differences in binding affinities between a protein and ligands with known affinities can be readily detected, but we also used this technique to identify TMM-6, a covalent ligand of gankyrin . To the best of our knowledge, TMM-6 is the first reported covalent binder of gankyrin. Another noncovalent binder was recently reported and was shown to stabilize expression of p53, highlighting the potential of gankyrin as a therapeutic target.[21] We are next interested in elucidating the impact of TMM-6 on cells that overexpress gankyrin (**Figure 5.1**).

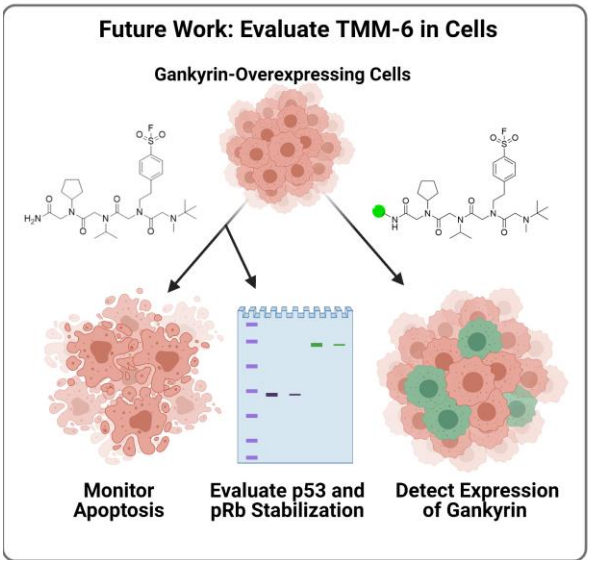

Figure 5.1 Future Directions for TMM-6. We next plan to evaluate the impacts of TMM-6 on cells that overexpress gankyrin. We plan to dose cells with TMM-6 and monitor the extent of apoptosis and levels of p53 and retinoblastoma protein. We hypothesize that TMM-6 could prevent gankyrin from enhancing degradation of these two cell cycle regulating proteins and result stabilizing their expression. This could lead to activation of apoptosis. We are also interested in using fluorescently labeled TMM-6 to monitor expression of gankyrin in cells during the onset and progression of cancers.

Aging and neurodegeneration are characterized by a decrease in proteasome activity.[6,26] Reduction in proteasome activity results in buildup of unwanted proteins that eventually leads to cell death if left unchecked. Our lab and others have begun to explore the impacts of small molecules that stimulate the proteasome on these pathologies.[4,27] Elucidating impacts of proteasome activity in aged humans is difficult, as humans have long lifespans. As a result, research has turned to the use of model organisms that undergo similar mechanisms of aging, such as *Saccharomyces cerevisiae*, or budding yeast.[28,29] The structure of yeast proteasome and

human proteasomes are remarkably similar.[11] Yeast can also be readily genetically manipulated to alter proteasome subunit expression and activity.[30] Importantly, genetic stabilization of proteasome expression has been shown to extend yeast lifespan, while repressing its expression shortens lifespan.[30] We sought to determine if dosage of yeast with reduced proteasome activity with small molecule stimulators could produce similar lifespan extension. This would provide more insight into the proteasome as a therapeutic target for aging.

We utilized a BY4741 yeast strain which is known to have a relatively long chronological lifespan (CLS).[31] This strain was selected because there are several commercially available isogenic strains, including *rpn4Δ* that is knocked down for the RPN4 transcription factor that controls expression of proteasome subunits.[32] Since the CLS of this strain was shown to be over one month, we first sought to optimize an assay to monitor CLS in response to dosing with proteasome stimulators. Through alterations in media composition, we successfully reduced the CLS from over 40 days, to just one week.[33,34] Following the work of other research groups, we also successfully scaled yeast culture conditions down to a deep well 96-well plate format which increased the number of stimulators that could be tested simtaneously.[35]

We used these optimized assay conditions to determine if ursolic acid (UA) and structurally similar compounds, betulinic acid (BA) and oleanolic acid (OA), could extend the CLS of the *rpn4Δ* yeast strain with reduced proteasome capacity. We found that dosage with UA and BA resulted in slight CLS extension. Although UA and its derivatives may not be very potent proteasome stimulators in this yeast model, we concluded that this assay could be used in future work to evaluate other proteasome stimulators in a biologically relevant environment. We further evaluated UA as a proteasome stimulator by monitoring degradation of α-synuclein, a protein prone to aggregation.[36] We found that dosage of UA in lysate of yeast induced to express α-synuclein resulted in a significant decrease in the amount of this protein. The results of this work indicate that we have successfully established a method to monitor yeast longevity in response to small molecules that modulate proteasome activity. Similarly, we concluded that UA provides slight lifespan extension in yeast with reduced proteasome activity.

Expression of the iCP has recently been implicated in a variety of diseases such as neurodegenerative diseases,[9,37] some cancers,[38,39] and autoimmune disorders.[40,41] The iCP is generally not expressed in the tissues impacted by these conditions unless they are exposed to inflammatory conditions. As a result, the iCP represents a way to distinguish between health and

diseased tissues. Our research group and others have begun to elucidate the impacts of modulating iCP activity to counteract the pathologies associated with these diseases. Here, we present that UA and its derivatives stimulate purified iCP. We further demonstrated this same phenomenon in cells induced to express the iCP. Currently, we are beginning to elucidate the impacts of iCP stimulation on MHC-I expression.

5.2 Future Directions

5.2.1 Expand OBOC Library Screening Technology

We have successfully demonstrated use of our OBOC library screening method to identify a covalent binder to gankyrin, TMM-6. However, we believe this technology could be expanded into a technique to identify pathogens and antibodies in human tissues. Autoimmune diseases are characterized by overexpress of autoantibodies that attack healthy tissues.[42,43] Current methods to diagnose these diseases are often not sensitive enough to detect the presence of these antibodies at early stages.[44] As a result, it can be difficult to intervene with therapeutics before significant disease progression. With our OBOC screening methods, we were able to reliably detect as little as 0.2 ng of antibody in a protein mixture.[19] We believe this could be expanded to sensitively detect antibodies that are overexpressed in autoimmune disorders.

We hypothesize that a ligand specific to an autoantibody could be synthesized on resin. Blood serum could then be exposed to the beads and the autoantibody would bind the ligand. Fluorescently labeled secondary antibodies could then be used to detect the autoantibody. The amount of fluorescent signal produced by the fluorescently labeled antibody binding the autoantibody could be quantified to reveal abnormal levels of antibodies in a blood sample. Small molecule ligands to autoantibodies would first have to be discovered using our OBOC screening method or other commercially available techniques. We believe repurposing this technology into a method to detect autoantibodies could result in a very sensitive diagnostic tool for autoimmune disorders.

Similarly, current techniques to identify blood cancers often involve invasive bone marrow biopsies or analyzing blood smears under a microscope for abnormal cells.[45] These methods require expertise in blood analysis, as abnormal cells must be manually counted. They are also not very sensitive, resulting in significant disease progression before some blood cancers can be

diagnosed. This results in poor prognosis and reduced patient lifespan. As a result, development of more sensitive diagnostic methods, such as the use of flow cytometry are underway.[46] We believe our OBOC screening method could be repurposed into a sensitive technique to identify cancer cells present in blood samples. This would not only expedite the diagnosis of certain blood cancers, but also result in a novel detection method.

Cancer cells often overexpress protein markers on the cell surface, providing a basis to discriminate between cancerous and normal cells.[47] We envision a method to detect these cells in which ligands specific to these proteins could be synthesized on resin. Blood samples could then incubate with the beads and only cancer cells that overexpress the target protein would bind the resin. We could then use fluorescently labeled secondary antibodies to detect the cancer cells bound to the bead. Since noncancerous cells do not overexpress the same types of proteins as cancer cells, fluorescence that results from an antibody binding a cell on-bead could be attributed to the presence of a cancerous cell. This would not only expedite the diagnosis of some blood cancers, but also offer a less invasive and potentially very sensitive method to detect blood cancers at earlier stages (**Figure 5.2**).

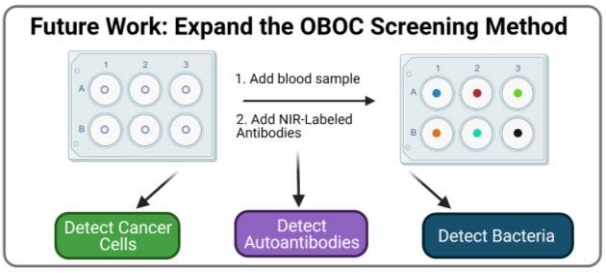

Figure 5.2 Expanding our OBOC Screening Technology. We plan to broaden the applications of our OBOC screening method into a technique to detect autoantibodies, bacteria, or cancer cells in patient blood samples. This could expedite the process of diagnosing autoimmune diseases, bacterial infections, and certain cancers.

5.2.2 Screen for New Proteasome Stimulators and Evaluate Lifespan Extension Properties

In this work, we presented an optimized assay to evaluate the impact of small molecule proteasome activity modulators on the lifespan of yeast with reduced proteasome capacity. Research suggests that reduction in proteasome activity is a hallmark of human aging, making the proteasome an interesting therapeutic target.[4,6] It can be difficult to study the impacts of chemical stimulation of the proteasome in humans because of their relatively long lifespan. However, yeast have emerged as an important tool to monitor lifespan, as they can be genetically manipulated to mimic human conditions.[28] We successfully optimized a method to monitor the chronological lifespan (CLS) of yeast by shortening the time required to acquire results and scaling down to a

96-well plate format. This assay could be used to rapidly elucidate the impacts of proteasome stimulators on aging.

Although UA and its derivatives were not especially potent, our optimized assay could be used to evaluate newly identified proteasome stimulators on aging. Importantly, it is difficult to for yeast to retain small molecules within the cell. This is partially because the cell wall prevents uptake of small molecules in the surrounding environment and the fact that yeast are equipped with several drug efflux pumps that rapidly expel compounds.[48] The BY4741 strain utilized in this study is known to have functional efflux pumps, which may have contributed to our observation of only slight lifespan extension in response to dosage with UA. There are commercially available strains of yeast that are knocked down for drug efflux pump expression, namely the *Δ8* BY4741 strain.[49] Since the drug efflux pumps in this strain are not fully expressed, it is easier for small molecules to be retained within the cell. Moving forward, we are interested in creating a double deletion strain of BY4741 that is knockdown for both the RPN4 transcription factor and the drug efflux pumps. This strain of yeast of could prove to be very helpful in determining the impacts of small molecule proteasome stimulators on aged yeast. We predict that better retention of small molecules such as UA by a double deletion strain will result in more significant lifespan extension than the single deletion strains.

Our optimized CLS assay bridges the gap between biochemical methods used to identify proteasome stimulators and evaluating their impacts in complex mammalian cellular environments. Yeast are relatively easier to work with than mammalian cells and several strains with reduced proteasome activity are commercially available.[32] This eliminates the need to optimize mammalian cells line or passage cells until they reach sufficient age to test small molecule stimulators. Similarly, this method could be further be used to evaluate the proteasome as a therapeutic target for aging.

5.2.3 Elucidate the Impacts of iCP Stimulators on MHC-I Expression

The iCP has recently emerged as a potential therapeutic target for a variety diseases such as neurodegenerative disorders,[37] autoimmune disorders,[40] and certain cancers.[38,41] Modulation of its activity could be viable strategy to specifically target diseased cells as most healthy cells do not express the iCP.[1] Our lab has recently developed a reporter probe that is recognized by the iCP and can be used in biochemical and cell-based assays.[50] In this work, we utilized this probe to

identify UA and its derivatives as iCP stimulators. We observed stimulation both biochemically and in cells induced to express the iCP.

Many viruses, such as human immunodeficiency virus (HIV), target the iCP to prevent it from generating antigenic peptides compatible with MHC-I complexes.[51–53] HIV deploys a protein called Tat which is known to form a heptameric ring structure that binds the alpha subunits of the iCP.[52] This prevents the iCP from degrading both cellular and viral proteins, resulting in a reduction in the pool of antigenic peptides in the cell. It is believed that this may partially contribute to a decrease in MHC-I expression on the outside of the infected cell and allow the virus to evade the immune system. Despite huge advancements in the therapies available to treat HIV, there is currently no cure. We hypothesize the iCP could represent a novel target for HIV therapies. Stimulating the iCP with a small molecule may rescue its inhibition by Tat and restore the pool of MHC-I compatible peptides. This could lead to an increase in the amount of MHC-I expressed on the outside of an infected cell and allow the immune system to recognize and clear it. Currently, we are beginning to elucidate the impacts of HIV Tat on iCP activity and effects of dosing Tat-expressing cells with iCP stimulators. We have recently demonstrated that MRC-5 cells induced to express the iCP and subsequently transfected with HIV Tat exhibit lower iCP activity than mock transfected cells (**Figure 5.3**). This indicates that the iCP could be an important target for therapeutic intervention.

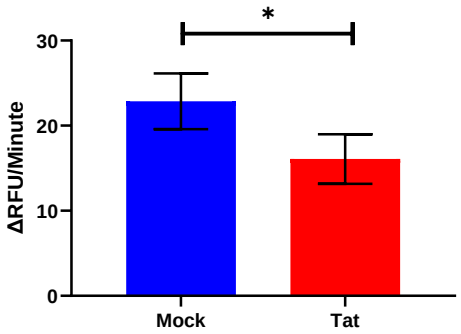

Figure 5.3 Tat-Transfected Cells Exhibit Reduced iCP activity. MRC-5 cells were induced to express the iCP by dosing with 5 ng/mL of IFN-γ for two days. Cells were then transfected with HIV Tat DNA. Mock-transfected or Tat-transfected cells were dosed with 31 µM of our iCP reporter probe, TBZ-1. Cleavage of the probe was monitored for 1.5 hours and the slopes of the resulting lines were graphed as bar graphs as shown above. This revealed that cells expressing HIV Tat have lower iCP activity than the mock transfected cells. This suggests the iCP could be an interesting target for therapeutic intervention.

Further characterization of UA is required to fully evaluate it as an iCP stimulator. Since we have demonstrated that cells induced to express the iCP that are transfected with HIV Tat show reduced iCP activity, we are next interested in determining if dosing these cells with UA could rescue its inhibition. Upon successfully stimulating the iCP in a Tat-transfected cell model, we will then turn our attention to determining the impacts of iCP stimulation on MHC-I expression by monitoring changes in the amount of MHC-I complexes on the outside of transfected cells

dosed with iCP stimulators by flow cytometry. We anticipate that stimulating the iCP will result in more MHC-I expression on the cell surface.

5.3 Final Conclusions

The discovery of small molecule binders to the proteasome has significantly aided in our understanding of the proteasome as a therapeutic target in a variety of diseases. However, standardized assays to screen for small molecule binders of the proteasome and evaluate their impacts in biologically relevant systems remain unavailable. This has resulted in inconsistencies in fully characterizing the role of the proteasome in diseases such as cancer, aging, and neurodegeneration. Similarly, until recently, research has primarily focused on discovering small molecules that modulate the catalytic subunits of the proteasome, leaving the remaining subunits largely underexplored. We believe that the set of assays presented in this work to discover small molecule binders to target proteins and evaluate the impacts of modulating proteasome activity in aged yeast will facilitate a better understanding of the proteasome as a therapeutic target. Identification of new small molecule binders to the noncatalytic subunits will allow for the development of probes that can be used to study the impacts of these subunits on proteasome function. Similarly, recent research has revealed that expression of the iCP is implicated in a variety of diseases and could emerge as an important therapeutic target. However, small molecule tools to probe its activity are limited, leaving a significant need to identify binders. The assays presented in this study could allow for the development of sensitive iCP probes and be used to answer questions regarding its therapeutic potential.

The discovery of small molecules that inhibit the proteasome has resulted new therapeutics for diseases such as cancer. Usage of these small molecules in the clinic has resulted in better prognosis and longer lifespans of cancer patients. However, the therapeutic benefit of proteasome stimulation in diseases such as neurodegeneration and aging remain largely underexplored. This is partially due to the lack of reported proteasome stimulators and assays to evaluate their impacts in aged cells. We believe the assays presented in this work will move the field of proteasome stimulation forward by facilitating rapid discovery and evaluation of small molecules that modulate proteasome activity.

5.4 References

(1) Kloetzel, P.-M. Ubiquitin and Proteasomes: Antigen Processing by the Proteasome. *Nat. Rev. Mol. Cell Biol.* **2001**, *2* (3), 179–188. https://doi.org/10.1038/35056572.

(2) Almond, J. B.; Cohen, G. M. The Proteasome: A Novel Target for Cancer Chemotherapy. *Leukemia* **2002**, *16* (4), 433–443. https://doi.org/10.1038/sj.leu.2402417.

(3) Chauhan, D.; Catley, L.; Li, G.; Podar, K.; Hideshima, T.; Velankar, M.; Mitsiades, C.; Mitsiades, N.; Yasui, H.; Letai, A.; Ovaa, H.; Berkers, C.; Nicholson, B.; Chao, T.-H.; Neuteboom, S. T. C.; Richardson, P.; Palladino, M. A.; Anderson, K. C. A Novel Orally Active Proteasome Inhibitor Induces Apoptosis in Multiple Myeloma Cells with Mechanisms Distinct from Bortezomib. *Cancer Cell* **2005**, *8* (5), 407–419. https://doi.org/10.1016/j.ccr.2005.10.013.

(4) Hwang, J. S.; Hwang, J. S.; Chang, I.; Kim, S. Age-Associated Decrease in Proteasome Content and Activities in Human Dermal Fibroblasts: Restoration of Normal Level of Proteasome Subunits Reduces Aging Markers in Fibroblasts From Elderly Persons. *J. Gerontol. Ser. A* **2007**, *62* (5), 490–499. https://doi.org/10.1093/gerona/62.5.490.

(5) Johnston-Carey, H. K.; Pomatto, L. C. D.; Davies, K. J. A. The Immunoproteasome in Oxidative Stress, Aging, and Disease. *Crit. Rev. Biochem. Mol. Biol.* **2015**, *51* (4), 268–281. https://doi.org/10.3109/10409238.2016.1172554.

(6) Kaushik, S.; Cuervo, A. M. Proteostasis and Aging. *Nat. Med.* **2015**, *21* (12), 1406–1415. https://doi.org/10.1038/nm.4001.

(7) McNaught, K. S. P.; Jenner, P. Proteasomal Function Is Impaired in Substantia Nigra in Parkinson's Disease. *Neurosci. Lett.* **2001**, *297* (3), 191–194. https://doi.org/10.1016/S0304-3940(00)01701-8.

(8) McNaught, K. S. P.; Belizaire, R.; Jenner, P.; Olanow, C. W.; Isacson, O. Selective Loss of 20S Proteasome Alpha-Subunits in the Substantia Nigra Pars Compacta in Parkinson's Disease. *Neurosci. Lett.* **2002**, *326* (3), 155–158.

(9) Díaz-Hernández, M.; Hernández, F.; Martín-Aparicio, E.; Gómez-Ramos, P.; Morán, M. A.; Castaño, J. G.; Ferrer, I.; Avila, J.; Lucas, J. J. Neuronal Induction of the Immunoproteasome in Huntington's Disease. *J. Neurosci. Off. J. Soc. Neurosci.* **2003**, *23* (37), 11653–11661.

(10) Chen, D.; Frezza, M.; Schmitt, S.; Kanwar, J.; Dou, Q. P. Bortezomib as the First Proteasome Inhibitor Anticancer Drug: Current Status and Future Perspectives. *Curr. Cancer Drug Targets* **2011**, *11* (3), 239–253.

(11) Groll, M.; Berkers, C. R.; Ploegh, H. L.; Ovaa, H. Crystal Structure of the Boronic Acid-Based Proteasome Inhibitor Bortezomib in Complex with the Yeast 20S Proteasome. *Structure* **2006**, *14* (3), 451–456. https://doi.org/10.1016/j.str.2005.11.019.

(12) Khan, M. L.; Stewart, A. K. Carfilzomib: A Novel Second-Generation Proteasome Inhibitor. *Future Oncol. Lond. Engl.* **2011**, *7* (5), 607–612. https://doi.org/10.2217/fon.11.42.

(13) Muli, C. S.; Tian, W.; Trader, D. J. Small-Molecule Inhibitors of the Proteasome's Regulatory Particle. *ChemBioChem* **2019**, *20* (14), 1739–1753. https://doi.org/10.1002/cbic.201900017.

(14) Tian, W.; Trader, D. J. Discovery of a Small Molecule Probe of Rpn-6, an Essential Subunit of the 26S Proteasome. *ACS Chem. Biol.* **2020**, *15* (2), 554–561. https://doi.org/10.1021/acschembio.9b01019.

(15) Trader, D. J.; Simanski, S.; Kodadek, T. A Reversible and Highly Selective Inhibitor of the Proteasomal Ubiquitin Receptor Rpn13 Is Toxic To Multiple Myeloma Cells. *J. Am. Chem. Soc.* **2015**, *137* (19), 6312. https://doi.org/10.1021/jacs.5b02069.

(16) Anchoori, R. K.; Jiang, R.; Peng, S.; Soong, R.; Algethami, A.; Rudek, M. A.; Anders, N.; Hung, C.-F.; Chen, X.; Lu, X.; Kayode, O.; Dyba, M.; Walters, K. J.; Roden, R. B. S. Covalent Rpn13-Binding Inhibitors for the Treatment of Ovarian Cancer. *ACS Omega* **2018**, *3* (9), 11917–11929. https://doi.org/10.1021/acsomega.8b01479.

(17) Lam, K. S.; Lebl, M.; Krchňák, V. The "One-Bead-One-Compound" Combinatorial Library Method. *Chem. Rev.* **1997**, *97* (2), 411–448. https://doi.org/10.1021/cr9600114.

(18) Olivos, H. J.; Bachhawat-Sikder, K.; Kodadek, T. Quantum Dots As A Visual Aid For Screening Bead-Bound Combinatorial Libraries. *ChemBioChem* **2003**, *4* (11), 1242–1245. https://doi.org/https://doi.org/10.1002/cbic.200300712.

(19) Maresh, M. E.; Trader, D. J. Development of a Method To Prioritize Protein–Ligand Pairs on Beads Using Protein Conjugated to a Near-IR Dye. *ACS Comb. Sci.* **2019**, *21* (3), 223–228. https://doi.org/10.1021/acscombsci.8b00165.

(20) Hintersteiner, M.; Auer, M. A Two-Channel Detection Method for Autofluorescence Correction and Efficient on-Bead Screening of One-Bead One-Compound Combinatorial Libraries Using the COPAS Fluorescence Activated Bead Sorting System. *Methods Appl. Fluoresc.* **2013**, *1* (1), 017001. https://doi.org/10.1088/2050-6120/1/1/017001.

(21) Chattopadhyay, A.; O'Connor, C. J.; Zhang, F.; Galvagnion, C.; Galloway, W. R. J. D.; Tan, Y. S.; Stokes, J. E.; Rahman, T.; Verma, C.; Spring, D. R.; Itzhaki, L. S. Discovery of a Small-Molecule Binder of the Oncoprotein Gankyrin That Modulates Gankyrin Activity in the Cell. *Sci. Rep.* **2016**, *6*, 23732. https://doi.org/10.1038/srep23732.

(22) Dawson, S.; Apcher, S.; Mee, M.; Higashitsuji, H.; Baker, R.; Uhle, S.; Dubiel, W.; Fujita, J.; Mayer, R. J. Gankyrin Is an Ankyrin-Repeat Oncoprotein That Interacts with CDK4 Kinase and the S6 ATPase of the 26 S Proteasome. *J. Biol. Chem.* **2002**, *277* (13), 10893–10902. https://doi.org/10.1074/jbc.M107313200.

(23) Higashitsuji, H.; Liu, Y.; Mayer, R. J.; Fujita, J. The Oncoprotein Gankyrin Negatively Regulates Both P53 and RB by Enhancing Proteasomal Degradation. *Cell Cycle* **2005**, *4* (10), 1335–1337. https://doi.org/10.4161/cc.4.10.2107.

(24) Higashitsuji, H.; Higashitsuji, H.; Itoh, K.; Sakurai, T.; Nagao, T.; Sumitomo, H.; Masuda, T.; Dawson, S.; Shimada, Y.; Mayer, R. J.; Fujita, J. The Oncoprotein Gankyrin Binds to MDM2/HDM2, Enhancing Ubiquitylation and Degradation of P53. *Cancer Cell* **2005**, *8* (1), 75–87. https://doi.org/10.1016/j.ccr.2005.06.006.

(25) Maresh, M. E.; Zerfas, B. L.; Wuthrich, B. S.; Trader, D. J. Identification of a Covalent Binder to the Oncoprotein Gankyrin Using a NIR-Based OBOC Screening Method. *RSC Adv.* **2021**, *11* (21), 12794–12801. https://doi.org/10.1039/D0RA10976B.

(26) Thibaudeau, T. A.; Anderson, R. T.; Smith, D. M. A Common Mechanism of Proteasome Impairment by Neurodegenerative Disease-Associated Oligomers. *Nat. Commun.* **2018**, *9* (1), 1–14. https://doi.org/10.1038/s41467-018-03509-0.

(27) Lee, C. K.; Klopp, R. G.; Weindruch, R.; Prolla, T. A. Gene Expression Profile of Aging and Its Retardation by Caloric Restriction. *Science* **1999**, *285* (5432), 1390–1393. https://doi.org/10.1126/science.285.5432.1390.

(28) Burtner, C. R.; Murakami, C. J.; Kennedy, B. K.; Kaeberlein, M. A Molecular Mechanism of Chronological Aging in Yeast. *Cell Cycle Georget. Tex* **2009**, *8* (8), 1256–1270. https://doi.org/10.4161/cc.8.8.8287.

(29) Mirisola, M. G.; Braun, R. J.; Petranovic, D. Approaches to Study Yeast Cell Aging and Death. *FEMS Yeast Res.* **2014**, *14* (1), 109–118. https://doi.org/10.1111/1567-1364.12112.

(30) Kruegel, U.; Robison, B.; Dange, T.; Kahlert, G.; Delaney, J. R.; Kotireddy, S.; Tsuchiya, M.; Tsuchiyama, S.; Murakami, C. J.; Schleit, J.; Sutphin, G.; Carr, D.; Tar, K.; Dittmar, G.; Kaeberlein, M.; Kennedy, B. K.; Schmidt, M. Elevated Proteasome Capacity Extends Replicative Lifespan in Saccharomyces Cerevisiae. *PLOS Genet.* **2011**, *7* (9), e1002253. https://doi.org/10.1371/journal.pgen.1002253.

(31) Jr, S. D.; Ch, M.; Cr, C.; Ra, W.; JL 4th, H. Gene-Nutrient Interaction Markedly Influences Yeast Chronological Lifespan. *Exp. Gerontol.* **2016**, *86*, 113–123. https://doi.org/10.1016/j.exger.2016.04.012.

(32) Wang, X.; Xu, H.; Ju, D.; Xie, Y. Disruption of Rpn4-Induced Proteasome Expression in Saccharomyces Cerevisiae Reduces Cell Viability Under Stressed Conditions. *Genetics* **2008**, *180* (4), 1945–1953. https://doi.org/10.1534/genetics.108.094524.

(33) Murakami, C. J.; Wall, V.; Basisty, N.; Kaeberlein, M. Composition and Acidification of the Culture Medium Influences Chronological Aging Similarly in Vineyard and Laboratory Yeast. *PLOS ONE* **2011**, *6* (9), e24530. https://doi.org/10.1371/journal.pone.0024530.

(34) Santos, J.; Leitão-Correia, F.; Sousa, M. J.; Leão, C. Nitrogen and Carbon Source Balance Determines Longevity, Independently of Fermentative or Respiratory Metabolism in the Yeast Saccharomyces Cerevisiae. *Oncotarget* **2016**, *7* (17), 23033–23042. https://doi.org/10.18632/oncotarget.8656.

(35) Carmona-Gutierrez, D.; Zimmermann, A.; Kainz, K.; Pietrocola, F.; Chen, G.; Maglioni, S.; Schiavi, A.; Nah, J.; Mertel, S.; Beuschel, C. B.; Castoldi, F.; Sica, V.; Trausinger, G.; Raml, R.; Sommer, C.; Schroeder, S.; Hofer, S. J.; Bauer, M. A.; Pendl, T.; Tadic, J.; Dammbrueck, C.; Hu, Z.; Ruckenstuhl, C.; Eisenberg, T.; Durand, S.; Bossut, N.; Aprahamian, F.; Abdellatif, M.; Sedej, S.; Enot, D. P.; Wolinski, H.; Dengjel, J.; Kepp, O.; Magnes, C.; Sinner, F.; Pieber, T. R.; Sadoshima, J.; Ventura, N.; Sigrist, S. J.; Kroemer, G.; Madeo, F. The Flavonoid 4,4'-Dimethoxychalcone Promotes Autophagy-Dependent Longevity across Species. *Nat. Commun.* **2019**, *10* (1), 651. https://doi.org/10.1038/s41467-019-08555-w.

(36) Witt, S. N.; Flower, T. R. Alpha-Synuclein, Oxidative Stress and Apoptosis from the Perspective of a Yeast Model of Parkinson's Disease. *FEMS Yeast Res.* **2006**, *6* (8), 1107–1116. https://doi.org/10.1111/j.1567-1364.2006.00135.x.

(37) Díaz-Hernández, M.; Martín-Aparicio, E.; Avila, J.; Hernández, F.; Lucas, J. J. Enhaced Induction of the Immunoproteasome by Interferon Gamma in Neurons Expressing Mutant Huntingtin. *Neurotox. Res.* **2004**, *6* (6), 463–468. https://doi.org/10.1007/BF03033282.

(38) Kuhn, D. J.; Orlowski, R. Z. The Immunoproteasome as a Target in Hematologic Malignancies. *Semin. Hematol.* **2012**, *49* (3), 258–262. https://doi.org/10.1053/j.seminhematol.2012.04.003.

(39) Niewerth, D.; van Meerloo, J.; Jansen, G.; Assaraf, Y. G.; Hendrickx, T. C.; Kirk, C. J.; Anderl, J. L.; Zweegman, S.; Kaspers, G. J. L.; Cloos, J. Anti-Leukemic Activity and Mechanisms Underlying Resistance to the Novel Immunoproteasome Inhibitor PR-924. *Biochem. Pharmacol.* **2014**, *89* (1), 43–51. https://doi.org/10.1016/j.bcp.2014.02.005.

(40) Basler, M.; Mundt, S.; Bitzer, A.; Schmidt, C.; Groettrup, M. The Immunoproteasome: A Novel Drug Target for Autoimmune Diseases. *Clin. Exp. Rheumatol.* **2015**, *33* (4 Suppl 92), S74-79.

(41) Zerfas, B. L.; Maresh, M. E.; Trader, D. J. The Immunoproteasome: An Emerging Target in Cancer, Autoimmune and Neurological Disorders. *J. Med. Chem.* **2019**. https://doi.org/10.1021/acs.jmedchem.9b01226.

(42) Nakamura, H.; Usa, T.; Motomura, M.; Ichikawa, T.; Nakao, K.; Kawasaki, E.; Tanaka, M.; Ishikawa, K.; Eguchi, K. Prevalence of Interrelated Autoantibodies in Thyroid Diseases and Autoimmune Disorders. *J. Endocrinol. Invest.* **2008**, *31* (10), 861–865. https://doi.org/10.1007/BF03346432.

(43) Graus, F.; Saiz, A.; Dalmau, J. Antibodies and Neuronal Autoimmune Disorders of the CNS. *J. Neurol.* **2010**, *257* (4), 509–517. https://doi.org/10.1007/s00415-009-5431-9.

(44) Conrad, K.; Roggenbuck, D.; Reinhold, D.; Sack, U. Autoantibody Diagnostics in Clinical Practice. *Autoimmun. Rev.* **2012**, *11* (3), 207–211. https://doi.org/10.1016/j.autrev.2011.05.014.

(45) Tests for Non-Hodgkin Lymphoma https://www.cancer.org/cancer/non-hodgkin-lymphoma/detection-diagnosis-staging/how-diagnosed.html (accessed Mar 8, 2019).

(46) Marti, G. E.; Stetler-Stevenson, M.; Fleisher, T. Diagnostic Flow Cytometry in Hematologic Malignancies. In *Hematologic Malignancies: Methods and Techniques*; Faguet, G. B., Ed.; Methods in Molecular Medicine™; Humana Press: Totowa, NJ, 2001; pp 179–215. https://doi.org/10.1385/1-59259-074-8:179.

(47) Wu, L.; Qu, X. Cancer Biomarker Detection: Recent Achievements and Challenges. *Chem. Soc. Rev.* **2015**, *44* (10), 2963–2997. https://doi.org/10.1039/c4cs00370e.

(48) Holmes, A. R.; Cardno, T. S.; Strouse, J. J.; Ivnitski-Steele, I.; Keniya, M. V.; Lackovic, K.; Monk, B. C.; Sklar, L. A.; Cannon, R. D. Targeting Efflux Pumps to Overcome Antifungal Drug Resistance. *Future Med. Chem.* **2016**, *8* (12), 1485–1501. https://doi.org/10.4155/fmc-2016-0050.

(49) Hoepfner, D.; Helliwell, S. B.; Sadlish, H.; Schuierer, S.; Filipuzzi, I.; Brachat, S.; Bhullar, B.; Plikat, U.; Abraham, Y.; Altorfer, M.; Aust, T.; Baeriswyl, L.; Cerino, R.; Chang, L.; Estoppey, D.; Eichenberger, J.; Frederiksen, M.; Hartmann, N.; Hohendahl, A.; Knapp, B.; Krastel, P.; Melin, N.; Nigsch, F.; Oakeley, E. J.; Petitjean, V.; Petersen, F.; Riedl, R.; Schmitt, E. K.; Staedtler, F.; Studer, C.; Tallarico, J. A.; Wetzel, S.; Fishman, M. C.; Porter, J. A.; Movva, N. R. High-Resolution Chemical Dissection of a Model Eukaryote Reveals Targets, Pathways and Gene Functions. *Microbiol. Res.* **2014**, *169* (2–3), 107–120. https://doi.org/10.1016/j.micres.2013.11.004.

(50) Zerfas, B. L.; Trader, D. J. Monitoring the Immunoproteasome in Live Cells Using an Activity-Based Peptide–Peptoid Hybrid Probe. *J. Am. Chem. Soc.* **2019**, *141* (13), 5252–5260. https://doi.org/10.1021/jacs.8b12873.

(51) Minor, M. M.; Slagle, B. L. Hepatitis B Virus HBx Protein Interactions with the Ubiquitin Proteasome System. *Viruses* **2014**, *6* (11), 4683–4702. https://doi.org/10.3390/v6114683.

(52) Apcher, G. S.; Heink, S.; Zantopf, D.; Kloetzel, P.-M.; Schmid, H.-P.; Mayer, R. J.; Krüger, E. Human Immunodeficiency Virus-1 Tat Protein Interacts with Distinct Proteasomal α and β Subunits. *FEBS Lett.* **2003**, *553* (1), 200–204. https://doi.org/10.1016/S0014-5793(03)01025-1.

(53) Dantuma, N. P.; Heessen, S.; Lindsten, K.; Jellne, M.; Masucci, M. G. Inhibition of Proteasomal Degradation by the Gly-Ala Repeat of Epstein–Barr Virus Is Influenced by the Length of the Repeat and the Strength of the Degradation Signal. *Proc. Natl. Acad. Sci. U. S. A.* **2000**, *97* (15), 8381–8385.

APPENDIX A. EXAMPLE STRUCTURES OF HITS FROM AN OBOC SCREEN AGAINST GANKRYIN.

The following data represents numerous example structures of the hits identified from both screens and several of the overlapping structures between the two screens. Structures were considered overlapping if they had similar amines in similar positions. The overlapping structures were selected for validation by the in-gel fluorescence experiment.

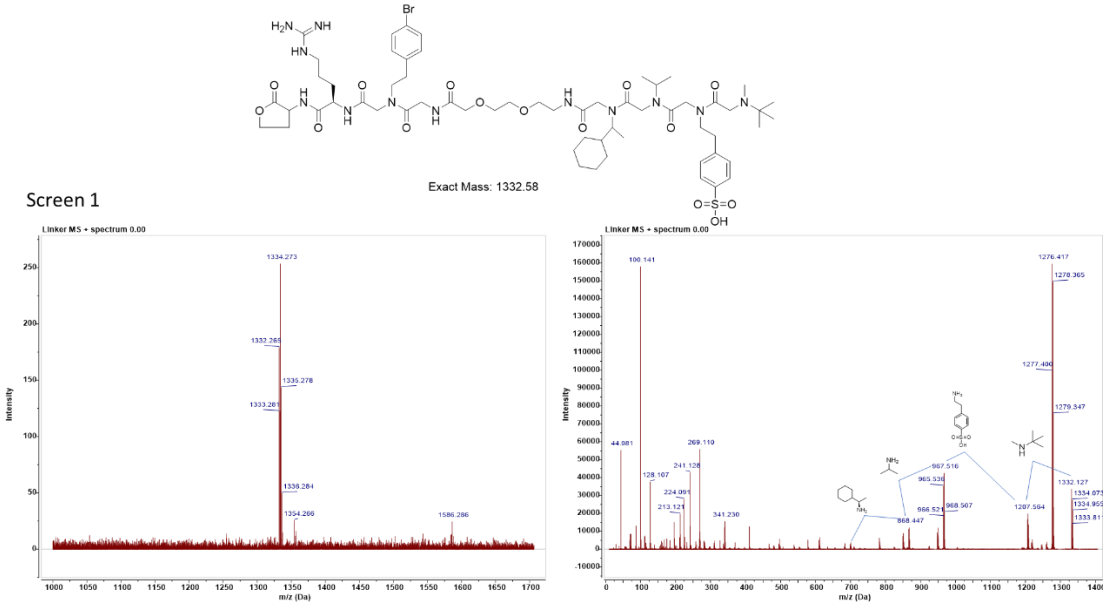

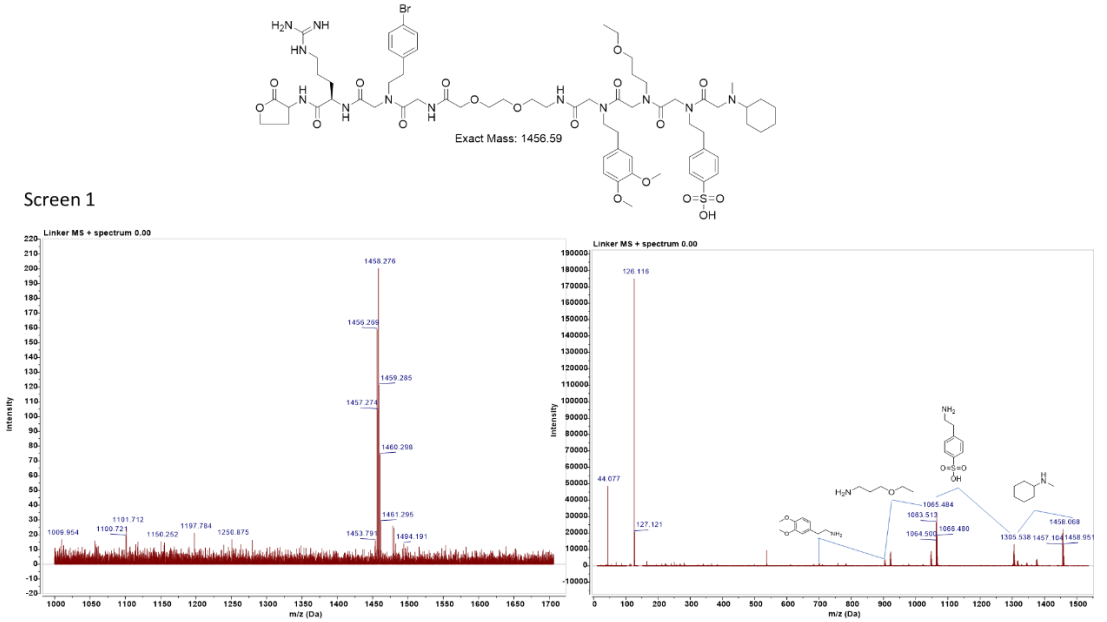

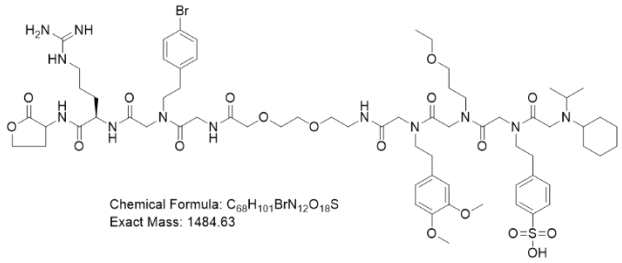

Chemical Formula: $C_{68}H_{101}BrN_{12}O_{18}S$
Exact Mass: 1484.63

Screen 1

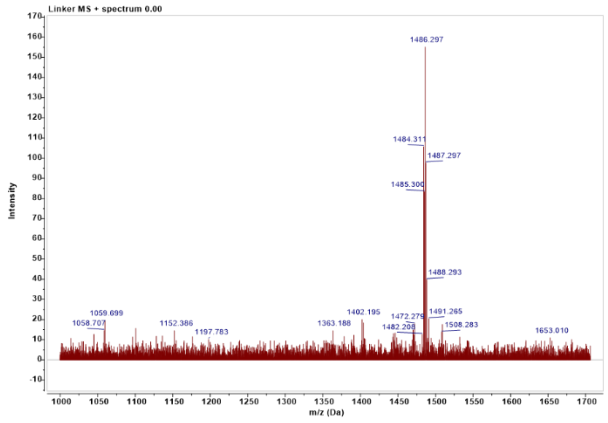

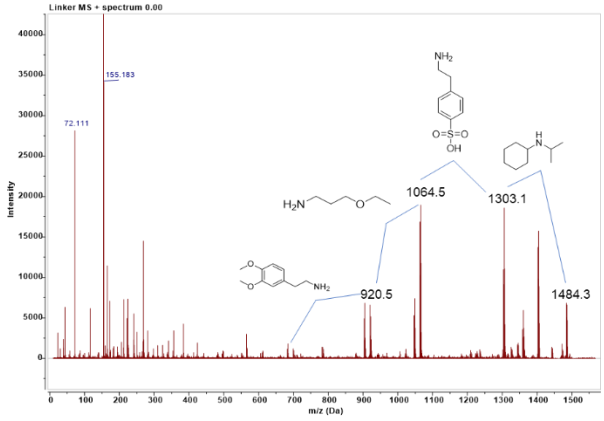

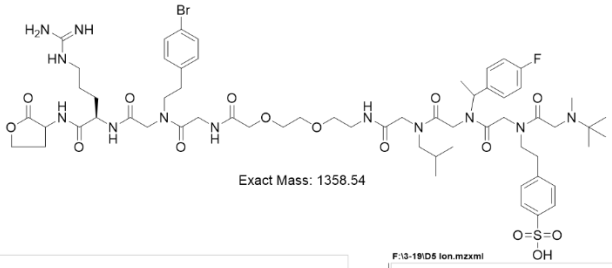

Exact Mass: 1358.54

Screen 2

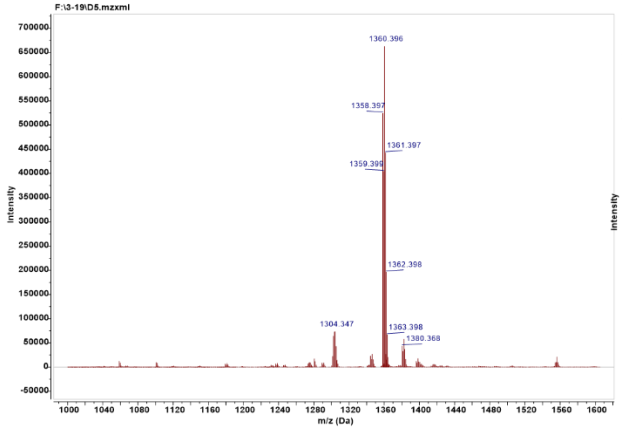

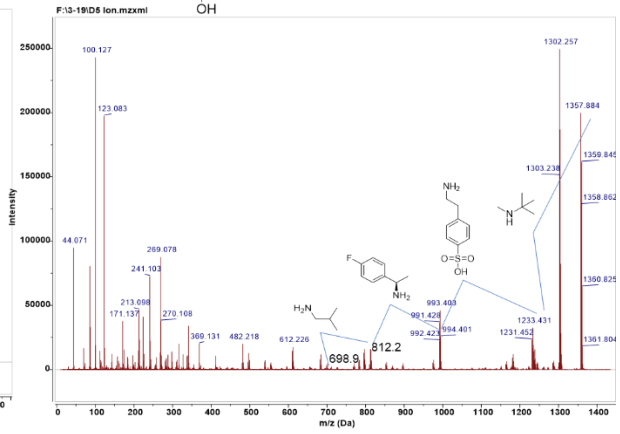

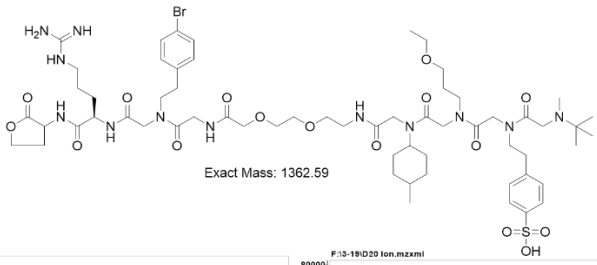

Screen 2

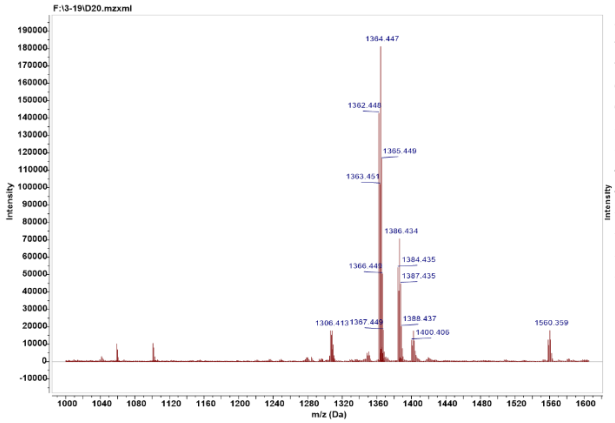

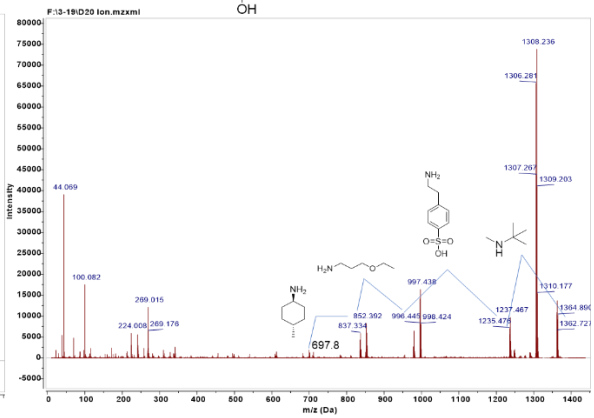

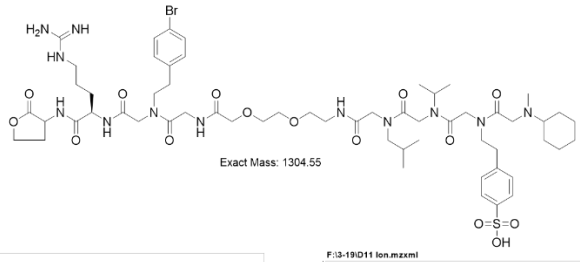

Screen 2

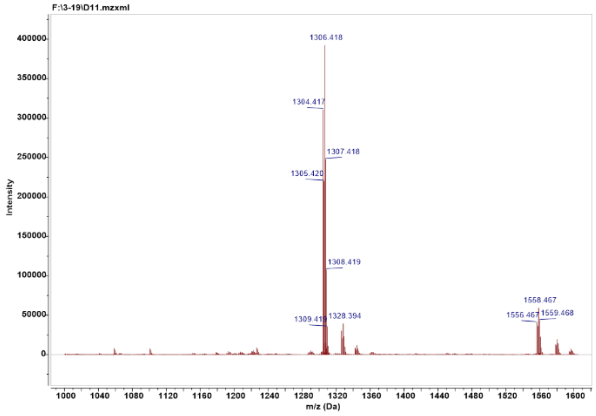

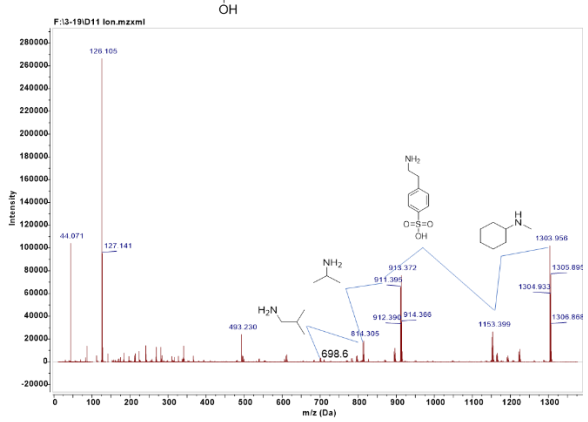

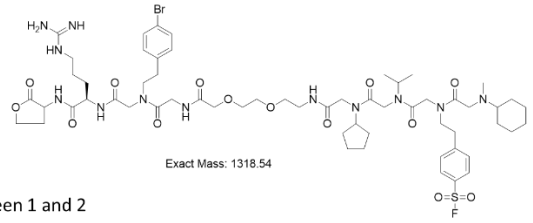

Exact Mass: 1318.54

Overlapping Structure from Screen 1 and 2

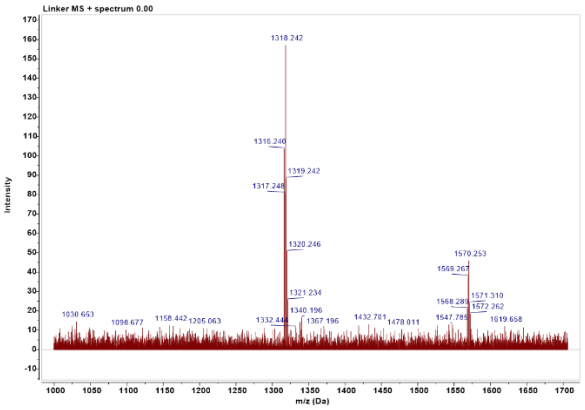

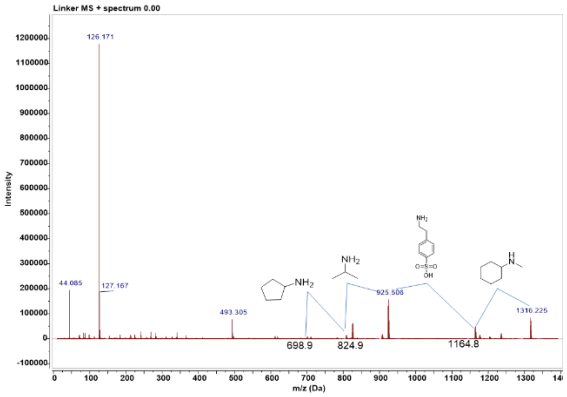

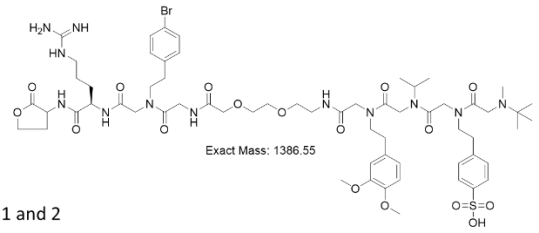

Exact Mass: 1386.55

Overlapping Structure from Screen 1 and 2

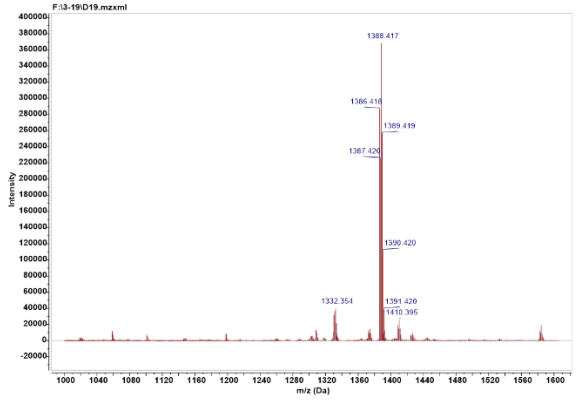

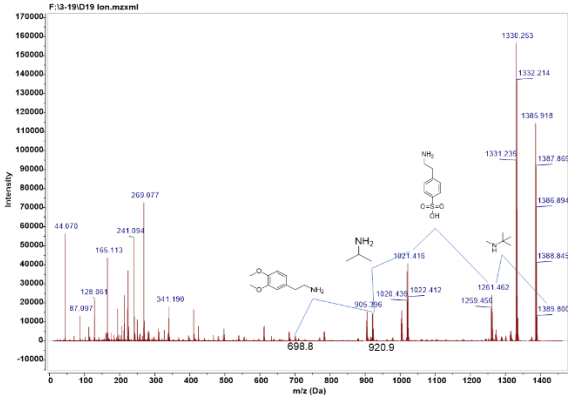

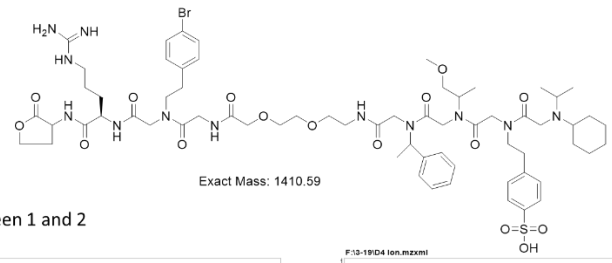

Exact Mass: 1410.59

Overlapping Structure from Screen 1 and 2

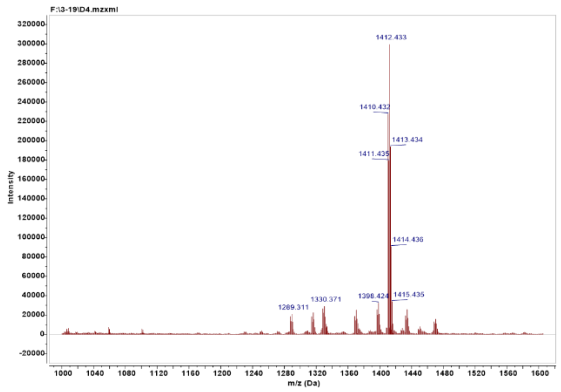

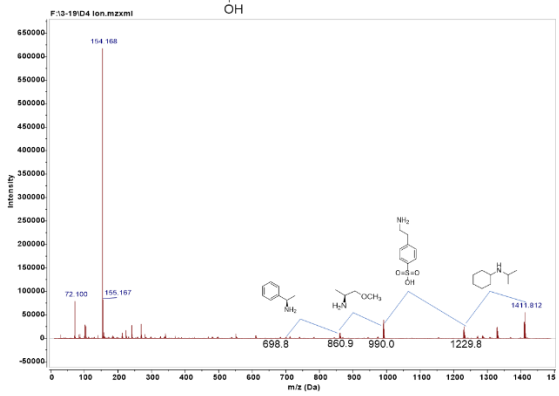

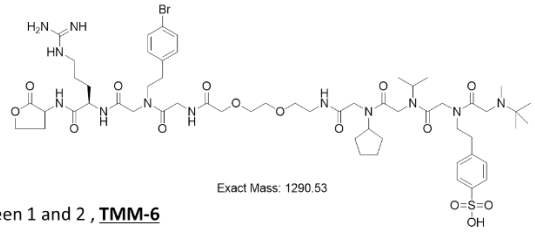

Exact Mass: 1290.53

Overlapping Structure from Screen 1 and 2 , **TMM-6**

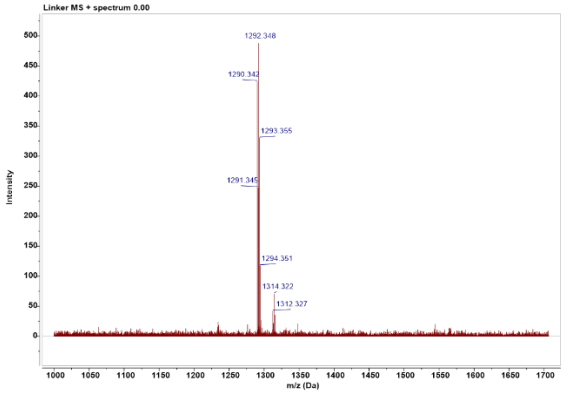

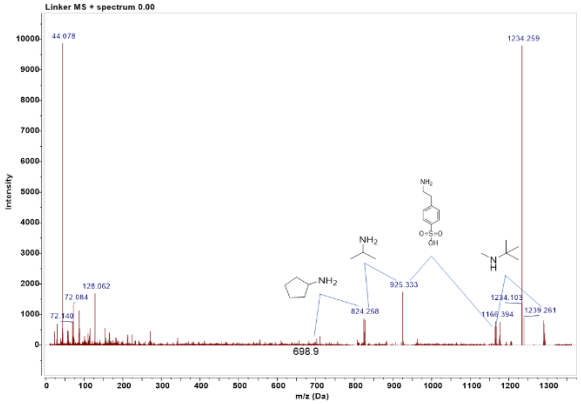

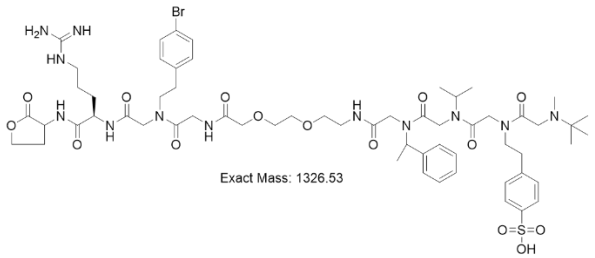

Overlapping Structure from Screen 1 and 2

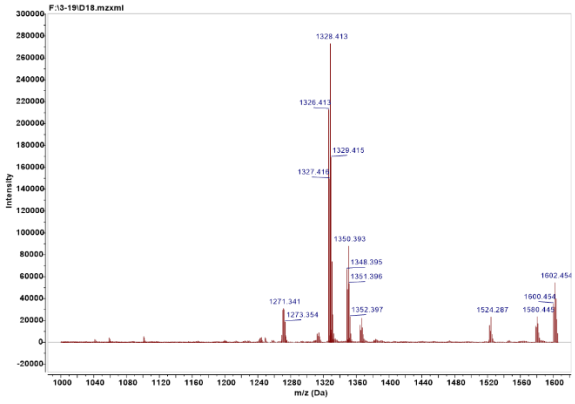

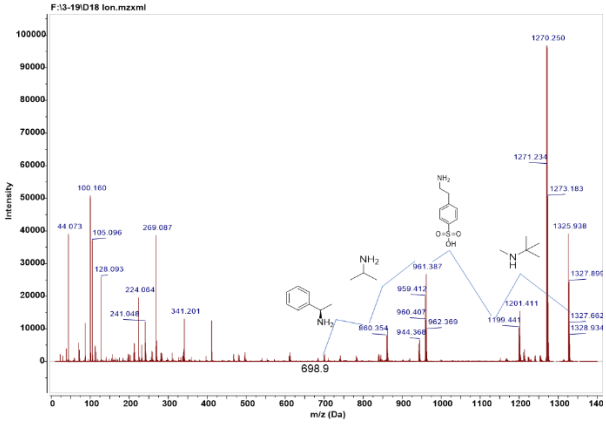

APPENDIX B. LC/MS TRACES OF FLUORESCENTLY LABELED LIGANDS FOR VALIDATION BY IN-GEL FLUORESCENCE

Shown below are several examples of LC/MS traces of the overlapping structures between the two screens that were selected for validation. Ligands were purified by RP-HPLC and the traces below represent injections of samples from the peaks from HPLC purification on an Agilent single quadrupole LC/MS system.

TMM-1

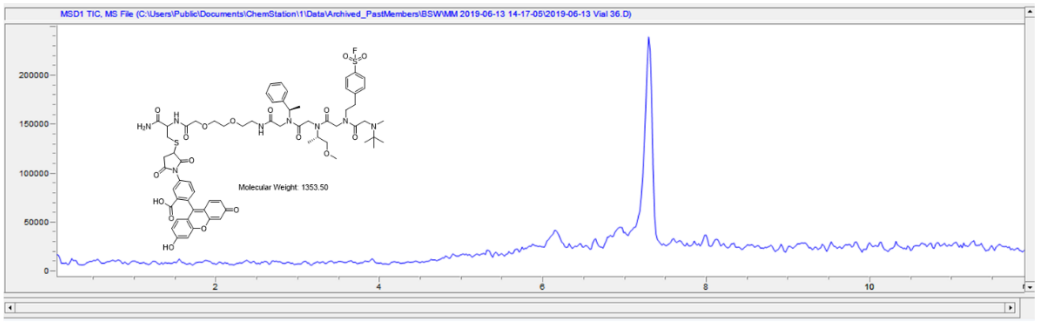

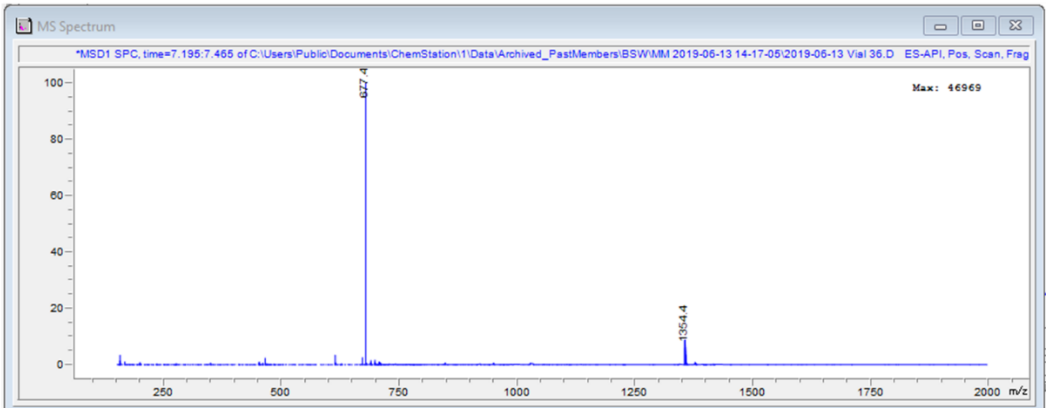

TMM-3

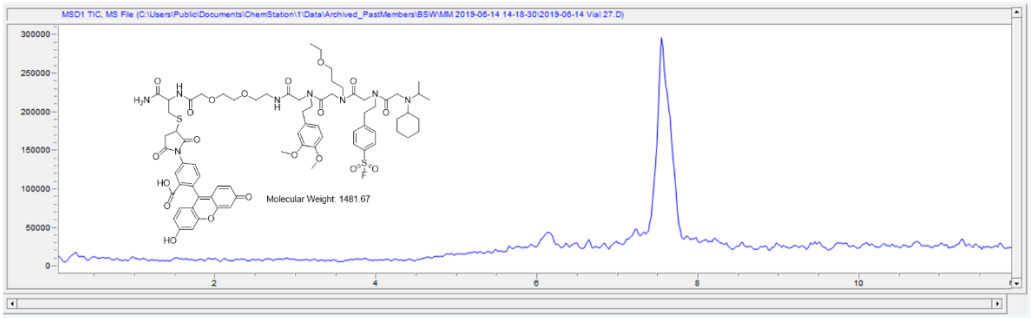
MSD1 TIC, MS File (C:\Users\Public\Documents\ChemStation\1\Data\Archived_PastMembers\BSW\MM 2019-06-14 14-18-30\2019-06-14 Vial 27.D)
Molecular Weight: 1481.67

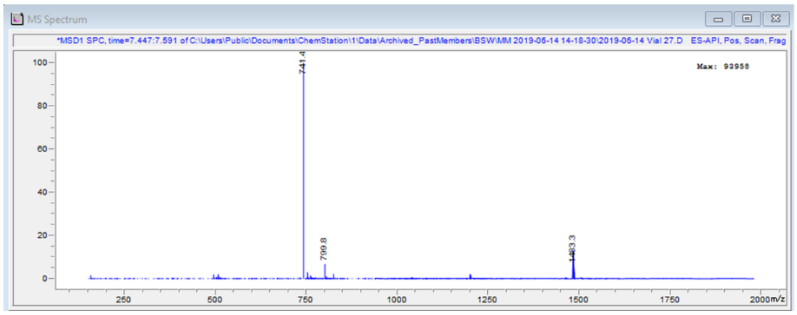
MS Spectrum
*MSD1 SPC, time=7.447:7.591 of C:\Users\Public\Documents\ChemStation\1\Data\Archived_PastMembers\BSW\MM 2019-06-14 14-18-30\2019-06-14 Vial 27.D ES-API, Pos, Scan, Frag
Max: 92958
741.4
799.8
1483.3
m/z

TMM-6

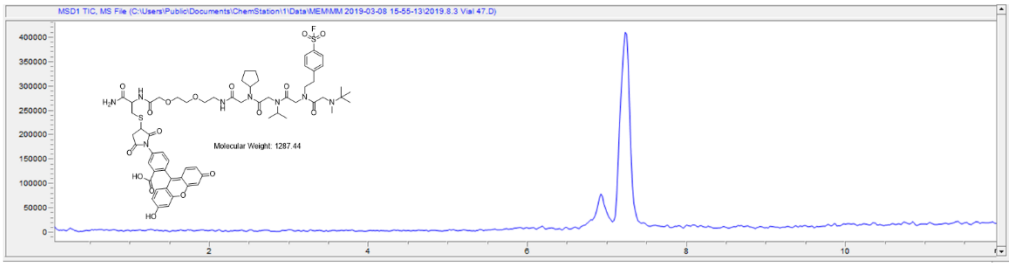
MSD1 TIC, MS File (C:\Users\Public\Documents\ChemStation\1\Data\MEM\MM 2019-03-08 15-55-13\2019.8.3 Vial 47.D)
Molecular Weight: 1287.44

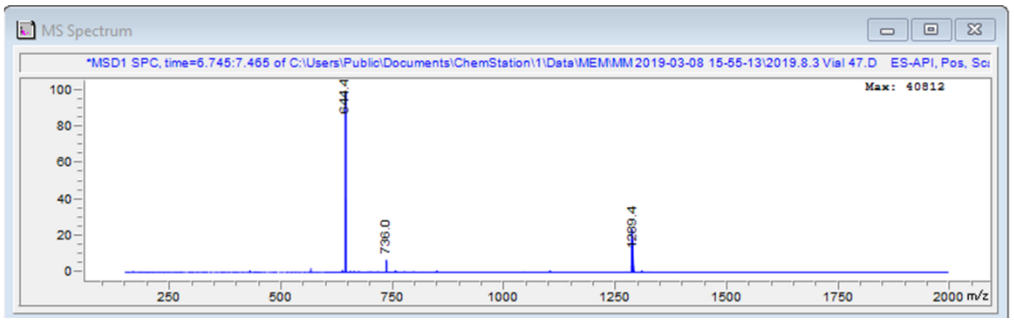
MS Spectrum
*MSD1 SPC, time=6.745:7.465 of C:\Users\Public\Documents\ChemStation\1\Data\MEM\MM 2019-03-08 15-55-13\2019.8.3 Vial 47.D ES-API, Pos, Sc
Max: 40812
644.4
736.0
1269.4
m/z

TMM-7

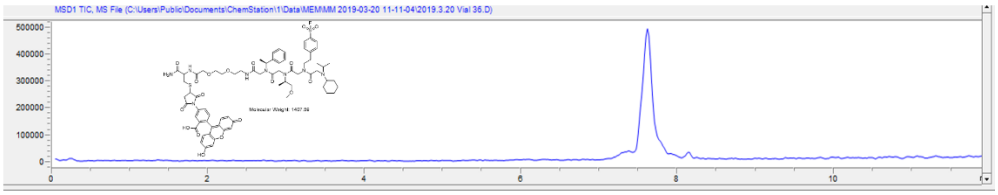
MSD1 TIC, MS File (C:\Users\Public\Documents\ChemStation\1\Data\MEMMM 2019-03-20 11-11-04\2019.3.20 Vial 36.D)

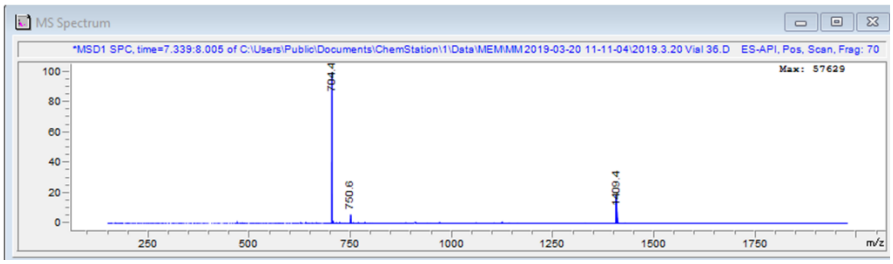
MS Spectrum
*MSD1 SPC, time=7.339:8.005 of C:\Users\Public\Documents\ChemStation\1\Data\MEMMM 2019-03-20 11-11-04\2019.3.20 Vial 36.D ES-API, Pos, Scan, Frag: 70
Max: 57629
704.4
750.6
1409.4
m/z

TMM-14

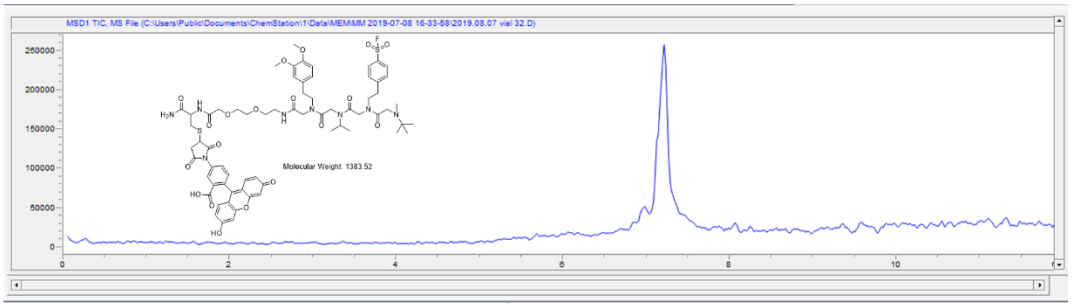
MSD1 TIC, MS File (C:\Users\Public\Documents\ChemStation\1\Data\MEMMM 2019-07-08 16-33-58\2019.08.07 vial 32.D)
Molecular Weight: 1383.52

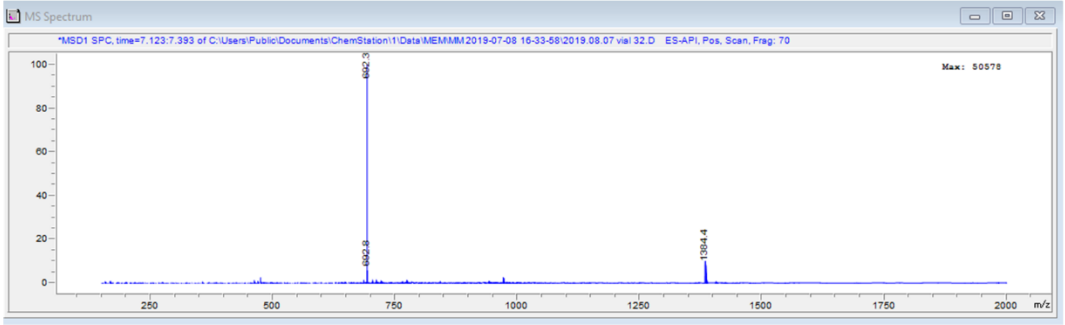
MS Spectrum
*MSD1 SPC, time=7.123:7.393 of C:\Users\Public\Documents\ChemStation\1\Data\MEMMM 2019-07-08 16-33-58\2019.08.07 vial 32.D ES-API, Pos, Scan, Frag: 70
Max: 50578
692.3
692.8
1384.4
m/z

Negative Control

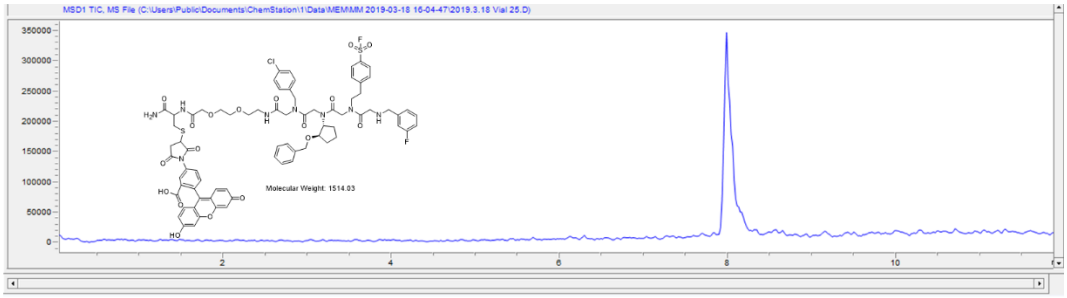

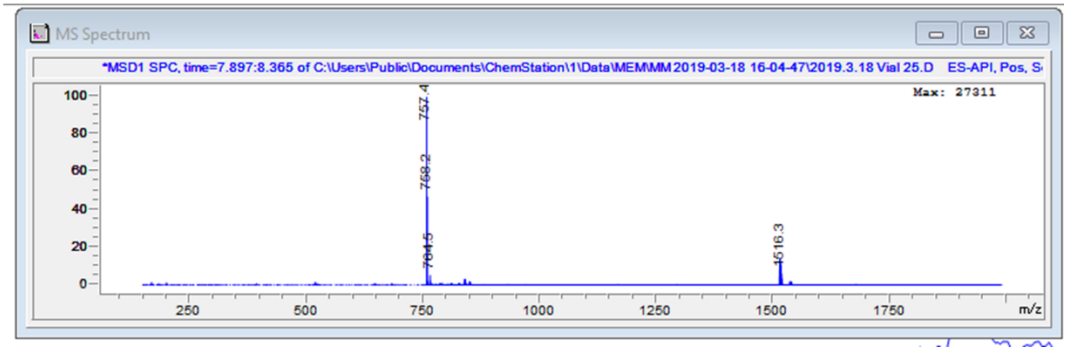

APPENDIX C GRAPHS FROM THE IN-GEL VALIDATION EXPERIMENTS

The following graphs represent examples of the quantified data from the in-gel fluorescence experiment in which purified gankyrin incubated with varying amounts of each fluorescently labeled ligands. The intensity of the protein band corresponding to the labeled ligand or negative control binding gankyrin was quantified and graphed using GraphPad Prism 9.0 software as shown below. TMM-6 was the only peptoid that produced higher fluorescence intensities than the negative control in the initial experiment, indicating that it was a true hit.

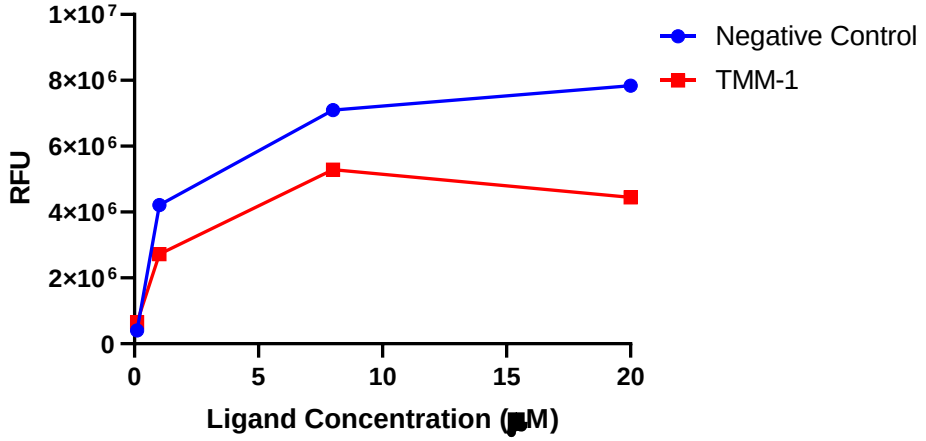

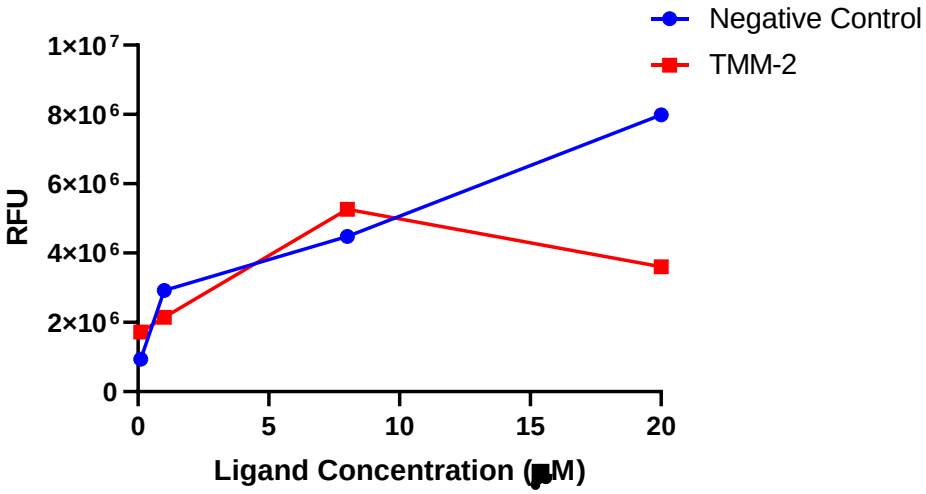

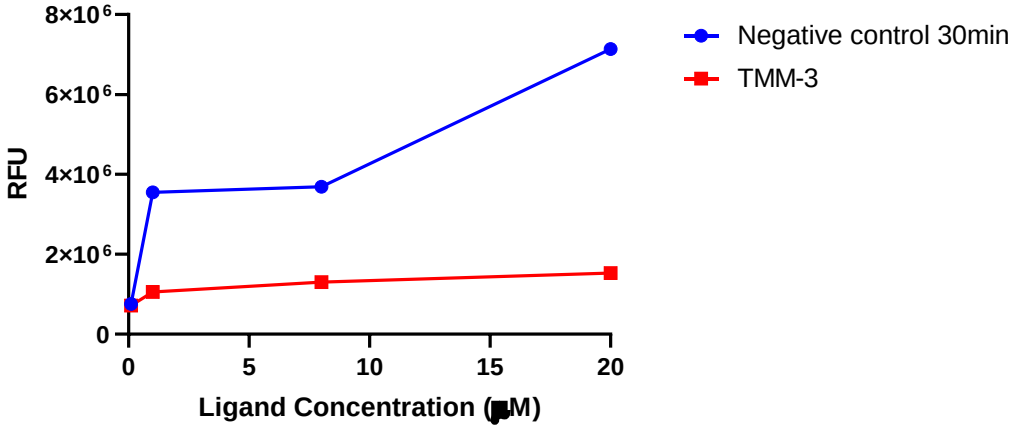
8×10⁶
6×10⁶
4×10⁶
2×10⁶
0
RFU
0
5
10
15
20
Ligand Concentration (μM)
Negative control 30min
TMM-3

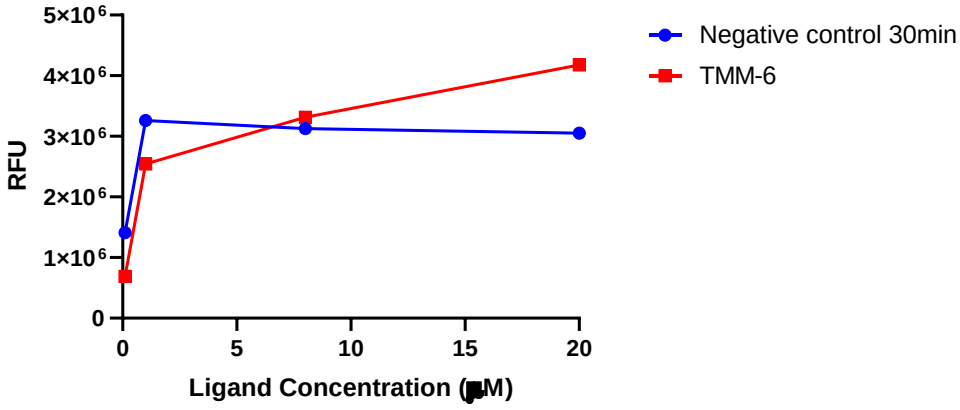
5×10⁶
4×10⁶
3×10⁶
2×10⁶
1×10⁶
0
RFU
0
5
10
15
20
Ligand Concentration (μM)
Negative control 30min
TMM-6

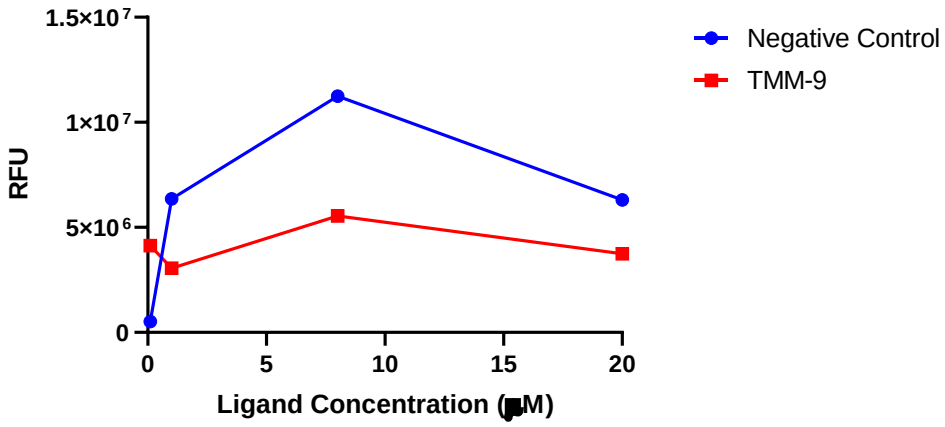
1.5×10⁷
1×10⁷
5×10⁶
0
RFU
0
5
10
15
20
Ligand Concentration (μM)
Negative Control
TMM-9

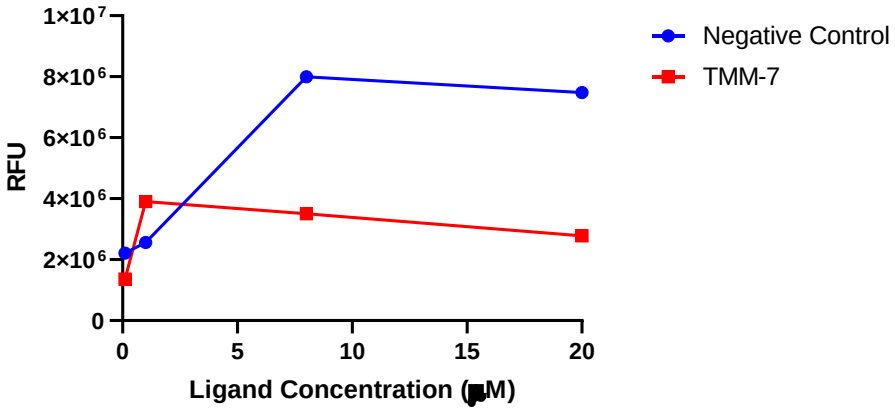
1×10⁷
8×10⁶
6×10⁶
4×10⁶
2×10⁶
0
RFU
0
5
10
15
20
Ligand Concentration (μM)
Negative Control
TMM-7

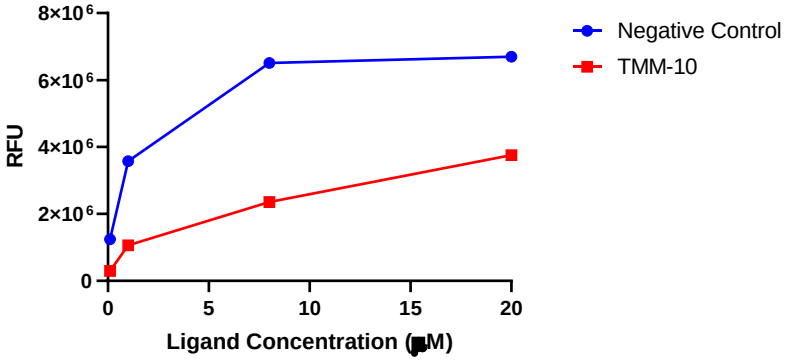
8×10⁶
6×10⁶
4×10⁶
2×10⁶
0
RFU
0
5
10
15
20
Ligand Concentration (μM)
Negative Control
TMM-10

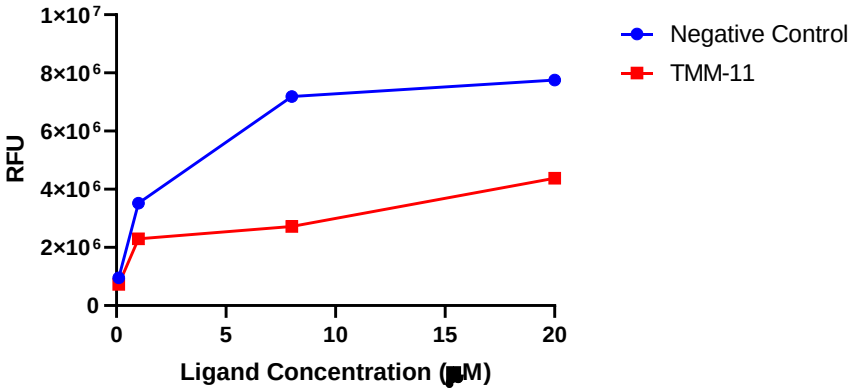
1×10⁷
8×10⁶
6×10⁶
4×10⁶
2×10⁶
0
RFU
0
5
10
15
20
Ligand Concentration (μM)
Negative Control
TMM-11

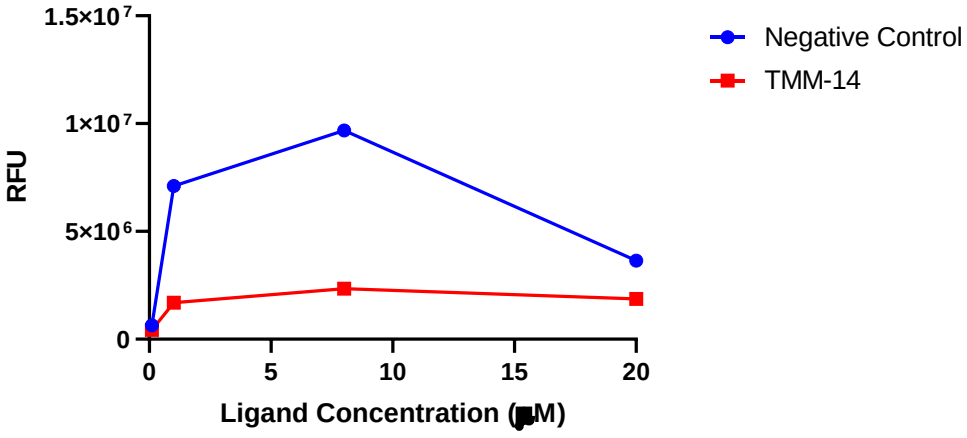
1.5×10⁷
1×10⁷
5×10⁶
0
RFU
0
5
10
15
20
Ligand Concentration (μM)
Negative Control
TMM-14

APPENDIX D. COPYRIGHT PERMISSION FOR REUSE OF PUBLISHED WORK FOR THIS DISSERTATION

American Chemical Society's Policy on Theses and Dissertations

If your university requires you to obtain permission, you must use the RightsLink permission system.
See RightsLink instructions at http://pubs.acs.org/page/copyright/permissions.html.

This is regarding request for permission to include **your** paper(s) or portions of text from **your** paper(s) in your thesis. Permission is now automatically granted; please pay special attention to the **implications** paragraph below. The Copyright Subcommittee of the Joint Board/Council Committees on Publications approved the following:

> Copyright permission for published and submitted material from theses and dissertations
> ACS extends blanket permission to students to include in their theses and dissertations their own articles, or portions thereof, that have been published in ACS journals or submitted to ACS journals for publication, provided that the ACS copyright credit line is noted on the appropriate page(s).
>
> Publishing **implications** of electronic publication of theses and dissertation material
> Students and their mentors should be aware that posting of theses and dissertation material on the Web prior to submission of material from that thesis or dissertation to an ACS journal may affect publication in that journal. Whether Web posting is considered prior publication may be evaluated on a case-by-case basis by the journal's editor. If an ACS journal editor considers Web posting to be "prior publication", the paper will not be accepted for publication in that journal. If you intend to submit your unpublished paper to ACS for publication, check with the appropriate editor prior to posting your manuscript electronically.

Reuse/Republication of the Entire Work in Theses or Collections: Authors may reuse all or part of the Submitted, Accepted or Published Work in a thesis or dissertation that the author writes and is required to submit to satisfy the criteria of degree-granting institutions. Such reuse is permitted subject to the ACS' "Ethical Guidelines to Publication of Chemical Research" (http://pubs.acs.org/page/policy/ethics/index.html); the author should secure written confirmation (via letter or email) from the respective ACS journal editor(s) to avoid potential conflicts with journal prior publication*/embargo policies. Appropriate citation of the Published Work must be made. If the thesis or dissertation to be published is in electronic format, a direct link to the Published Work must also be included using the ACS Articles on Request author-directed link − see http://pubs.acs.org/page/policy/articlesonrequest/index.html

* Prior publication policies of ACS journals are posted on the ACS website at
http://pubs.acs.org/page/policy/prior/index.html

If your paper has **not** yet been published by ACS, please print the following credit line on the first page of your article: "Reproduced (or 'Reproduced in part') with permission from [JOURNAL NAME], in press (or 'submitted for publication'). Unpublished work copyright [CURRENT YEAR] American Chemical Society." Include appropriate information.

If your paper has already been published by ACS and you want to include the text or portions of the text in your thesis/dissertation, please print the ACS copyright credit line on the first page of your article: "Reproduced (or 'Reproduced in part') with permission from [FULL REFERENCE CITATION.] Copyright [YEAR] American Chemical Society." Include appropriate information.

Submission to a Dissertation Distributor: If you plan to submit your thesis to UMI or to another dissertation distributor, you should not include the unpublished ACS paper in your thesis if the thesis will be disseminated electronically, until ACS has published your paper. After publication of the paper by ACS, you may release the entire thesis (**not the individual ACS article by itself**) for electronic dissemination through the distributor; ACS's copyright credit line should be printed on the first page of the ACS paper.

10/10/03, 01/15/04, 06/07/06, 04/07/10, 08/24/10, 02/28/11

Author reusing their own work published by the Royal Society of Chemistry

You do not need to request permission to reuse your own figures, diagrams, etc, that were originally published in a Royal Society of Chemistry publication. However, permission should be requested for use of the whole article or chapter except if reusing it in a thesis. If you are including an article or book chapter published by us in your thesis please ensure that your co-authors are aware of this.

Reuse of material that was published originally by the Royal Society of Chemistry must be accompanied by the appropriate acknowledgement of the publication. The form of the acknowledgement is dependent on the journal in which it was published originally, as detailed in 'Acknowledgements'.

Future Medicinal Chemistry Journal Policy:

Are you planning on using our material in a thesis/dissertation?

Express permission is not required for this purpose, authors are able to re-use or adapt their article for use in their thesis/dissertation, provided a suitable acknowledgement to the original publication is included (see "Acknowledgement" section below). Authors may also deposit their thesis/dissertation in an online, institutional repository if required by their institution.

The above only applies to use in a thesis/dissertation; for other types of re-use authors should refer to the relevant sections on this page, and for self-archiving information here: https://www.future-science.com/authorguide.

VITA

Marianne Elizabeth Maresh is the daughter of Anthony Maresh Jr. and Faye Maresh. She was raised in Michigan and received her Bachelor of Science in Biological Science in May of 2016 from Wayne State University in Detroit, Michigan. During her time as Wayne State University, Marianne completed an Honors Thesis titled, "Determining the Effects of KLHDC3 on Herpes Simplex Virus 1 Viral DNA Replication" under the supervision of Dr. Haidong Gu. She graduated summa cum laude with University and Departmental Honors. Marianne then enrolled in the Purdue University Interdisciplinary Life Sciences (PULSe) Program in August of 2016. She joined the Department of Medicinal Chemistry and Molecular Pharmacology where she completed her doctoral research with Professor Darci J. Trader. Marianne received several fellowships during her doctoral research such as the Bilsland Dissertation Fellowship, SIRG Graduate Research Assistantship, Lilly Endowment Gift, and partial funding from the Lynn Fellowship, in addition to several travel awards.

PUBLICATIONS

1. Maresh, M.E.; Chen, P.; Hazbun, T.R.; Trader, D.J. A Yeast Chronological Lifespan Assay to Assess Activity of Proteasome Stimulators. *Under Review.*

2. Maresh, M. E.; Zerfas, B. L.; Wuthrich, B. S.; Trader, D. J. Identification of a Covalent Binder to the Oncoprotein Gankyrin Using a NIR-Based OBOC Screening Method. *RSC Adv.* **2021**, *11* (21), 12794–12801.

3. Tian, W.; Maresh, M.E.; Trader, D.J. Approaches to Evaluate the Impact of a Small Molecule Binder to a Non-catalytic Site of the Proteasome, *ChemBiochem*, Accepted, **2021**. https://doi.org/10.1002/cbic.202100023

4. Maresh, M. E.; Salazar, A.F.; Trader, D. J. Methods for the Discovery of Small Molecules to Monitor and Perturb the Activity of the Human Proteasome. *Future Med. Chem.,* ASAP, **2020**. https://doi.org/10.4155/fmc-2020-0288

5. Zerfas, B.L.; Maresh, M.E.; Trader, D.J. The Immunoproteasome: An Emerging Target in Cancer, Autoimmune, Neurological Disorders, *J. Med. Chem*. **2020**, *63* (5), 1841-1858.

6. Maresh, M. E.; Trader, D. J. Development of a Method To Prioritize Protein–Ligand Pairs on Beads Using Protein Conjugated to a Near-IR Dye. *ACS Comb. Sci.* **2019**, *21* (3), 223–228.